UNIVERSITÀ
DEGLI STUDI
FIRENZE

Interference in Wireless Communication Systems: Mitigation and Exploiting

by

Giulio Bartoli

Submitted to the Department of Information Engineering
in partial fulfillment of the requirements for the degree of

DOCTOR OF PHILOSOPHY

in Computer Science, Systems and Telecommunications
Cycle XXVI, Disciplinary Scientific Area ING-INF/03

February 2014

Author .....
Department of Information Engineering
December 31, 2013

Certified by .....
Romano Fantacci
Full Professor, Thesis Supervisor

.....
Dania Marabissi
Assistant Professor, Thesis Supervisor

.....
Norman C. Beaulieu
Full Professor, Thesis Supervisor

Accepted by .....
Luigi Chisci
Ph. D. Coordinator

Years 2011/2013

Interference in Wireless Communication Systems: Mitigation and Exploiting

by

Giulio Bartoli

Submitted to the Department of Information Engineering
on December 31, 2013, in partial fulfillment of the
requirements for the degree of
DOCTOR OF PHILOSOPHY

Abstract

The opportunity to transfer information from a location to another has always held a position of capital importance for the mankind. The relevance of telecommunications is uncontested due to countless reasons, spanning from philosophical to tactical. The increasing demand for high data rate services is the driving force of the scientific research in this area. In order to provide the final user with a fast and reliable service, many technical challenges have to be completed. For what concerns the physical layer of communications, increasing the data rate usually involves a detrimental effect on the reliability of the link.

Theoretical bounds of reliable transmission has been derived for channels affected by additive white Gaussian noise (AWGN). The performance in AWGN channel is a useful benchmark, because wireless communication systems are usually affected by further problems. One of the most discussed impairments that heavily deteriorates the performance is the interference, which is the topic discussed here.

This thesis embeds the most of the author's works during his Ph.D. course. In particular, each section is or contains an excerpts of publications. In the first chapter, the impact of impulsive interference on multi-carrier systems is analysed and a novel transmission scheme to improve the performance is proposed. Sec. 1.2 and Sec. 1.3 are based on references [1, 2], respectively.

Chapter 2 derives from [3, 4] and shows how impulsive interference can be modelled as an additive noise through the Laplace distribution. Hence, the structure of the optimum receiver is provided and discussed for this particular distribution.

Chapter 3 concerns interference produced by terminals belonging to the same system, in particular the LTE standard. Indeed, the high frequency reuse, aiming to maximize spectrum efficiency, leads to intra-system interference which limits the benefits of this approach. This chapter gathers [5–7].

Finally, Chapter 4, following from [8, 9][1], deals with a different approach to manage interference coming from terminals of the same system: rather than avoid or mitigate, the physical layer network coding exploits mutual interference to increase the transmission rate.

Thesis Supervisor: Romano Fantacci, Full Professor

Thesis Supervisor: Dania Marabissi, Assistant Professor

Thesis Supervisor: Norman C. Beaulieu, Full Professor

[1] The other publications achieved during this Ph.D. are [10–14]

List of Publications

[1] G. Bartoli, R. Fantacci, D. Marabissi, L. Micciullo, C. Armani, and R. Merlo, "A Novel Mitigation Scheme for JTIDS Impulsive Interference on LDACS System Based on Sensing and Symbol Retransmission," *J. Signal Process. Syst.*, vol. 73, no. 3, pp. 255–266, Jun. 2013.

[2] G. Bartoli, R. Fantacci, D. Marabissi, L. Micciullo, and D. Tarchi, "Detection and Mitigation of Impulsive Interference on OFDM Signals Based on Spectrum Sensing, Blanking and Symbol Retransmission," *Wireless Personal Communications*, pp. 1–17, Feb. 2014. [Online]. Available: http://dx.doi.org/10.1007/s11277-014-1658-6

[3] N. C. Beaulieu, G. Bartoli, D. Marabissi, and R. Fantacci, "The Structure and Performance of an Optimal Continuous-Time Detector for Laplace Noise," *IEEE Commun. Lett.*, vol. 17, no. 6, pp. 1065–1068, Jun. 2013.

[4] G. Bartoli, N. C. Beaulieu, R. Fantacci, and D. Marabissi, "Optimal Data Rate for Reliable Packet Communications in Laplace Noise," *IEEE Commun. Lett.*, vol. 18, no. 1, pp. 2–5, Jan. 2014.

[5] G. Bartoli, R. Fantacci, B. K. Letaief, D. Marabissi, N. Privitera, P. Pucci, and J. Zhang, "Beamforming for Small Cells Deployment in LTE-Advanced and Beyond," *IEEE Wireless Commun. Mag.*, vol. 21, no. 2, Apr. 2014.

[6] G. Bartoli, R. Fantacci, D. Marabissi, and M. Pucci, "Physical Resource Blockclustering method for an OFDMA cognitive femtocell system," *Physical Communications*, Oct. 2013. [Online].
Available: http://www.sciencedirect.com/science/article/pii/S1874490713000591

[7] ——, "LTE-A femto-cell interference mitigation with MuSiC DOA estimation and null steering in an actual indoor environment," in *Proc. IEEE Int. Conf. Commun. (ICC)*, Budapest, Hungary, Jun. 2013, pp. 2707–2711.

[8] G. Bartoli, D. Marabissi, R. Fantacci, and S. Simoni, "Subcarriers Suppression Methods for OFDM Systems with Decode-and-Forward Network Coding," *IEEE Trans. Wireless Commun.*, vol. 12, no. 12, pp. 6034–6042, Dec. 2013.

[9] G. Bartoli, R. Fantacci, D. Marabissi, and R. Simoni, "Physical Layer Network Coding in Multipath Channel: Effective Precoding-Based Transmission Scheme," in *Proc. IEEE Global Telecommun. Conf. (GLOBECOM)*, Houston, US-TX, Dec. 2011, pp. 1–5.

[10] G. Bartoli, R. Fantacci, D. Marabissi, L. Micciullo, and M. Fossi, "Carrier Allocation Method for AeroMACS System in Airport Channel," *IEEE Trans. Aerosp. Electron. Syst.*, vol. 49, no. 2, pp. 786–797, Apr. 2013.

[11] G. Bartoli, R. Fantacci, F. Gei, D. Marabissi, and L. Micciullo, "A Novel Emergency Management Platform for Smart Public Safety," *International Journal of Communication Systems*, Dec. 2013. [Online]. Available: http://dx.doi.org/10.1002/dac.2716

[12] G. Bartoli, R. Fantacci, and D. Marabissi, "AeroMACS: A New Perspective for Mobile Airport Communications and Services," *IEEE Wireless Commun. Mag.*, vol. 20, no. 6, pp. 44–50, Dec. 2013.

[13] G. Bartoli, R. Fantacci, D. Marabissi, D. Tarchi, and A. Tassi, "Downlink cross-layer scheduling strategies for long-term evolution and long-term evolution-advanced systems," *Wireless Commun. and Mobile Computing*, Jun. 2013. [Online]. Available: http://dx.doi.org/10.1002/wcm.2406

[14] G. Bartoli, A. Tassi, D. Marabissi, D. Tarchi, and R. Fantacci, "An Optimized Resource Allocation Scheme Based on a Multidimensional Multiple-Choice Approach with Reduced Complexity," in *Proc. IEEE Int. Conf. Commun. (ICC)*, Kyoto, Japan, Jun. 2011, pp. 1–6.

Acknowledgements

Saying thanks, here, just once, wouldn't be enough for me.
I think the true acknowledgement must be shown everyday.

Contents

List of Figures

List of Tables

Chapter 1

Impulsive Interference on OFDM Systems

Abstract

The impact of systems producing impulsive interference on OFDM receivers is addressed here. First, a practical case study is analysed and a sensing and mitigation technique based on Orthogonal Frequency Division Multiplex (OFDM) symbol retransmission is proposed. In particular, future digital air/ground communication systems (LDACS) will operate on the L-Band where the coexistence with existing legacy systems shall be guaranteed. A scheme to detect and mitigate the JTIDS impulsive interference on LDACS-1 system is described in the first section. The idea advised here is based on the transmission of two copies of the symbols received with interference that are suitably combined at the receiver after a blanking operation of the corrupted samples. Two alternatives are presented, that differ for the adopted retransmission policy, namely *full combining* scheme, where all the symbols are transmitted twice, and *partial combining* scheme, which foresees the retransmission of only those symbols where interference has been detected. Both these methods remove efficiently the interference without affecting the useful information and exploiting profitably the diversity gain against noise through the soft combining approach.

Then, the proposed scheme is extended for any OFDM system affected by impulsive interference. Indeed, the increasing number of wireless devices and systems operating on the same area leads to significant interference problems of impulsive nature that need to be solved. The aim is to generalize the detection and mitigation technique proposed in the first section, for interference generated by an impulsive noise source on an OFDM system. The problem and the proposed method are analysed either theoretically and by means of simulations for an interference with fixed duration.

Performance in terms of bit error rate and throughput is compared with the case without mitigation and with the classical blanking method showing significant improvements. The reduction of the transmission rate, due to the retransmissions, is well compensated by the improvement of the data reliability that leads to an increase of useful data correctly received.

1.1 Introduction

Orthogonal Frequency Division Multiplexing (OFDM) is a transmission technique widely adopted in recent years in high data rate communication systems. It is a multi-carrier modulation technique, with orthogonal sub-carriers, that exhibits several advantages over the

single carrier modulation approaches, such as a higher bandwidth efficiency and the capability of mitigating frequency-dependent distortion across the channel band with a consequent simplified equalization in multipath fading environments. For these reasons OFDM has been selected as the air-interface of many wireless standards such as Third Generation Partnership Project (3GPP) Long Term Evolution (LTE/LTE-Advanced), Wireless Metropolitan Area Networks (IEEE 802.16), Wireless Local Area Network (IEEE 802.11), Digital audio/video broadcasting (DAB/DVB) and wired systems such as power line communications (PLCs).

Performance of OFDM systems can be affected not only by thermal noise but also by Impulsive Noise (IN). The problem of IN in OFDM transmission is well-known in PLCs [15], while only recently it has been investigated for wireless systems where the increasing number of wireless devices and systems leads to a dense spatial reuse and a severe co-channel interference that can be impulsive. In addition, IN can be generated by other sources like lightning discharges or man-made noise.

In an OFDM system the IN is spread over all the subcarriers due to the Discrete Fourier Transform (DFT) operation performed at the receiver side. This is an advantage compared to the single carrier systems in case of low interference power, but it becomes a disadvantage if IN is powerful, as may happen in PLC and dense cellular networks.

In this case, OFDM has low immunity to impulsive noise, and performance is heavily affected [16, 17]: without any interference mitigation, the OFDM system is not able to meet the QoS requirements especially in high data rate systems.

The most known solutions to counteract the impulsive interference are clipping and blanking [18, 19]. In both methods IN is detected when the signal amplitude exceeds a certain threshold. On one hand, blanking sets to zero the samples where the noise has been detected, removing the signal together with noise, on the other hand clipping truncates the amplitude of the samples to a certain value, where the noise is present, to reduce its impact.

Both methods operate with non-linear operations, making the OFDM signal subcarriers no more orthogonal, thus resulting in an increased inter-carrier interference (ICI). This degrades the performance especially in multi-user communication systems [20], requiring additional ICI cancellation schemes.

In [21] the authors provide an improvement of blanking non-linearity through an iterative reduction of ICI caused by blanking operation. In [22, 23] IN suppression techniques jointly with frequency domain equalization are investigated. Alternative schemes show a noise reduction based on data detection (i.e., decision directed) and cancellation in order to estimate and remove the noise. These schemes are quite effective but present high computational costs [24, 25]. In [26], the authors propose a decision direct approach for mitigating the impulsive noise in xDSL environments.

This chapter proposes a new method to detect and remove the impulsive noise based on spectrum sensing and symbols retransmission. This sensing and retransmission technique has a low complexity compared to other mitigation schemes and is particularly suitable when the IN affects often the signal, making an interleaving approach not useful [27].

The impulsive noise is detected by resorting to a spectrum sensing algorithm based on energy detector. Spectrum sensing algorithms have gained popularity since the introduction of the Cognitive Radio concept [28]; among others, the energy detector presents low computational cost and is the most useful when the signal to be detected is unknown [29]. Our proposal is to exploit a combination of symbols retransmission and blanking operation after the interference detection.

According to the soft symbol combining principle [30], in order to increase the performance in continuous ARQ (Automatic Repeat reQuest) based communication systems, the symbol is transmitted two times whenever the impulsive interference is detected: the first

replica of the symbol is stored and soft combined with the second replica. Before the soft combining operation, the samples affected by IN are zeroed on each copy, in order to remove the impulsive interference without losing useful information. An additional gain is introduced by the soft combining against AWGN noise. The scheme is based on the idea that, even if two consecutive replicas of the same packet are affected by IN, the samples affected by the interference can be considered as statistically independent.

1.1.1 The aeronautical environment

We start our analysis by considering a specific case study: the interference produced by the Joint Tactical Information Distribution System (JTIDS) on the aeronautic L-band Digital Aeronautical Communication System (LDACS). Indeed, the growth of air traffic in national and international airports leads to the need of an advanced and efficient Air Traffic Management (ATM) system able to support the requirements of future air transportation system [31]. The joint efforts of Eurocontrol and ICAO (International Civil Aviation Organization) towards the definition of a new ATM system generation, have recently yielded two parallel projects: the SESAR (Single European Sky ATM Research) [32] in Europe and the NextGen (Next Generation Air Transportation System) [33] in the United States. One of the main aspects of the future ATM system is the provision of enhanced communication capabilities. Hence, Future Communication Systems (FCSs) definition is an important part of the ATM updating program. Since the COCR (Communications Operating Concepts and Requirements) operational requirements cannot be fulfilled by a single technology, the communication infrastructure will be implemented as a complex system, integrating existing as well as new communication technologies [10]. Among these, the new LDACS for air/ground communications is currently under development. Due to the heavy congestion of the VHF band, the Eurocontrol/FAA Action Plan17 (AP17) [34] identified the L-Band (from 960 MHzto 1213 MHz) as the best candidate band for air/ground data links, primarily due to its propagation characteristics. At present time, two different alternatives are under evaluation for LDACS technology, named LDACS-1 and LDACS-2. The former is a Frequency Division Duplex (FDD) system exploiting the OFDM (Orthogonal Frequency Division Multiplex) technique, that is very effective against the inter symbol interference. The latter option, LDACS-2, is a Time Division Duplex (TDD) system utilizing the CPFSK (Continuous-Phase Frequency-Shift Keying) modulation, that allows to reduce the out-of-band emissions. One of the two alternatives will be selected depending on the results of the ongoing studies. With reference to this one important aspect that will determine the choice of the most appropriate data link solution is the spectral compatibility with existing legacy systems operating in L-Band (e.g., DME, SSR, UAT, JTIDS/MIDS). The focus here is on the investigation of interference effect of JTIDS / Multi-functional Information Distribution System (JTIDS/MIDS)[1] on LDACS-1 system. JTIDS is a military radio technology employed as digital data link used for several purposes such as mission management, identification in surveillance and air control. Its signal results to be very robust to interference and jamming thanks to the adoption of appropriate countermeasures like frequency hopping and spread spectrum coding. On the contrary, JTIDS interference on the LDACS-1 signal can be very disruptive due to its high transmission power. In addition, JTIDS frequency hopping is performed over a large range of frequencies spanning almost the whole L-Band: hence, the probability of having collisions between the LDACS-1 and the JTIDS signal is very high. Impulsive noise on an OFDM system is spread over all the subcarriers by means

[1]MIDS is the NATO implementation of JTIDS.

of the DFT (Discrete Fourier Transform). This is an advantage with respect to single carrier systems until the interference power is low but becomes a disadvantage if impulsive noise becomes high. In this case OFDM is vulnerable to impulsive noise that gives rise to a strong performance loss [16], [17]. In general, without any interference mitigation the OFDM system is not able to meet the QoS requirements, especially in the case of high data rate systems. Influence of interference of JTIDS on LDACS-1 was previously investigated in [35], where the LDACS-1 performance in terms of Bit Error Rate (BER) is evaluated considering a pulse blanking mitigation technique and ideal interference detection. More in general, impulsive interference on OFDM systems is a well-known problem in Power Line Communications (PLCs), and recently is investigated also for wireless systems. In fact the increasing number of wireless devices and systems leads to a dense spatial reuse and severe co-channel interferences that can be modelled as impulsive. Main solutions to counteract this type of interference are clipping and blanking [18], [36], [19]. In both methods impulsive noise is detected if the signal amplitude exceeds a threshold. Blanking technique sets to zero the samples where the noise has been detected and signal is removed together with noise. Clipping method truncates the amplitude of the samples where the noise is present to reduce its impact. Both are nonlinear operations and the result is that OFDM signal is no longer orthogonal and consequent Inter-Carrier Interference (ICI) degrades the performance especially in multiuser communications systems, requiring additional countermeasures [20]. Some joint advanced schemes have been proposed. In [21] author provides an improvement of blanking nonlinearity through an iterative reduction of ICI caused by the blanking operation. In [22], [23] impulsive noise suppression techniques in conjunction with frequency domain equalization are investigated. Alternative schemes present a noise reduction method based on data detection (i.e., decision directed) and cancellation in order to estimate and remove the noise. These schemes are quite effective but present high computational cost [24], [25].

1.2 JTIDS Interference on LDACS Receiver

This section proposes a new approach to detect and remove the impulsive noise based on the joint use of spectrum sensing per sample, symbols retransmission and soft combining. It presents low complexity and is suitable when the impulsive noise is often present, affecting many symbols and, hence, making interleaving techniques [37] ineffective.

In the first phase, impulsive noise is detected by resorting to a spectrum sensing algorithm based on energy detector. In the of Cognitive Radio context, different sensing techniques have been proposed to detect interference in [38], [28], among them the energy detector presents low computational cost and is the most useful when the signal to be detected is unknown [29]. After the interference sensing phase the proposed method foresees the joint use of symbols retransmission and blanking operation. According to the soft symbol combining principle [30], to increase the performance in continuous ARQ based communication systems [39], whenever the JTIDS interference is detected, the symbol is transmitted two times: the first copy of the symbol is not discarded but stored and soft combined with its new received copy. Before the combining operation, the samples affected by impulsive noise are zeroed. In that way the impulsive interference is removed without losing useful information. An additional gain is introduced by the soft combining against the AWGN noise, increasing the system performance. In particular two different alternatives are presented, called *full* and *partial combining*, that differ for the retransmission policy. These schemes are based on the idea that even if two consecutive copies of the same symbol are affected by impulsive noise, the samples affected by the interference are statistically independent.

Table 1.1: LDACS-1 possible allocation bands (Bn with n=1,...,4).

B1	$964 - 970$ MHz
B2	$985 - 1009$ MHz
B3	$1048 - 1072$ MHz
B4	$1150 - 1156$ MHz

1.2.1 Impulsive transmitter and OFDM receiver model

In the system under consideration the LDACS-1 signal is affected by the interference of a JTIDS signal operating on the same band. For the LDACS-1 system we refer to the latest available specifications [40]. It is based on the FDD approach and is designed to operate in the lower part of the L-band with a bandwidth of $B_{LDACS} = 498.05$ kHz. The possible allocation bands foreseen for the system, either for Forward Link (FL) and Reverse Link (RL), are reported in Tab. 1.1.

LDACS-1 is an OFDM-based communication system where the available spectrum is shared between a large number of subcarriers. Data symbols are efficiently modulated on these subcarriers by resorting to the use of the Inverse DFT (IDFT) in transmission and the DFT at the receiving end. According to [40], we consider an OFDM system with a total number of available subcarriers, N, equal to 64 where only $N_u = 50$ are used to carry information. The bit stream is first mapped into complex QPSK symbols v_k, with $k = 0, \cdots, N_u$. After a serial to parallel (S/P) conversion, the block of N_u symbols, $\mathbf{v} = [v_0, \cdots, v_{N_u-1}]$, is transformed into a block of N symbols $\mathbf{c} = [c_0, \cdots, c_{N-1}]$ by inserting $(N - N_u)$ zeros in correspondence of the first 7 and the last 6 subcarriers, and on the DC subcarrier.

The i-th transmitted OFDM symbol results to be

$$s_i(n) = \sum_{k=0}^{N-1} c_k \cdot e^{j\frac{2\pi}{N}nk} \quad \text{for} \quad \begin{cases} n = 0, ..., N-1 \\ i = -\infty, \cdots, \infty \end{cases} . \tag{1.1}$$

Then, a cyclic prefix of length N_g, equal to 11 samples, is inserted by repeating the final part of the OFDM symbol, $s_i(n)$, resulting in the transmitted signal $\hat{s}_i(n)$, with duration T_s equal to 120 μs. The base-band signal is up-converted to the radio frequency and transmitted through the channel. We consider a frequency selective multipath fading channel with discrete impulse response $h_i(n)$ shorter than the cyclic prefix, so that, by removing the cyclic prefix at the receiving end, the ISI is deleted. By using the cyclic prefix, the convolution between the transmitted signal and $h_i(n)$ is a cyclic convolution, hence, the down-converted i-th received symbol can be defined as:

$$\hat{r}_i(n) = \hat{s}_i(n) \otimes h_i(n) + n_i(n) + u_i(n) \tag{1.2}$$

where $n_i(n)$ is white Gaussian noise term, with zero mean and variance $N_0/2$ introduced by the communication channel and $u_i(n)$ represents the impulsive noise due to the JTIDS signal as described in the following. The useful received signal $r_i(n)$ is obtained by removing the cyclic prefix.

Then the signal $r_i(n)$ is processed by the DFT block. The DFT output for the k-th

subcarrier, before equalization, is

$$\begin{aligned} Z_i(k) &= \frac{1}{N}\sum_{n=0}^{N-1} r_i(n)\cdot e^{-j\frac{2\pi}{N}nk} \\ &= S_i(k)\cdot H_i(k) + N_i(k) + U_i(k) \end{aligned} \tag{1.3}$$

where $S_i(k)$, $H_i(k)$, $N_i(k)$ and $U_i(k)$ are the samples of the transmitted symbol, channel impulse response, AWGN and JTIDS interference contributions, respectively, in the frequency domain, on the k-th subcarrier of the i-th symbol. The channel coefficients can be written as

$$H_i(k) = \alpha_i(k)e^{\phi_i(k)} \tag{1.4}$$

where $\alpha_i(k)$ and $\phi_i(k)$ are the attenuation and the phase rotation of the channel impulse response at the k-th subcarrier of the i-th symbol, respectively. We assume a fading channel whose amplitude varies with a Rice distribution, with Ricean factor equal to $K = 10$ dBand normalized power $\Omega = 1$. The signal is equalized by the means of a Zero Forcing operation assuming perfect knowledge of the channel response.

JTIDS is a TDMA (Time Division Multiple Access) system operating in the frequency range $[960 - 1215]$ MHz [41]. Each time slot is composed by a sequence of N_p pulses of length $T_p = 6.4$ μs and spaced by $T_{int} = 6.6$ μs: each pulse contains 5 bits multiplied for a spreading sequence of 32 chips, modulated through the MSK (Minimum Shift Keying). The chip duration is 200 ns, with a consequent bandwidth of 5 MHz. Then, the total bandwidth is filtered and reduced to 3 MHz. Each pulse is transmitted over a different carrier frequency selected among $N_{ch} = 51$ possible values according to a specific hopping pattern. In particular the N_{ch} frequencies are spaced of 3 MHz, from 969 MHzto 1206 MHz. JTIDS is a military system and the hopping sequences represent a classified information, for this reason we consider here randomly generated sequences where each frequency has the same probability to be selected. JTIDS has a bandwidth that is significantly wider than that of LDACS-1, hence, when JTIDS transmits on a band near to the LDACS-1 central frequency the entire LDACS-1 signal is affected by the interference. One or two hopping frequencies can interfere with LDACS signal depending on its exact frequency allocation. We can conclude that JTIDS interference on LDACS-1 signal is not deterministic but it depends on several parameters. In particular JTIDS transmission results to be intermittent in both the time and frequency (due to frequency hopping) domains, and the probability that a JTIDS pulse interferes with LDACS-1 signal can be expressed as:

$$P_p = \frac{q}{N_{ch}}\eta\frac{N_p * (T_p + T_{int})}{T_{slot}} \tag{1.5}$$

It depends on:

- the probability that JTIDS is transmitting on the hopping frequencies that are near to the LDACS-1 central frequency, that is $\frac{q}{N_{ch}}$ with $q = 1, 2$. For simplicity here we do not consider multi-frequency JTIDS networks (i.e., simultaneous transmission on more frequencies following orthogonal hopping patterns, and, hence, $q > 2$);

- the probability that the JTIDS time slot is active, that is $\frac{N_p(T_p+T_{int})}{T_{slot}}$, where:

  - $N_p = [72, 258, 444]$ is the number of pulses in a JTIDS time slot (the standard value is $N_p = 258$);

- $T_{slot} = 7,8125$ msis the overall JTIDS time slot duration, which includes an inactive period where the transmitter is in idle mode;

- the probability that JTIDS time slot is effectively used, η, which corresponds to the time slot duty factor (TSDF): the percentage of time slots occupied in a JTIDS frame. It depends on the number of JTIDS active users on the LDACS-1 area (i.e., that can interfere): for a single user the maximum value[2] is 50%. The TSDF can reach the value of 100% for a higher number of users.

In order to have the same sampling frequency as the LDACS signal, the JTIDS pulse is decimated and then the two signals are summed at sample level. This decimation operation extends the pulse duration and reduces the amplitude, making the JTIDS signal more difficult to detect. Hence, when the power of the interfering signal is high, the decoding is difficult for all the samples carried by the OFDM symbol.

Interference evaluation

The development of a new system operating in a frequency band densely populated by legacy systems introduces the need of a careful evaluation of coexistence issue. This section presents a preliminary compatibility assessment. A qualitative evaluation of the mutual interference can be derived by the joint representation of JTIDS and LDACS-1 spectrum in nominal band and in Out of Band and Spurious Domain. It permits to put in evidence potentially critical scenarios. The signals have been generated in Time Domain (TD) taking into account the standards mandatory features [40], [41] that directly affect the spectrum shape. For LDACS-1, an OFDM signal with 64 subcarriers has been generated in FD and transformed in TD by means of a IDFT. Then a raised cosine window that aims to reduce out-of-band radiations has been applied. Later, the signal has been transformed in FD and filtered with the spectral mask. For JTIDS an impulse of 6.4 μs duration has been produced and modulated with a spreading sequence of 32 chips each of 200 ns duration and CPFSK modulated. Once transformed the signal to FD, the spectrum mask has been applied. Fig. 1-1 shows LDACS and JTIDS power spectrum when an offset (Δf) equal to 5 MHzbetween the central frequencies of the two systems is assumed. It is evident that JTIDS heavily interferes with the LDACS-1 due to its high transmission power. It can be noted that the results are similar even under higher frequency offsets (i.e., translating the LDACS-1 spectrum).

The effect of JTIDS interference can be also evaluated analytically following an approach based on the MCL (Minimum Coupling Loss) method [42]. The power of the interfering signal, $I(d)$, at a give distance d between JTIDS transmitter and LDACS receiver can be calculated by means of a link budget [43], defined as

$$I(d) = P_{RX}(d) + OCR + DC \tag{1.6}$$

where:

- $P_{RX}(d)$ is the interfering signal power received by the victim system defined as $P_{RX} = P_{TX} + G_{RX} + G_{TX} - L_{TX} - L_{RX} - P(d)$ It is function of the transmitting power P_{TX}, the antenna gains (G_{TX} and G_{RX}) and the cable losses (L_{TX} and L_{RX}) of the two systems and the path loss $P(d)$, which is in turn dependent on the distance d.

[2]This analysis considers the maximum values of the TSDF because they represent the worst case from an interference point of view.

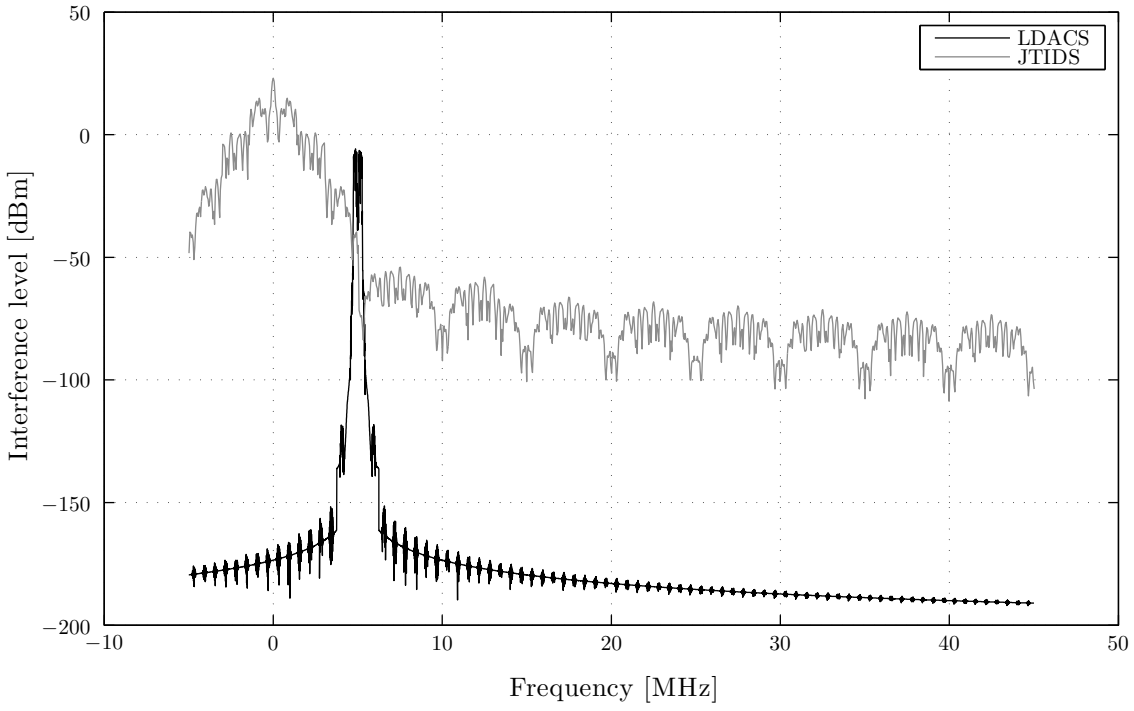

Figure 1-1: JTIDS and LDACS spectra with a frequency offset equal to 5 MHz.

- OCR is the Off Channel Rejection factor that takes into account the capability of the victim receiver to reject the interferer signal for a given frequency offset among the two systems and is calculated as described in [44][3]

- DC takes into account the transmitter duty cycle that is equal to $P_p(T_p/(T_p + T_{int})$.

The value of $I(d)$ is compared to the maximum level of interference I_{MAX} allowed by the system to have reliable communications[4].

The goal is to detect the minimum distance, d_{min}, at which the interference level is tolerated (i.e., $I(d_{min}) = I_{MAX}$). The coexistence between the two systems is guaranteed if d_{min} is lower than the minimum operational distance that in a first evaluation can be assumed equal to the minimal vertical separation of the aircraft that is 300 m.

Fig. 1-2 shows the results obtained assuming a JTIDS user on the ground that interferes with a LDACS-1 airborne aircraft. Used parameters depend on the scenario and are summarized in Tab. 1.2. The figure shows that even beyond 370 km, which is assumed to be the LDACS-1 cell radius [40], $I(d)$ is higher than I_{MAX} and d_{min} cannot be identified in the range of distances considered in the figure. Spectrum compatibility between the two systems is not guaranteed.

The results of different scenarios are reported in Tab. 1.3, where the link budget parameters have been changed accordingly. The considered TSDF is always 50% and the JTIDS maximum transmission power is assumed to be 1000 W.

In all the considered cases the minimum distance that guarantees a tolerable interference level is much higher than the minimum operational distance. Even if this is only a theo-

[3]OCR depends on the power spectral density of the interfering signal and on the receiver IF filter frequency response

[4]I_{MAX} can be usually obtained by system specifications, however at current state LDACS-1 specifications have not defined this value and we refer to the value defined for B-AMC (Broadband Aeronautical Multicarrier Communication) system from which LDACS-1 specifications have been derived.

Table 1.2: Link Budget Parameters.

P_{TX}	L_{TX}	G_{TX}	G_{RX}	L_{RX}	$TSDF$
1000 W	3 dB	6 dBi	0 dBi	3 dB	50%

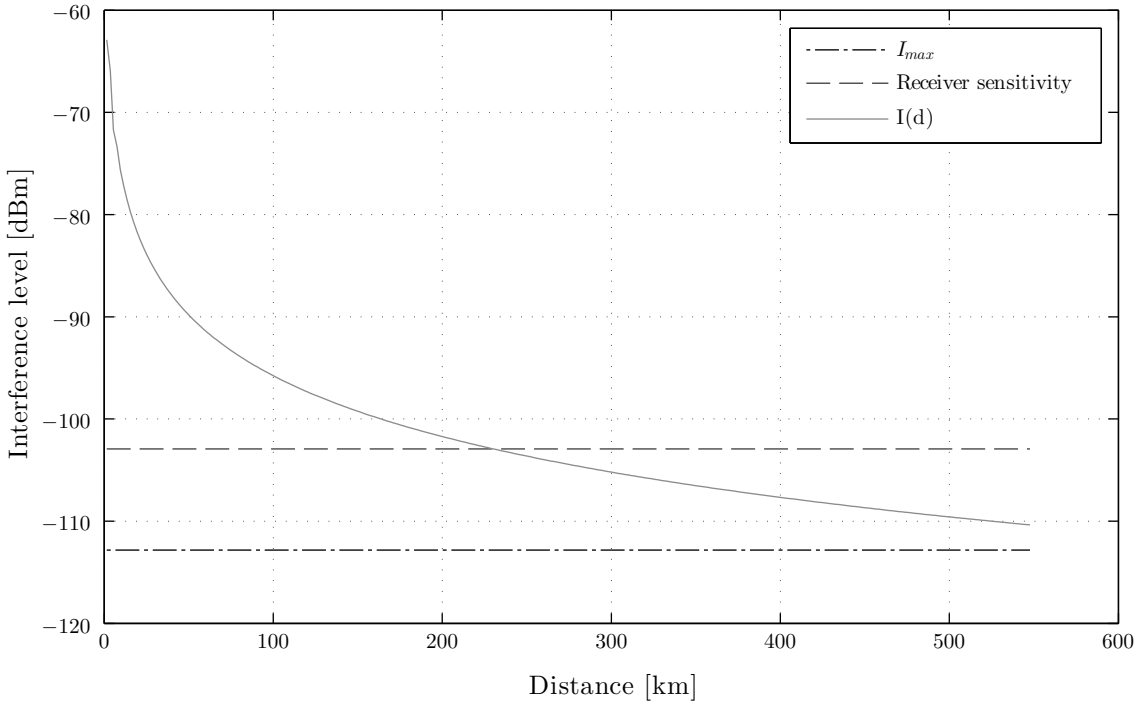

Figure 1-2: JTIDS Interference on L-DACS1 FL (Aircraft on the Ground on Airborne Aircraft).

retical analysis and considers the worst case, it shows that the JTIDS/LDACS-1 spectrum compatibility needs of further investigations and the adoption of countermeasures.

1.2.2 Interference sensing and mitigation

This section describes the proposed sensing and mitigation method. In particular two, different alternatives are presented. In the first one (named *full combining*) we suppose that all the symbols are transmitted twice and the interference sensing is performed on the signal resulting from combination of the two replicas. It was previously proposed in [45]. The second option (named *partial combining*), originally proposed here, considers a scheme where only the OFDM symbols corrupted by the interference are retransmitted and, hence, the sensing is performed on the signal replicas before combining. In the first case it is possible to obtain a more reliable interference detection at the expense of a reduction of the transmission capacity. In the second case, interference detection is more affected by the useful signal fluctuations but it permits to save transmission capacity. Furthermore, when JTIDS interference is present, the probability that even the successive retransmissions of the OFDM symbols can be affected by interference is very high. In a system with a HARQ mechanism, this should lead to a high number of retransmission and delays. The joint use of blanking and retransmission can overcome this problem.

The first operation common to both the proposed schemes is the interference detection,

Table 1.3: Compatibility Results.

Scenario	Distance
Ground Station on Airborne Aircraft	$d > 370$ km
Airborne Aircraft on Airborne Aircraft	$d > 370$ km
Airborne Aircraft on Ground Station	$d > 370$ km
Ground Station on Ground Station	$d > 370$ km
Ground Aircraft on Ground Aircraft	$d > 26.6$ km
Ground Station on Ground Aircraft	$d > 370$ km
Ground Aircraft on Ground Station	$d > 46.5$ km

that is used to determine which samples are corrupted. This is performed by adapting a well known spectrum sensing scheme: the energy detector (ED). This detector is well-known in the Cognitive Radio networks where a secondary user (SU) looks for spectrum holes that are not used by the primary licensed user (PU). Free spectrum portion can be used by the SU for transmission. The ED scheme is blind and does not require the knowledge of the interfering system features[5], in addition it presents very low complexity. In general, the ED computes the energy of the samples received during a specified sensing period and compares it with a threshold, which depends on the power of the noise at the receiver. If the energy is over the threshold, it is assumed that another system is transmitting. The detector performance depends on the threshold choice and the accuracy is proportional to the duration of the sensing period, which can be performed only for a limited time: if the number of collected samples is sufficient, it is possible to reach any desired performance even under low Signal to Noise Ratio (SNR) conditions. Usually, during the sensing period the receiver exclusively listens the spectrum and does not receive any communication.

We propose a modified energy detector. The spectrum sensing is not performed on a dedicated interval but together with communication. In addition, the goal is to know which samples are affected by the JTIDS interference instead of detecting spectrum holes. By adapting the sensing concept, it is possible to exploit a sliding window to compute the mean energy of successive portions of the signal. If the value exceeds a certain threshold, we assume the interference affects that portion of the signal. A significant difference with the traditional spectrum sensing is represented by the impact of the sensing period on the performance: increasing the window length does not leads to an improvement, since the energy of the pulse is spread on a longer interval making more difficult to discriminate which samples are affected. The window length depends on the duration of the interfering signal that cannot be exactly known because the pulse is filtered at the receiving end, however a rough estimation of the JTIDS signal duration results in $L = T_p \cdot f_s = 4$ samples, where f_s is the sampling frequency. We adopt a windowing size, W, equal to $L + 1$ samples.

In order to get refined results, the sliding window analyses every sample of the received symbol: each value returning from the windowing operation is referred to a specific sample, since the windows are partially overlapped. The n-th sample of the i-th symbol in output

[5]JTIDS is a military system and many features of the system are not known.

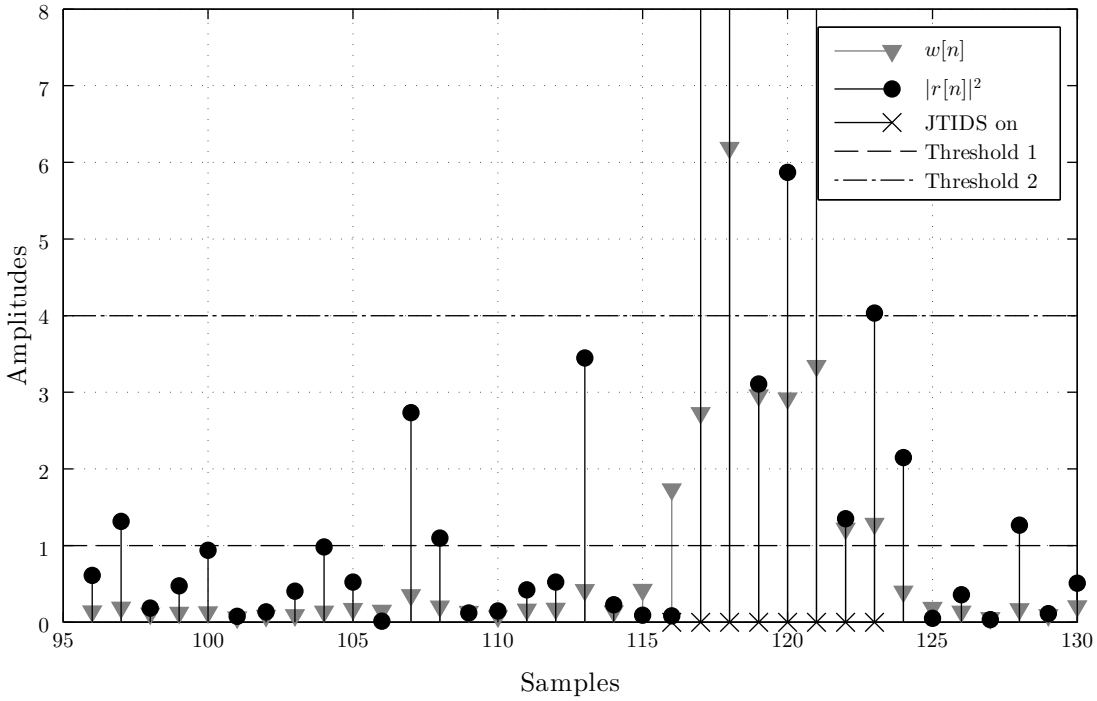

Figure 1-3: Windowing effects on spectrum sensing.

from the sliding window is

$$w(n) = \sum_{j=-\frac{W-1}{2}}^{+\frac{W-1}{2}} a_j \cdot \|r_i(n-j)\|^2 \tag{1.7}$$

where the a_j terms are the window weight and are selected in order to give more weight to the central sample.

Fig. 1-3 shows an example of the windowing effects. It is possible to note that windowing reduces significantly the fluctuations of the signal thus permits to better discriminate the interference selecting an optimal threshold value. In fact, by performing the windowing operation (i.e.,$w(n)$) and considering the $Threshold1$ value, it is possible to detect all the samples affected by interference. On the contrary, observing directly the received signal (i.e.,$||r(n)||^2$) an optimum threshold value is more difficult to be selected: with $Threshold1$ some missing detections and many false alarms occur. Increasing the threshold ($Threshold2$) permits to reduce the false alarms but increases the missing detections.

In is straightforward to note that the window output obviously depends also on LDACS-1 signal, which is based on an OFDM transmission and, hence, it is characterized by a high peak to average ratio. This can increase the probability of false alarm. To counteract this aspect, and taking into account the length of the JTIDS signal, this probability can be reduced by observing M consecutive window outputs: the outputs $w[n]$ are compared with a threshold, if at least $M = L - 1$ consecutive outputs are over the threshold we assume the interference is present on correspondent received samples.

After sensing operation the interference is removed by means of a blanking operation. Blanking simply puts to zero the received samples where the interference has been detected and leaves unchanged the other samples.

The difference among the two proposed alternatives is that:

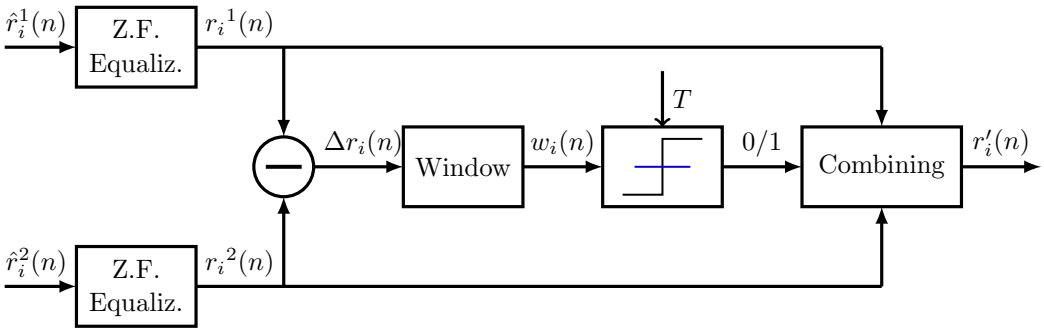

Figure 1-4: Full combining scheme.

- in *full combining* all the symbols are transmitted twice and hence the sensing is performed on the difference of the two signal replicas;
- in *partial combining* the sensing is performed on the received signal and the sensing decision is used to select which symbols must be retransmitted.

Full combining scheme

In *full combining* scheme two replicas of all the symbols are always available. This can be exploited in order to improve the interference detection performance [45]. *Full combining* scheme is pictured in Fig. 1-4

To detect exactly which samples are affected by interference the proposed method performs a sample by sample difference between the two copies of the symbol that has been previously equalized to remove the channel effect. In that way the dependence on the LDACS-1 signal fluctuation is removed. Assuming a perfect channel zero-forcing equalization, the difference on the n-th sample of the i-th symbol is

$$\Delta r_i(n) \doteq r_i^1(n) - r_i^2(n). \tag{1.8}$$

Since each signal r_i^l, with $l = 1, 2$, is

$$r_i^l(n) = s(n) + \frac{u_i^l(n)}{\alpha_i^l} + \frac{n_i^l(n)}{\alpha_i^l}. \tag{1.9}$$

The difference Δr_i can be expressed as

$$\Delta r_i(n) = \frac{u_i^1(n)}{\alpha_i^1} - \frac{u_i^2(n)}{\alpha_i^2} + \frac{n_i^1(n)}{\alpha_i^1} - \frac{n_i^2(n)}{\alpha_i^2} \tag{1.10}$$

where:

- $r_i^l(n)$ is the n-th received sample of the i-th symbol of the l-th transmission after equalization
- $u_i^l(n)$ is the JTIDS interference on n-th sample of the i-th symbol of the l-th transmission
- $n_i^l(n)$ is the AWG noise on n-th sample of the i-th symbol of the l-th transmission
- α_i^l is the Ricean fading term on the i-th symbol of the l-th transmission, assumed constant on an OFDM symbol.

Table 1.4: Analysed cases.

$CASE$	q	$TSDF$	N_p	P_p
$Standard$	1	50%	258	$4.2E-3$
$Worst$	2	100%	444	$2.3E-2$

In Eq.s (1.9) and (1.10) the fading coefficients appears in the denominators because the signal is equalized. The difference $\Delta r_i(n)$ depends on the JTIDS interference and the noise power: the LDACS-1 signal fluctuation does not affect the detection procedure.

The windowing operation is performed along the difference signal samples $\Delta r_i(n)$ and the result is compared with a threshold, T. The threshold comparison output is 1 if the sample is above the threshold or 0 otherwise. Finally the combining block checks if windowed signal keeps above the threshold for at least $M = L - 1$ consecutive samples (i.e., it receives at least M consecutive ones). In that case it is assumed that the interference is present in those samples. At this step, it is possible to know which samples are affected by the interference but it is needed to determine if the interference is introduced by the first, $r_i^1(n)$, or the second $r_i^2(n)$ copy of the received signal. Hence, the combining block performs a comparison of the two signals before combining. Indicating as $\overline{n}_q$, with $q = 0, 1, ..., Q-1$ the samples affected by the interference, for each $\overline{n}_q$ the values of $r_i^1(\overline{n}_q)$ and $r_i^2(\overline{n}_q)$ are compared: the maximum is blanked while the minimum is doubled. The resulting signals are summed together, and the final i-th symbol can be expressed as

$$r_i'(n) = \begin{cases} r_i^1(n) + r_i^2(n) & \text{if } n \neq \overline{n}_q, \quad \forall \overline{n}_q \\ 2 \cdot r_i^1(n) & \text{if } n = \overline{n}_q, r_i^1(\overline{n}_q) < r_i^2(\overline{n}_q) \\ 2 \cdot r_i^2(n) & \text{if } n = \overline{n}_q, r_i^1(\overline{n}_q) > r_i^2(\overline{n}_q). \end{cases} \tag{1.11}$$

Demodulation and decision are performed on r_i' signal.

Partial combining scheme

In the *partial combining* scheme interference detection is applied on the received signal in order to detect which symbols are affected by interference and thus requiring a new transmission of these symbols. *Partial combining* is pictured in Fig. 1-5.

In this case the windowing operation is performed along the symbol $r_i^1(n)$ and the result is compared with a suitable threshold. When the windowed signal keeps above the threshold for at least $M = L - 1$ samples, the interference is assumed to be present in those samples and in the relative symbols. Following an HARQ mechanism the receiver requires a new transmission of the corrupted symbols that are not discarded but stored after removing the interference by the means of a blanking operation. Indicating as $\overline{n}_q$, with $q = 0, 1, ..., Q-1$ the samples affected by the interference, the resulting i-th symbol becomes

$$\overline{r}_i^1(n) = \begin{cases} r_i^1(n) & \text{if } n \neq \overline{n}_q \\ 0 & \text{if } n = \overline{n}_q \end{cases} . \tag{1.12}$$

In presence of JTIDS interference, the probability that even the second transmission is affected by the interference is very high, for this reason sensing is performed also on the second received signal, $r_i^2(n)$ and the eventual interference is removed by the means of a blanking operation like in (1.12), obtaining $\overline{r}_i^2(n)$. Finally, the two copies of the i-th symbol

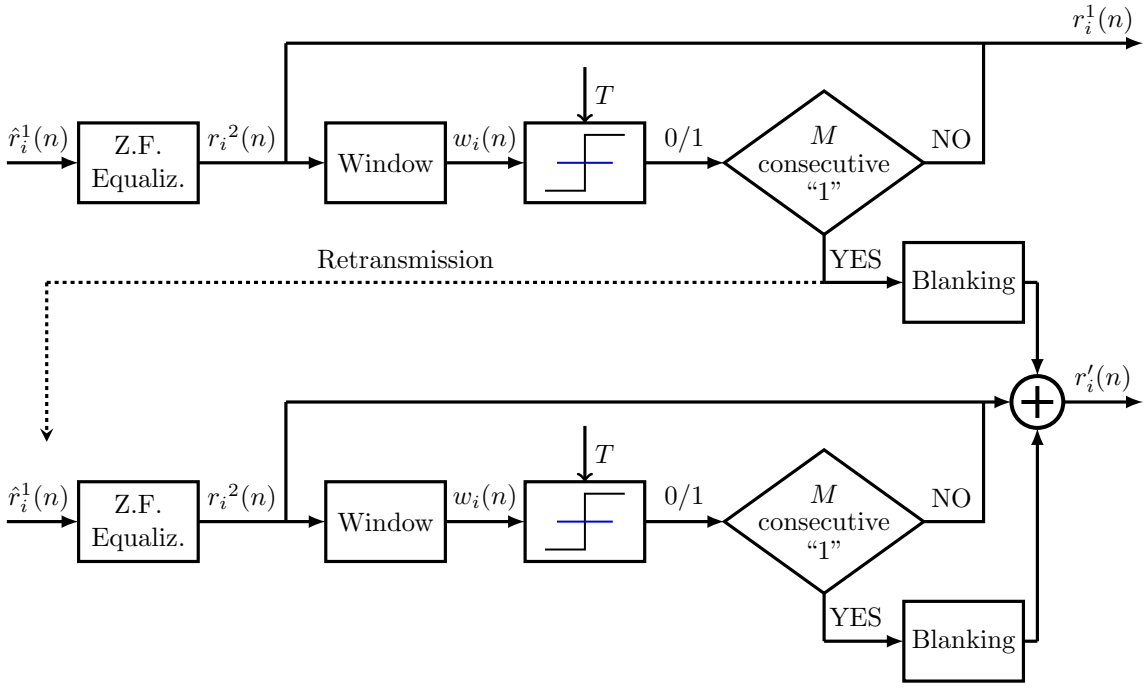

Figure 1-5: Partial combining scheme.

are softly combined

$$r'_i(n) = \overline{r}_i^1(n) + \overline{r}_i^2(n). \tag{1.13}$$

Demodulation and decision on corrupted symbols are taken on r'_i rather then r_i^1.

1.2.3 Numerical results

In order to study the effectiveness of the proposed mitigation method, the performance of our system has been simulated and compared with that of a classical blanking method and with the system that does not adopt any interference mitigation technique. For the blanking scheme case, the same windowing interference detection method presented in Sec. 1.2.2 has been considered. The JTIDS interference has been characterized by considering two profiles, named *standard* (STD) and *worst* (WORST), reported in Tab. 1.4. From this table we can see that the probability of interference between the two systems is quite high, especially for the WORST case.

Since the performance of the proposed method depends on the threshold value, T, an optimization process has been carried out. Fig.s 1-6 and 1-7 show the Bit Error Rate (BER) as a function of the threshold value for different system configuration. In particular the optimum threshold behaviour has been evaluated through computer simulations, either for the proposed and the blanking methods for different Signal to Noise Ratio (SNR) (Fig. 1-6) and for different interference parameters (Fig. 1-7).

These figures highlight the existence, for each method, of an optimum value of T for which we have the lowest BER. We can note that the optimum threshold value does not change significantly when the SNR or the interference configuration change even if cancellation benefits are more evident for higher SNR values and when the interference is more frequent (in Fig. 1-7 only the curves of the proposed methods are reported for a better readability, but the same simulations have been carried out also for the blanking method, leading to similar results). In addition Fig. 1-7 shows that the performance of the proposed methods

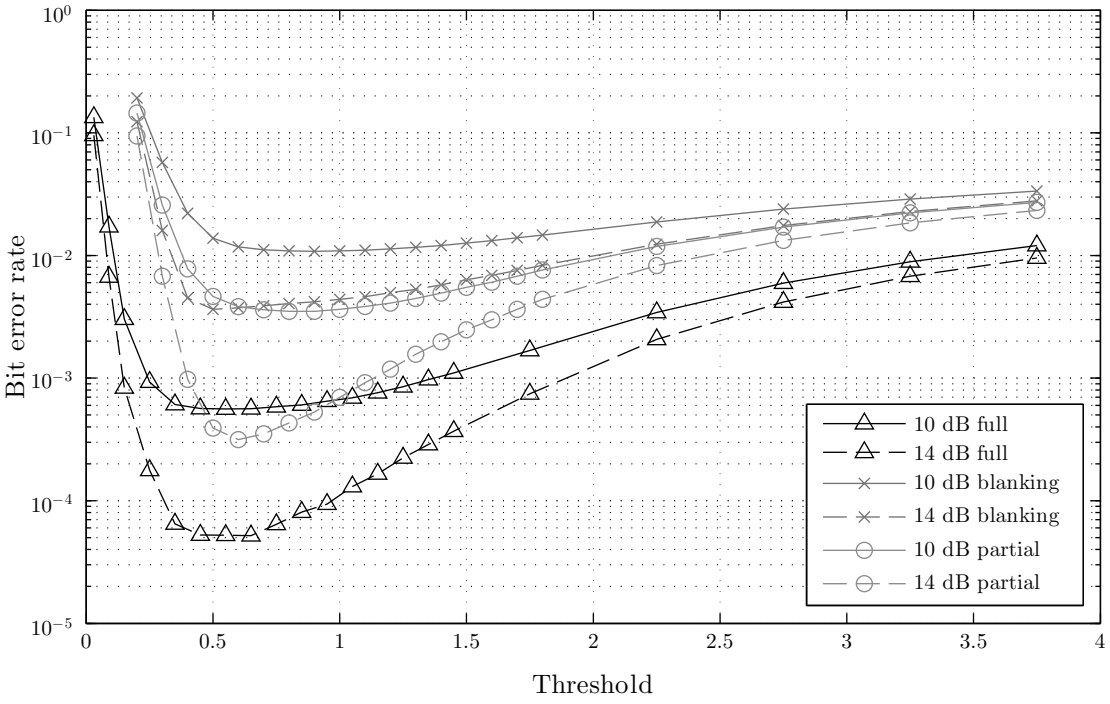

Figure 1-6: BER as a function of the threshold for different SNR (SIR=0 dBin the Worst Case).

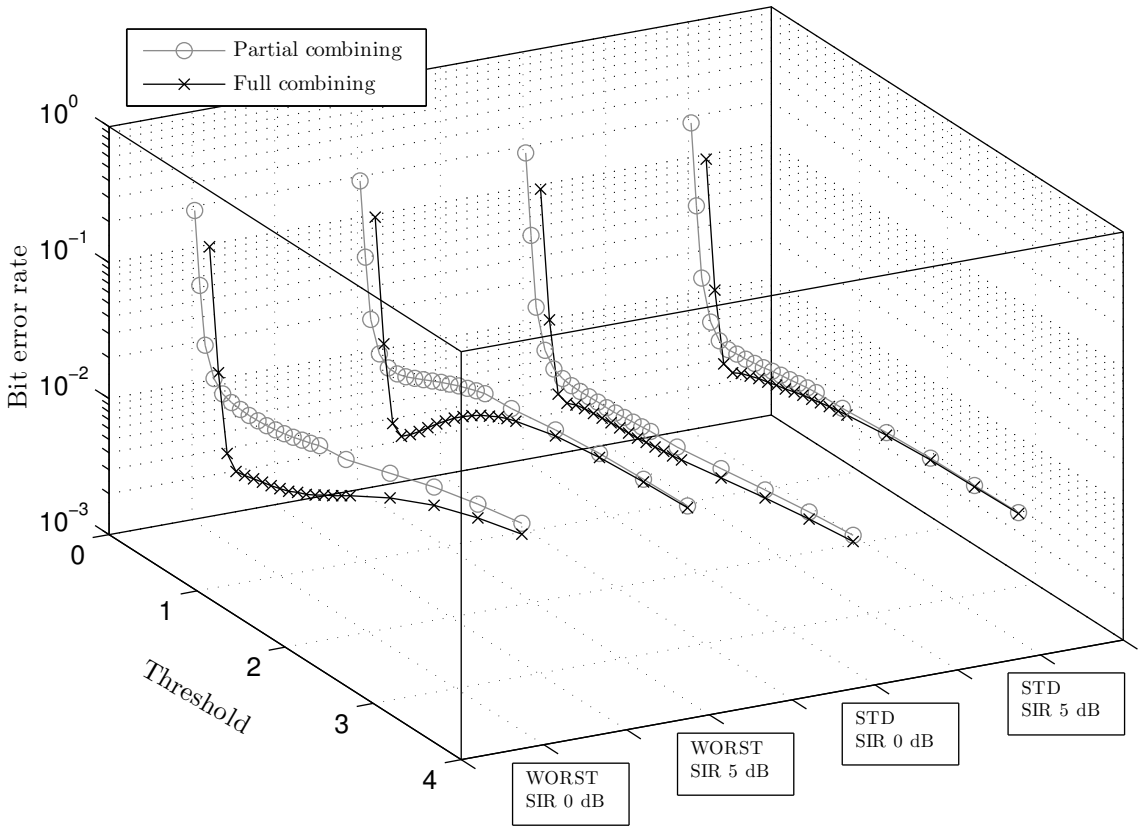

Figure 1-7: BER as a function of the threshold for different SIR and interference profiles (SNR=10 dB).

does not change significantly when the SIR changes. This is because when the SIR is high the interference is harder to be detected but it has a minor impact (at least, on a BER basis). On the other hand, when the SIR is low, the detection and the recombination become more reliable. It is important to underline that JTIDS power is very high if compared with LDACS-1 transmission power and low SIR values can often occur. Simulations with SIR values lower of 0 dBhave been carried out, showing performance very close to the case of SIR equal to 0 dB, for this reason the results are not reported here. In general, observing the threshold optimization figures we can observe that a slope close to zero is visible around the optimum T value and we can deduce that a value of T close to the optimum does not affect notably the receiver performance. The optimum T determination has to be performed only for specific target applications and service scenarios. The following results were obtained for an optimum threshold value, different for each method, which was determined by computer simulation, as outlined above.

In *partial combining* scheme the threshold choice affects also the system throughput because it determines the number of retransmissions as shown in Fig. 1-8. From this figure it is possible to see that the maximum useful throughput (i.e., the amount of OFDM symbols correctly received on a given time period) is achieved for threshold values that are almost the same of those for which we have minimum BER. We can note that for low threshold values (up to the value for which the maximum throughput is reached) the results are independent of the SIR value. This is because all the interference is detected for both values of SIR. When the threshold increases, there is a range of values for which having lower SIR leads to a higher interference detection probability and, hence, a higher interference mitigation. Conversely there is a following range of values for which missing detection probability increases, thus having higher SIR leading to a residual interference that has less detrimental effects.

The interference detection and mitigation capabilities of the proposed methods are evident also by observing BER performance. Fig. 1-9 represents the BER as a function of SNR. The performance of the proposed methods is compared with that of the classical blanking method and the case without mitigation and without interference. Standard and Worst cases are considered. It is evident that for both the proposed methods the interference effects are almost completely removed, in fact the partial combining method permits to approach the performance of the case without interference, and the full combining scheme presents almost a 3 dBgain thanks to the diversity combining. Only for high SNR and high interference (worst case) the BER results to be slightly affected by the residual interference. The proposed methods present in all the cases a significant gain if compared with the case without mitigation, that is heavily deteriorated, and the blanking method. In particular, for high SNR values blanking operation reaches more rapidly a performance floor due to the fact that the signal is removed together with the interference and ICI is introduced by the nonlinearities. This is more evident in the worst case.

In order to evaluate the effect of retransmission on throughput we have to take into account that symbol retransmission leads to a reduction of the transmission capacity, on the other end, useful received throughput increases thanks to the reduced error rate. Fig. 1-10 presents final useful received throughput in terms of number of correct OFDM symbols received, evaluated taking into account transmission capacity loss due to retransmission. It is evident that despite the retransmissions, *full combining* scheme presents an advantage also in terms of throughput for low SNR values, while *partial combining* scheme results to be always the best choice for high SNR values, especially when the interference is high (worst case).

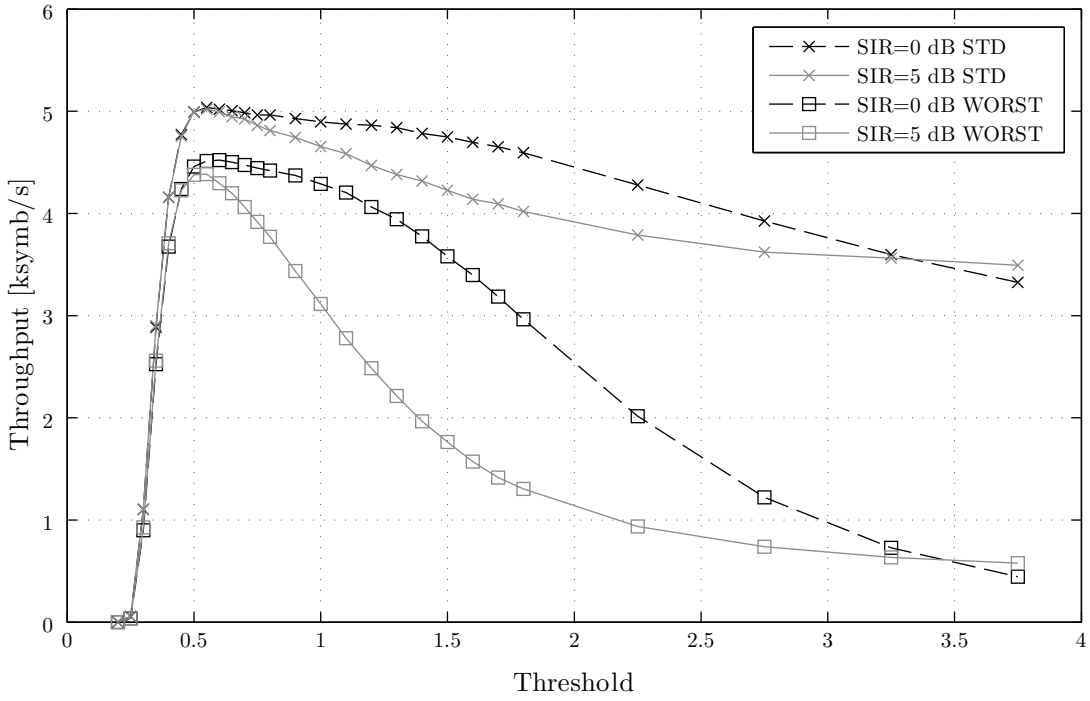

Figure 1-8: Throughput as a function of the threshold for different SIR and interference profiles (SNR=10 dB).

1.2.4 Summarising

This section proposes a new method to detect and mitigate impulsive interference that a JTIDS system operating in a frequency hopping regime generates on a LDACS system. The proposed method is based on symbol retransmission. In particular two different alternatives are presented: in the first considered, namely *full combining* scheme, two copies of the symbols are always transmitted in order to improve both interference detection and mitigation. Conversely, in the second considered alternative, named *partial combining* scheme, only the symbols affected by the interference are transmitted twice thus increasing system throughput. In both cases, before symbol combining, detected interference is blanked. The results show that both alternatives permit to efficiently mitigate the effects of interference, thus approaching BER performance of the case without interference and with additional gain of diversity combining. Performance has been compared also with that of a classical blanking method showing a better behaviour of the proposed methods. Finally, having more reliable data permits to compensate the reduction of transmission capacity due to retransmissions: throughput performance shown that *full combining* scheme presents the highest throughput in low SNR regime and *partial scheme* in high SNR regime.

1.3 Generalized Analysis

This section aims to analyse the use of *partial combining* method in any OFDM system affected by impulsive interference. We use here a different notation, to underline the difference from the previous section.

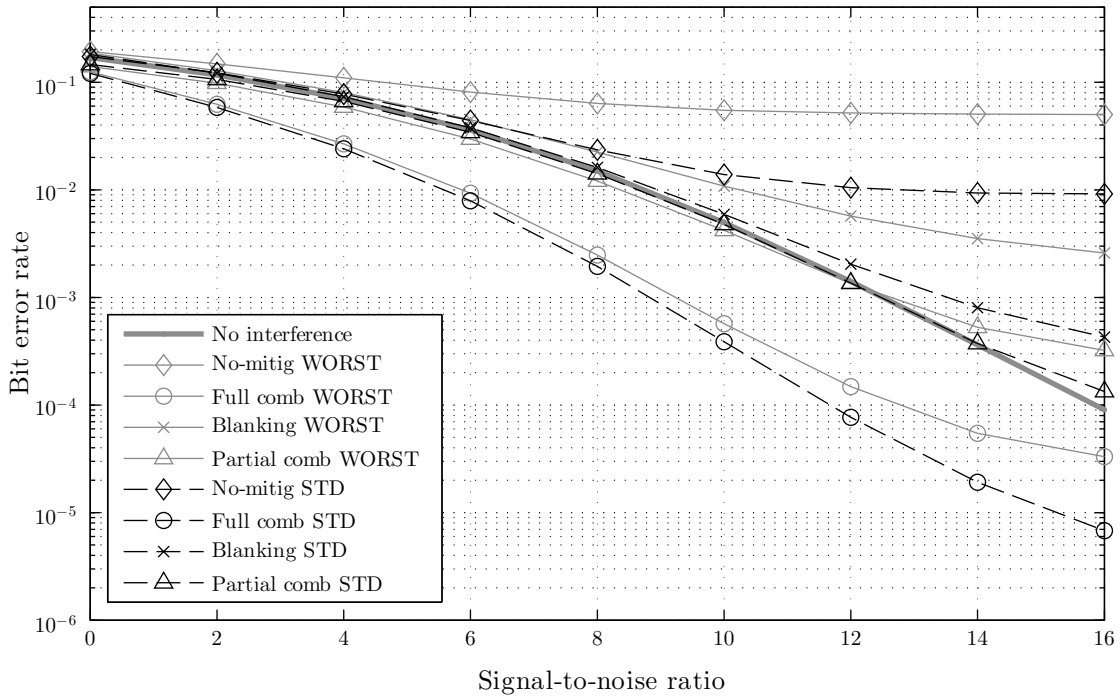

Figure 1-9: BER comparison as a function of SNR when SIR=0 dB, worst and standard cases

1.3.1 System model

In OFDM communication systems the available spectrum is divided in several subcarriers. Data symbols are efficiently modulated on the subcarriers by resorting to the use of the inverse DFT (IDFT) in transmission and the DFT at the receiving end. We focus here on an OFDM-based communication system with K subcarriers. The information bit streams are coded with the concatenation of an outer Reed-Solomon (RS) code and an inner variable-rate convolutional code in packets of 2500 bits, and then mapped into a base-band symbol c_k with $k = 0, \cdots, N_{\text{FFT}} - 1$ using QPSK modulation scheme, where $K = N_{\text{FFT}}$. The information sequence results to be

$$s(n) = \sum_{k=0}^{K-1} c_k \cdot e^{j\frac{2\pi}{K}nk} \quad n = 0, \cdots, K-1. \tag{1.14}$$

A cyclic prefix with length N_g symbols is considered by repeating the final part of the OFDM symbol, $s(n)$, resulting in the transmitted signal $\hat{s}(n)$. The base-band signal is up-converted to the radio frequency and transmitted through the channel. The channel is modelled here as a frequency selective multipath fading channel following a Rayleigh distribution, with a discrete impulse response $h(n)$ shorter than the cyclic prefix, which allows the cancellation of ISI effect at the receiver side. Hence, the received signal can be defined as

$$\hat{r}(n) = \hat{s}(n) \otimes h(n) + v(n) + u(n) \tag{1.15}$$

where $v(n)$ $\mathcal{N}(0, \sigma_v^2)$ represents the Additive White Gaussian Noise (AWGN), while $u(n)$ denotes the IN. The useful received signal $r(n)$ is obtained by removing the cyclic prefix.

Some statistical or empirical models have been proposed in the literature to model the IN, but they refer to specific environments and interference sources [26, 46, 47]. Even if the

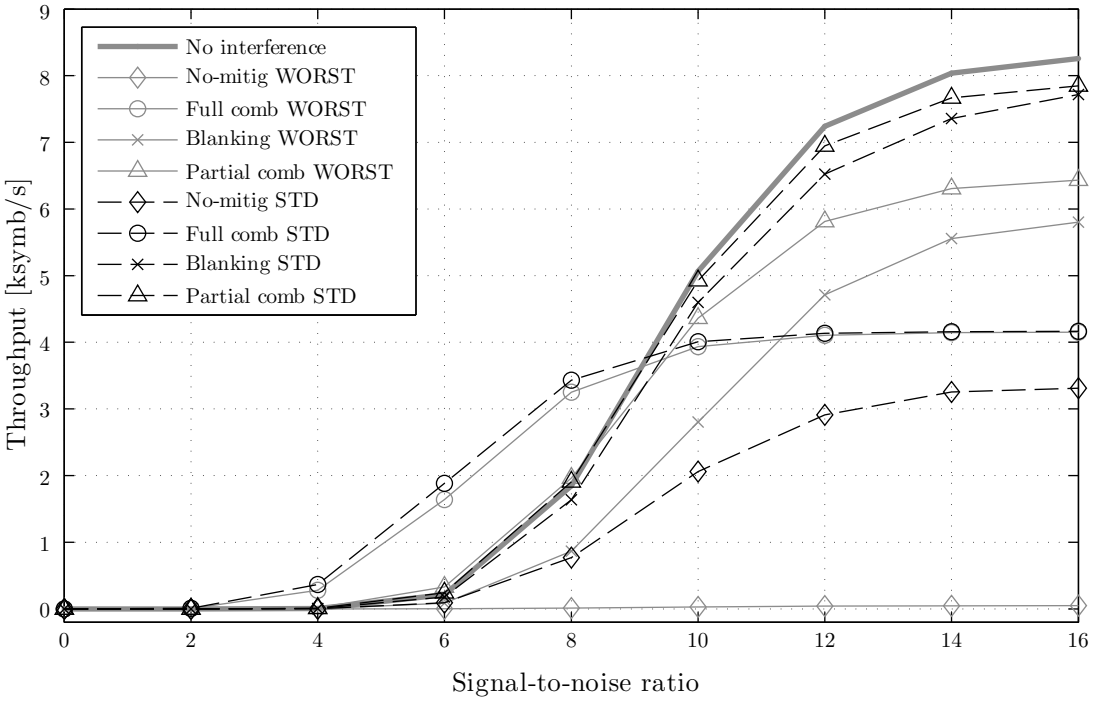

Figure 1-10: Throughput of the proposed and blanking methods as a function of SNR when $SIR = 0$ dB.

characterization of impulsive noise is quite difficult, two features are in common among all the impulsive interference sources: the energy is concentrated in short time periods and its power is much higher than the background noise. For this reason we model the IN as a Gaussian pulse with duration D, such that

$$D \ll T_s \tag{1.16}$$

where T_s is the OFDM symbol duration. In addition, the probability that the IN affects a certain OFDM symbol is P_i (i.e., in average one symbol every $\frac{1}{P_i}$ is affected by the interference). The position of the interference within the OFDM symbol is considered random with uniform distribution. The signal $r(n)$ is processed by the DFT block at the receiver side. The DFT output for the k-th subcarrier, before equalization, is

$$\begin{aligned} Z(k) &= \frac{1}{K}\sum_{n=0}^{K-1} r(n)\cdot e^{-j\frac{2\pi}{K}nk} \\ &= S(k)\cdot H(k) + V(k) + U(k) \end{aligned} \tag{1.17}$$

where $S(k)$, $H(k)$, $N(k)$ and $U(k)$ are the samples in the frequency domain of the transmitted signal, channel impulse response, AWGN and IN contribution on the k-th subcarrier, respectively. The signal is equalized by exploiting a Zero Forcing equalization algorithm by dividing each subcarrier signal $Z(k)$ by the channel response $H(k)$[6].

[6]We assume to have a perfect knowledge of the channel response for equalization purposes.

1.3.2 Proposed interference mitigation method

This section presents the proposed method to counteract the effects of an impulsive interference on an OFDM signal. In particular, it is composed of a first stage of IN detection, and then a new mitigation strategy based on symbols retransmission.

Interference detection

Interference detection is needed to determine which samples and, hence, which symbols, are corrupted by interference in order to put in act suitable countermeasures. In particular, we consider here a spectrum sensing approach based on the energy detector. This method is blind, hence it does not require any knowledge of the interfering system features, and can be implemented by resorting to a low complexity algorithm.

In general, spectrum sensing is used to determine if a signal is present or not on a given area. To this aim, the energy detector estimates the energy of the samples received during a dedicated period (i.e., the communication is avoided in this interval) and compares it with a certain threshold, whose value is set depending on the background noise power at the receiver. If the energy is over the threshold, another system is assumed to be present and transmitting, i.e., the interference is present.

The detection accuracy is proportional to the duration of the sensing period: if the number of collected samples is sufficient, it is possible to reach any desired performance even in low Signal to Noise Ratio (SNR) regime. A modified energy detector is proposed in order to know which samples of the received signal are affected by the interference. Hence, the sensing is not performed on a clear interval but on the whole received signal.

By adapting the sensing concept, we exploit a sliding window for estimating the average energy of a portion of the signal. If the value exceeds a certain threshold, we assume that interference affects that portion of the signal.

A significant difference with the traditional spectrum sensing is represented by the impact on the performance of the sensing period: an increasing in the window length does not necessarily lead to an improvement, because the energy of the pulse is spread on a longer interval making more difficult to discriminate which samples are affected. The choice of the window length, W, is shown in Sec. 1.3.4.

In order to get refined results, the sliding window is partially overlapped, each value returning from the windowing operation is referred to a specific sample. The n-th sample of the signal in output from the sliding window is computed as

$$w(n) = \sum_{i=-\frac{W-1}{2}}^{+\frac{W-1}{2}} a_i \cdot \|r(n-i)\|^2. \tag{1.18}$$

where the a_i terms are the window weights.

The interference detection phase produces as output the value “1” if the interference is present on a given sample, “0” otherwise.

Interference mitigation

The sensing decision is used to request a new transmission of the symbols where the interference has been detected during the previous sensing phase. The receiver does not discard the corrupted symbols, which are stored after removing the interference by means of a blanking operation. Then, they are softly combined with the new transmitted replica. Blanking puts

to zero the received samples where the interference has been detected, while leaves unchanged the other samples. Indicating with n_i, where $i = 0, 1, ..., I-1$, the samples affected by the interference on the first received signal $r_1(n)$, the resulting signal after blanking operation becomes:

$$\bar{r}_1(n) = \begin{cases} r_1(n) & \text{if} \quad n \neq n_i \\ 0 & \text{if} \quad n = n_i \end{cases}, \quad \forall n_i. \tag{1.19}$$

Even the second transmission of the symbol, $r_2(n)$, may be affected by interference; for this reason, the sensing procedure and the blanking operation as in (1.19) are repeated also for the second replica of the symbol, obtaining the signal $\bar{r}_2(n)$. Finally the two copies of the symbols are softly combined, giving

$$r'(n) = \bar{r}_1(n) + \bar{r}_2(n). \tag{1.20}$$

Demodulation and decision on corrupted symbols are performed on $r'(n)$. A block diagram of the proposed method is presented in Fig.1-11.

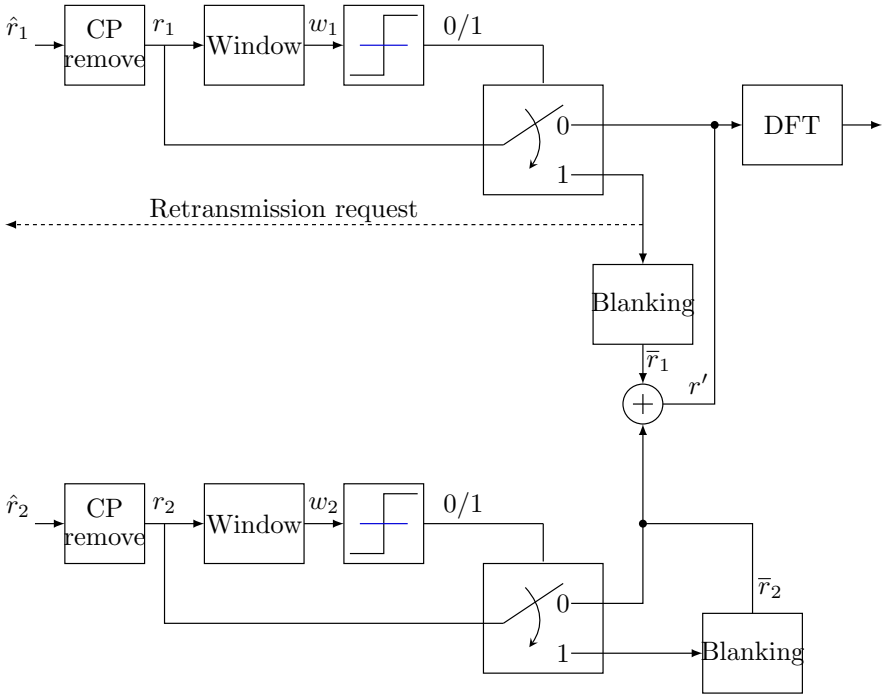

Figure 1-11: Block diagram of the proposed method in the OFDM receiver.

1.3.3 Theoretical analysis

In this section a theoretical analysis of the proposed method is presented. We focus here on an AWGN channel[7] and on an impulsive noise that has a Gaussian distribution. Thus, the total noise $v'(n) = v(n) + u(n)$ affecting the signal has a Gaussian distribution when interference is present. The impulsive noise is spread on the whole OFDM symbol by means of the DFT operation, hence, denoting with d the number of samples affected by the interference the bit

[7]The results can be easily extended to a Rayleigh fading channel by averaging the performance with the Rayleigh distribution.

error probability can be expressed as

$$P_e(d) = Q\left(\sqrt{\frac{S}{\sigma_v^2 + \frac{d}{K}\sigma_i^2}}\right) \tag{1.21}$$

where $Q(\cdot)$ is the Q-function, S is the useful signal power and σ_i represents the power of each interference sample.

To remove the dependence on d, it is necessary to find its probability density function (pdf), $f_d(x)$. This can be calculated by averaging all the possible interference configurations within a generic OFDM symbol with the related probability of occurrence. To this aim, the characteristics of the impulsive interference must be taken into account. As stated before, interference has fixed time duration equal to D, and P_i is the probability that an OFDM symbol is affected by the interference. Hence, to derive $f_d(x)$ we consider a time axis divided in slots of duration D, and the probability that a slot is affected by the interference is defined by p, that can be derived by P_i (i.e., $P_i = 1 - (1-p)^N$ where N is the number of slots in the OFDM symbol defined in what follows).

In the most general case, the interference timing is different from the timing of the OFDM signal and the symbol length K (i.e., the number of samples of an OFDM symbol in the time domain after the CP removal) is not a multiple of D. Hence, at the beginning and at the end of the OFDM symbol the interference can affect less than D samples (i.e., part of the interference is on the next symbol or on the CP that has been removed). To take into account this aspect we denote with t the time offset between the OFDM symbol and the slots timing. It is straightforward to note that t may assume values in the interval $[0; D-1]$; when $t = 0$ the interference and signal timings are aligned[8].

Hence, the impulsive interference can affects an initial portion of signal of duration t, a certain number of central slots of duration D, and/or a final portion of signal with duration R, as depicted in Fig. 1-12.

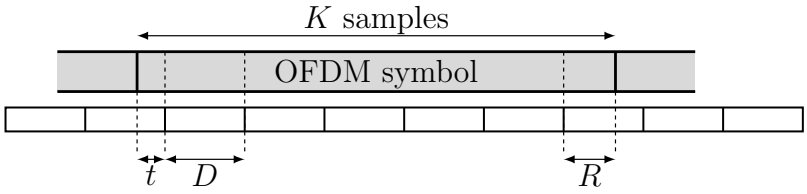

Figure 1-12: Interference and symbol timing comparison.

For any given value of K, t and D, the duration of the final slot is

$$R = K - t - \lfloor (K-t)/D \rfloor D \tag{1.22}$$

where $\lfloor s \rfloor$ denotes the greatest integer minor than s, and the total number of slots in an OFDM symbol is

$$N = \lfloor (K-t)/D \rfloor + 2. \tag{1.23}$$

The interference can affect m slots in the OFDM symbol, with $m = 1, \cdots, N$. In addition, it produces a less detrimental effect on the performance if it is on the first or the last slot because in this cases the duration is shorter than D. For this reason, we have to distinguish among four main cases:

[8]In general, even if the interference and signal timings are aligned at the beginning of an OFDM symbol, in the next one they will not be synchronized unless K and CP are multiples of D.

- l=1, the interference is on the first t samples but not on the last R;
- l=2, the interference is on the last R samples but not on the first t;
- l=3, the interference is neither on the first t samples nor on the last R;
- l=4, the interference is both on the first t samples or on the last R.

The probability density function of d, $f_d(x)$, can be derived as the sum of the probabilities, $P_{m,t,l}$, to have $d = x$ for all the values of m, t, and l, that is

$$f_d(x) = Pr(d = x) = \sum_{m,t,l\,:\,d_{m,t,l}=x} P_{m,t,l} \quad , \quad \text{for } x = 0, 1, \cdots, K. \tag{1.24}$$

The probabilities $P_{m,t,l}$ are derived in the Appendix A. Following (1.21) and (1.24), the mean bit error probability of the system without any interference mitigation, P_e^I, can be expressed as

$$P_e^I = E_x\left[Q\left(\sqrt{\frac{S}{\sigma_v^2 + \frac{x}{K}\sigma_i^2}}\right)\right] \tag{1.25}$$

$$= \sum_{x=0}^{K} Q\left(\sqrt{\frac{S}{\sigma_v^2 + \frac{x}{K}\sigma_i^2}}\right) f_d(x) \tag{1.26}$$

Let us consider now the proposed retransmission and combining technique. To derive a closed form expression of the error probability we consider an ideal sensing phase. We are interested in validating the main element of the proposed method that is the joint use of blanking and retransmission. Each sample corrupted by the interference is blanked, and combined with the corresponding sample of an OFDM symbol replica. Sensing and blanking are applied on the second replica too, and retransmission occurs only if at least one sample of the OFDM symbol is corrupted by interference. It is straightforward to note that with ideal sensing the performance does not depend on the SIR. The retransmitted OFDM symbols have twice the SNR of the others, but each sample affected by interference in any replica leads to an increase of the power of the noise equal to $\frac{\sigma_v^2}{K}$.

However, this is true only if the same sample is not interfered in both the symbol replicas. In this case, the signal is just blanked and the effect on the performance is more detrimental and complex. On the other hand, the probability that a sample is affected by interference in both replicas is equal to p^2, which means that for small values of p can be considered negligible. Hence, we give here only a lower bound of the mean bit error probability, assuming the absence of the aforementioned condition. In this case, the mean bit error probability of the mitigated system, P_e^M, can be expressed as:

$$P_e^M = Q\left(\sqrt{2\frac{S}{\sigma_v^2}}\right) f_d(0) + \sum_{x_1=1}^{K}\sum_{x_2=0}^{K} Q\left(\sqrt{\frac{S}{\sigma_v^2\left(1 + \frac{x_1+x_2}{K}\right)}}\right) f_d(x_1) f_d(x_2) \tag{1.27}$$

that is the sum of the error probability when interference is not present in the first replica and the re-transmission does not occur, and of the error probability of all the possible combinations of interference on the first and/or on the second replica. In the next section, the theoretical results will be validated through simulations.

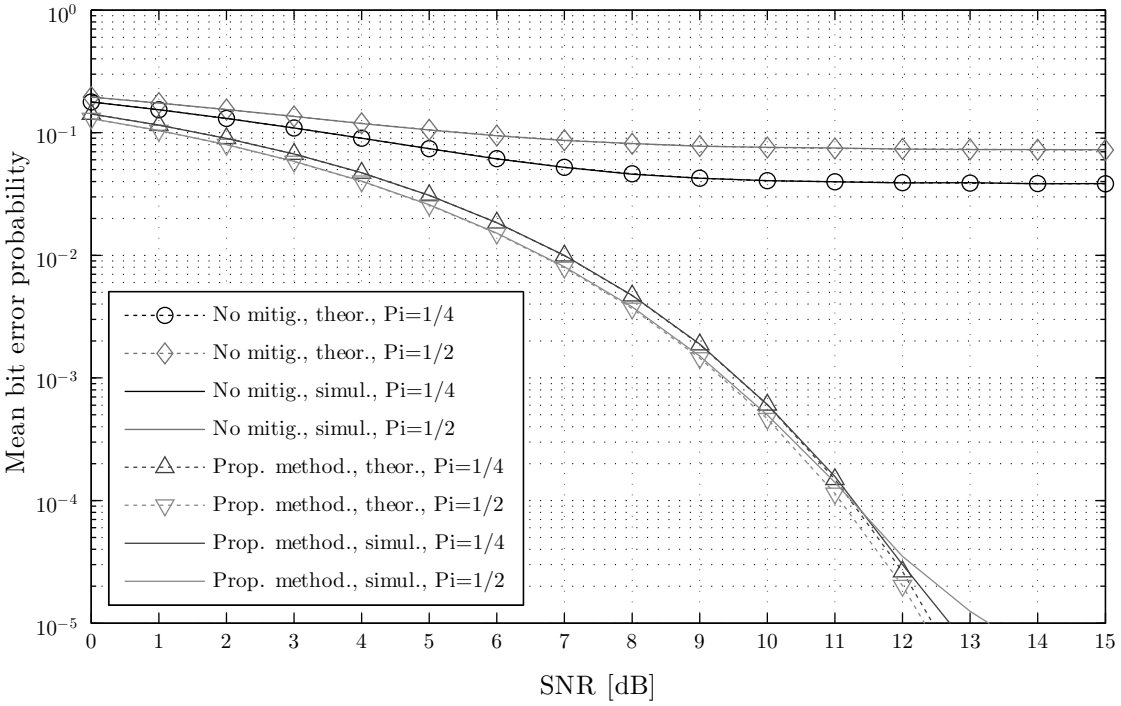

Figure 1-13: Bit Error Probability of the proposed method when $D = 4$. Theoretical analysis vs simulations.

1.3.4 Numerical results

In order to demonstrate the effectiveness of the proposed mitigation method, we provide here some numerical results.

First, we validate the theoretical analysis provided in Sec. 1.3.3. To this end, Fig. 1-13 presents the bit error probability of the proposed system obtained by means of theoretical analysis and computer simulations. The curves are compared with those of a system without interference mitigation for different interference probabilities P_i, when $D = 4$. It is possible to see that there is a good match between the two curves that slightly diverge at high Signal to Noise Ratio (SNR). In facts, as explained before, the theoretical analysis does not consider the case in which the same samples of both the replicas are affected by the interference, hence, is a lower bound of the performance. To derive these results we assumed an AWGN channel and omitted the channel coding gain.

The following system performance has been derived by means of computer simulations, taking into account also the multipath Rayleigh channel, the coding gain and the sensing phase. The obtained performance is compared with that of a classical blanking method and that of a system that does not adopt any interference mitigation technique. For what concerns the blanking technique, the same interference windowing detection method presented in Sec. 1.3.2 has been considered.

The parameters assumed in deriving our numerical results are:

- Number of subcarriers $K = 64$;
- Variable length of impulse noise, $D = 4, 8$ samples;
- Variable probability of interference P_i ;
- QPSK modulation scheme;

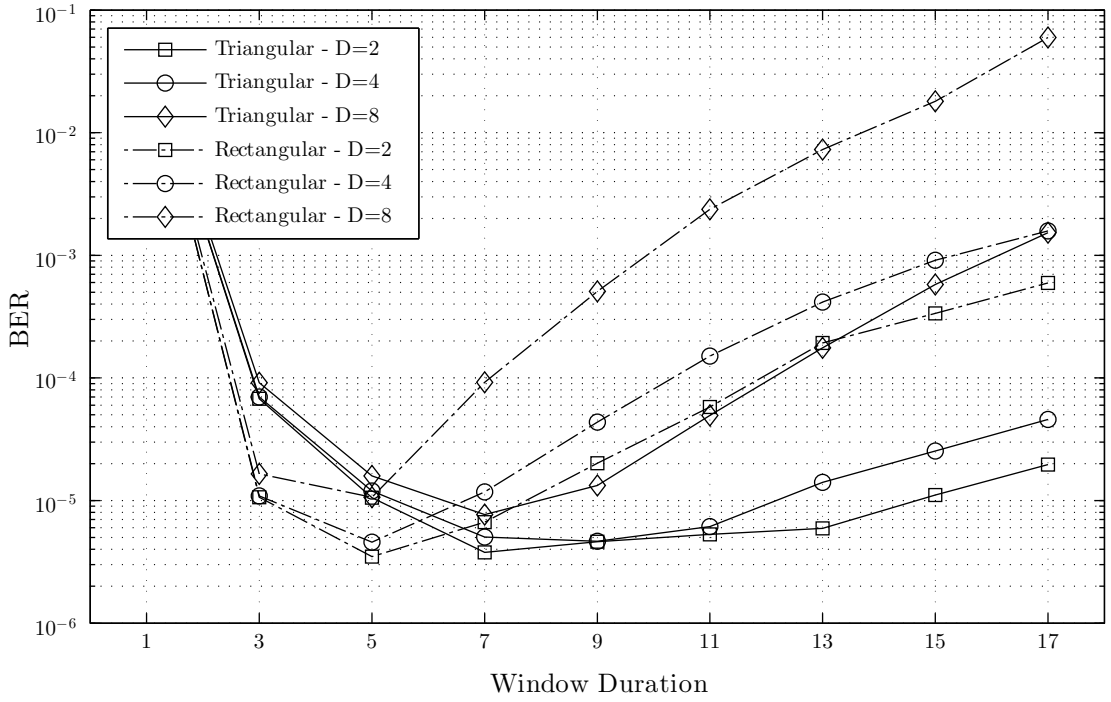

Figure 1-14: BER for different windows weights and lengths ($SIR = 0$ dB, $P_i = 1/4$, and $D = 2, 4, 8$).

- Variable Signal to Interference Ratio (SIR) ;
- The ITU-R pedestrian channel model [48], with 4 active paths and maximum delay spread equal to 410 ns.

A cyclic prefix consisting of $K/4$ samples has been assumed to counteract the multipath effects.

The sensing phase is based on a windowing operation, hence we have verified the dependence of the system performance on the window parameters (i.e, length and weights). The Fig. 1-14 presents the behaviour of the Bit Error Rate (BER) as a function of the window length, using different window weights (i.e., rectangular and triangular shapes with normalized coefficients) when the interference duration varies. From this figure we can see that the choice of the window weights has not a deep impact on the system performance if the right length of the window is chosen. We selected the triangular window with $W = 7$ to derive the following results because it presents a slope close to zero around the optimum value of W, which leads a value of the window length close to the optimum to not affect notably the performance.

Since the performance of the proposed method depends on the threshold value, T, an optimization process has been carried out: Figs. 1-15 and 1-16 show the BER as a function of the threshold value for different system configurations. In particular, the optimum threshold behaviour has been evaluated for the proposed method and the blanking alternative for different SNR values and for different interference parameters (P_i,D, SIR). These figures highlight the existence of an optimum value of T allowing the lowest BER. It is interesting to notice that such optimum value does not changes significantly with the SNR (Fig. 1-15) and interference parameters. Furthermore, from Fig. 1-15 it is evident that, in general, a slope close to zero is evident around the optimum T value. Hence, we can conclude that a value of T close to the optimum does not affect notably the receiver performance and, therefore,

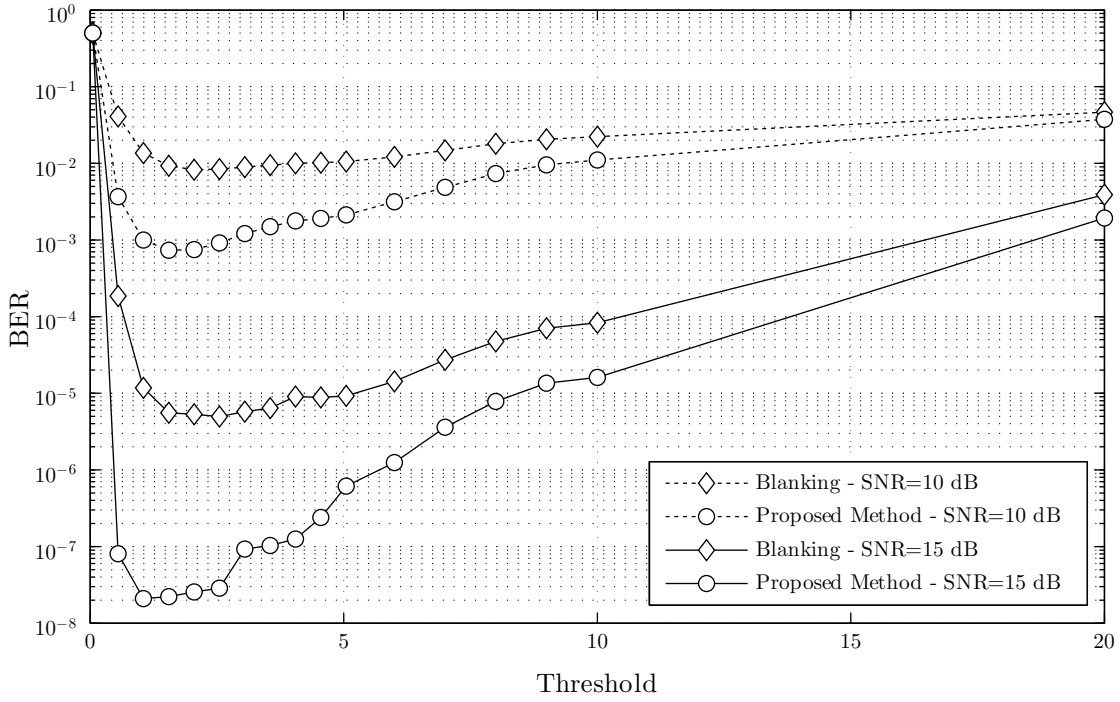

Figure 1-15: BER of the proposed method and blanking as a function of the threshold for different SNR values ($SIR = 0$ dB, $D = 4$ OFDM samples, $P_i = 1/4$

the optimization of T could be performed only for specific target applications and service scenarios.

The following results were obtained with the optimum threshold, as previously described. Fig. 1-16 shows that the performance of the proposed method does not change significantly when the SIR changes because the interference is correctly detected and removed when its power is sufficiently higher than the useful signal power.

The BER performance as a function of SNR is depicted in Figs. 1-17 and 1-18. In particular, in Fig. 1-17, the performance of the proposed method is compared with that of the classical blanking method and the cases without mitigation and without interference. It is possible to see that the proposed method allows to approach the performance of the case without interference. It presents a significant gain compared to the case without mitigation and the blanking method. In particular for high SNR values, blanking operation presents a degradation of the performance due to the fact that the signal is removed together with the IN, and ICI is introduced by the non-linearities, while the proposed method overcomes these problems. In addition, it presents a gain due to the symbol combining. Fig. 1-18 shows the BER when the interference parameters change. A good behaviour is evident in the figure under all the operational conditions.

In order to evaluate the effect of retransmission on the transmitting rate we can assume to have an ideal interference detection (i.e., the probability of false alarm and missing detection equal to 0). Consequently, the probability of having a retransmission is equal to the probability of having interference on a symbol, i.e., P_i. It means that the transmitted capacity is reduced of $100/(\frac{1}{P_i} + 1)\%$. However, the useful received throughput (i.e., the amount of packets correctly received on a given time period) increases thanks to the reduced error rate, as shown in Fig. 1-19.

In addition, the proposed method reduces the delay due to retransmission mechanism of classical ARQ schemes, which require a retransmission every time the symbol is incorrectly

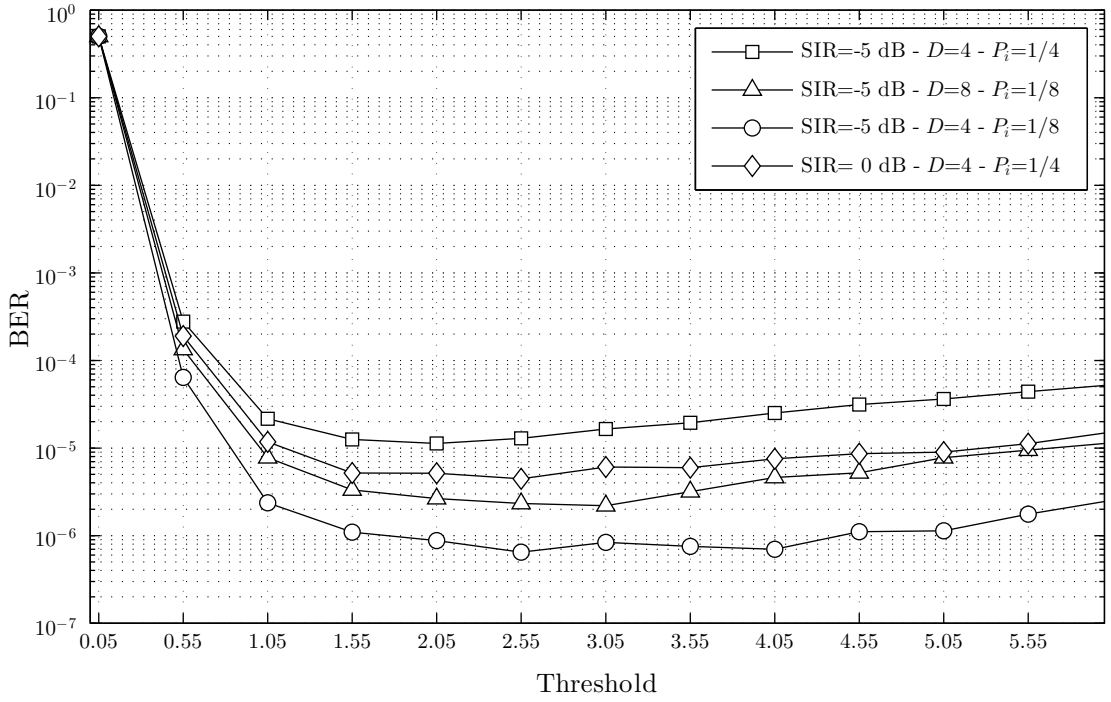

Figure 1-16: BER of the proposed method as a function of threshold for different interference configurations ($SNR = 10$ dB)

received due the presence of the interference. Indeed, even the successive retransmissions can be affected by interference, and hence, many attempts could be needed to correctly recover the information with a consequent long delay. This problem is overcome by the proposed method where the interference is removed by each copy sample by sample.

1.4 Conclusion

In this chapter a mitigation technique for the interference generated by an impulsive source affecting an OFDM signal has been proposed. After the interference detection phase, based on energy detection, the interference is removed by means of a blanking operation and then the retransmission of the corrupted symbols is requested. Finally, the two replicas of the symbol are soft combined. After a parameters analysis and optimization, the performance of the proposed method has been presented in comparison with the classical blanking method, showing a significant gain in terms of BER that leads to an increased number of corrected received bits, thus compensating the reduction of the transmission capacity introduced by the retransmissions.

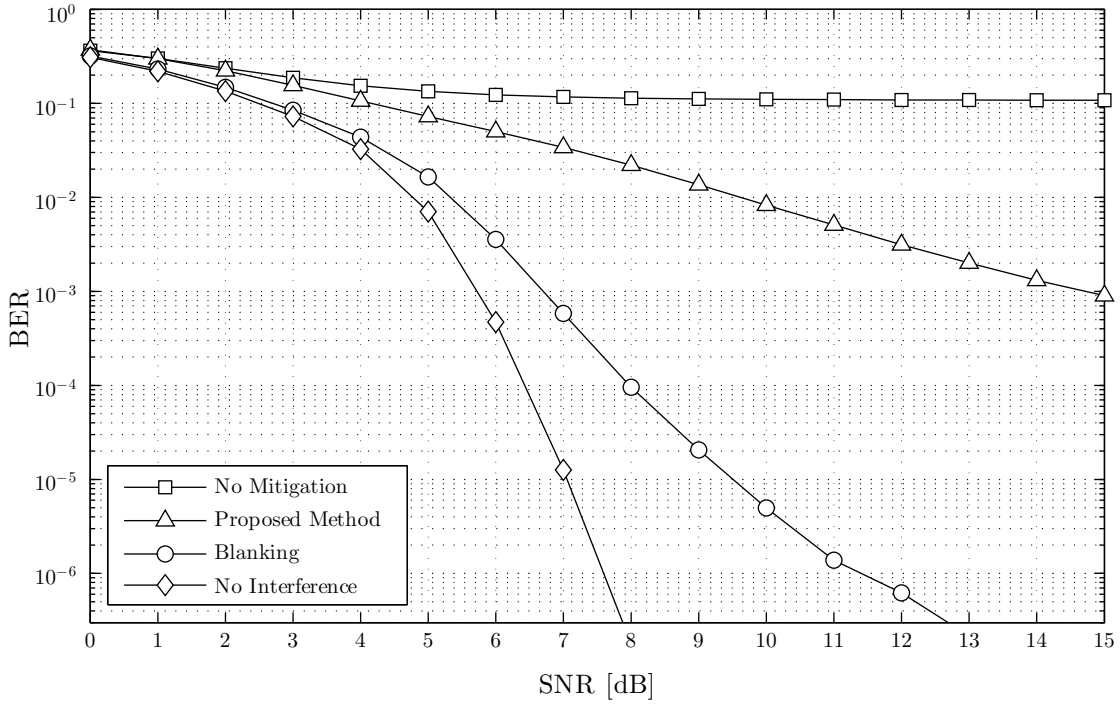

Figure 1-17: BER comparison as a function of SNR when $SIR = 0$ dB, $P_i = 1/4$ and $D = 4$ OFDM samples.

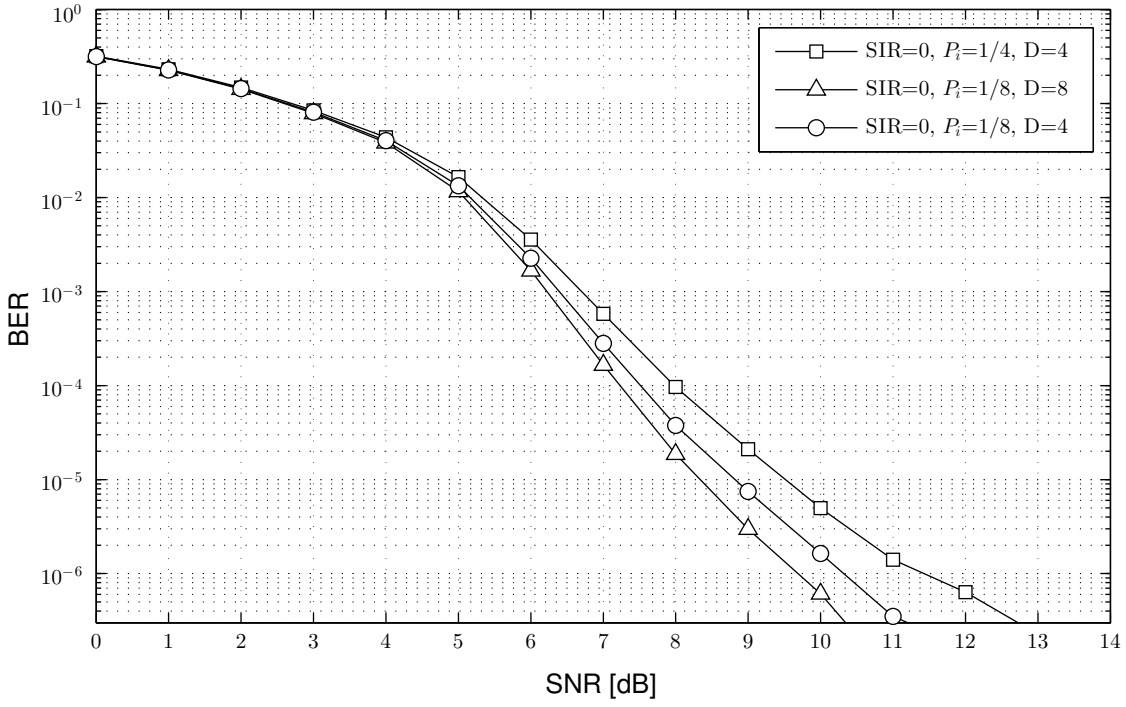

Figure 1-18: BER as a function of the SNR for different interference configuration.

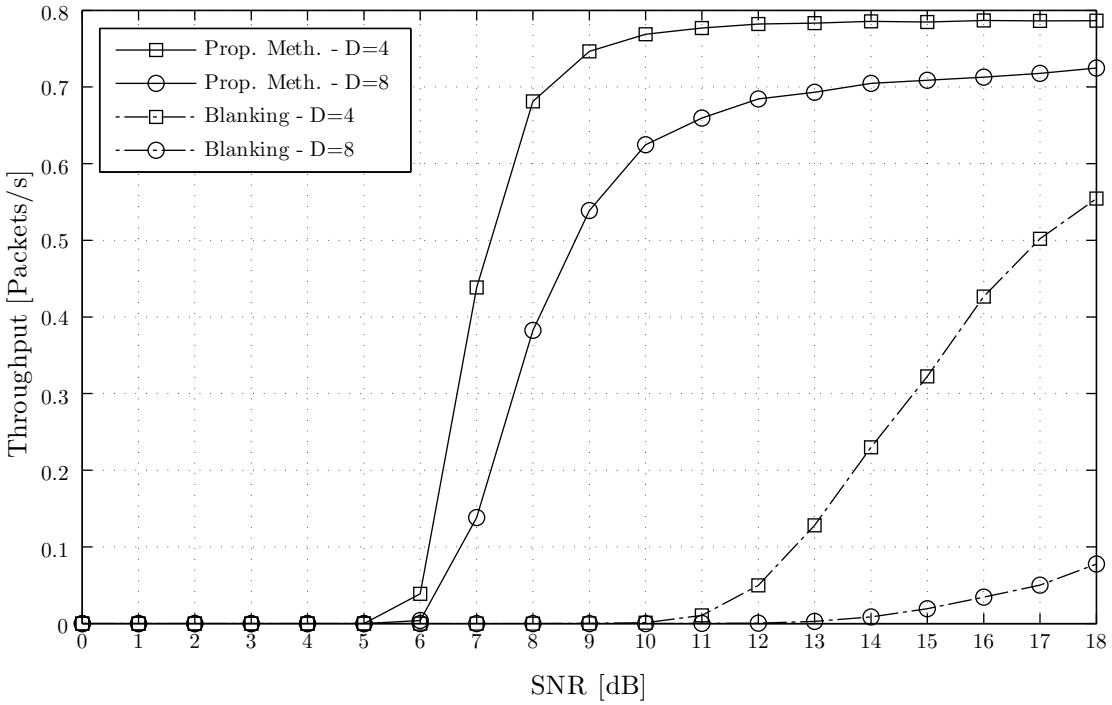

Figure 1-19: Throughput of the proposed and blanking methods as a function of SNR when $SIR = 0$ dB, $P_i = 1/4$ and $D = 4, 8$ OFDM samples

Chapter 2

Laplace Distribution Modelling Impulsive Noise

Abstract

Laplace distribution can be used to model white impulsive noise. An optimal detector for a known signal in Laplace noise is determined. The analysis starts with a sampled digital receiver, leading to an asymptotic analysis when the number of samples approaches infinity. The optimum detector for Laplace noise achieves twice the signal-to-noise ratio of the matched filter for Gaussian noise. The theoretical analysis is corroborated by computer simulations.

Furthermore, a practical receiver is analysed. The transmission rate is optimized for a selective automatic repeat request (SR-ARQ) scheme to minimize the mean delay. The optimization procedure is proposed in relation to the use of the soft-limiting detector of the previous section. The superiority of the optimized SR-ARQ scheme over different alternatives is clearly shown.

2.1 Introduction to Laplace Noise

Impulse Noise is a type of noise characterized by transient short-duration disturbances distributed essentially uniformly over the useful passband of a transmission system. In general it may require modelling beyond the amplitude distribution, such as modelling the impulse arrival time distribution. The white Laplace noise is a special case where the noise process at different time instances is considered statistically independent, while the first-order amplitude distribution follows a Laplace probability distribution function (PDF). The Laplace PDF, which has heavier tails than the Gaussian PDF, has found historical use to model impulsive noise, such as atmospheric noise in extremely low frequency communications. The white Laplace noise model has found application in [49–53].

The interest in the Laplace noise model is due to its importance in signal detection and processing when it is necessary to model impulsive noise. Furthermore, recent research in ultra-wide bandwidth (UWB) wireless systems, [54, 55], has led to renewed interest in Laplace noise, because the multi-user interference in UWB systems can be well modelled by the Laplace probability density function (PDF). Many UWB systems can be considered equivalent to a binary data communication system operating in Laplace noise. A key benefit of the white Laplace model is its tractability compared to other heavy-tailed models; the white Laplace model leads to relatively simple receiver designs.

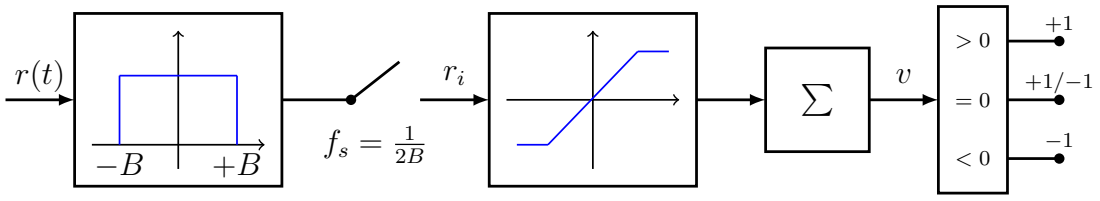

Figure 2-1: Block diagram of the receiver model.

2.2 Optimal Detector in Laplace Noise

The matched filter is well known as the optimum continuous-time detector for digital signals corrupted by additive white Gaussian noise processes. The matched filter is optimum in the sense that it maximizes the signal-to-noise ratio (SNR), which operation, in the absence of any noise and/or interference components that are non-Gaussian, is also optimal in the sense of minimizing the symbol error rate (SER). To the best of the authors' knowledge, the only optimal analog signal detector known is the matched filter for Gaussian noise. In this section, we reveal the corresponding optimum signal detection structure that achieves the minimum SER for detection of data signals corrupted by an additive strictly white Laplace random process.

The optimum detector that bases its decision on a number of discrete, independent Laplace samples is well known [49, 51, 56, 57]. The corresponding discrete time detector for samples corrupted by additive, independent Gaussian noise is the digital matched filter (DMF) [58]. However, to the best of the authors' knowledge, there is no discussion in any of the literature regarding the structure of the optimum continuous-time signal detector for signals immersed in a white Laplace noise process.

2.2.1 Detector model

Let us consider an antipodal modulation, where the binary information symbol $d = \pm 1$ modulates an arbitrary pulse shape $s(t)$ lasting T seconds. Hence, the transmitted baseband signal can be expressed as $ds(t)$. The binary symbol d takes values $+1$ and -1 with equal probability. The signal is transmitted over an additive white Laplace noise channel to the receiver. The system model is shown in Fig. 2-1 [59]. The channel corrupts the transmitted signal with additive noise $n(t)$ creating the signal $x(t) = ds(t) + n(t)$. After prefiltering, signal $r(t)$ is input to the detector. The detector outputs its estimate, $\hat{d}$, of the transmitted information symbol. Without loss of generality, we will assume that $s(t) \geq 0$ for all $t \in [0, T]$. If $s(t) < 0$ in some regions of $[0, T]$, the signal $r(t)$ can be multiplied by -1 in those regions. To develop the continuous-time receiver, we will proceed by studying a digital sampling receiver with noise-limiting prefilter. The white noise continuous-time receiver will be realized by increasing the sampling frequency and the prefilter bandwidth without limit to obtain a white noise channel and a continuous-time receiver. The prefilter is ideal lowpass with cutoff frequency, B. The received signal $s(t)$ is sampled at rate $2B$ and the sampled received signal can be written as

$$\{r_i\}_{i=1}^{M} = d\{s_i\}_{i=1}^{M} + \{n_i\}_{i=1}^{M} \tag{2.1}$$

where $M = 2BT$ is the total number of samples and n_i represents the Laplace noise sample, with zero mean and variance $\sigma_n^2 = N_0 B$. This signal model with ideal lowpass filter and sampling rate $2B$ achieves zero crossings in the noise autocorrelation function at the sampling

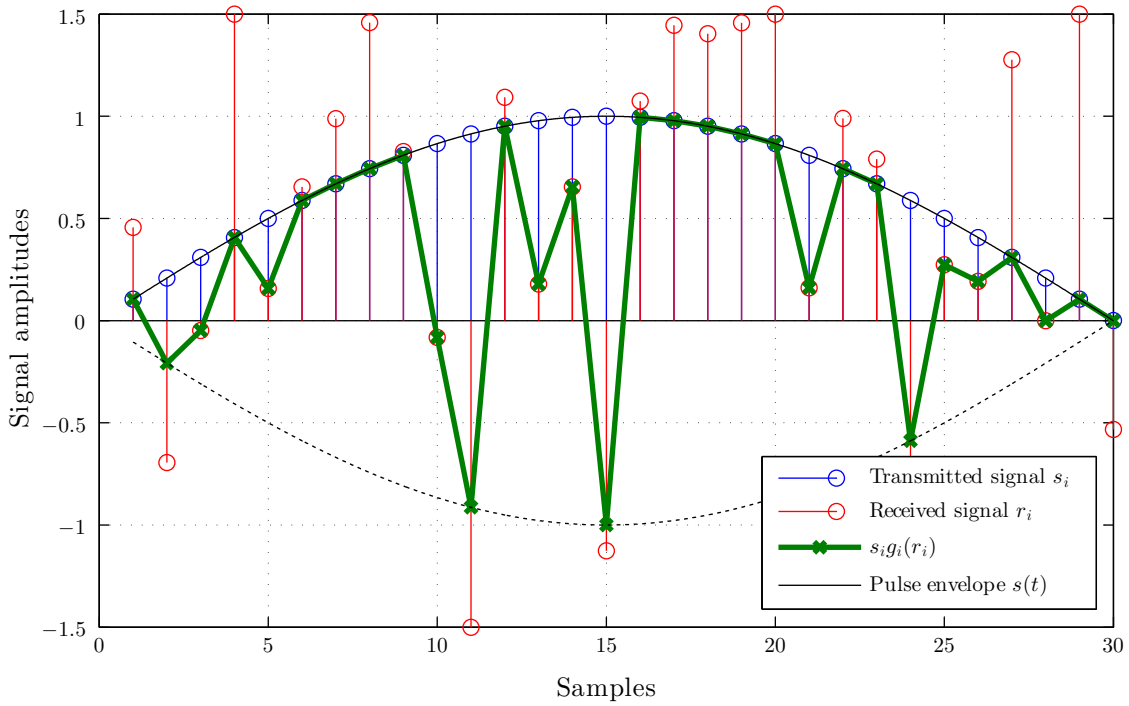

Figure 2-2: The effect of the optimum receiver on noisy signal pulse samples.

instants, and hence, the samples are uncorrelated [50, 59]. The Laplace probability density function (PDF) for the random variable X is defined as [49, 51, 56, 57]

$$X \sim \mathcal{L}(\lambda, c) \quad , \quad f_X(x; c, \lambda) = \frac{1}{2c} e^{-\frac{|x-\lambda|}{c}} \tag{2.2}$$

where λ represents the location parameter and is equal to the mean, while c is related to the variance as $\sigma_n^2 = 2c^2$. Then, the white Laplace noise samples n_i are outcomes of random variables $N_i \sim \mathcal{L}(0, \frac{\sigma_n}{\sqrt{2}})$. From [57], the optimum sampled detector generating the test statistic v, can be expressed as

$$v = \sum_{i=1}^{M} s_i g_i(r_i) \gtrless 0 \tag{3a}$$

where g_i denotes the nonlinearity

$$g_i(x) = \begin{cases} -1 & \text{if} \quad x \leq -s_i \\ \frac{x}{s_i} & \text{if} \quad -s_i \leq x \leq s_i \\ 1 & \text{if} \quad x \geq s_i \end{cases} . \tag{3b}$$

The optimum detector (3a) decides $\hat{d} = 1$ if $v > 0$ and $\hat{d} = -1$ if $v < 0$; if $v = 0$, a fair coin toss determines $\hat{d}$.

Fig. 2-2 shows the effect of the nonlinearity g_i on the received signal. The optimal receiver limits the excursion of the received signal samples to not exceed the pulse shape samples $\{s_i\}_{i=1}^{M}$.

To obtain the optimum analog detector, note that the time spacing between the samples

is $\Delta t = \frac{T}{M}$ and multiply the sum in (3a) by $\frac{T}{M}$ to get

$$\tilde{v}(i\Delta t) = \frac{T}{M}\sum_{i=1}^{M} s(i\Delta t)g(r(i\Delta t), i\Delta t) \gtrless 0 \tag{2.4}$$

where $\tilde{v}$ in (2.4) is an equivalent statistic to v in (3a). Then, one obtains

$$\lim_{M\to\infty} \tilde{v}(i\Delta t) = \int_0^T s(t)g(r(t), t)dt \gtrless 0 \tag{5a}$$

where

$$g(x,t) = \begin{cases} -1 & \text{if} \quad x \le -s(t) \\ \frac{x}{s(t)} & \text{if} \quad -s(t) \le x \le s(t) \\ 1 & \text{if} \quad x \ge s(t) \end{cases} \tag{5b}$$

by the fundamental theorem of calculus [60], and the detector decides $\hat{d} = 1$ and $\hat{d} = -1$ corresponding to the superiority and the inferiority of the inequality, respectively. Eqs. (5a) and (5b) represent a fundamental novel result. It is the optimum continuous-time (analog) detector for binary signalling in strictly white Laplace noise.

The detector structure (5a) is optimal in the sense that it achieves the minimum probability of error. This follows because the structure (3a) is maximum likelihood for all numbers of samples, and because the prefilter implements ideal bandlimiting, provided that the noise is strictly white. A strictly white noise process is one whose samples are independent [61, p. 385]. This is a stronger condition than the white noise condition, which implies that samples are uncorrelated. The prefiltering scheme in Fig. 2-1 guarantees that the Laplace samples are uncorrelated. To rigorously assert optimality it is further required to specify that the samples are strictly white. We conjecture that uncorrelatedness is sufficient for optimality, but are unable to prove this conjecture. Invoking the sampling theorem for bandlimited random processes [61, Ch. 10-5], it is clear that the detector performance cannot be improved by processing additional, correlated (dependent) samples obtained by oversampling, because correlated samples are weighted linear combinations (sinc interpolations) of the uncorrelated samples.

2.2.2 Performance analysis

The receiver performance is determined by the mean and the variance of the random test statistic V. The mean is defined as

$$\mu_V = E\big[V\big] = \sum_{i=1}^{M} s_i E\big[Y_i\big]. \tag{2.6}$$

Note that $\{y_i\}_{i=1}^M = \{g_i(r_i)\}_{i=1}^M$ are outcomes of random variables following a double truncated Laplace density, $f_{Y_i}(\,\cdot\,)$. That is, for $d = 1$,

$$f_{Y_i}(x) = \begin{cases} F_{N_i}(-2s_i)\delta(x+1) & \text{if} \quad x = -1 \\ \mathcal{L}\left(1, \frac{c}{s_i}\right) & \text{if} \quad -1 \le x \le 1 \\ (1 - F_{N_i}(0))\delta(x-1) & \text{if} \quad x = 1 \end{cases} \tag{2.7}$$

where $F_{N_i}(\,\cdot\,)$ denotes the Laplace cumulative distribution function (CDF) of the random variable N_i

$$F_{N_i}(x) = \frac{1}{2}\left[1 + \operatorname{sgn}(x)\left(1 - e^{-\sqrt{2}\frac{|x|}{\sigma_n}}\right)\right] \tag{2.8}$$

where $\operatorname{sgn}(\,\cdot\,)$ denotes the signum function, so

$$F_{N_i}(-2s_i) = \frac{1}{2}e^{-2\frac{s_i}{c}} \tag{2.9}$$

$$F_{N_i}(0) \quad = 1 - F_{N_i}(0) = \frac{1}{2}. \tag{2.10}$$

The mean of Y_i can be expressed as

$$\begin{aligned}\mu_{Y_i} &= E\big[Y_i\big] \\ &= -F_{N_i}(-2s_i) + \int_{-1}^{1} y f_{Yi}(y)dy + \big(1 - F_{N_i}(0)\big) \\ &= 1 - \frac{c}{s_i}\left(\frac{1 - e^{-\frac{2s_i}{c}}}{2}\right).\end{aligned} \tag{2.11}$$

Defining $\{z_i\}_{i=1}^{M} = \{s_i/c\}_{i=1}^{M}$ we can rewrite (2.11) as

$$\mu_{Y_i} = 1 - \frac{\sinh z_i}{z_i}e^{-z_i}. \tag{2.12}$$

and hence the mean of the test variable can be expressed as

$$\mu_V = \sum_{i=1}^{M} z_i c\left(1 - \frac{e^{z_i}}{z_i}\sinh(z_i)\right) \tag{2.13}$$

The variance is defined as

$$\begin{aligned}\sigma_V^2 &= E\left[(V - \mu_V)^2\right] \\ &= E\left[\left(\sum_{i=1}^{M} s_i g_i(r_i) - \sum_{i=1}^{M} s_i \mu_{y_i}\right)^2\right] \\ &= E\left[\left(\sum_{i=1}^{M} s_i\big(Y_i - \mu_{Y_i}\big)\right)^2\right] \\ &= \sum_{i=1}^{M} s_i^2 E\left[\big(Y_i - \mu_{y_i}\big)^2\right]\end{aligned} \tag{2.14}$$

where the last step is based on the assumption of uncorrelated noise samples which is valid

for our model. One has

$$\begin{aligned}\sigma_{Y_i}^2 &= E\left[\left(Y_i - \mu_{Y_i}\right)^2\right] \\ &= \left(1+\mu_{Y_i}\right)^2 F_{y_i}(-2s_i) + \int_{-1}^{1} y^2 f_{Y_i}(y)dy + (1-\mu_{Y_i})^2 F_{Y_i}(0) \\ &= \frac{1}{z_i^2}\left(1 - 2z_i e^{-2z_i} - e^{-2z_i}\cosh^2(z_i)\right) \qquad (2.15) \\ &= \frac{-2z_i + 2e^{z_i}\sinh z_i - \sinh^2 z_i}{z_i^2 e^{2z_i}}. \qquad (2.16)\end{aligned}$$

Hence, the mean and the variance of the test statistic V can be expressed through the moments of the random variables, Y_i, as

$$\mu_V = \sum_{i=1}^{M} s_i \mu_{Y_i} \qquad (2.17)$$

$$\sigma_V^2 = \sum_{i=1}^{M} s_i^2 \sigma_{Y_i}^2. \qquad (2.18)$$

The test statistic V is a sum of independent soft-limited Laplace random variables, hence, for large values of M, V follows a Gaussian distribution due to a central limit theorem [62, p. 58]. When $d = +1$ has been transmitted, an error occurs if $V < 0$. Hence, using the Gaussian approximation (GA) the error probability can be approximated as

$$P_{e,GA} \cong Q\left(\frac{\mu_V}{\sigma_V}\right). \qquad (2.19)$$

Eq. (2.19) holds when M is large enough. In particular when M approaches infinity the sampled digital detector converges to the time-continuous detector.

The performance of the optimal analog detector in white Laplace noise is computed as follows. We evaluate the ratio between the mean and the standard deviation of the test statistic when M approaches infinity, namely

$$\lim_{M\to\infty} \frac{\mu_V}{\sigma_V} = \lim_{M\to\infty} \frac{\mu_V}{c} \cdot \left(\lim_{M\to\infty} \frac{\sigma_V^2}{c^2}\right)^{-\frac{1}{2}}. \qquad (2.20)$$

By recalling the definition of z_i we have

$$z_i = \frac{s_i}{c} = 2s_i\sqrt{\left(\frac{T}{N_0 M}\right)} \qquad (21a)$$

and hence

$$\lim_{M\to\infty} \frac{\sinh(z_i)}{z_i} = 1. \qquad (21b)$$

Eq. (21b) states that $\sinh(z_i) \approx z_i$ and $\sinh^2(z_i) \approx z_i^2$, when M approaches infinity. Hence,

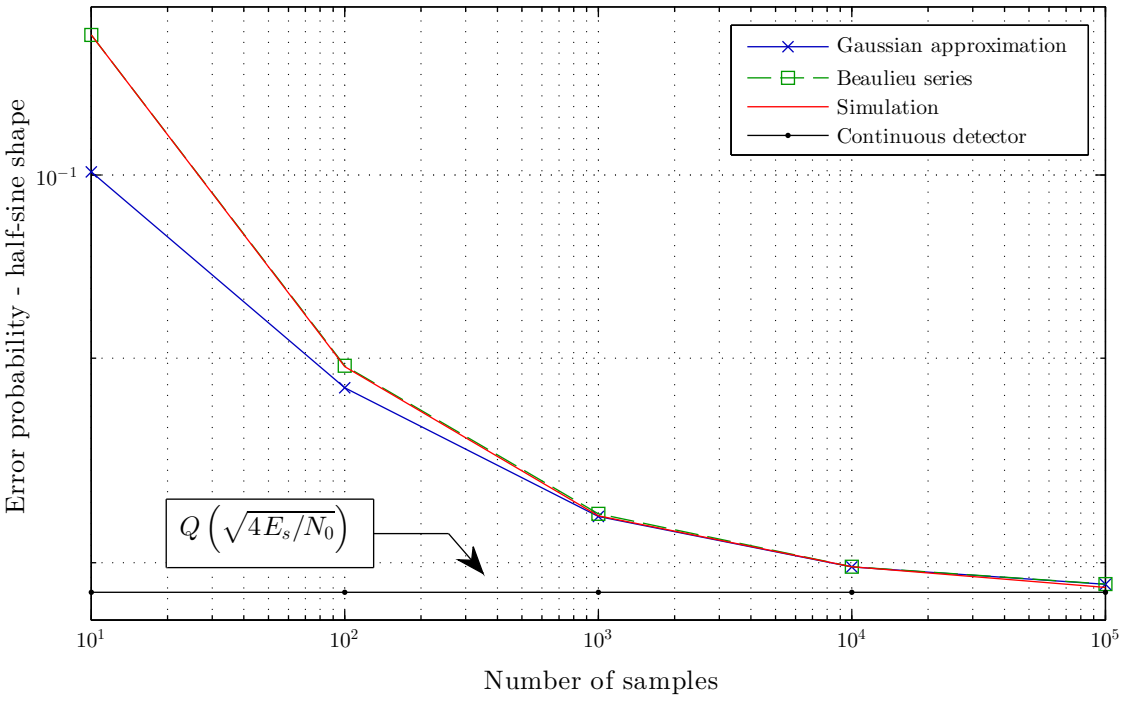

Figure 2-3: The detector performance when the E_s/N_0 ratio is equal to -3 dB.

the limiting ratio of μ_V to c can be expressed as

$$\begin{aligned}
\lim_{M\to\infty}\frac{\mu_V}{c} &= \lim_{M\to\infty}\sum_{i=1}^{M} z_i\left(1-\frac{\sinh z_i}{z_i}e^{-z_i}\right)\\
&= \lim_{M\to\infty}\sum_{i=1}^{M} z_i\left(1-e^{-z_i}\right) = \lim_{M\to\infty}\sum_{i=1}^{M} 2z_i e^{-\frac{z_i}{2}}\sinh\left(\frac{z_i}{2}\right)\\
&= \lim_{M\to\infty}\sum_{i=1}^{M} z_i^2 e^{-\frac{z_i}{2}} = \lim_{M\to\infty}\sum_{i=1}^{M} 2\frac{s_i^2}{\sigma_n^2}\\
&= 2\frac{\lim_{M\to\infty}\sum_{i=1}^{M}\frac{T}{M}s_i^2}{\frac{N_0}{2}} = 4\frac{\int_0^T |s(t)|^2dt}{N_0} = \frac{4E_s}{N_0}.
\end{aligned} \tag{2.22}$$

The limiting variance is

$$\begin{aligned}
\lim_{M\to\infty}\frac{\sigma_V^2}{c^2} &= \lim_{M\to\infty}\sum_{i=1}^{M}\frac{-2z_i+2e^{z_i}\sinh z_i-\sinh^2 z_i}{e^{2z_i}}\\
&= \lim_{M\to\infty}\sum_{i=1}^{M} -2z_i+2z_ie^{z_i}-z_i^2 = \lim_{M\to\infty}\sum_{i=1}^{M} 4z_ie^{\frac{z_i}{2}}\sinh\frac{z_i}{2}-z_i^2\\
&= \lim_{M\to\infty}\sum_{i=1}^{M} z_i^2\left[1+2\left(e^{\frac{z_i}{2}}-1\right)\right] = \lim_{M\to\infty}\sum_{i=1}^{M} z_i^2\left[1+z_ie^{\frac{z_i}{4}}\right]\\
&= 4\frac{\int_0^T |s(t)|^2dt}{N_0}+4\frac{\int_0^T |s(t)|^3dt}{N_0}\lim_{M\to\infty}\frac{\sqrt{2}}{\sigma_n} = \frac{4E_s}{N_0}.
\end{aligned} \tag{2.23}$$

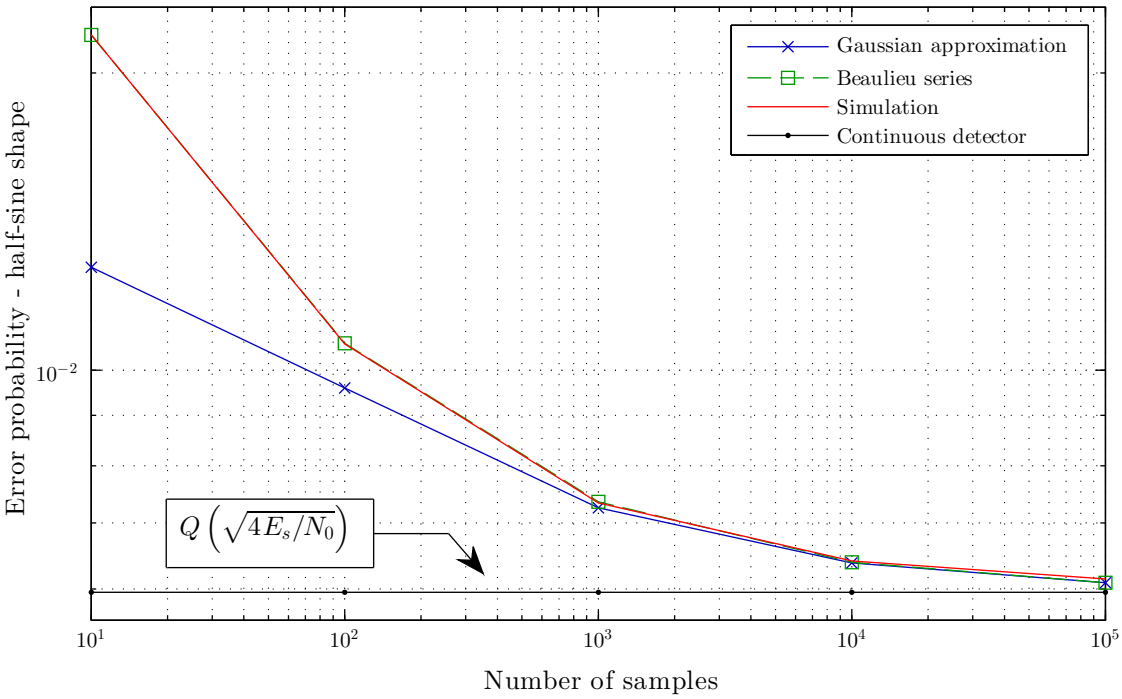

Figure 2-4: The detector performance when the E_s/N_0 ratio is equal to 2 dB.

In (2.23) we can see that the variance depends also on the third power of the pulse shape, but the second term approaches 0 when M is large. By combining (2.22), (2.23) and (2.20) one has

$$\lim_{M\to\infty} \frac{\mu_V}{\sigma_V} = \sqrt{\frac{4E_s}{N_0}} \tag{2.24}$$

and the probability of error for the continuous time detector is given by $P_{e,GA} = Q\left(\sqrt{\frac{4Es}{N_0}}\right)$. This is an interesting and intriguing result that states the proposed detector for Laplace noise achieves twice the E_s/N_0 achieved by the matched filter detector for Gaussian noise.

2.2.3 Numerical results

In this section, the theoretical analysis is validated through computer simulations. In deriving our results we use a half-sine pulse, that is

$$s_i = \sqrt{2}\sin\left(\frac{\pi}{M}i\right). \tag{2.25}$$

We are interested in how the performance behaves for a fixed E_s/N_0 value when the number of samples M varies. Figs. 2-3, 2-4 and 2-5 show the simulated error probability of the detector when the E_s/N_0 ratio is equal to -3, 2 and 7 dB, respectively[1]. In these figures we also compare the accurate performance with the performance as estimated by the Gaussian approximation (GA), expressed through (2.19). Note that [57] has shown that the GA is not accurate for this case when $M < 1000$. For this reason, we do the BER calculation using the Beaulieu series [63], which was shown to be the far superior method for computing the statistics of Laplace random variables in [57]. The series is truncated to $L = 1000$ terms

[1]The prefilter distorts the pulse, but the distortion decreases rapidly to zero as M increases for smooth pulses [59]. Figs. 2-3 - 2-5 show results for $M > 10$ ignoring small distortion.

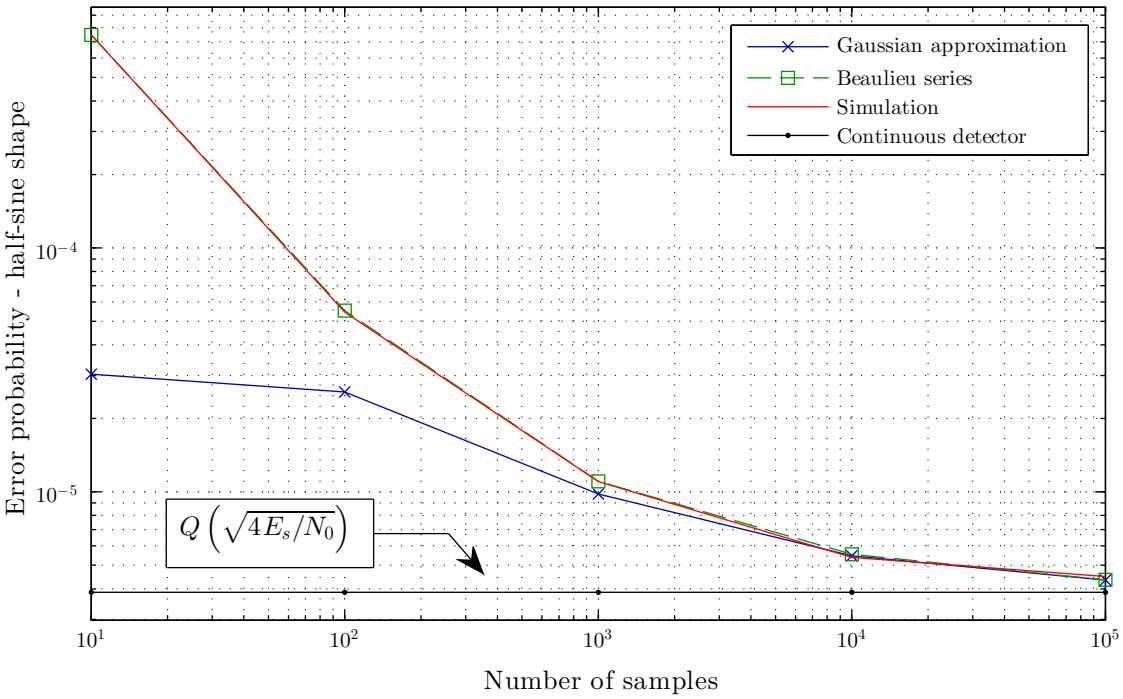

Figure 2-5: The detector performance when the E_s/N_0 ratio is equal to 7 dB.

and the period of the square wave, P, is selected as $P = \alpha\left(2\sum_{i=1}^{M} s_i\right)$, where $\alpha = 1.1$ to prevent the overlap between the square wave and the lower bound of the test statistic PDF. The results in the figures show that when M is large enough, the performance of the discrete sampled detector converges to that of the continuous-time detector. It is seen in Figs. 2-3, 2-3 and 2-5 that Gaussian approximation is poor for high E_s/N_0 values and sample size less then 1000, while the Beaulieu series gives a tractable and precise calculation of the error probability in all cases. The results clearly show, as expected, that the analog optimal detector outperforms its sampled versions.

2.3 Optimal Rate Transmission in Laplace Noise

Reliable data transfer is of paramount importance in several applications as vehicular, military and industrial communication systems that often operate in hostile environments affected by severe impulsive noise.

A typical approach adopted to counteract impulsive noise effects and allow reliable communications is the use of Automatic Repeat Request (ARQ) schemes [64]. The basic ARQ principle is that whenever errors are detected in a packet at the receiving end, the transmission of a new copy of the packet is requested from the transmitter by sending back a negative acknowledgement (NACK). The transmission of copies of the same packet is stopped only when a positive acknowledgement (ACK) is received at the transmitting end meaning that a previous transmission attempt for that packet was successful (i.e., the packet was received errors-free at least once). Many alternatives for basic and hybrid ARQ schemes are available in the literature. Among them, here we consider the Selective Repeat ARQ (SR-ARQ) scheme, where unnecessary packet retransmissions are avoided [64]. The performance of a SR-ARQ scheme is usually dependent on the mean transmission delay [65] defined as the time elapsed from the beginning of the first packet transmission attempt to the time of the

arrival at the transmitting end of the first ACK message for this packet. Furthermore, since the mean packet transmission delay is a critical parameter for several applications, we will adopt it as the performance measure in carrying out our analysis devoted to deriving the optimum data rate value that allows the best performance under Laplace noise propagation conditions.

2.3.1 Variable rate model

Let us consider that data are transmitted according to a binary PSK modulation scheme [66], with each binary information symbol d taking values ± 1 with equal probability, and modulating an arbitrary pulse shape $s(t)$ known at the receiver end of time duration T. Moreover, we assume that the modulated signal $ds(t)$ is transmitted over an additive white Laplace noise channel of bandwidth B to the receiver.

The channel corrupts the transmitted signal with additive Laplace noise $n(t)$ creating the signal

$$r(t) = ds(t) + n(t) \quad \text{with} \quad 0 < t < T. \tag{2.26}$$

The studies on the optimal (in the maximum likelihood sense) digital receiver for Laplace noise [3], shown in Fig. 2-1, indicate that the performance in terms of error probability can get a remarkable improvement by combining several independent signal samples for each transmitted symbol. In practical applications the channel bandwidth B is usually fixed and hence it is not possible to arbitrarily increase the prefilter bandwidth and, accordingly, the sampling frequency. The underlying idea is to extend the symbol duration by a factor m (thus reducing the signal bandwidth $\tilde{B}$ with respect to the maximum allowed B), so that m statistically independent signal samples are available at the receiver for each data symbol Moreover, this allows maintaining the receiver sampling frequency and the prefilter bandwidth constant. In particular, eq. (2.26) becomes

$$r(t) = ds\left(\frac{t}{m}\right) + n(t) \quad \text{with} \quad 0 < t < mT. \tag{2.27}$$

The received signal $r(t)$ is sampled at rate $2\tilde{B}$ and the sampled received signal can be written as

$$\{r_i\}_{i=1}^{m} = d\{s_i\}_{i=1}^{m} + \{n_i\}_{i=1}^{m} \tag{2.28}$$

Hence, increasing the symbol duration is possible to collect m samples, making more reliable the link but decreasing the transmission rate.

In any ARQ based system the performance is strictly affected by the reliability of the wireless medium. A higher decoding error probability means longer transmission delays. We suppose the presence of an optimal value of m allowing the minimal transmission delay. For this reason, we are interested in deriving the bit error probability in Laplace noise. As seen in the previous section, the two most practical methods for achieving this goal are represented by the Gaussian approximation (GA) and the Beaulieu series (BES) [63]. However, the GA is a good approximation only when the number of samples is very high, i.e., $m > 1000$. The second method, i.e., the BES, allows expressing the complementary cumulative distribution function of a sum of r.v.s by means of a series decomposition. In particular, the terms of the BES for the Laplace detector decision statistic have been derived in [57]. Hence, the Laplace detector error probability with m independent samples available at the receiver can

be expressed as

$$P_e(m) = \frac{1}{2} - \sum_{\substack{l=0 \\ l\ odd}}^{\infty} \frac{2}{\pi l} \left(\prod_{i=1}^{m} \sqrt{A_{i,l}} \right) \sin \left(\sum_{i=1}^{m} \arctan\left(\theta_{i,l}\right) \right) \tag{29a}$$

$$A_{i,l} = \frac{\cos^2(\omega_l s_i) + \sinh^2\left(\frac{s_i}{c}\right) + \frac{\sin(2\omega_l s_i)}{\omega_l c} + \frac{e^{\frac{2s_i}{c}}}{(\omega_l c)^2}}{\left[1 + \frac{1}{(\omega_l c)^2}\right] e^{\frac{2s_i}{c}}} \tag{29b}$$

$$\theta_{i,l} = \frac{1 + \omega_l c \left\{ e^{-\frac{2s_i}{c}} \left[\omega_l c - \cot(\omega_l s_i)\right] \right\}}{1 + \omega_l c \left\{ e^{-\frac{2s_i}{c}} \left[\omega_l c + \tan(\omega_l s_i)\right] \right\}} \tan(\omega_l s_i) \tag{29c}$$

$$\omega_l = \frac{\pi l}{\sum_{i=1}^{m} |s_i|}. \tag{29d}$$

This expression can be used to derive numerically the error probability without resorting to computer simulations even when the value of m is small.

Let us consider the use of a SR-ARQ scheme to allow reliable data transfer on a link basis (i.e., between a transmitter and a receiver directly connected). Under the assumption of an ideal error detecting code (i.e., a code able to detect all the error patterns) and considering each packet formed by L bits, we have that the probability of receiving a packet with errors is given by

$$P_L(m) = 1 - (1 - P_e(m))^L \tag{2.30}$$

where $P_e(m)$ is the error probability of a bit given by (29a).

From the preceding, according to standard theory [64], the mean packet transmission delay normalized to the nominal packet duration time LT, is

$$\mu(m) = \frac{m + \delta}{1 - P_L(m)} \tag{2.31}$$

where δ is the delay (normalized with respect to LT) elapsed from the packet transmission completion to when an acknowledgement message for that packet transmission attempt is received at the transmitting side, usually referred as round trip time. From the preceding, it is possible to note that reducing the data signal bandwidth by a factor m means increasing by the same factor the data signal duration and hence the mean packet transmission delay.

Therefore, our aim here is to find the value of m, namely m_{opt}, which minimizes $\mu(m)$ in relation to specific channel propagation conditions. In particular, we have

$$m_{opt} = \arg\min_{m} \frac{m + \delta}{(1 - P_e(m))^L}. \tag{2.32}$$

The m_{opt} values derived by (2.32) guarantees the best trade-off between a high data reliability at the receiving end and a low packet transmission delay. The application of the proposed SR-ARQ scheme does not require a significant implementation complexity increase compared to the classical alternative. For the proposed scheme it is only needed that the transmitter is aware about the available signal-to-noise ratio at the receiving end. This information can be easily provided by conventional approaches and, usually, it is planned to be available in the most common communication standards. Moreover, it will be shown in the next section that even if the transmission rate is reduced by a factor m_{opt}, i.e., the transmission time

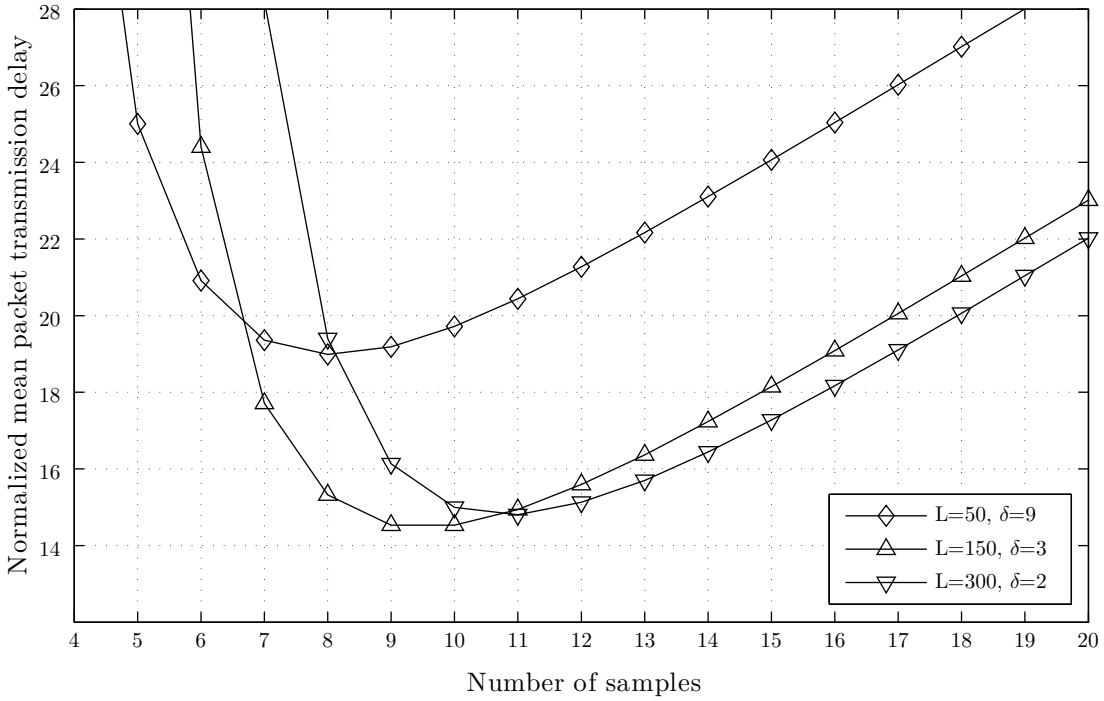

Figure 2-6: Normalized mean packet transmission delay for different packet sizes and SNR equal to 0 dB.

of any information packet is m_{opt} times longer than the nominal value, the proposed rate optimized SR-ARQ scheme lowers the overall mean delivery delay with respect to different alternatives.

2.3.2 Numerical results

The numerical results, carried out by the means of computer simulations, aim to evaluate the performance advantages achieved by adopting the optimal data rate reduction value m_{opt} derived by (2.32). The assumed transmit rate of the system, R, has been considered equal to 675 Mb/s (which is the nominal bit rate in UWB systems) and the distance between users, w, equal to 100 m. Hence the acknowledgement delay δ can be expressed as

$$\delta = \frac{2Rw}{\tilde{c}L} \tag{2.33}$$

where $\tilde{c}$ is the speed of light.

Basically, it is necessary to estimate the SNR and δ during the connection start up. Then, it is possible to evaluate the transmission delay for increasing values of m iteratively. This evaluation process can be stopped when $\mu(m) > \mu(m+1)$, due to the convexity of the objective function.

Figs. 2-6 and 2-7 show the normalized mean packet transmission delay for different size of the packets and, hence, from (2.33) different values of δ, when the SNR value is 0 dB and 6 dB, respectively, as a function of the symbol duration increase factor m. These figures highlight the presence of an optimal rate which allows the transmission delay minimization. The trend of m_{opt} as a function of the SNR is shown in Fig. 2-8 for three different values of L.

In order to further highlight the performance benefits of the proposed rate optimized

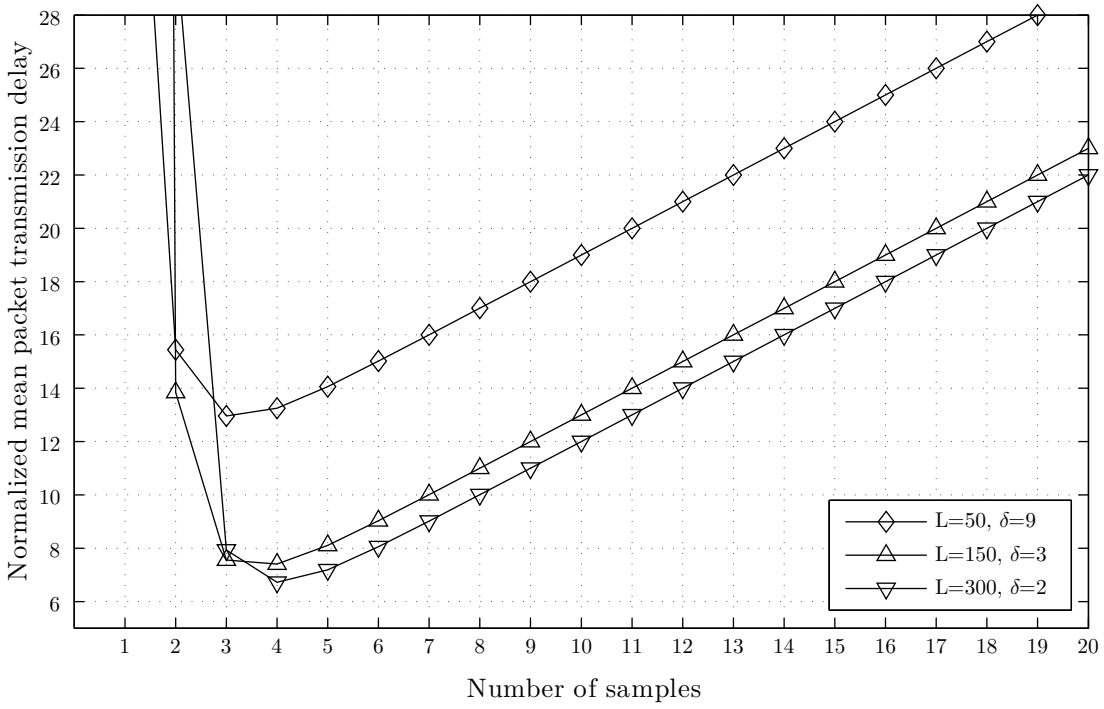

Figure 2-7: Normalized mean packet transmission delay for different packet sizes and SNR equal to 6 dB.

SR-ARQ (ORSR-ARQ) scheme, we compare the achieved mean packet transmission delay $\mu(m_{opt})$ with that obtained by means of a classic SR-scheme (with $B = \tilde{B}$ and hence, $m = 1$) and a SR-ARQ scheme employing the popular soft combining principle originally proposed by Chase in [67], named CSR-ARQ hereafter, with $m = 1$.

In the former case, data symbols are transmitted at the maximum allowed data rate, so that only when the sampling rate is equal to one sample for each data symbol, is the statistical independence among different Laplace noise samples preserved. Hence, the decision statistic for the optimal digital receiver for Laplace noise related to the $j-th$ received data symbol is

$$v = s_1 g_1 (r_1) . \tag{2.34}$$

Hence, it follows that the Laplace detector bit error probability and the related probability of receiving a packet with errors, can be derived by (29a) and (2.30), respectively by setting $m = 1$.

Likewise, for the case of the CSR-ARQ scheme, according to the soft combining principle, a cumulative test statistic is formed on a recursive mode for each symbol of a received packet. Denoting with $v^{(j)}$ the test statistic after $j-1$ failed transmission attempts of the same packet, after the reception of the following copy of the same packet, we have

$$v_1^{(j)} = v^{(j-1)} + s_1 g_1 \left(r_1^{(j)} \right) \tag{2.35}$$

where $r_1^{(j)}$ represents the received signal at the j-th attempt.

From the preceding, it is straightforward to verify that CSR-ARQ allows the same symbol error probability compared to that of ORSR-ARQ when $j = m_{opt}$. Hence, the probability to

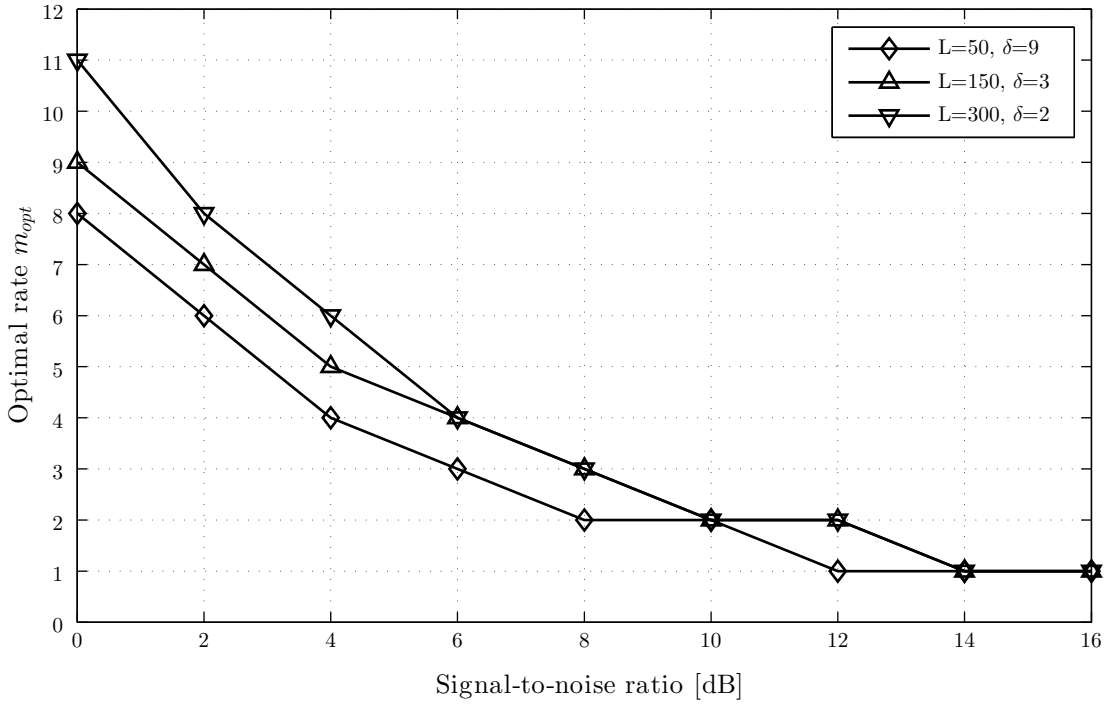

Figure 2-8: Optimal rate as a function of the SNR value.

receive an error-free packet on the n-th transmission after $n-1$ attempts is [68]

$$p(n) = \Big(1 - P_L(n)\Big) \prod_{l=0}^{n-1} P_L(l) \tag{2.36}$$

with $n = 1, 2, \cdots, \infty$ and $P_L(0) = 1$ to simplify the notation. Therefore, the normalized mean packet transmission delay for Chase combining is

$$\begin{aligned} \mu_C &= \sum_{n=1}^{\infty} n(1+s)p(n) \\ &= (1+s)\Big\{ \sum_{n=1}^{\infty} n[1 - P_L(n)] \prod_{l=0}^{n-1} P_L(l) \Big\}. \end{aligned} \tag{2.37}$$

Fig. 2-9 shows the performance of the proposed ORSR-ARQ scheme when the signal-to-noise ratio varies and the comparisons with the performance achieved by the SR-ARQ and CSR-ARQ schemes previously introduced. We can see that the proposed scheme clearly outperforms the other alternatives. In particular, we can note from the figure a critical behaviour for the SR-ARQ scheme under high error probability conditions, i.e., it does not allow reliable data transmissions. Finally, we can note that, as expected, the performance gain with respect to the CSR-ARQ scheme decreases when the SNR grows.

2.4 Conclusion

In this chapter, we derived the structure of the optimal signal detector in white Laplace noise and assessed its performance analytically using the Gaussian approximation and the

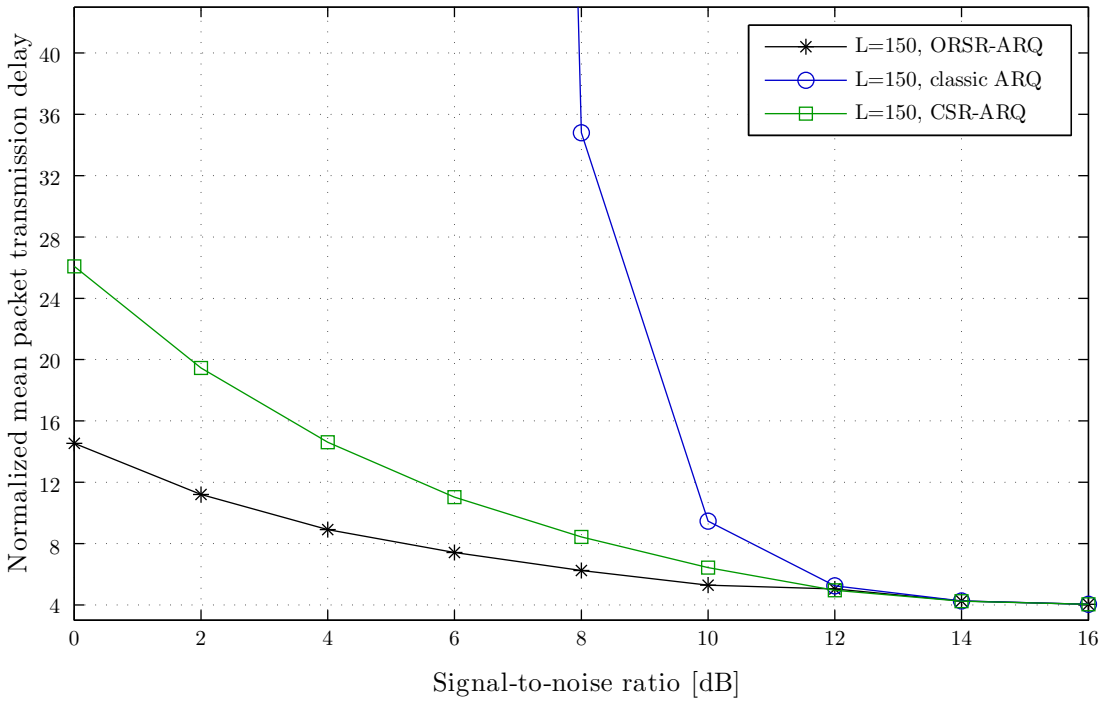

Figure 2-9: Normalized mean packet transmission delay comparison.

Beaulieu series, and by simulation. While the Gaussian approximation is poor even for hundreds of samples, the Beaulieu series gives precise results for all numbers of samples. The optimum detector for Laplace noise achieves exactly double the E_s/N_0 achieved by the matched filter for Gaussian noise.

Then, an optimal rate selection criterion for detectors in Laplace noise has been proposed. The presented approach is suitable to practical system with fixed sampling frequency. The performance in terms of mean packet transmission delay has been numerically derived by means of the Beaulieu series, which is used to provides a good approximation of the symbol error probability in Laplace noise even when the available samples are only a few and it is not possible to exploit the Gaussian approximation. The proposed optimized SR-ARQ scheme has been compared to the classical SR-ARQ scheme and to a SR-ARQ scheme adopting the Chase combining principle, showing an improvement of performance in both the cases.

Chapter 3

Intra-System Interference: LTE Heterogeneous Networks

Abstract

The integration of traditional macro-cells with cells of reduced dimensions, i.e., small-cells, is expected to be one of the main enhancements for Long Term Evolution systems. Small-cells will integrate the macro-cells coverage where greater capability and higher throughput will be needed. This heterogeneous network deployment presents many potential benefits but also many challenges that need to be resolved. In particular, multi-antenna techniques and processing in the spatial domain will be key enabling factors to mitigate these issues. This chapter starts presenting a complete overview of the main small-cell deployment approaches and the benefits provided by beamforming techniques. Then, a particular scenario is analysed in details.

A cognitive method is proposed to counteract the interference generated by the small-cell on the macro-cell downlink communications. Coordination between the two cells is supposed to be unavailable. The estimation of the direction of arrival of the user equipments signals is used to place nulls in the low power cell transmissions by means of a suitable null steering algorithm. The system operates under actual propagation conditions assuming multipath components with a very large angle spread and considering a variable number of macro-cell user equipments. This challenges either the capabilities of the direction of arrival estimation algorithm or null steerer. For this reason the scheme operates on a physical resource blocks basis. First, we focus on the residual interference produced on the macro-cell terminals by using zero forcing (ZF) beamforming. The obtained numerical results show that the system is able to significantly reduce the interference for small system bandwidths in all the operational conditions. On the other hand, when the bandwidth increases good performance is obtained if a physical resource blocks clustering is adopted in order to increase the dimension of the snapshot used for direction of arrival estimation. Then, two cognitive resource allocation methods that work using the angle of arrival of the signals instead of the channel state information. Both methods reduce the interference toward the macro-cell User Equipments (MUEs) using ZF beamforming to avoid transmission in the MUEs direction. At the same time they maximize the capacity of the small-cell with a suitable allocation of the time-frequency resources to the small-cell UEs (FUEs). In particular, the former method selects the FUEs that maximize the beamforming gain, while the latter selects the FUEs that have the highest angle separation with the MUEs. The second is sub-optimal but significantly reduces the complexity. The performance of the proposed methods is compared with that of a conventional maximum gain beamforming and conventional ZF beamforming.

The results show that the proposed methods achieve a good trade off between maximization of the small-cell capacity and reduction of the interference level at the MUEs side.

However, the possibility to operate on more than a single resource block would carry significant benefits to the proposed method. This is possible if the small-cell has knowledge about how the resources are allocated by the macro-cell. Assuming the lack of coordination between the cells, we consider a cognitive small-cell base station that is able to sense the environment and identify the set of PRBs allocated to a given user by the macro-cell base station. A PRBs clustering method is proposed. Initially, suitable inputs are derived and then provided to the K-means algorithm for a clustering refinement. The method proposed here is able to correctly gather together the PRBs of each user. Performance comparisons with a hierarchical clustering method is presented. The benefits of PRBs clustering on direction of arrival estimation are shown in order to prove the effectiveness of the proposed methods.

3.1 Introduction to LTE Heterogeneous Networks

The demand for communication services that require ever increasing data rates and quality has led to a continuous evolution of mobile communication systems. One of the most promising radio access technologies that is under active consideration is the Long Term Evolution (LTE) defined by the Third Generation Partnership Project (3GPP). LTE is able to satisfy new communication requirements, thanks to its low latency and high spectral efficiency that guarantee high data rates and real time services [69]. LTE is designed to meet high-speed data and media transport as well as high-capacity voice support thanks to key technologies such as MIMO (Multiple Input Multiple Output) and OFDM (Orthogonal Frequency Division Multiplexing). However, LTE technology is continuously evolving to meet future requirements. LTE Release 10 (LTE-Advanced) includes all features of Releases 8/9 and adds several innovations. It foresees the possibility of increasing the system capacity by integrating basic macro-cell (eNodeB or eNB) coverage with low power cells often referred to as femto or pico cells [70]. In particular, multiple-input multiple-output (MIMO) systems with up to 8×8 antenna arrays are considered as key elements, supported with the flexible reference signal structures.

However, these technologies are reaching their theoretical limits and it is commonly agreed that a network composed of only macro-cells will not be able to satisfy the current forecast of the mobile data traffic explosion. The 3GPP is working toward a further evolution of LTE Release 12 and beyond (also referred as LTE-B) in which the heterogeneous network deployment represents one of the main enhancements [71]. In heterogeneous deployment the territory coverage and, consequently, the service supply shall be guaranteed not only by the traditional macro-cells, but also shall be integrated with small-cells, above all in areas requiring high peaks of data transfer or in special environments, where coverage shall be improved or a reserved access shall be guaranteed. It is attractive for operators to offer extended services and represents new market opportunities. It offers many other advantages such as high-data rate, reduced network cost and energy saving.

Two different approaches have been proposed for the deployment of small-cells in future LTE networks: *sharing the same frequency* band with the macro-cell or using *separated higher frequency* bands [70]. Starting from LTE-Release 10, the concept of small-cells has been introduced, referring to a low power, short range wireless access point that coexists in the same geographical area of the macro-cell sharing the same spectrum. With the promising advantages, this type of small-cells deployment also causes several practical issues, especially

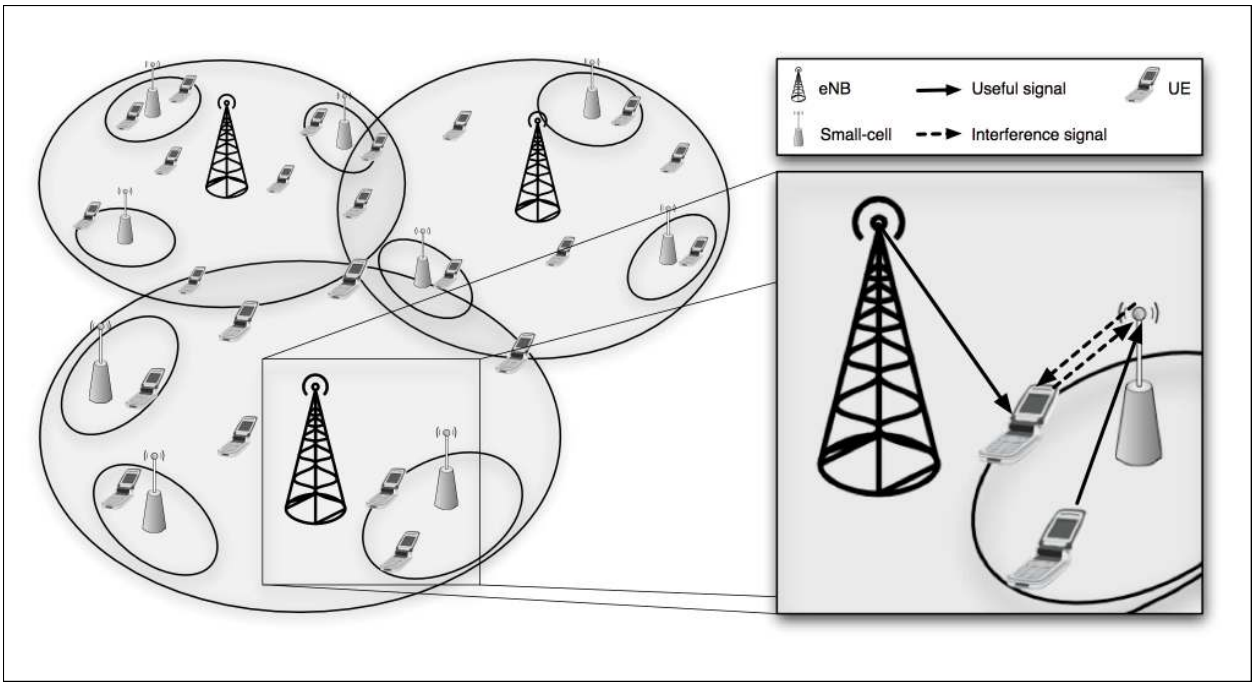

Figure 3-1: Heterogeneous interference scenario with the spectrum sharing approach.

in terms of inter-cell interference. Indeed, an inefficient deployment of the small-cell network may degrade the performance of the whole cellular system. A possible alternative for future small-cell deployments is to seek new spectrum resources in higher bands, e.g., even beyond 10 GHz, which have not been exploited in cellular systems. This will lead to separated frequency band deployment of macro-cells and small-cells, which may then simplify the network operation.

In both deployment scenarios, multi-antenna techniques and processing in the spatial domain will be key enabling factors. This chapter presents some candidate beamforming techniques that can be adopted to overcome the impairments that arise from a heterogeneous network deployment. By considering a *spectrum sharing* deployment, beamforming techniques can be used to reduce intra-cell and inter-cell interference, while in *separated high frequency* deployment they are useful to compensate the increased path loss. In particular, the high beamforming gain offered by the emerging Massive MIMO can be an essential improvement for the small-cells. Using higher frequency bands, typical millimetre techniques, and Massive MIMO antenna patterns, a common ground between the benefits of these two techniques can be reached thanks to the reduced dimension of the antenna elements.

Low power nodes can be operator-deployed or user-deployed Home-eNB (HeNB), but in both cases they have to operate without interfering with the macro-cell. In the operator-deployed case, interference reduction can be solved by using proprietary protocols that allow the coordination among the two cells, but may not guarantee the interoperability among different manufacturer devices. When the small-cell is user-deployed, the two systems do not know their mutual presence and they do not have any coordination among them. Hence, interference reduction becomes an issue of primary importance. In particular, a user close to the low power cell but not admitted to connect with it, can be subjected to strong interference that can destroy the downlink (DL) communication received from the macro-cell base station. In particular, three types of small-cells can be deployed depending on the access mode:

- *closed access mode*: the access is restricted to a limited set of user equipments (UEs).

Small-cell is user-deployed;

- *open access mode*: the access is open and small-cell is deployed directly by an operator to eliminate coverage holes;
- *hybrid access mode*: small-cell is usually user-deployed and, hence, some users have the priority.

After an overview of the main coordinated interference mitigation techniques, we focus on a user deployed HeNB with restricted (closed) access through a Cognitive Radio-based approach [72]. The cellular network is modelled as a Cognitive Network with the macro-cells and femto-cells representing the primary and secondary systems, respectively. The small-cell can transmit over the spectrum allocated to a primary system, simultaneously, but without affecting its reception (*Underlay* Cognitive Networks). The small-cell must have cognitive capabilities in order to learn from the environment and adapt its transmission by means of distributed power control algorithms and/or suitable resource allocation schemes [73]. Several works concern with resource allocation in cognitive OFDMA systems considering subcarrier allocation [74–77], power allocation [78]. In [79, 80], well-known frequency reuse allocation schemes are proposed for a joint femto/macro cell allocation.

In order to know if a resource is used or not by the primary user, *spectrum sensing* is needed. Traditionally, spectrum sensing is considered as measure of the spectrum energy in order to detect if a frequency band is occupied or not by the primary user on a given time. However, with the recent advances in multi-antenna technologies space and angle dimensions can be exploited thanks to the use of multiple antennas. MIMO schemes have been considered in Cognitive systems to enhance the performance of single antenna spectrum sensing techniques [81–84]. A different approach is to use beamforming at the secondary system transmitter in order to maximize its performance while the interference to the primary system receiver is minimized [85–88]. This operation, named Cognitive Beamforming (CB), requires solving optimization problems to find optimal pre-coding vectors and power allocation strategies with complex numerical solutions. In addition, CB is based on the knowledge of all the propagation channels over which the secondary transmitter interferers with the primary receiver. This is impracticable in actual scenarios as the two systems operate in an independent manner and the primary system ignores the presence of the secondary one. Partial solutions to this problem have been proposed by [89,90]. In [89] the use of an effective interference channel that can be observed at the secondary system instead of the full channel knowledge is proposed for a Time Division Duplex (TDD) systems. In [90] only partial information regarding the channel between the secondary system and the primary system are supposed to be available. CB has also been considered for small-cells in [91] assuming non-perfect channel knowledge. However, multiple antenna systems introduce also another resource dimension that is the direction of arrival (DOA) (or angle of arrival). In [92] after detecting the presence of a primary system the secondary system determines the direction of arrival of the primary signal but how the DOA information can be used is not considered. On the contrary, [93] assumes a perfect knowledge of primary signal DOA in order to insert a null in the direction of the primary system. In particular, cognitive beamforming reduces the interference at the primary system and satisfies the demand for high data rate at the secondary system at the same time. It can be jointly used with resource allocation schemes as in [94, 95] where Zero Forcing Beam Forming (ZFBF) is combined with a user selection procedure. In particular, [94] and [95] proposed joint resource allocation and ZFBF in Cognitive network with a high number of users. Beamforming weights are selected to reduce mutual inference among different systems taking advantage from spatial separation

between users. These methods are based on semi-orthogonal user selection. They require the knowledge of the channel state information of the interference links. However, this can be too complex in some scenarios. On the other hand, DOA estimation and actual propagation conditions in multipath indoor channels have not been taken into account.

All the above cited methods are effective only if the knowledge of the environment acquired during the first sensing interval is reliable. This may depend on many factors, but, in particular, in a mobile communication channel the multipath fading and the AWGN noise fluctuations reduce the sensing accuracy. In addition, DOA estimation capabilities are affected by angle dispersion of the multipath components: even when only one primary UE is located within the small-cell coverage area, each propagation path entails a different DOA of the signal, making the accuracy of the estimation critical. Furthermore, the quality of the estimation is strongly conditioned by the number of samples collected during the sensing period: in particular, if only few samples are available, the acquired knowledge can be not accurate. However, if the HeNB does not know which physical resource blocks (PRBs[1]) compose the sub-channel allocated to a given MUE, the estimate takes place only on the smallest resource portion (i.e., the PRB). In order to have an accurate knowledge of the surrounding environment and, hence, to perform a suitable resource allocation, the HeNB should know which PRBs belong to a specific sub-channel. However, in closed access mode, this knowledge is not provided *a priori*.

In this chapter we will discuss the two major small-cells deployment approaches. Section 3.2 presents the main research trends about the heterogeneous deployment supported by beamforming technique. In particular, Sec. 3.2.1 will focus on the spectrum sharing deployment. After an introduction of the main interference scenarios, beamforming approaches in cognitive small-cells and in CoMP systems will be presented. Sect. 3.2.2 describes the separated higher bandwidth deployment, by focusing on beamforming with Massive MIMO systems. Furthermore, the cognitive approach using beamforming technology is examined in depth in Sections 3.3 and 3.4. Finally, Section 3.5 presents a novel method to acquire the knowledge of the resource allocation

3.2 Heterogeneous Deployment Research Trends

3.2.1 Overview on spectrum sharing deployment

In this section, we will consider the spectrum sharing deployment, where inter-cell interference is the main bottleneck. However, beamforming techniques can be used to efficiently exploit the spatial domain to separate small and macro-cells. In the following subsections, we will first distinguish between two typical deployment scenarios of small-cells, i.e., the unplanned deployment and the coordinated deployment. The role of beamforming will then be discussed for each scenario.

Interference scenarios

Low-power base stations can be either user deployed or operator deployed. If the low power nodes are installed in an ad-hoc manner, directly by the end users, and can be moved, activated/deactivated at any moment (Unplanned Deployment), the traditional network planning and optimization becomes inefficient, since the operator cannot control such nodes.

[1]A PRB is the smallest time-frequency resource that can be allocated to a user

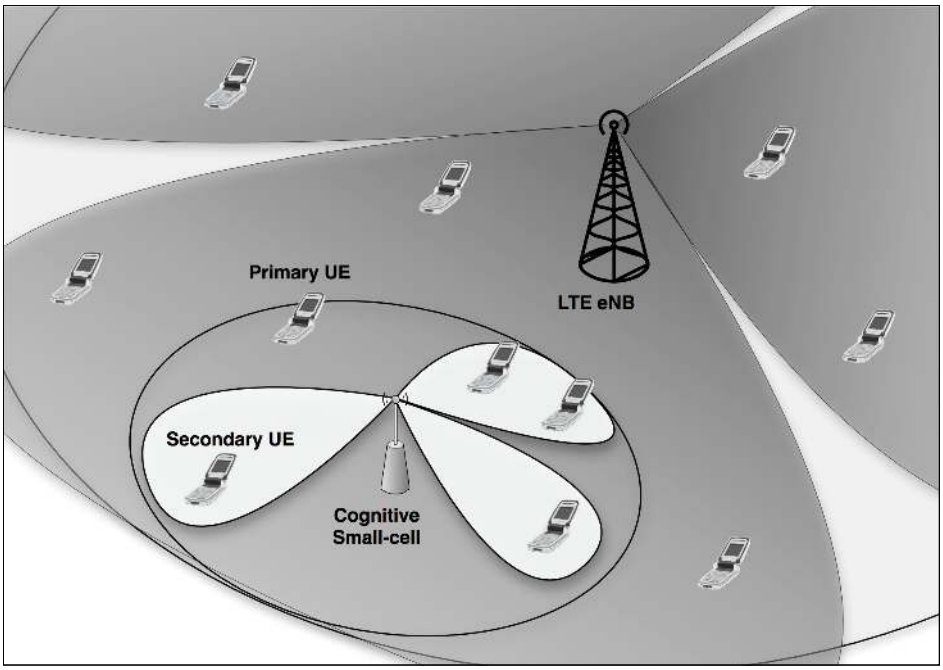

Figure 3-2: Cognitive small-cell beamforming

Therefore, new decentralized interference reduction schemes shall be introduced, which operate independently in each cell and with only local information. Low power nodes shall have *cognitive* capabilities, i.e., shall be able to monitor the network status and optimize their transmissions/receptions to improve coverage and reduce interference. On the contrary, when small-cells are installed by the operator, the transmission is coordinated by the network (Coordinated Deployment) and more efficient solutions to manage interference have been proposed to be included in the standard under definition:

- **CoMP (Coordinated MultiPoint)**. It introduces the possibility of transmitting in a coordinated way from different network points toward users that are on the cell edge and more vulnerable to interferences. Different operation modes have been supposed, from the easiest selection of the best transmission point, to the joint transmission from different network points or coordinated scheduling and beamforming schemes.

- **eICIC (enhanced InterCell Interference Coordination)**. Macro and small-cells use the same frequency channels, but they adopt a joint optimal resource allocation with the goal of using orthogonal portions of the resources to prevent co-channel interference.

Finally there are two different operating modes for small-cells, which bring different interference scenarios.

- The small-cell can be operated in the *closed access* mode and consequently some macro-cell users may be in its coverage range, but not allowed to connect. The small-cell may cause a high interference to nearby macro-cell users in DownLink (DL) transmission; on the contrary, the macro-cell user may interfere on UpLink (UL) data received at the small-cell.

- The small-cell can also be *open access*, where all users are free to connect with the small-cell. However, this will generate a load balancing problem, if each user is associated

to the small-cell only based on the received signal power, as in this case almost all users would connect to the macro-cell with the consequent reduction of advantages derived from a heterogeneous development of the network. Consequently, small-cell Range Extension solutions are suggested, which, on their turn, generate interference problems.

A general representation of a heterogeneous deployment scenario using the spectrum sharing approach is given in Fig.3-1.

Beamforming in cognitive small-cells

Interference management in heterogeneous networks can be achieved with a careful cell planning. However, in some cases, it can be very expensive and it is not even possible in an Unplanned Deployment scenario. In this case, interference management can be considered from a Cognitive Network point of view where the macro-cell is the primary system that has higher priority on the resource usage and the small-cell represents the secondary system that has lower priority.

Cognitive capabilities permit the system to autonomously identify the presence of other systems through a periodic sensing that is essential to identify the unoccupied portions of spectrum. The knowledge about the surrounding environment is used to adapt the transmission by means of power control algorithms and/or suitable resource allocation schemes in order to limit the mutual interference. The simplest way to perform a proper transmission is to use blanking techniques to avoid transmitting in regions occupied by the primary system, in this case the macro-cell. Power management algorithms can then be applied and solved by means of game theory. This technique allows to obtain orthogonal signals but reduces the spectral efficiency. In the following, we will present some more promising approaches for decentralized interference management via beamforming.

Beamforming With the recent advances in multi-antenna technologies, beamforming can be exploited to allow co-channel frequency allocation with a spatial separation of the interfering signals. Complex scenarios with many small-cells can be addressed. These techniques can be used by each secondary system, whether the system around it is a primary or another secondary system.

Small-cell is equipped with an antenna array made up of correlated elements with a distance of $\lambda/2$, by means of the radiated beam can be modeled. Steering accuracy and null beams selectivity grow linearly with the number of elements composing the antenna system.

To use of beamforming at the secondary transmitter would allow to maximize its performance while the interference to the primary receiver would be minimized. This operation, also known as Cognitive Beamforming (CB), requires solving optimization problems to find optimal precoding vectors and power allocation strategies with complex numerical solutions. CB is based on the knowledge of all the propagation channels over which the secondary transmitter interferes with the primary receiver. This is impracticable in actual scenarios as the two systems operate in an independent manner and the primary system ignores the presence of the secondary one. In [91], a CB scheme working under non-perfect channel knowledge was proposed, which would be a more practical approach. Other works, e.g., [96], focused on the optimization of the total capacity depending on the choice of the preset antenna patterns. This solution presents high complexity due to the best pattern selection search process.

Multi-antenna systems introduce also another resource dimension, namely, the direction of arrival (DOA). In particular, the small-cell beam can be steered toward a direction that maximize the information signal while nulls can be placed in the directions of arrival of

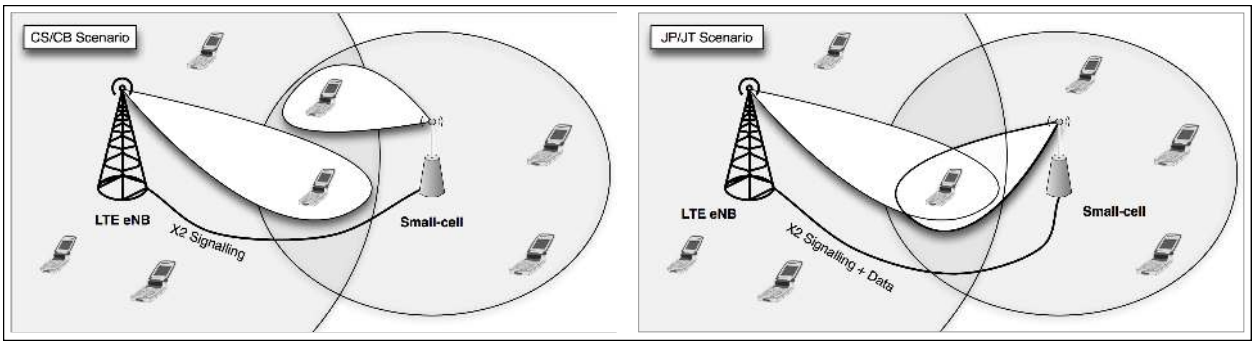

Figure 3-3: CS/CB and JP/JT approaches for CoMP.

the primary system signals as depicted in Fig.3-2. This scheme requires knowledge of the DOA of the multiple signals received from the Macro-cell User Equipments (MUEs), and the performance is strongly dependent on the propagation channel and on the number of antenna elements (i.e., the number of nulls which can be realized is limited by the number of elements of the multi-antenna system). An interesting method is proposed in [7] for small-cell interference suppression focusing on problems that arise for practical system. In particular, using a periodic sensing phase the directions of arrival of MUE signals are estimated by means of a suitable DOA Estimation algorithm. The method to calculate DOA is based on the eigenvector decomposition of the autocorrelation matrix of the received signal. This kind of method is widely explained in literature, and its high accuracy and simplicity compared to other approaches are often underlined.

The described approaches can be further improved through a cross-layer resource allocation algorithm, so that the interference reduction will be more effective, as each user of the secondary service will be allocated in correspondence of the resources of its best primary user.

Sensing Cognitive approaches can be very effective only if the knowledge of the environment is reliable. The amount of resources dedicated to sensing is an interesting trade-off and it requires to be carefully evaluated according to the operating scenario where small-cells are placed. The computational complexity depends on the sensing period and the complexity of the sensing algorithm. In addition, the sensing accuracy depends on many factors, such as the propagation channel, the angle dispersion of the multipath components and the number of samples collected during the sensing period. This last point is very important. In LTE, the smallest physical resource unit that can be allocated is a Physical Resource Blocks (PRB) that consists of 12 contiguous subcarriers. Using a single PRB to acquire knowledge about a MUE can be insufficient, leading to inaccurate estimates. The possibility of gathering together all the PRBs allocated to a given user shall represent a significant improvement (see Section 3.5).

In an Unplanned Deployment, the small-cell has no knowledge about the resource allocation performed by the macro-cell. Some works assumed that the small-cell is able to decode the control channel sent by the macro-cell, but it is not always possible. Another possibility is to apply suitable algorithms that estimate which PRBs belong to the same MUE, for example, exploiting the mutual projection of the eigenvectors obtained from each PRB. With these methodologies, the cognitive approach of beamforming will be an efficient and practical way to suppress interference in the Unplanned Deployment scenario.

Beamforming with CoMP

The small-cells may also be deployed by the same operator. In this way, different tiers of access nodes can be interconnected through an interface, as the X2 interface in LTE provided for the information interchange between TPs. Such coordinated deployment is radically different from the cognitive-based schemes explained previously. With efficient coordination, the signal received from other cells can be used constructively and it can be an information resource rather than an interference source. This is the basic idea behind the Coordinated Multi-Point.

The CoMP schemes can be considered as an evolution of the ICIC, that is a technique to reduce the interference through a coordination between neighbouring cells. So far, ICIC algorithms proposed in the literature are based on two approaches: Frequency Reuse Partitioning and Power Control. The CoMP evolution brings higher flexibility of the exchanged information, ranging from a static or semi-static approach to dynamic joint decision about the scheduling. It allows to take full advantage of the increased capacity offered by heterogeneous systems especially by means of beamforming algorithms, which allow the spatial reuse of the resources by avoiding mutual interference and efficiency loss.

In general, joint resource allocation can be managed with:

- *hierarchical* schemes, where an eNB set elects a master (usually one eNB or the Mobility Management Entity-MME) to be in charge of coordinating some operations and the decision-making on behalf of the group.

- *horizontal* schemes, where the same algorithm runs at each CoMP node and it will return the same resource allocation pattern.

3GPP has highlighted two approaches for CoMP that mainly differ on the required network signalling overhead. These are shown in Fig.3-3 and described in what follows.

The former LTE CoMP scheme is named **Coordinated Scheduling/Coordinated Beamforming (CS/CB)**. It is based mostly on the sharing of information provided by each terminal to its TPs (Transmission Point), as well as other information exchanged among TPs to contribute to a joint decision. In this context, the data addressed to a specific UE is transmitted by a single TP, while other TPs can use the same radio resources (i.e., the same PRBs) to transmit to angularly separated UEs using beamforming. There have been a number of proposals aiming to reduce the coordination complexity and the required side information, e.g., it was proposed in [97] that interference can be suppressed through spatial cancellation with multiple antennas at the base station, which would require only local side information. For the CS/CB approach, the signalling increase is limited and the X2 interface provides adequate capacity. This scheme also allows to borrow some techniques devised for cognitive small-cells, as both the schemes are based on the use of spatial diversity. On the other hand, the key role of beamforming in CS/CB will be much more effective than in cognitive beamforming, since more accurate side information is available.

The latter CoMP scheme proposed by the 3GPP is named **Joint Processing/Joint Transmission (JP/JT)**. When a higher signalling overhead is supported, more sophisticated cooperation can be applied. In JP/JT, data transmission for each UE is done simultaneously by multiple TPs. Hence, the UE can combine multiple copies of the signal to improve the received signal quality. The waste of resources due to multiple transmissions is compensated by beamforming that allows to spatially reuse the same resources to transmit toward angularly separated UEs.

This scheme requires that the user data is available at all TPs, so the main challenge is represented by the high capacity requirement of the backhaul links, which represents a

Table 3.1: Spectrum sharing techniques comparison

	Cognitive Systems	**Coordinated Systems**
Deployer	User/Operator	Operator
Network signalling overhead	Low	High
Capacity loss	During sensing step	No
Environmental information amount	Low	Up to high
Environmental information accuracy	Low-medium	High
Hardware requirement	Sensing equipment	High data rate back-haul

bottleneck for this solution. One efficient approach to reduce the signaling overhead and the backhaul requirement of JP/JT is clustered cooperation [98], where TPs within the same cluster will coordinately serve users in this cluster and some form of inter-cluster interference management may also be performed. For the further evolution along this path, as the operators are starting to upgrade their backhaul links, a more radical approach for coordination has been recently proposed, which is the cloud radio access network (C-RAN) [99]. In this new architecture, all the baseband signal processing is shifted to a single baseband unit pool, thanks to the high-capacity backhaul links which will normally be supported by optic fibers. Such a network architecture will enable efficient centralized resource allocation and interference management, which can then greatly improve both the network capacity and energy efficiency.

In conclusion, in many emerging scenarios, where the high density of heterogeneous systems will stress the problems due to the interference, the benefits offered by CoMP are very attractive. However, it is challenging to implement in practical systems. In particular, two main issues should be addressed. One is the dynamic settlement of the CoMP areas and the topology updating algorithms for the TPs involved in a joint process; the other is the signalling overhead as well as the impairment in the available side information, e.g., imperfect channel state information. Lots of efforts have been put on these aspects, and there is no doubt that CoMP will be an essential part in future communication networks.

3.2.2 Separated bands deployment

One of the most discussed proposals to overcome inter-cell interference is to deploy small-cells in a higher frequency band. Indeed, the limited available spectrum makes dedicated deployment of small-cells in the current cellular band very unlikely. On the other hand, large bandwidths at higher frequencies ($f_c > 10$ GHz) are still unexplored, primarily due to the harsh propagation conditions of the radio channel. The main challenge is represented by the path loss, which is proportional to a power (usually greater than 2) of the carrier frequency and, hence, any signal in high frequency band would suffer a deep attenuation. For example, assuming the system is moved from 2 to 20 GHz, the received signal would suffer an attenuation penalty of at least 100 dB, which will in turn reduce the system

Table 3.2: Different frequency techniques comparison

	Conventional Bands	**mmWave Bands**
Carrier frequency	≤ 3 GHz	$\approx$ 30 GHz
Available spectrum	Low	High
Supported antennas	$\leq$10	$\approx$100
Beamforming performance	Low-medium	High
Channel conditions	-	High atmospheric absorption Low penetration depth

coverage. Hence, it becomes of cardinal relevance for future deployments to find transmission techniques aiming to improve the quality of the link in order to counteract this drawback.

In particular, Massive MIMO represents a particular interesting technology. It consists of using a very large number of antennas to fully exploit the spatial diversity among the users. A possible application is to form very narrow beams to provide a significant gain that can partially counteract the increased path loss. One of the major problems of Massive MIMO in conventional operating bands is the dimension of the antenna system, which may be acceptable for large installation like the LTE eNB, but is completely inappropriate for domestic use. On the other hand, in a high operating frequency range, the antenna element dimension becomes smaller and then this technology will be more applicable.

From the above discussion, high frequency deployment and Massive MIMO are closely related. Massive MIMO can be seen as an enabling technology for communications in high frequencies, and, at the same time, the small antenna size at high frequency makes Massive MIMO practical.

Massive MIMO

Massive MIMO represents a new research field that spans communication theory, propagation characterization and the associated electronic component design. Recently, this topic has attracted great attention from both academic and industry, thanks to its great potential in improving communication performance [100]. Massive MIMO systems consist of equipping base stations with antenna arrays composed of a large number (i.e., a hundred or more) of small antennas plugged together. Ideally, with a widely separated antenna array, each additional element adds a degree of freedom that can be exploited, which introduces very attractive advantages. In [101], it is demonstrated that if the number of base station antennas M is much larger than the number of antennas per terminal K, such that $M/K \gg 1$, then deploying more and more antennas is always beneficial, i.e., the effects of fast fading and correlated noise decreases toward zero, even in low SNR (Signal to Noise Ratio) environments. By relying on very simple signal processing, Massive MIMO can increase the link capacity and at the same time improve the radiated energy-efficiency [102, 103]. This is achieved by focusing signal strength in a specific direction and creating very narrow radiated beams. Hence, it is possible to efficiently transmit independent data flows to different user terminals during the same time-frequency block, thus exploiting spatial separation of the users (*multi-user* beamforming). It is straightforward to note that strategy can be used symmetrically in

the uplink, by using the high beam resolution to split in the angular domain different signals arriving in the same time/frequency slot.

The creation of very narrow beams also permits to reduce the inter-symbol interference thus decreasing the spectrum inefficiencies of the cyclic prefix in OFDM (Orthogonal Frequency Division Multiplexing) symbols. In addition, the total available transmission power is spread among the M antennas, allowing the reduction of per-antenna power consumption. In [103], it has been showed that for an eNB equipped with a linear detector, Massive MIMO can decrease the amount of per-user transmission power. The amount of saved power is inversely proportional to the size of the antenna array in the case of perfect Channel State Information (CSI), while to the square-root of the number of antennas for imperfect CSI. This leads to the general complexity reduction of radio frequency front-end of the eNBs and also allows to apply inexpensive low-power components. The usage of Massive MIMO also leads to a significant reduction of latency on the air interface, since it dramatically reduces the probability of having fading dips affecting received signals. Finally, robustness regarding intentional and unintentional jamming is increased thanks to the presence of many excess degrees of freedom that can be used to eliminate signals coming from jammers.

We conclude that by implementing small-cells equipped with Massive MIMO is possible to efficiently use the available frequency resource, reduce the interference and assure improved transmission capabilities. However there are some main challenges that need to be addressed.

Challenges in Massive MIMO

In theory, Massive MIMO systems can achieve all the performance improvements as stated above. In practice, the design of very large array systems suffer from several implementation issues that need to be resolved.

Antenna dimension The realization of Massive MIMO systems requires that more than hundred small antennas are placed at the eNB front-end [104]. This leads to the implementation of 2-D or 3-D antenna arrays where the coupling effects among antenna elements are more evident, thus reducing the system capacity. In addition, there is a need of a significant physical space to accommodate the antennas. The deployment in higher radio spectrum for small-cells means that the base station antennas can be designed without the need of large spaces, easing the placement problem.

Channel state information To correctly operate massive MIMO systems need to acquire CSI. Traditionally, in multi-antenna systems, pilots are sent by each antenna element in the DL. This is not possible when the number of antenna elements is very high, as the number of pilot symbols would become too high, especially in mobility scenarios with short channel coherence time. As a consequence, massive MIMO systems shall operate in the TDD (Time Division Duplexing) mode, where channel reciprocity can be exploited and CSI will be estimated at the eNB. However, when the number of user equipments is high, acquiring reliable and updated CSI will still be challenging and represent an interesting research topic. In particular, in mobility conditions the support of control signaling and connectivity when operating with high directive links is not trivial.

Signal processing When the number of antenna elements increases, the complexity of the algorithms used to determine suitable precoding vectors or decoding processes also increases. This requires suitable optimizations especially for small-cells deployment, since in this case the transmission points have less computational resources. To provide very accurate narrow beams that can follow UEs represents an important issue to be investigated, especially in the mobility environment. A possible solution is the use of low complexity algorithms which can be implemented directly in hardware. The loss of performance due to

the simplicity of the algorithm would be compensated by effects of the high antenna number.

3.3 Cognitive Zero Forcing Beamforming in Actual Environment

Focusing on a user deployed HeNB with restricted access, this section proposes a system to reduce the interference due to a small-cell on the DL of a primary system (i.e., LTE macro-cell) by exploiting the angle dimension. The small-cell is equipped with a multiple antenna system and is able to estimate the DOAs of the multiple signal replicas received from different Macro-cell User Equipments (MUEs) by using suitable sensing intervals in the uplink frame. The small-cell will then transmit using a null steering algorithm, also known as ZF beamforming, in order to reduce the interference toward the MUEs. The proposed approach takes into account actual propagation conditions. Assuming that the small-cell is placed indoor, then the signals transmitted by the MUEs will follow different propagation paths that can have very different DOAs [105] that are varying in time. This leads to a number of received signals that is higher than the number of antennas. The proposed solution is to work on a PRB (Physical Resource Block) basis, where the PRB is the smallest resource unit that can be allocated to a UE in a LTE frame, because the resource allocation of the macro-cell is supposed to be unavailable.

3.3.1 System model

In the operating scenario considered here, the secondary system is represented by a user-deployed HeNB and the primary system is the macro-cell base station (eNB). Thus, the UEs of the primary service that are located within the small-cell coverage receive the DL signal of the eNB with partial or complete overlap of the HeNB downlink with a consequent performance degradation. Both systems are modeled according to the 3GPP LTE-Advanced standard [106], by considering FDD (Frequency Division Duplexing) mode and different bandwidths ($1.25 - 20.0$ MHz). In order to take into account the worst interference conditions, we assume that the two systems operate with the same carrier frequency, $f_0 = 2$ GHz, and bandwidth. The HeNB must be able to perform DOA estimation and digital steering. Hence, it is equipped with a linear array of antennas consisting of L equally spaced elements. The number of antennas has been selected in order to take into account the device dimension. It is well known in the literature that as the number of antenna elements increases the system performance improves. In particular, the DOA estimation becomes more accurate and the number of resolvable directions grows linearly with the number of the antennas as well as the beam directivity (or the null selectivity). On the other hand, a high number of antenna elements leads to higher computational load and higher antenna dimension.

Considering that the array elements are uniformly spaced with $d = \lambda/2$ and $f_0 = 2$ GHz, the spacing D required to deploy L antennas is

$$D = \frac{(L-1)c}{2f_0} \tag{3.1}$$

where c is the light speed. This means that each antenna element requires 7.5 cm (about 3 inches). Here we assume a HeNB provided by $L = 4$ antennas, leading to a total dimension $D = 22.5$ cm. This choice allows us to perform accurate beamforming operations [107] while the device dimension are similar to those of other household devices, e.g., WiFi access points.

Table 3.3: Number of replicas in indoor ITU-R M.1225 channel

B (MHz)	1.25	2.50	5.0	10.0	15.0	20.0
$\mathbf{F_s}$ (MHz)	1.92	3.84	7.68	15.36	23.04	30.72
Paths	1	2	3	4	4	4

A grater number of antennas would lead to better performance but also to an unlikely bulky structure.

The proposed system takes into account multipath propagation effects using the tapped-delay-line model defined in the ITU-R M.1225 Reccomendation [48]. Two different Power Delay Profiles (PDPs) are considered:

- Outdoor-A for the eNB and the MUEs links;
- Indoor-A for the HeNB and the MUEs links.

Considering M signal replicas, the propagation channel can be represented by a vector $\mathbf{h}$

$$\mathbf{h} = [\alpha_1 e^{j\phi_1}, \quad \alpha_2 e^{j\phi_2}, \quad \cdots \quad , \alpha_M e^{j\phi_M}]^T \tag{3.2}$$

where α_i and ϕ_i with $i = 1, 2, \cdots, M$ are attenuation and phase, respectively, of the i-th signal replica. These are independent random variables whose statistical distribution is Rayleigh for α_i and uniform in $[-\pi, \pi]$ for ϕ_i according to [48]. The number of resolvable paths, M, depends on the PDP, but also on the system bandwidth and the sampling frequency of the receiver since the signal is received through a set of time domain samplings as shown in Table 3.3. In addition to the channel phase shift we have to take into account also the phase shift due to the DOAs of the signals. The received signal replicas arrive to the antennas through a series of rays arranged in clusters, each one from a different direction. The power distribution of the rays forming the cluster has a strong angular concentration, therefore the average value is the best candidate to feature the angle of arrival of the whole cluster [105, 108]. The DOAs of different clusters received by the indoor HeNB vary depending on the environment and the scatters position and thus an uniform angular distribution of clusters in $[0, 2\pi]$ is the more realistic choice [105].

The i-th signal replica arrives on the antennas forming the angle θ_i with array perpendicular. The propagation delay of the i-th signal between two consecutive antenna elements is:

$$\tau = \frac{d \sin(\theta_i)}{c} = \frac{\sin(\theta_i)}{2 f_0}. \tag{3.3}$$

By considering $\tau \ll T_s$, where T_s is the sampling period, the arriving signal phase is rotated by $2\pi f_0 \tau$. Hence, the n-th sample of the signal received by l-th antenna element can be expressed as

$$r_l[n] = \sum_{m=1}^{M} x[n - \tau_m] \alpha_m e^{j[\phi_m + \pi(l-1)\sin(\theta_m)]} + v_l[n] \tag{3.4}$$

where $x[n]$ is n-th sample of the transmitted signal, τ_m is the delay introduced by the m-th propagation path expressed in samples, and $v_l \sim \mathcal{N}(0, \sigma_v^2)$ is the AWGN noise with zero mean and variance σ^2.

Let us denote the $\mathbf{s}(\theta)$ vector containing $s_l(\theta) = e^{j\pi(l-1)\sin(\theta)}$ elements, with $l = 1, 2, \cdots, L$ and $i = 1, 2, \cdots, M$, usually referred to the literature as steering vector, since it can be used

to steer the antenna system on the direction θ. Let

$$\mathbf{S} = [\mathbf{s}(\theta_1), \quad \mathbf{s}(\theta_2), \quad \cdots, \quad \mathbf{s}(\theta_M)] \tag{3.5}$$

denote the matrix containing the steering vectors of the incoming signals DOAs, the received signal can be expressed in matrix form by

$$\mathbf{r} = \mathbf{S} \cdot \mathrm{diag}(\mathbf{h}) \cdot \mathbf{x} + \mathbf{v} \tag{3.6}$$

where $\mathbf{x} = \left[x[n - t_1], \cdots, x[n - t_M]\right]^T$ and $\mathrm{diag}(\,\cdot\,)$ denotes the diagonal matrix.

3.3.2 Adaptive interference suppression method

In this section, we describe the method to reduce the HeNB interference on the MUEs during the DL reception. The HeNB performs a first phase of sensing during which it identifies the directions of arrivals of the primary users signals. The HeNB schedules one OFDM symbol in each-sub frame in the uplink transmission to estimate the DOA and track the MUEs mobility. In particular the LTE uplink frame supplies one OFDM symbol in each slot as reserved for the transmission of the Sounding Reference Signals (SRSs) usually allocated to the UEs to provide channel state information (CQI) to the eNB. The sensing procedure can take place in one of these OFDM symbols, once for each subframe. In the second phase, the proposed method calculates the suitable weights to modify the radiation pattern in order to place zeros in correspondence with the estimated directions during its DL transmission. However, an ideal implementation of this scheme is not possible in actual scenarios. Any DOA estimation algorithm can detect up to $L - 1$ directions of arrival and the Null Steerer algorithm can place $L - 1$ nulls in the sought directions. When more than one MUE is present in the small-cell area, and each one is characterized by a PDP composed of multiple replicas, it is very likely that the number of received signals is higher than $L - 1$.

To solve this problem, the proposed system works on a PRB-wise way. In LTE the smallest resource unit that can be allocated to a user is a PRB. It is defined as a set of 12 contiguous subcarriers [106] over two consecutive OFDM symbols. Each PRB, at a given time, can be allocated to only one user. Performing DOA estimation and null steering on each PRB permits to estimate $L-1$ DOAs for each PRB and, hence, to separate the MUEs signals in reception and transmission. In [7], the authors proposed a system where all the subcarriers are allocated to a single user, and thus the number of received signals depends only on the PDP of the channel. In that way the snapshot (i.e., the available samples on which the DOA estimation algorithm works) used to estimate the DOA is composed by all the subcarriers. However, this system does not take into account the actual LTE multiple access scheme based on PRBs and the presence of multiple users. Performing DOA estimation on a reduced snapshot (i.e., the PRB) reduces the estimation accuracy.

DOA estimation

The sensing stage used by the HeNB to estimate the signal DOAs lasts 71.43 ns (1 OFDM symbol) and it is performed on the SRSs sent by the MUEs. We consider a widely known family of DOA estimation algorithms known as MuSiC (Multiple Signal Classification). It is based on the decomposition of the autocorrelation matrix of the received signal and the knowledge of the amount of incident signals on the antenna.

The Root-MUSIC has been selected [109]. At the first stage the MuSiC algorithms estimated the autocorrelation matrix from the received signal samples. Then eigenvalues

and eigenvectors are properly derived. The received signal autocorrelation matrix is defined as

$$\begin{aligned}\mathbf{R_r} &\triangleq E\big[\mathbf{r}\mathbf{r}^H\big] \\ &= E\big[\mathbf{S}\ \mathrm{diag}(\mathbf{h})\ \mathbf{x}\mathbf{x}^H \mathrm{diag}(\mathbf{h})^H \mathbf{S}^H\big] + E\big[\mathbf{v}\mathbf{v}^H\big] \\ &= \mathbf{S}\mathbf{P}\mathbf{S}^H + \sigma_v^2 \mathbf{Id}_L \end{aligned} \tag{3.7}$$

where $\mathbf{Id}_L$ is the identity matrix with dimension $L \times L$, $\cdot^H$ represents the hermitian transformation and $\mathbf{P}$ is defined as

$$\mathbf{P} = E\big[\mathrm{diag}(\mathbf{h})\ \mathbf{x}\mathbf{x}^H \mathrm{diag}(\mathbf{h})^H\big]. \tag{3.8}$$

The eigenvectors are sorted in a descending order according to the value of the corresponding eigenvalue and divided two subspaces with the first called signal subspace $\mathbf{U}_S$ and it is made up of the N eigenvectors with greater eigenvalues. The second one is called the noise subspace $\mathbf{U}_V$ and it is composed by the remaining eigenvectors with smaller eigenvalues. N is equal to the number of received signals if it is lower than $L-1$ or to $L-1$, otherwise. In particular, if N is not known, the two subspaces can be split by relying on power of uncorrelated noise incident on the antenna. Indeed, all the eigenvalues corresponding to the signal subspace eigenvectors are greater than the noise power

$$\lambda_1 > \lambda_2 > \cdots > \lambda_N > \lambda_{N+1} = \cdots = \lambda_L = \sigma^2 \tag{3.9}$$

The two subspaces are orthogonal to each other due to the algebraic construction, and therefore, they are disjoint. Moreover, their union contains all the steering vectors. It follows that calculating the value of the projection on the noise subspace of each steering vector ($\|\mathbf{s}^H(\theta)\mathbf{U}_V\|$), the lowest N projection values are related to the N signal directions of arrival.

In particular, the classic formulation of MuSiC, named Spectral MuSiC looks for the peaks of the function

$$P_{SM}(\theta) = \frac{1}{\|\mathbf{s}^H(\theta)\mathbf{U}_V\|}. \tag{3.10}$$

When the steering vector is orthogonal to the noise subspace, its projection is zero and the function has a peak. However, the peaks of (3.10) are strongly influenced by the received signal-to-noise ratio (SNR) value. The Root-MuSiC scheme considered here tries to solve this impairment. The localization of the functional peaks is replaced by the evaluation of the roots of the polynomial in the denominator of (3.10). This is carried out through a problem reformulation in the z domain, so that the roots closest to the unit circle may be determined. The denominator of (3.10), in case of an antenna array with equispaced elements, can be written as:

$$\begin{aligned} P_{SM}(\theta)^{-1} &= \mathbf{s}^H(\theta)\mathbf{Q}\mathbf{s}(\theta) \\ &= \sum_{p=1}^{L}\sum_{q=1}^{L} e^{-j\pi(p-1)\sin\theta} Q_{p,q} e^{j\pi(q-1)\sin\theta} \\ &= \sum_{l=-L+1}^{L-1} q_l e^{-j\pi l \sin\theta} \end{aligned} \tag{3.11}$$

where $\mathbf{Q} = \mathbf{U}_N \mathbf{U}_N{}^H$ and $q_l \triangleq \sum_{l=-q} Q_{p,q}$ is the sum elements of $\mathbf{Q}$ on the l-th diagonal.

Evaluating the peaks of $P_{SM}(\theta)$ is equivalent to compute the polynomial roots of $D(z)$ on the unit circle, where the polynomial is defined as:

$$D(z) = \sum_{l=-L-1}^{L-1} q_l z^{-l} \tag{3.12}$$

This leads to an improvement of the DOA estimation accuracy for low SNR values and allows us to distinguish even close signals. In addition, Root MuSiC does not require the selection of a suitable threshold for the selection of the peaks.

When the number of received signal N is higher than $L-1$, the splitting of the two subspaces (i.e., signal and noise) can still be enforced to $L-1$ and 1 respectively. However the noise subspace is interfered by the useful signal and they are no longer disjoint. This leads to a loss of the DOA estimation capabilities that increases with N. In general, the number of received signals, N, is given by the number of MUEs in the HeNB coverage area, K, multiplied for the number of multipath components, M. In order to manage efficiently a number of received signals higher than $L-1$ the PRB-wise algorithm is introduced. Root MuSiC algorithm is performed for each PRB estimating up to $L-1$ DOAs. The signal received during the stage of sensing is transformed into the frequency domain, splitted in PRB parts and later they are transformed back into the time domain to achieve a snapshot of 12 temporal samples. When the number of incident signals is greater than $L-1$ only the most powerful signals are selected. By operating on a PRB basis it is possible to separate the users' signals because each PRB is allocates to a different user.

Zero forcing beamforming

The estimated directions are used as input to a ZF beamforming algorithm that returns L complex weights w_l with $l = 1, \cdots, L$, by placing the radiation pattern nulls at the selected directions. In particular, the null steering algorithm is based on the same theoretical construct of the classic beamformer and it generates a vector of L weights consisting of complex numbers that adjusts the amplitude and the phase of the output signal from each antenna. Hence, it is possible to select a main direction of steering and the location of the $L-1$ nulls[2].

The modified radiation pattern is obtained by multiplying the time domain signal and the suitable weights. The w_l weights are obtained by imposing that the steering vector $\mathbf{s}(\varphi)$ is equal to 1 and the steering vectors $\mathbf{s}(\theta_1), \mathbf{s}(\theta_1), \ldots \mathbf{s}(\theta_{L-1})$ are zero. Mathematically the just described constraint is achieved by identifying the matrix of the steering vectors of interest $\mathbf{A} = \big[\mathbf{s}(\varphi), \quad \mathbf{s}(\theta_1), \quad \mathbf{s}(\theta_2), \quad \cdots, \mathbf{s}(\theta_K)\big]$ and $\mathbf{c} = [1, 0, \cdots, 0]^T$ that is the vector of the related constraints. In general, $\mathbf{A}$ is not a square matrix and the weights are obtained by solving

$$\mathbf{w}^H = \mathbf{c}^H \mathbf{A}^H (\mathbf{A}\mathbf{A}^H)^{-1}. \tag{3.13}$$

The algorithm limits are inherited from the linear arrays theory and therefore each weights vector is able to model $L-1$ nulls, it is not enough to reduce the interference of all MUEs that can be found in the HeNB coverage. As for the DOA estimation algorithm also the null steering is performed in a PRB-wise way. One weights vector is generated for each PRB and then it is used to weight the subcarriers belonging to that PRB.

Operating in this way on each group of 12 subcarriers different weights are obtained and

[2]In the radiation pattern of a linear array with L antenna elements there are always $L-1$ nulls and L beam.

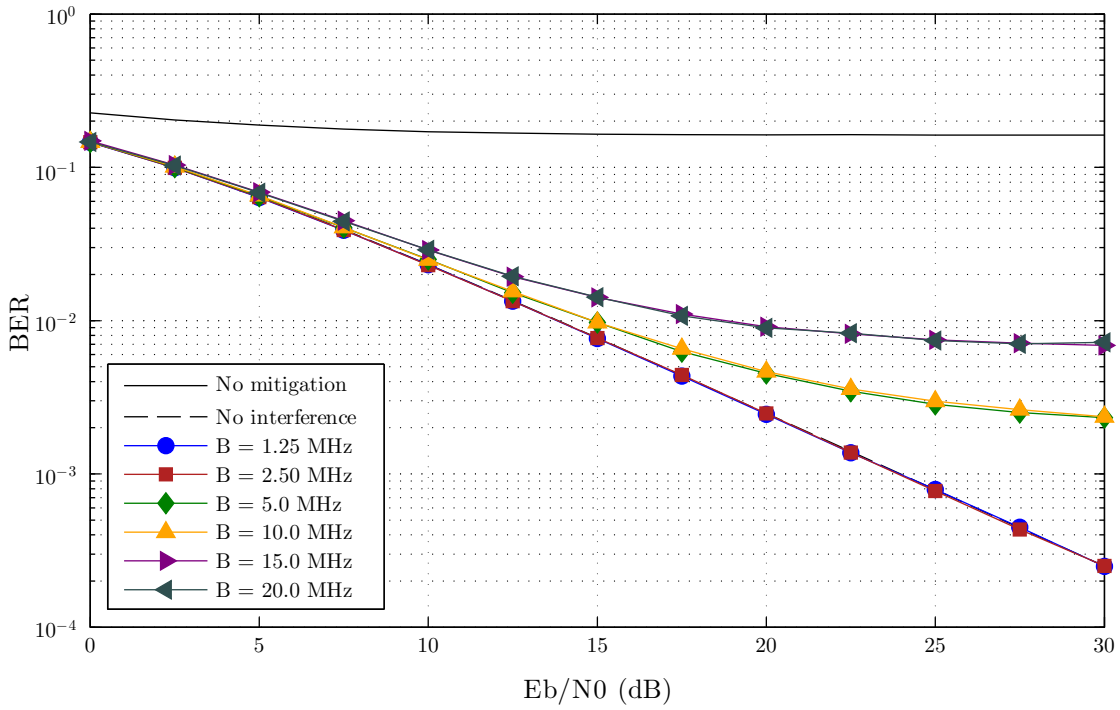

Figure 3-4: Macro-cell DL BER performance of the proposed system when ideal DOA estimates are available at HeNB.

thus nulls in different positions depending on the group of selected frequencies. The radiation pattern has deep selectivity in the neighbourhood of nulls for each group of frequencies, similar to a notch filter, allowing to obtain a strong reduction of the interference.

Snapshot issue

The interference mitigation scheme described above is mainly subject to errors due to DOAs estimation. Fig. 3-4 shows the Bit Error Rate (BER) experienced by the MUEs in the DL communication when the proposed interference mitigation system is applied and the DOAs of the received signal replicas are perfectly known at the HeNB. The BER performance is expressed as a function of the ratio between the received energy per bit, E_b, and the noise spectral density, N_0, for different operational bandwidths (i.e., for a different number of resolvable multipath components, see Table 3.3). It is possible to note that if the number of multipath components introduced by the propagation channel is lower than L the system is able to completely eliminate the small-cell interference. The performance worsen for the highest operational bandwidths because the number of resolvable paths is higher than $L-1$ and there is a residual interference due to the 4th path that cannot be deleted. DOA estimation errors weaken the effectiveness of the proposed scheme because the Null Steerer places the nulls to the wrong directions as shown in Section 3.3.3.

In general, the failure in the DOA estimation depends mainly on three factors: the number of antenna elements, the SNR value of the received signal during sensing and the size of the snapshot. As stated in Section 3.3.1, the number of antenna elements is one of the main operational constraints we have considered. In addition we selected a DOA estimation algorithm able to provide a high accuracy even when the received signal is degraded (i.e., low SNR values). The third factor, the snapshot size, is widely addressed in the literature [109, 110]. Usually MuSiC algorithms optimally work for oversized snapshots which

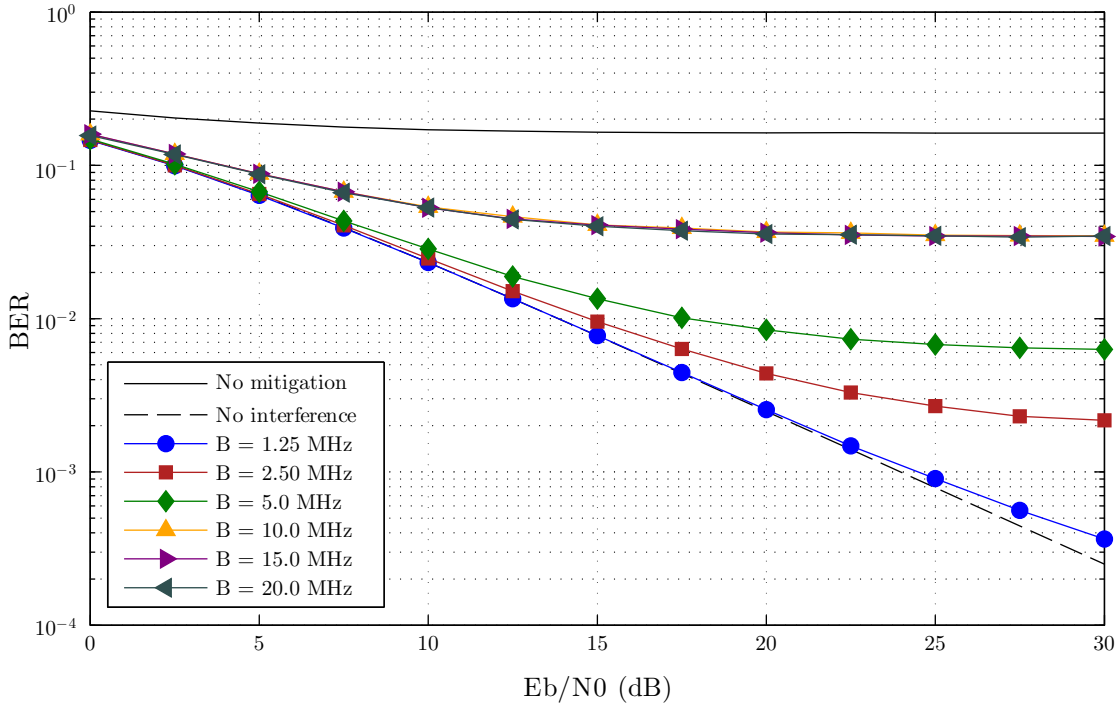

Figure 3-5: Macro-cell DL BER performance of the proposed system. E_b/N_0 of $link_1 =$ dB

are not available at the receiver in certain contexts. The main solution proposed in the literature is to rely on a high number of antennas, even doubly the number of the signals to be detected. Alternatively, the data received during the different sensing stages could be temporarily collected averaging the values of the autocorrelation matrix. However, the resource allocation of the MUEs should remain unchanged for the averaging time and it cannot be guaranteed. The solution could be increasing the snapshot dimension in the frequency domain by gathering together PRBs belonging to the same user. This would also lead a reduced computational complexity because Root-MuSiC and Null Steering algorithms would be carried out fewer times. However, it requires the knowledge of the MUEs uplink resource allocation that cannot be known a priori. Indeed, in LTE there is a wide variability in the frequency allocation of the PRBs that depends on the system bandwidth, but also on the number of active UEs, the selected scheduling algorithm and the type of data flows. This problem can be addressed by introducing algorithms able to group the PRBs belonging to the same users. We refer to two possible methods for PRBs clustering. The first one is based on a preliminary row estimation of the DOA of the main signal component on each PRB and the second on the similarity of eigenspaces signal belonging to the same user.

As shown in the next section, the efficiency of the DOA estimation algorithm depends on the number of used PRBs. Hence, it varies between a lower and an upper bound. The worst case occurs when the PRBs clustering information is not available (i.e., it is no possible to estimate which PRBs belongs to the same user) or each PRB is allocated to a different user. It follows that the size of the used snapshot by the DOA estimation is the equal to the PRB size and some inaccuracies are introduced when the number of incident signals is high. Instead, the upper bound is reached when all the PRBs are assigned to a single user and this information is available at the HeNB. In this case the snapshot is made up of all the subcarriers and the proposed system achieves good performance also for high system bandwidth. This particular case coincides with considering an OFDM system like in [7].

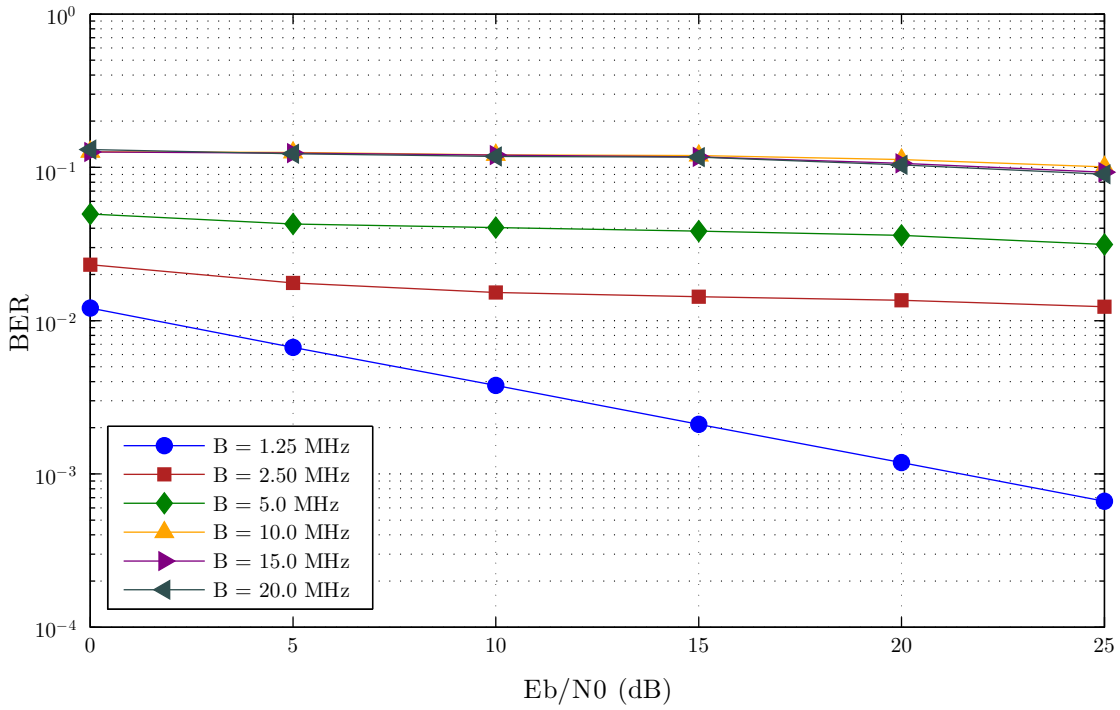

Figure 3-6: DOA estimation errors.

3.3.3 Performance analysis

This section presents sample numerical results obtained through computer simulations in order to validate the proposed system.

In order to facilitate the description of the results we shall use the following notations as:

- $link_1$ the link between the MUE and the HeNB that is used for DOA estimation;
- $link_2$ the macro-cell DL connecting the eNB and the MUE.

Firstly, the BER of the macro-cell downlink communications is evaluated when the proposed interference mitigation scheme is applied at the HeNB. The values are derived as a function of the $link_2$ E_b/N_0 when $link_1$ E_b/N_0 is equal to 10 dB. From Fig. 3-5 it can be observed that performance worsen with the increasing of the number of signals replicas generated by the propagation channel. For bandwidths greater than 5 MHz the number of propagation paths exceeds the estimation capabilities of MuSiC algorithm and the number of nulls that can be placed in the transmission radiation pattern by the HeNB. Hence, the MUE receives interference form some propagation paths that cannot be detected and canceled. This leads to a performance floor. However,a significant perfromance improvement is evident respect to the case without mitigation. The curves for $B > 5$ MHz have a common trend due to the same Power Delay Profile of the channel. It is important to underline that in actual scenarios user-deployed HeNB, likely will have small operational bandwidths. In this case the proposed system achieves very good performance.

As stated before the proposed algorithm performance strongly depends on the precision of the DOA estimation. For this reason Fig. 3-6 presents the DOA estimation error performed by the Root-MuSiC as a function of the E_b/N_0 received on $link_1$. The value of the *Weighted Euclidean DOA error* is computed weighting the error with weights, g_i, proportional to the magnitude of each replica, i.e., $g_i = E\left[{\alpha_i}^2\right]$, where α_i is defined in equation (3.2).

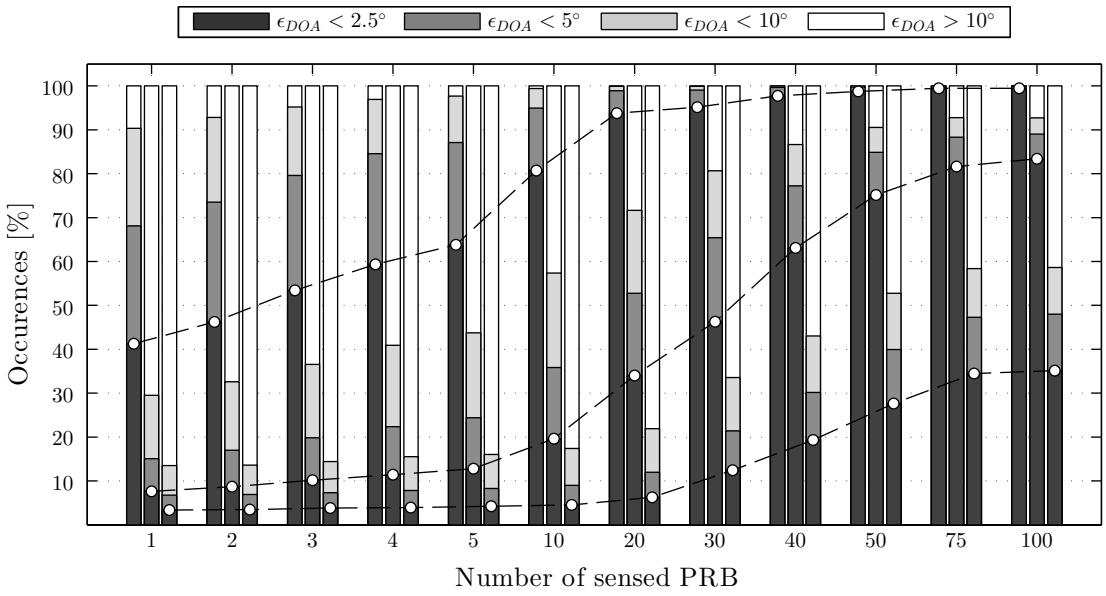

Figure 3-7: DOA estimation precision as a function of the PRBs in the snapshot used for sensing.

When $B = 1.25$ MHz the error curve decreases linearly with the E_b/N_0 and DOA estimates are very accurate. As the bandwidth increases also the DOA estimation error increases due to the contribute of the weakest signal replicas. It can be noted that there is not a significant performance improvement neither for high E_b/N_0 values. However, DOA estimation capabilities can be improved by increasing the snapshot used by the Root MuSiC algorithm, as explained in Section 3.3.2.

Fig. 3-7 shows the precision of the DOA estimates as a function of the number of PRBs that compose the snapshot used for sensing, in the worst case, i.e., $B = 20$ MHz. For each abscissa value there are three bars representing the DOAs estimation error occurrences of the three, $(L-1)$, estimated paths. Different shades of gray are used to distinguish the interval of errors: $[0, 2.5°], [2.5°, 5°], [5°, 10°]$. It can be seen that the first path is always detected with high accuracy, even with a limited number of PRBs. Conversely, the second and third paths DOA estimates presents a good precision by increasing the number of sensed PRBs.

Clearly by gathering together PRBs belonging to the same user it is possible to improve significantly the performance of the proposed interference suppression method even for high system bandwidth.

3.4 Angular Resource Allocation

This section proposes a joint beamforming and resource allocation scheme for a LTE-A system which utilizes the angular information (i.e., DoA) of the primary and secondary User Equipments (UEs) instead of the channel state information of the interference links. In particular, the femto-cell acquires information about the geographical position of the Macro-cell UEs (MUEs) and Femto-cell UEs (FUEs) without making use of any form of coordination with the macro-cell. The surrounding environment is heard by means of a periodic sensing phase and the DoAs are estimated thanks to the presence of a multiple antenna system [7]. DoA information is exploited to allocate the time-frequency resources to the FUEs that minimize the interference toward the primary MUEs and maximize the

femto-cell capacity. In particular, two methods are proposed here. The first represents the optimal solution, it determines the achievable gain for each FUE in each resource unit and performs an optimal allocation that maximizes the capacity of the FUE with the constraint of avoiding the transmission in the MUE directions. The second is a faster heuristic method, based only on the information obtained from the sensing step (i.e., DoA), thus reducing the computation complexity. Both methods represent a very simple transmit strategy that can be easily implemented in practice. Performance is presented in terms of femto-cell capacity and MUEs error probability in order to evaluate either the effects on the secondary or primary systems. DoA estimation errors have been taken into account. The performance of the proposed methods is compared with that of a conventional Beamforming that maximizes the small-cell capacity without taking into account the MUEs presence and with that of a ZFBF that avoids transmission in the intended directions but does not perform suitable resource allocation to the FUEs.

3.4.1 System model

We consider a cognitive user-deployed femto-cell (Home eNB, HeNB) that shares the spectrum resource with a primary macro-cell in a LTE-A heterogeneous network, as illustrated in Fig. 3-8. Both systems are modelled according to the 3GPP LTE-Advanced standard [106], considering FDD (Frequency Division Duplexing) mode. In order to take into account the worst interference condition, we suppose the two systems operate with the same carrier frequency, f_0, and bandwidth. The small-cell base station is equipped with L antennas spaced of $d = \lambda/2$, and it serves K_F secondary users. There is not any coordination with the macro-cell base station (eNB), hence the DownLink (DL) signal received by the MUEs that are located in the HeNB coverage area, is interfered by the signal transmitted by the HeNB. LTE-A considers an OFDMA system where the time-frequency resources are divided into units called Physical Resource Blocks (PRBs), representing the smallest elements that can be allocated. In particular, in LTE-A, a PRB is made up of $S = 12$ subcarriers over six[3] consecutive OFDM symbols. The time-frequency resources are then organized in frames, that are divided in subframes, each one made up of two time slots. The number of PRBs per slot, J, depends on the system bandwidth (i.e., $6 \leq J \leq 100$). In order to allow the femto-cell to share the spectrum with the macro cell, suitable beamforming weights are used to eliminate the interference toward the MUEs. The knowledge of the signals DoAs is acquired by means of a first phase of sensing, as described in Section 3.3.2.

The AoA information is used to limit the interference toward the MUEs through a preprocessing of the signal transmitted by the HeNB. It allows to perform null beams in the selected transmission directions. In particular let θ_m^M be the AoA of the m-the replica of the signal transmitted by the MUE and θ_m^F the AoA of the m-th replica of the signal transmitted by the FUE. Beamforming weights $\mathbf{w}_j = \left[w_{1,j}, \cdots, w_{L,j}\right]^T$ for the transmission on PRB_j, are obtained by imposing the projection on $\mathbf{s}(\theta_1^F)$ equal to 1 and the projection on $\mathbf{s}(\theta_1^M), \cdots, \mathbf{s}(\theta_K^M)$ equal to 0 [109].

We denote with $\mathbf{A_j} = \left[\mathbf{s}(\theta_1^F), \quad \mathbf{s}(\theta_1^M), \quad \mathbf{s}(\theta_2^M), \quad \cdots, \mathbf{s}(\theta_K^M)\right]$ the matrix containing the steering vectors of interest for the PRB_j (whose dimension is $L \times (K+1)$) The beamforming weights are calculated as explained in Section 3.3.2, recalling here the equation for convenience we have

$$\mathbf{w}_j^H = \mathbf{c}^T \mathbf{A}_j^H (\mathbf{A}_j \mathbf{A}_j^H)^{-1}. \tag{3.14}$$

Value $w_{l,j}$ is used to weight the signal transmitted on the j-th PRB by the l-th antenna.

[3]We assume long Cyclic Prefix length.

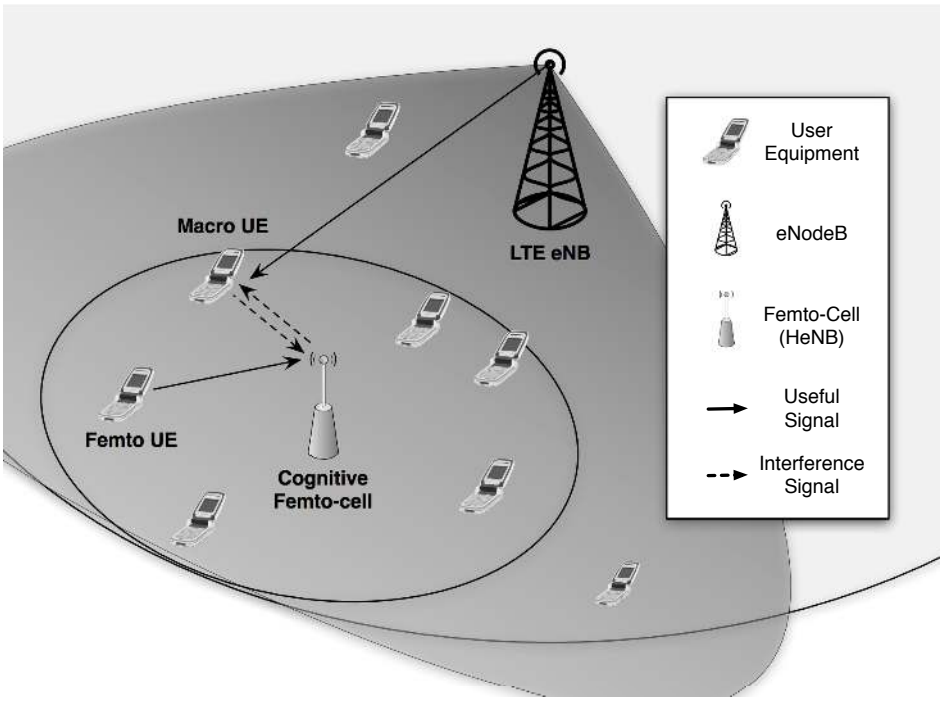

Figure 3-8: Considered scenario set up by a macro-cell, some MUEs, a small-cell and its FUEs.

3.4.2 Proposed schemes

In this section the proposed resource allocation schemes are presented. The idea is to make use of the angular information about the users (either FUEs or MUEs) to improve the capacity of the small-cell and to eliminate the interference effect on the primary users (i.e., MUEs). In particular, the proposed methods integrate a ZFBF scheme with a suitable policy for resource allocation. Differently from previous works [94, 95] the proposed method does not use channel state information to detect quasi-orthogonal user, but only the estimates of the AoA of the signals arrived to the HeNB. In addition, the proposed schemes work on a PRB basis. Indeed, each PRB can be used by a MUE to communicate, and this MUE is characterized by its own AoAs. The HeNB selects the FUE that has less effect on this primary user (i.e, MUE) and, at the same time, that achieves the highest capacity. Let assume that the j-th PRB is used by the macro-cell to communicate with a MUE that is in the coverage area of the small-cell. The signal transmitted by this MUE is received by the HeNB antennas with a set of AoAs, $(\theta_1^M, \theta_2^M, \cdots, \theta_M^M)$. The HeNB is able to detect $K \leq L-1$ AoAs related to the most powerful multipath components. For simplicity in what follow we assume that $M = K \leq L-1$ [4]. The FUE i-th, is characterized by a set of M AoAs, $(\theta_{1,i}^F, \theta_{2,i}^F, \cdots, \theta_{M,i}^F)$, with $i = 1, \cdots, K_F$.

In particular, we propose two resource allocation schemes. The first allocates the PRB_j to the FUE that presents the Maximum Beamforming Gain (MBG). The second is a Location Aware (LA) resource allocation scheme: it allocates the PRB to the FUE that has the highest angle separation from the MUE. It is a very simple heuristic that achieves performance close to the MBG solution, but with very reduced complexity.

[4]The effects of $M > L-1$ on ZFBF have been considered in [7]

3.4.3 Maximum Beamforming Gain resource allocation

As stated before, this method selects the FUE that achieves the maximum beamforming gain in each PRB, avoiding the transmission towards corresponding MUE directions. For the j-th PRB and the i-th FUE the matrix containing the steering vectors is

$$\mathbf{A_{i,j}} = \left[\mathbf{s}(\theta_{1,i}^F), \quad \mathbf{s}(\theta_1^M), \quad \mathbf{s}(\theta_2^M), \quad \cdots, \mathbf{s}(\theta_K^M)\right] \tag{3.15}$$

and the beamforming weights are calculated as in (3.14), substituting A_j with $A_{i,j}$. Finally the beamforming gain, $G(\theta_{1,j}^F)$ of the i-th FUE in the direction of its main propagation path can be expressed as:

$$G(\theta_{1,i}) = |\mathbf{w}_{i,j}^H \mathbf{s}(\theta_{1,i})|^2 = |\mathbf{s}^H(\theta_{1,i})(\mathbf{A}_{i,j}\mathbf{A}_{i,j}^H)^{-1}\mathbf{s}(\theta_{1,i})|^2. \tag{3.16}$$

The resource allocation scheme looks for the FUE $\hat{i}$ that maximizes the beamforming gain

$$G(\theta_{1,\hat{i}}^F) = \max_i \{G(\theta_{1,i}^F)\}. \tag{3.17}$$

The algorithm is described in Procedure 1.

Procedure 1 Proposed MBG Algorithm

DEFINITIONS

K_F: number of small-cell UEs
J: number of PRB
θ_m^M: the AoA of the m-th path of the Macro-cell UE that communicates on a given PRB, with $m = 1, \cdots, M$
$\theta_{1,i}^F$: the AoA of the main path of the i-th FUE
S: scheduling matrix with dimension $K_F \times J$, with:

$$S[u,k] = \begin{cases} 1 & \text{if PRB } j \text{ is assigned to user } i \\ 0 & \text{otherwise} \end{cases}$$

ALGORITHM

Beamforming weights and gain computation
for $j \leftarrow 1$ to J **do**
  for $i \leftarrow 1$ to K_F **do**
    $\mathbf{A}_{i,j} = \left[\mathbf{s}(\theta_{1,i}^F), \quad \mathbf{s}(\theta_1^M), \quad \mathbf{s}(\theta_2^M), \quad \cdots, \mathbf{s}(\theta_K^M)\right]$
    $\mathbf{w}_{i,j}^H = \mathbf{s}^H(\theta_{1,j}^F)(\mathbf{A}_{i,j}\mathbf{A}_{i,j}^H)^{-1}$.
    $G(\theta_{1,j}^F) = |\mathbf{s}^T(\theta_{1,j}^F)(\mathbf{A}_{i,j}\mathbf{A}_{i,j}^H)^{-1}s(\theta_{1,j}^F)|^2$
  end for
end for
PRB allocation:
for $j \leftarrow 1$ to J **do**
  for $i \leftarrow 1$ to K_F **do**
    if $\arg\max_t \{G(\theta_{1,t}^F)\} = i$ **then**
      $S[i,j] = 1$
    else
      $S[i,j] = 0$
    end if
  end for
end for

3.4.4 Location Aware resource allocation

This resource allocation scheme is suboptimal compared to the previous one but presents lower computational complexity. The assumption is that the beamforming gain increases as much as the FUE to MUE angle separation increases. In particular, we refer to the angle separation between the main propagation paths of the two users. When the FUE is near to the MUE, the null beam is cloe to the direction of transmission and this can affect the performance of the FUE. For this reason, the proposed Location Aware (LA) resource allocation scheme selects, for each PRB, the FUE that presents the highest angular distance with the MUE. This scheme is very simple because it does not require additional computation, the only needed information is the AoA calculated during the sensing phase. The procedure is described in Procedure 2. Then the beamforming weights are calculated only for the selected FUE as in (3.14)

Procedure 2 - Proposed LA Algorithm

DEFINITIONS

K_F: number of small-cell UEs

J: number of PRB

θ_m^M: the AoA of the m-th path of the Macro-cell UE that communicates on a given PRB, with $m = 1, \cdots, M$

$\theta_{1,i}^F$: the AoA of the main path of the i-th FUE

S: scheduling matrix with dimension $K_F \times J$, with:

$$S[u,k] = \begin{cases} 1 & \text{if PRB } j \text{ is assigned to user } i \\ 0 & \text{otherwise} \end{cases}$$

ALGORITHM

PRB allocation

for $j \leftarrow 1$ to J **do**
  for $i \leftarrow 1$ to K_F **do**
    if $\arg\max_t \{\theta_{1,t}^F - \theta_1^M\} = i$ **then**
      $S[i,j] = 1$
    else
      $S[i,j] = 0$
    end if
  end for
end for

3.4.5 Performance analysis

This section presents the numerical results obtained by means of computer simulations. The performance of the two proposed methods is compared with that of a conventional beamforming scheme that maximizes the capacity of the femto-cell without taking into account the presence of the MUE ("Conventional BF"), and with that of a ZFBF that performs a random allocation of the PRBs without taking into account the beamforming gain ("ZFBF with random allocation"). These two curves represent the upper and lower bounds of the proposed methods performance. In particular, the highest capacity is achieved with conventional BF that maximizes the beamforming gain of each FUE, independently on the presence of the Macro-cell UEs. In this case the beamforming gain toward the main propagation path is equal to $G(\theta_{1,i}^F) = L$. Conversely, through the ZFBF the beamforming gain is calculated as

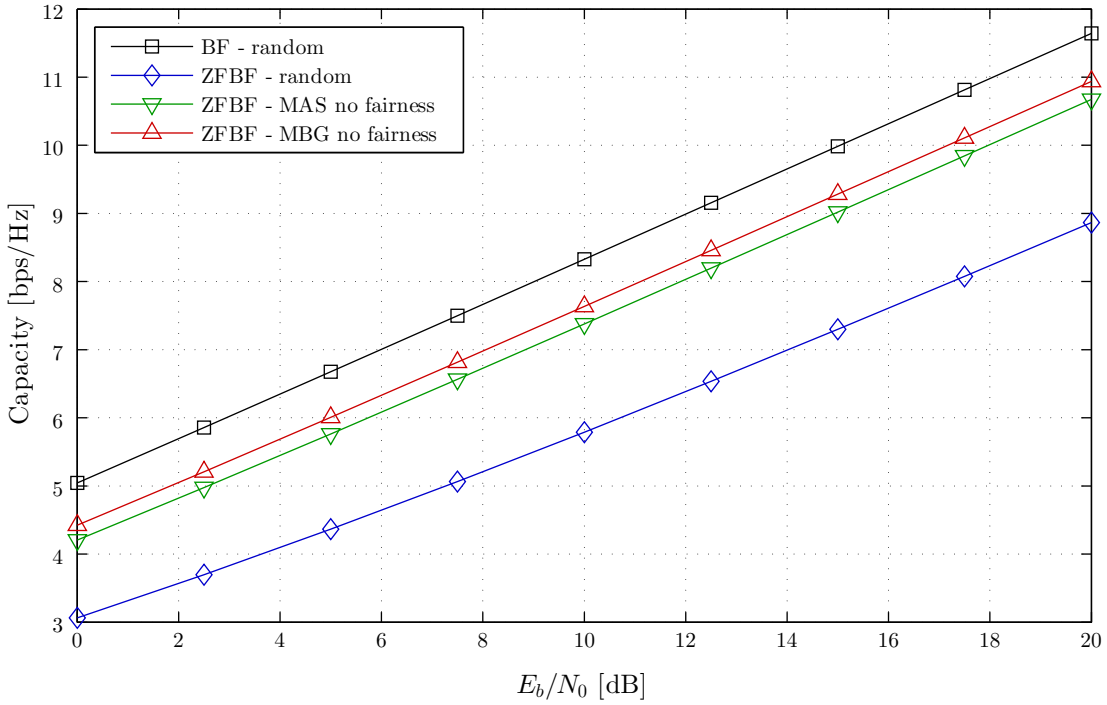

Figure 3-9: Femto-cell mean capacity when the proposed resource allocation schemes are used.

in eq.(3.14) when the FUE (and hence its AoA) is randomly chosen. In deriving the results we assume the following working hypothesis

- bandwidth $B = 2,5$ MHz
- multipath indoor propagation channel in accordance with [48]
- number of FUE $K_F = 3$
- number of antennas $L = 4$
- number of PRB, $J = 12$.

We consider the worst case, where all the PRBs are used for communication with a MUE in the HeNB coverage area.

Fig. 3-9 presents the mean capacity of the femto-cell as a function of the ratio between the Energy per bit and N_0 (E_b/N_0). As expected the highest capacity is obtained with conventional BF while the ZFBF with random PRB allocation represents the worst case. The proposed methods present intermediate results. We can note that the sub-optimal LA resource allocations scheme has performance very close to the optimal MBG, saving significant computational complexity.

The benefits of the proposed resource allocation methods must be evaluated taking into account also the error probability either of the femto-cell or the macro-cell UEs. Indeed the goal of our schemes is to obtain a good trade-off between increasing the femto-cell capacity and reducing the interference toward the MUEs. Figs. 3-10 and 3-11 represent the P_e of the femto-cell and the macro-cell, respectively. The curves are derived as a function of the E_b/N_0 of the relative links (i.e., E_b/N_0 of the small-cell DL in Fig.3-10 and E_b/N_0 of the macro-cell DL in Fig.3-11). The behaviour of the curves in Fig. 3-10 follows that of the capacity and

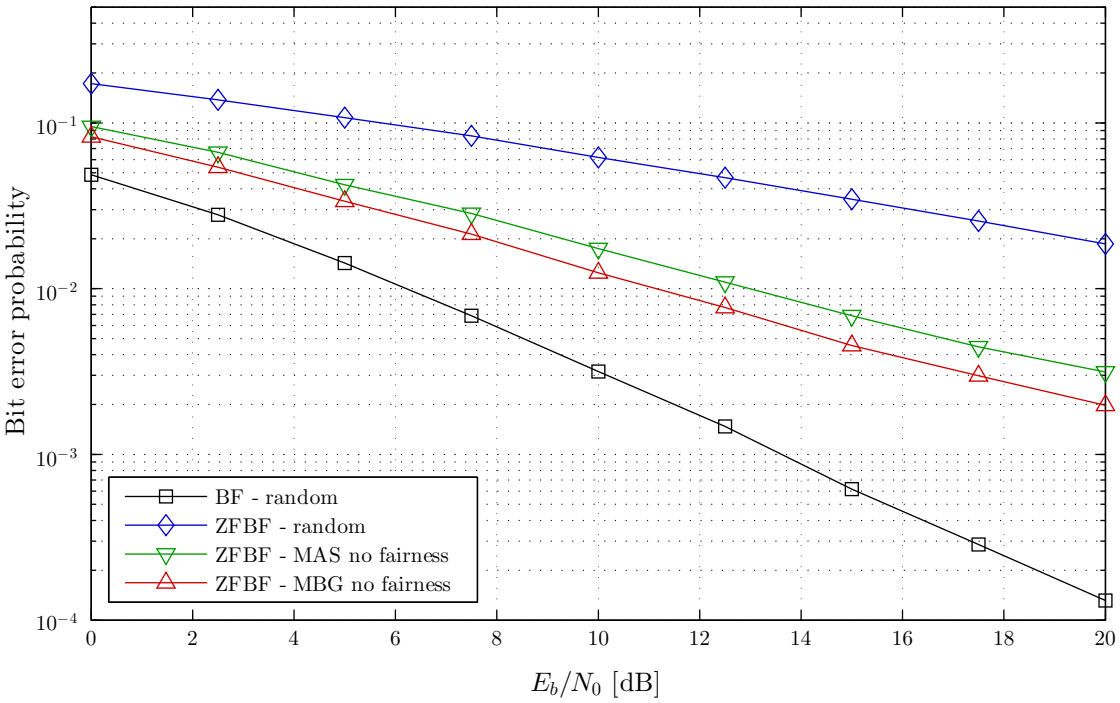

Figure 3-10: Bit error probability of the femto-cell DL.

the same considerations can be drown. For what concerns the MUEs P_e, we can notice that the proposed methods and the ZFBF achieve the same results, because the interference is completely removed in both cases. Conversely, the Conventional BF presents very high P_e.

The proposed methods are based on the knowledge of the AoA. Hence, the performance can be affected by errors in the AoA estimation. Figs. 3-12 and 3-13 show the P_e of the two cells, when the AoA is estimated by means the MuSiC algorithm, as a function of the sensing E_b/N_0. In particular considering the femto-cell (Fig.3-12) the sensing E_b/N_0 corresponds to the DL E_b/N_0. Therefore we can note that the performance follows the ideal AoA case with an obvious performance worsening that affects mainly the conventional BF scheme. In addition in presence of AoA estimation errors the differences among the two proposed methods, MBG and LA, tends to reduce. Hence, we can state that the AoA estimation errors mainly affect the determination of the maximum BF gain. Differently, in Fig. 3-13 the sensing E_b/N_0 is that of the link between the MUE and the HeNB while the E_b/N_0 of the DL MUE is fixed at 12 dB. It is possible to see that the performance has only a little improvement when the sensing E_b/N_0 increases, because the MuSiC is able to provide good estimates even for low values. The P_e worsening achieved by the macro-cell UE (if compared with the results in Fig. 3-11 at 12 dB) is comparable with that of the femto-cell.

3.5 PRB Clustering for LTE Allocation

This section investigates a method to gather together the PRBs belonging to the same user (i.e., to the same sub-channel) exploiting the similarity of signals DOA for grouping. We suggest to apply a modified K-means [111] clustering algorithm to a particular data set, represented by mutual projections of the eigenvectors of each PRB autocorrelation matrix. In particular, a new method to determine the inputs needed by the K-means algorithm is proposed.

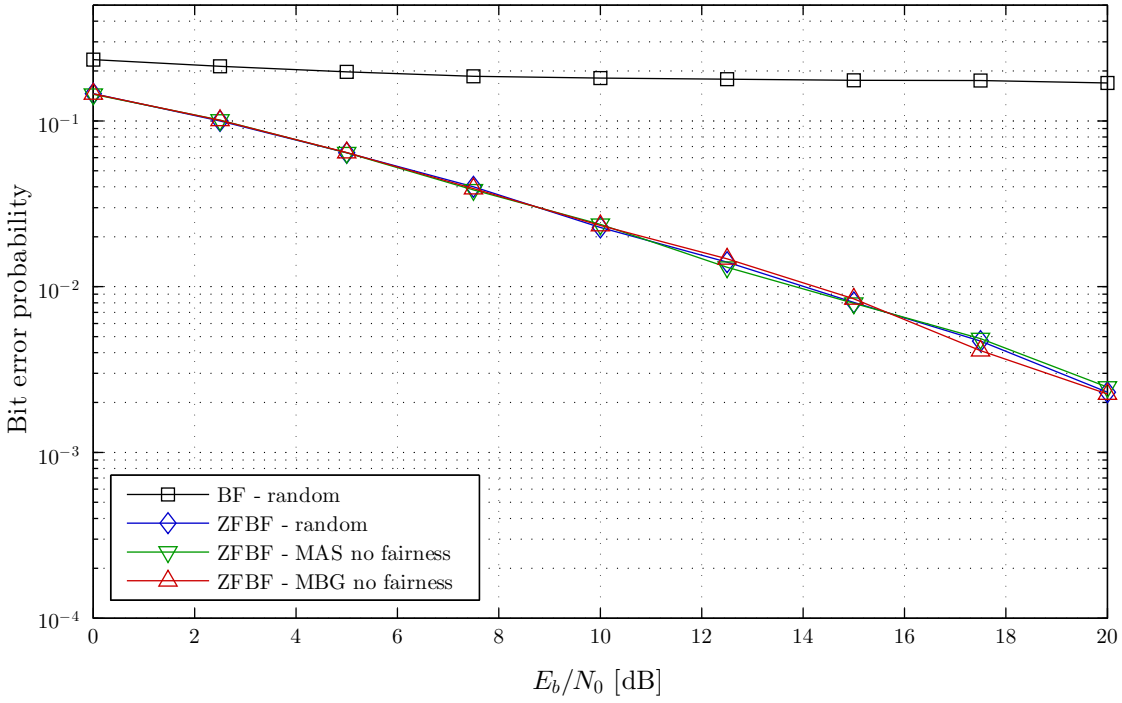

Figure 3-11: Bit error probability of the macro-cell DL.

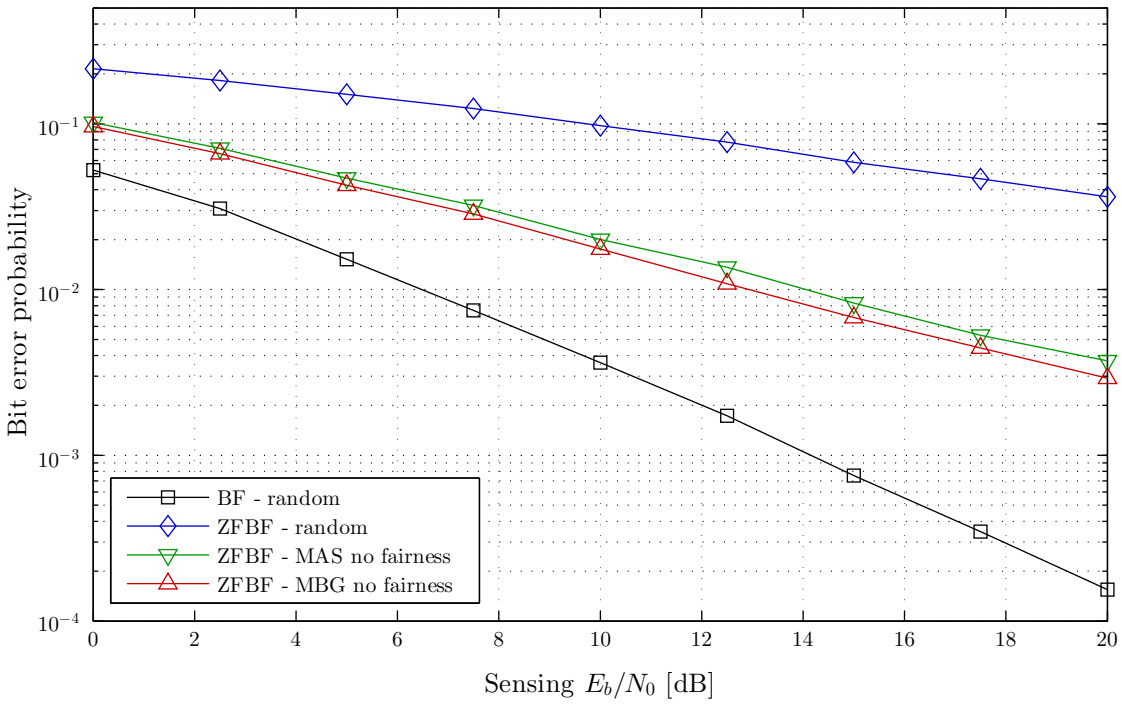

Figure 3-12: Bit error probability of the femto-cell DL in presence of AoA estimation errors.

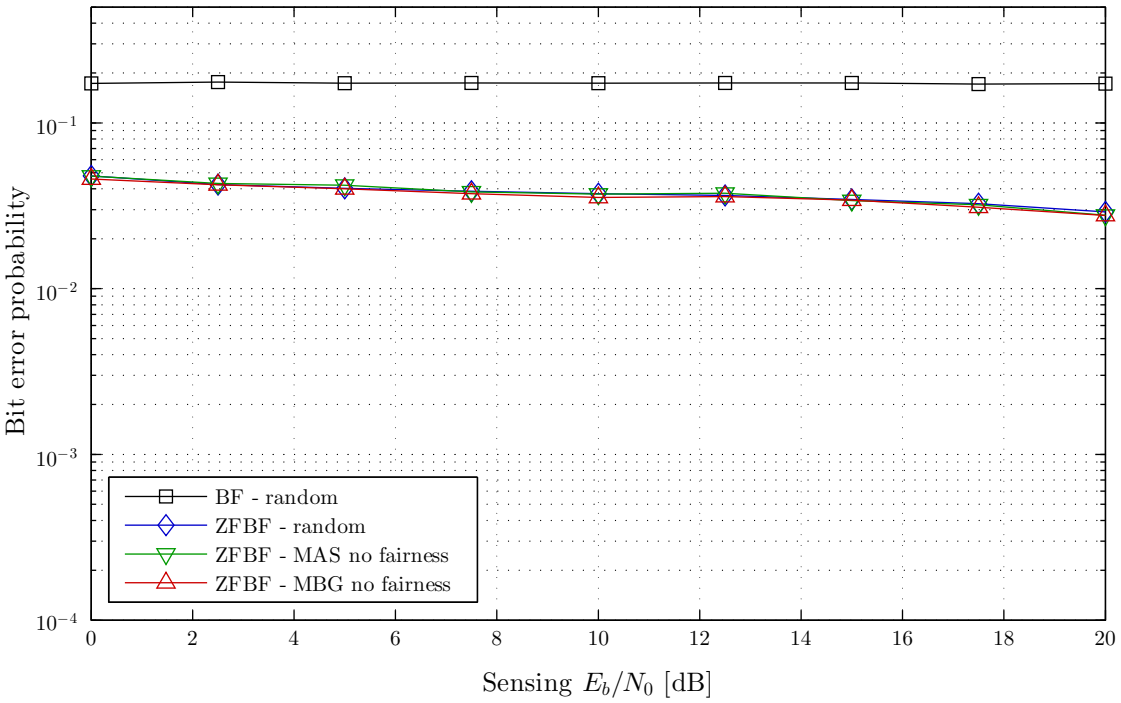

Figure 3-13: Bit error probability of the macro-cell DL in presence of AoA estimation errors. The Macro-cell DL link has $E_b/N = 12$dB.

The results show how this method allows the detection of the PRBs allocation with great accuracy by means of the proposed initialization procedure that provides the number of clusters and accurate cluster centres. The performance of the method is compared with that of a hierarchical approach for which inputs are not needed a priori and with that of a K-means algorithm that receives its inputs from a first hierarchical stage. Finally, we show the benefits of PRBs clustering in the DOA estimation performance, especially when the number of paths increases making difficult the DOA estimation.

3.5.1 System model

We consider an LTE-A network where a user-deployed HeNB is placed in an indoor area to improve the coverage offered by a macro-cell eNB representing the primary signal. Both systems are modelled according to the 3GPP LTE-Advanced standard [106,112], considering FDD (Frequency Division Duplexing) mode. In order to take into account the worst interference condition, we suppose the two systems operate with the same carrier frequency, f_0, and bandwidth. In particular the frequency carrier has been assumed equal to 2 GHz. In this scenario the macro-cell UEs (MUEs) that are located within the small-cell coverage area receive the downlink signal of the eNB with partial or complete overlap of the HeNB downlink, with a consequent performance degradation. For this reason, the HeNB has cognitive capabilities to acquire the knowledge of the surrounding environment and then to activate the selected interference mitigation strategies [7,76–78,92,93] for its downlink transmissions. In particular, we focus on the first phase, the acquisition of the knowledge of the environment within the HeNB coverage area.

We refer to an OFDMA system where the time-frequency resources are divided into units called PRBs that represent the smallest elements that can be allocated. In particular, in

LTE, a PRB is made up of $S = 12$ subcarriers over 6 or 7[5] consecutive OFDM symbols. The time-frequency resources are then organized in frames, that are divided in subframes, each one made up of 2 time slots. The number of PRBs per slot, P, depends on the system bandwidth (i.e., $6 \leq P \leq 100$).

During a slot the eNB allocates to each active MUE a sub-channel made up of a disjoint set of PRBs. PRBs in each sub-channel may be not contiguous and the number of PRBs allocated to a MUE depends on many factors (e.g., number of active UEs, system bandwidth, type of data flow) and on the scheduling algorithm adopted by the eNB in each frame. Therefore, there is a wide variability in the allocation of PRBs to the sub-channels.

If K_M is the number of active MUEs during a slot period, the k-th MUE (MUE_k) with $k = 1, \ldots, K_M$, can communicate using the sub-channel S_k that is made up of P_k PRBs so that:

- $\sum_{k=1}^{K_M} P_k \leq P$
- if $PRB_j \in S_k \Rightarrow PRB_j \notin S_q \quad with \quad \begin{cases} q \neq k; \quad q, k = 1, \cdots, K_M \\ j = 1, \cdots, P \end{cases}$.

Introducing the matrix T of dimension $K_M \times P$, whose element $t_{k,j}$ is one if PRB_j has been assigned to user k and zero otherwise, we can write the n-th sample of the signal transmitted by MUE_k as

$$s_k[n] = \sum_{j=1}^{P} t_{k,j} \sum_{s=1}^{S} \chi_k(j,s) e^{j\frac{2\pi}{N}[((j-1)S+s]n} \tag{3.18}$$

where $\chi_k(j,s)$ represents the symbol sent on the s-th subcarrier of the j-th PRB by the k-th MUE, and N is the total number of the OFDM subcarriers.

The Cognitive HeNB has to estimate information regarding the K ($K \leq K_M$) MUEs located in its coverage area so that it can adopt a suitable interference mitigation scheme.

To achieve this goal, the small-cell schedules one OFDM symbol in each subframe in the uplink transmission as sensing period. In particular, the LTE uplink frame supplies one OFDM symbol in each subframe as reserved for the transmission of Sounding Reference Signals (SRSs) usually allocated to the UEs to provide channel state information (CQI) to the eNB. The sensing procedure of the HeNB can take place in these OFDM symbols. In addition, we assume the HeNB is equipped with a linear array of antennas consisting of L equally spaced elements.

The number of antennas considered here has been selected in order to have a good trade off between performance and limited device dimension, and the distance between two consecutive antenna elements is $d = \lambda/2$. Indeed, it is well known in the literature that the system performance improves as the number of antenna elements increases. On the other hand a high number of antenna elements leads to higher computational load and greater antenna dimensions.

The signal transmitted by the k-th MUE is received by the HeNB through different propagation paths due to multiple scatterers and obstacles. In particular, the multipath propagation effects are modelled using the tapped-delay-line model defined in ITU-R M.1225 Recommendation for indoor communications (Indoor-A model) [48]. The propagation channel can be represented by a vector $\mathbf{h}_k = [h_{1,k}, h_{2,k}, \cdots, h_{M,k}]^T$, where $(\cdot)^T$ denotes the transpose operator, whose entry $h_{m,k}$ represents the channel gain for the m-th signal replica

[5]Depending on the cyclic prefix length.

transmitted by the k-th MUE. Each element $h_{m,k}$ is distributed as a circularly-symmetric complex Gaussian random variable, $h_{m,k} \sim \mathcal{CN}(0, \sigma^2_{m,k})$.

The received signal replicas arrive at the antennas through a series of rays arranged in clusters, each one from a different direction, depending on the position of the scatterers accountable for multipath. The power distribution of rays that form the cluster has strong angular concentration, therefore the average value is the best candidate to feature the angle of arrival of the whole cluster. The DOAs of different clusters received by the indoor HeNB vary depending on the environment and the scatterers position, thus an uniform angular distribution of clusters in $[0, 2\pi]$ is the more realistic choice [105].

The m-th signal replica of the k-th MUE signal arrives at the antennas forming the angle $\theta_{m,k}$, $m = 1, 2, \cdots, M$, with the array axis. The propagation delay of the m-th signal between two consecutive antenna elements is

$$\delta_{m,k} = \frac{d \sin(\theta_{m,k})}{c} = \frac{\sin(\theta_{m,k})}{2 f_0}. \tag{3.19}$$

Considering $\tau \ll T_s$, where T_s is the sampling period, the arriving signal phase is rotated by $2\pi f_0 \delta_{m,k}$. Hence, the n-th sample of the signal received by l-th antenna element of the HeNB can be expressed as

$$x_l[n] = \sum_{k=1}^{K_M} c_k \sum_{m=1}^{M} s_k[n - \tau_{m,k}] h_{m,k} e^{j[\pi(l-1)\sin(\theta_{m,k})]} + v_l[n] \tag{3.20}$$

with $l = 1, \cdots, L$, and $\tau_{m,k}$ is the delay introduced by the m-th propagation path expressed in samples, and $v_l \sim \mathcal{N}(0, \sigma^2_v)$ is the AWGN noise with zero mean and variance σ^2_v. The term c_k is equal to one if the MUE_k is located in the HeNB coverage area, or zero otherwise. To simplify the notation and without loss of generality, in what follows we consider $K = K_M$, and hence we omit term c_k (i.e., $c_k = 1 \quad \forall k = 1; \cdots, K_M$). The samples of the received signal are used to estimate the autocorrelation matrix needed by the PRBs clustering method proposed below.

3.5.2 Proposed PRBs clustering methods

A cognitive HeNB needs to acquire the knowledge of the surrounding environment and, in particular, information regarding the MUEs that are in its coverage area. With this information it is possible to carry out some countermeasures to limit its interference on the primary system. The accuracy of the environment knowledge depends on the portion of signal that can be used to perform the estimate of the intended parameter (e.g., DOA, Signal to Interference plus Noise Ratio, Interference Level), but if the PRBs allocation in the macro-cell is not known at the HeNB, the measures can be done only on a single PRB. This section proposes a method to gather together the PRBs belonging to the same MUE, in order to extend the snapshot (i.e., the available samples) that can be used for the measurements. In particular, we propose a modified version of K-means clustering algorithm. Hence, in this section we first briefly introduce the main concepts of clustering with particular reference to the K-means algorithm. Then the proposed approach is detailed. Hierarchical clustering is introduced as a comparison method.

Clustering algorithms

Clustering algorithms are used to group the elements of a data set in K groups, on the basis of suitable attributes/features [113]. They perform better when elements belonging to the same cluster are similar each other and different from the elements of other clusters.

Clustering algorithms can be classified in two main classes:

- Partitional
- Hierarchical

Partitional methods start from an initial partition of data and move elements of the data set iteratively from one group to another until a stabilization is reached. The K-means is the most known and used partitional cluster analysis method thanks to its simplicity and fast execution speed [111, 114]. It has been used in a variety of domains.

The procedure can be easily described as follows:

- *initialization*: the number of clusters, K, is known; K initial cluster centres are chosen randomly;
- *iterations*: each data element is assigned to the nearest centre; then the centres are recomputed as the centre of mass of all points assigned to it; the iterations are repeated until the process stabilizes or a maximum number is reached.

Hierarchical approaches proceed through a series of steps that build a tree structure (called dendrogram) by either merging or splitting elements so as to optimize some criterion. Each step corresponds to a different number of clusters. The most common procedure is agglomerative (i.e., merging), it means that groups are merged until the number of clusters reaches the expected one [115].

K-means algorithm has two main drawbacks: the number of clusters K must be known and the performance strongly depends on the choice of the cluster centres. Indeed, it has been demonstrated that K-means algorithm gives different results selecting different initial cluster centres and the better results are obtained when the initial partition is close to the final solution [116]. For this reason many works in the literature presented methods to improve the selection of cluster centres supposing the number of clusters known *a priori*. The determination of the number of clusters is considered a more challenging issue [114]. A typical but not very efficient approach is to run K-means independently for different values of K choosing the best value of K based on a predefined criteria. Another viable solution is to combine the strength of both approaches (i.e., hierarchical and iterative) trying to discard their disadvantages by using a two-stage procedure where a hierarchical algorithm is used to define the number of clusters and cluster centres, then these results are used as starting points for subsequent partitional clustering (i.e., K-means) [117].

Indeed, in hierarchical methods the number of clusters can be derived examining the incremental changes in the observed metrics (the euclidean distance in our case). A large increase implies that dissimilar clusters have been merged; thus, the number of clusters prior to the merger is most appropriate [115].

The performance of the proposed method is compared with that of a hierarchical agglomerative single-link[6] clustering method [113] and with that of a two-stage K-means clustering algorithm where the number of clusters K is provided by the hierarchical agglomerative algorithm and the cluster centres are selected randomly.

[6] the distance between two clusters is the minimum of the distances between all pairs of patterns drawn from the two clusters

Proposed method

As stated before, in traditional K-Means algorithm, the parameter value K is given in advance and randomly initial cluster centres are selected. We propose here an improved K-means algorithm based on a two stage procedure. During the first stage, newly proposed here, the number of clusters K and the initial cluster centres are determined. During second stage the K-means algorithm is used to refine clustering using the inputs provided by first stage.

In particular, in the case considered here, we are interested in identifying the resource assignment in an OFDMA system. To this goal we consider a new application of the clustering algorithm where:

- the data set is represented by the eigenvectors of the autocorrelation matrix of the signal received by each PRB
- the number of cluster, K, represents the number of MUEs in the HeNB coverage area
- each cluster represents a subchannel S_k

Data set

The clustering algorithm must be applied using suitable attributes to identify which time-frequency resources (i.e., PRBs) have been assigned to the same user by the eNB. Indeed, the selection of the attributes used to group the elements is one of the fundamental step in cluster analysis. In the considered case the attribute must be characterized by an information that is specific of a given user. To this goal we propose to use the information regarding the DoA of the incoming signals. We assume that two signals arriving from the same direction belong to the same user[7].

Let us consider the autocorrelation matrix of the signals received on PRB_j,

$$\mathbf{C}_{\tilde{x}\tilde{x}}^{(j)}[s] = E\left[\tilde{\mathbf{x}}^{(j)}[s]\left(\tilde{\mathbf{x}}^{(j)}[s]\right)^H\right] \tag{3.21}$$

with $j = 1, \cdots, P$, where $(\cdot)^H$ denote the Hermitian operator and the l-th element of the vector $\tilde{\mathbf{x}}^{(j)}[s]$ represents the s-th sample received on PRB_j on the l-th antenna in the time domain. It can be expressed as

$$\tilde{x}_l^{(j)}[s] = \sum_{k=1}^{S} w_k^{(j)} \sum_{n=1}^{N} x_l[n] e^{-j2\pi\frac{nk}{N}} e^{j2\pi\frac{ks}{S}} \tag{3.22}$$

with $s = 1, \cdots, S$, where $w_k^{(i)}$ is a weight which filters the subcarriers belonging to the j-th PRB defined as

$$w_k^{(j)} = \begin{cases} 1 & \text{if} \quad (j-1)S+1 \leq k \leq jS \\ 0 & \text{otherwise} \end{cases} . \tag{3.23}$$

Hence, the autocorrelation matrix of the signal received on PRB_j can be estimated as[8]

$$\widehat{\mathbf{C}}_{\tilde{x}\tilde{x}}^{(j)} = \frac{1}{S}\sum_{s=1}^{S} \tilde{\mathbf{x}}^{(j)}[s]\tilde{\mathbf{x}}^{(j)^H}[s] \tag{3.24}$$

[7]The probability that two users have the same DoA is low.

[8]$\tilde{\mathbf{x}}^{(j)}[s]$ with $s = 1, \cdots, S$ are independent and identically distributed random variables.

In order to obtain a comparison metric between two PRBs, the autocorrelation matrix of the signals received on each PRB is decomposed through the Singular Value Decomposition, i.e.,

$$\widehat{\mathbf{C}}_{\tilde{x}\tilde{x}}^{(j)} = \mathbf{U}_j \mathbf{\Lambda}_j \mathbf{U}_j^H \tag{3.25}$$

where each column of $\mathbf{U}_j$, $\mathbf{u}_l^{(j)}$ with $l = 1, \cdots, L$, represents an eigenvector of $\widehat{\mathbf{C}}_{\tilde{x}\tilde{x}}^{(j)}$ and $\mathbf{\Lambda}_j$ is a diagonal matrix which contains the relative eigenvalues $\lambda_{l,j}$. For each PRB_j, $j = 1, \cdots, P$, the eigenvector relative to the greatest eigenvalue, $\mathbf{u}_{\tilde{l}_j}^{(j)}$ with $\tilde{l}_j = \arg\max_l \lambda_{l,j}$, contains most of the information regarding the DOAs of the signals received in the considered PRB_j. Hence, these eigenvectors can be suitable attributes to aggregate PRBs: signals coming from same direction will have similar eigenvectors while signals coming from different directions will have different eigenvectors. We define the matrix $\mathbf{U}$ as $\mathbf{U} = [\mathbf{u}_{\tilde{l}_j}^{(1)}, \cdots, \mathbf{u}_{\tilde{l}_j}^{(P)}]$, whose dimensions are $L \times P$.

In order to evaluate similarity among the elements of the data set we build the matrix $\mathbf{R}$, whose dimension are $P \times P$, defined as $\mathbf{R} = |\mathbf{U}^H \mathbf{U}|$. The element $r_{i,j}$ of the matrix $\mathbf{R}$ is the magnitude of the projection of the first eigenvector of the i-th PRB on the first eigenvector of the j-th PRB, i.e.,

$$r_{i,j} = \left| \left(\mathbf{u}_{\tilde{l}_j}^{(i)} \right)^H \mathbf{u}_{\tilde{l}_j}^{(j)} \right|. \tag{3.26}$$

The element $r_{i,j}$ expresses how the PRB_i is correlated to PRB_j, hence it expresses the similarity between the DOAs of the signal received by PRB_i and PRB_j. Note that the elements of the matrix may assume values in the interval $[0; 1]$, where 1 denotes perfect match between two PRBs, while 0 means that they are orthogonal and hence completely uncorrelated.

Fig. 3-14 represents an example of $\mathbf{R}$ in the case of $K = 3$ users when $P = 6$ and with contiguous PRBs frequency allocation[9].

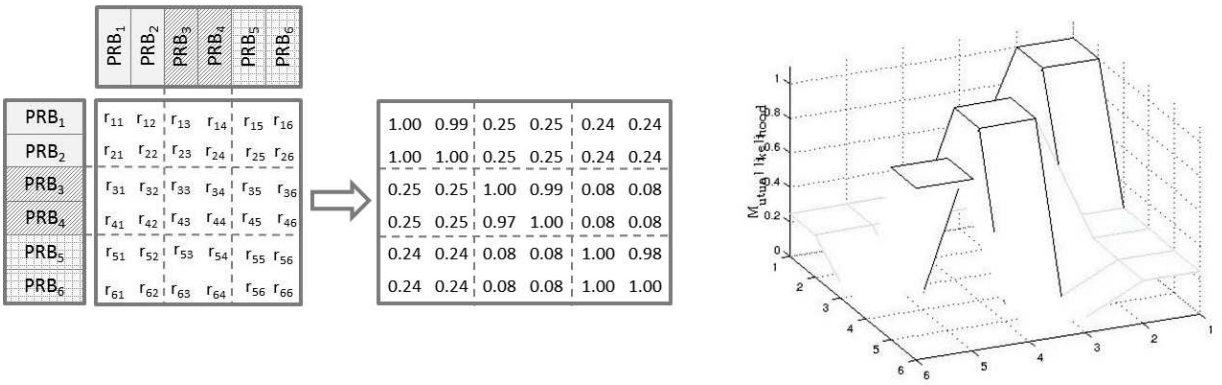

Figure 3-14: Example of matrix $\mathbf{R}$ with 3 users and contiguous frequency allocation.

In this example we see that 3 clusters can be clearly identified, they represent the sub-channels allocated to the users. We want to stress that this is a simple case that is used for a clear explanation. In general, when the number of clusters grows, the clusters discrimination is more complicated due to the multipath channel propagation and different directions of arrival of the incoming signals.

[9]The subchannel of k-th user is $S_k = \{PRB_{(k-1)K+1}, \cdots, PRB_{kK}\}$, with $k = 1, 2, 3$

Stage 1: Identification of the number of clusters and cluster centres

This subsection describes the first stage of the clustering algorithm that is newly proposed here. It is used to determine the number of clusters (i.e., the number of MUEs in the HeNB area) and suitable initial cluster centres. The algorithm is made up of two thresholding and row deletion operations that are detailed in Procedure 3.

In the first operation, at the t-th iteration (with $t = 1, \cdots, P$) the thresholding is operated on matrix $\tilde{\mathbf{R}}^{(t)}$ where $\tilde{\mathbf{R}}^{(1)} = \mathbf{R}$. A row of $\tilde{\mathbf{R}}^{(t)}$ is selected: rows are selected successively, while the first row (i.e., $t = 1$) is randomly chosen. If the j-th element of the selected i-th row is over the threshold Γ, all the elements of the j-th row (with $i \neq j$) of $\tilde{\mathbf{R}}^{(t)}$, are put to zero (all the corresponding PRBs are assumed to belong to the same cluster). This thresholding operation is used to know which PRBs are strongly similar, for this reason Γ should assume high values.

Fig. 3-15 shows the results of this first step when the second row is selected as starting point. $\tilde{\mathbf{R}}^{(6)}$ represents the result of the first stage.

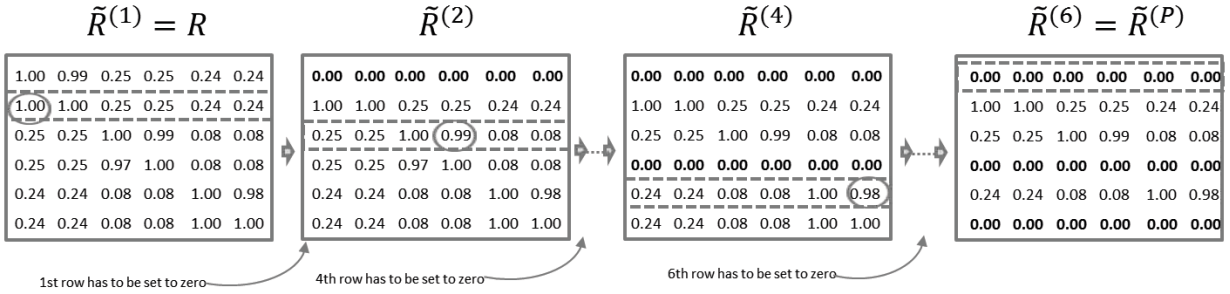

Figure 3-15: First thresholding and rows deletion operation.

The number of rows of $\tilde{\mathbf{R}}^{(P)}$ different from zero represents a rough estimation of the number of clusters, K'.

The second operation is used to refine this result by exploiting the whole information contained in each row of $\tilde{\mathbf{R}}^{(P)}$. The idea is that the similarity between PRB_i and PRB_j depends not only on the correlation between them, but also on the correlation of each one with all the other PRBs (i.e., if two PRBs are both similar to a third PRB maybe there is a correlation also among them).

Let $\mathbf{q}' = [q'_1, \cdots, q'_{K'}]$ be a vector of length K' that contains the indexes of the rows of $\tilde{\mathbf{R}}^{(P)}$ that are different from zero. We can define the upper triangular matrix $\mathbf{Z}$, whose dimensions are $K' \times K'$, so that its (i, j) element is defined as the correlations between the non-zero rows of $\tilde{\mathbf{R}}^{(P)}$, $\tilde{\mathbf{r}}_i^{(P)}$,

$$z_{i,j} = \begin{cases} \dfrac{\tilde{\mathbf{r}}_{q'_i}^{(P)} \left[\tilde{\mathbf{r}}_{q'_j}^{(P)}\right]^T}{\sqrt{\|\tilde{\mathbf{r}}_{q'_i}^{(P)} \tilde{\mathbf{r}}_{q'_j}^{(P)}\|}} & \text{if} \quad i < j \\ 0 & \text{i} \geq j \end{cases} . \tag{3.27}$$

A second thresholding operation[10] is performed on $\mathbf{Z}$. The proposed procedure looks for elements that are higher than the selected threshold. If G is the number of elements of $\mathbf{Z}$ that are higher than Γ, it means that too many centres at the first step have been found:

- the final number of cluster centres is $K = K' - G$;

[10]The threshold value here is the same of the first step.

- if element $z_{i,j}$ of $\mathbf{Z}$, is over the threshold, the q'_j-th row of matrix $\tilde{\mathbf{R}}^{(P)}$ is put to zero resulting in matrix $\tilde{\mathbf{R}}^{final}$;

- a new vector $\mathbf{q} = [q_1, \cdots, q_K]$ of length K is defined as the vector that contains the indexes of the rows of $\tilde{\mathbf{R}}^{final}$ that are different from zero.

If $G = 0$ we have: $K' = K$, $\mathbf{q} = \mathbf{q}'$ and $\tilde{\mathbf{R}}^{(P)} = \tilde{\mathbf{R}}^{final}$ as in the example reported in Fig. 3-16.

The final results of the first stage of the proposed algorithm are:

- the number of cluster K,

- the initial cluster centres; these are the rows of $\mathbf{R}$ whose indexes are included in $\mathbf{q}$. In particular the set of initial cluster centres $\mathbf{C}^{(0)}$ is $\mathbf{C}^{(0)} = [\mathbf{c}_1^{(0)}, \cdots, \mathbf{c}_K^{(0)}]$ with $\mathbf{c}_i^{(0)} = \mathbf{r}_{q_i}, \quad i = 1, \cdots, K$.

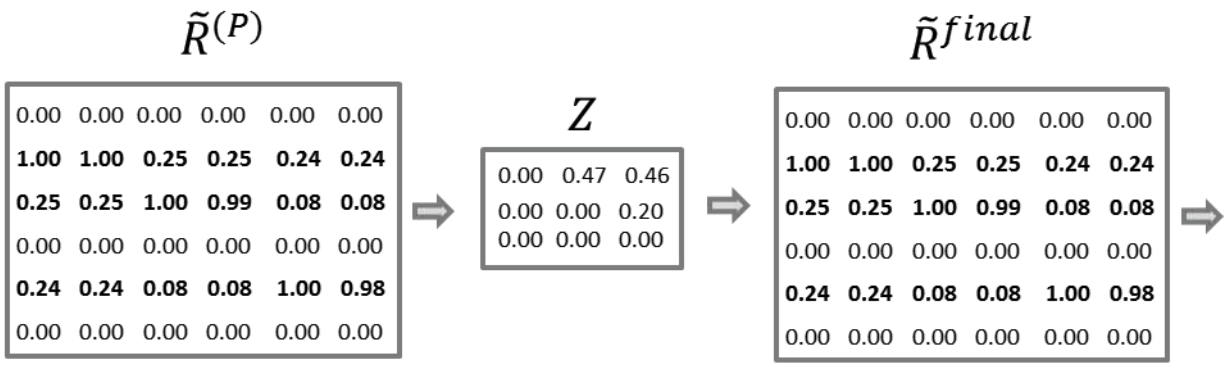

Figure 3-16: Second thresholding and rows deletion operation.

The performance of the proposed method is dependent on the threshold Γ, but an accurate optimization is not needed. Threshold Γ is used to determine which elements are strongly correlated and, hence, a high value of Γ must be selected. We have verified that a value of $\Gamma = 0.95$ is always correct. Indeed, even if the algorithm can find too many clusters (i.e., $K' > K$) during the first step, the second step reduces this selection.

STAGE 2: K-means Clustering

In the second stage the classical K-means algorithm is applied using the inputs provided by the first stage. In particular, the data set is represented by the rows of matrix $\mathbf{R}$ and the set of initial cluster centres is $\mathbf{C}^{(0)}$. Each cluster corresponds to a sub-channel S_k with $k = 1, ..., K$.

The algorithm works iteratively. At iteration t we have:

- the euclidean distance among all the cluster centres, derived at previous iteration, $c_i^{(t-1)}$ $(i = 1, \cdots, K)$ and all the rows of $\mathbf{R}$, $\mathbf{r_j}$ $(j = 1, \cdots, P)$ is calculated as:

$$d_j(\mathbf{c}_i^{(t-1)}) = \|\mathbf{r}_j - \mathbf{c}_i^{(t-1)}\| \tag{3.28}$$

- each PRB_j, with $j = 1, \cdots, P$, is assigned to the sub-channel S_k with $k = 1, \cdots, K$, if $d_j(\mathbf{c}_k^{(t-1)})$ is lower than $d_j(\mathbf{c}_i^{(t-1)})$ for all $i \neq k$

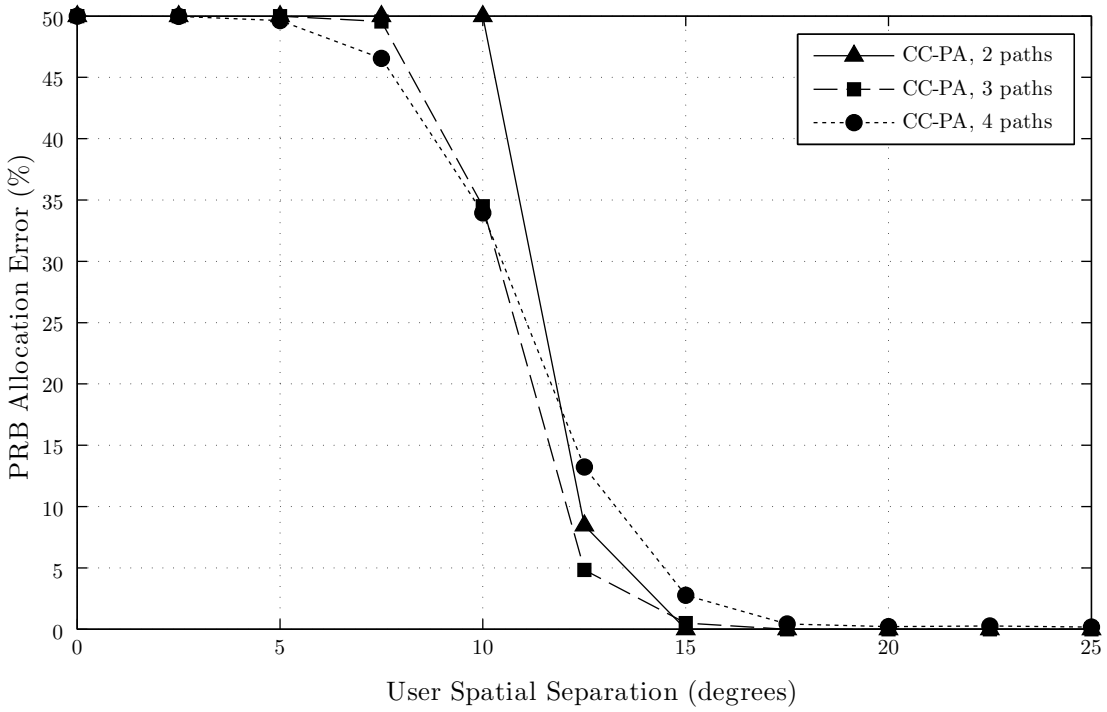

Figure 3-17: Mean percentage error for different number of multipath components when the angle separation between two users varies.

- a new set of cluster centres, $\mathbf{C}^{(t)}$, is calculated, whose elements are

$$\mathbf{c_k^{(t)}} = \sum_{j:\, PRB_j \in S_k} \frac{\mathbf{r}_j}{P_k^{(t)}} \quad k = 1, \cdots, K \tag{3.29}$$

where $P_k^{(t)}$ is the number of elements belonging to cluster k-th at iteration t. The iterations stop when the algorithm converges or when the maximum number of iterations is reached.

3.5.3 Numerical results

This section presents the numerical results obtained by means of computer simulations in order to validate the scheme proposed in the previous section. We assume the HeNB equipped with a linear array of L antennas and the presence of a variable number of MUEs in its coverage area. The number of PRBs allocated to each MUEs varies and the allocation can be either contiguous or interleaved. The propagation channel between the MUEs and the HeNB is characterized as a multipath indoor channel with 4 paths, where each path has a DOA that is uniformly distributed over 360 degrees. The number of PRBs is assume equal to $P = 100$.

First we want to verify the choice of the attributes of the data set used for clustering (i.e., DOA information). We focus on a scenario with two MUEs (i.e., $K = 2$) and analyze the PRBs clustering performance in terms of mean percentage error in the PRBs allocation as a function of the angle separation between the users. In particular, the received signal is obtained as the sum of different multipath components received with different DOAs, hence, we refer here to the angle separation between the DOAs of the main signal component of the users (i.e., the main path). In order to evaluate the effect of secondary multipath components, Fig. 3-17 shows the results for different number of multipath components when

the Signal to Noise Ratio (SNR) at the HeNB receiver is equal to 15 dB and $L = 4$. We can see that the proposed method (Cluster Centres - Proposed Approach, CC-PA) has good performance only when the separation between the users is beyond a critical angle. As expected, when the users are too close, the proposed algorithm is not able to separate the two clusters. This is due the choice of the clustering data set whose attributes are based on the similarity of the DOA of the incoming signals. Therefore, if the signals of two users arrives at the antennas from the same direction, they cannot be distinguished. However, the probability that the main propagation path of two different MUEs comes from the identical direction can be considered very low. In addition we can see that the performance are almost the same changing the number of multipath components. It depends on the fact that the contribution of the main path is always dominant. However, we can observe that until the first paths of the two users are not sufficiently separated, having a higher number of paths is better because it implies higher diversity among users. Conversely, increasing the separation angle there are crossing points among the curves because the main paths separation becomes dominant.

The effectiveness of the proposed clustering method compared with other alternatives is shown in Fig. 3-18. This figure represents the performance of the K-means with the proposed algorithm as a function of the number of MUEs in the coverage area of the small-cell assuming $L = 4$. The performance of a agglomerative single-link hierarchical clustering (Hierarchical) algorithm and a K-means algorithm that uses as inputs the number of clusters estimated by the hierarchical procedure and random cluster centres (Cluster Centres - Hierarchical & Random Selection, CC-H& RS), are reported as comparison. The figure shows that when the number of clusters and the cluster centres are calculated with the proposed method, the percentage of PRBs allocation errors is lower compared to the other methods, especially for a high number of clusters. In particular, as demonstrated in the literature, K-means suffers for an inaccurate selection of the clusters centres that leads to high errors because in some cases the algorithm is not able to converge. Hierarchical clustering has better performance than the K-means with random initial centres, but it is outperformed by the proposed method since it suffers for higher inaccuracy in the estimation of the number of clusters, as evident in Fig. 3-20.

The performance of the clustering methods is shown as a function of the SNR value in Fig. 3-19 for different numbers of clusters (i.e., MUEs). It is possible to note that the SNR effect on the proposed method is negligible, while the other two methods for an inaccurate estimates of K at low SNR values (i.e., both methods uses the parameter K estimated by the hierarchical approach). This results depends on the particular data set that has bee selected, indeed the effect of the noise is negligible because it is reduced by the mutual projection of the PRB correlation matrix eigenvectors. This operation is repeated two times in the proposed method (calculating the matrix $\mathbf{Z}$), and hence it is more robust at low SNR values.

The performance comparison between CC-PA and the CC-H& RS allows the evaluation of the benefits of our method in terms of the selection of the cluster centres. However, the proposed method is used also to determine the number of clusters K that is a parameter needed by any clustering algorithm. Fig. 3-20 shows the mean percentage error on the determination of the number of clusters of the proposed K-means method and the value K calculated by means of a hierarchical approach for different number of antennas, $L = 4, 6, 8$. It is possible to see that our methods achieves better performance and there is a significant improvement by increasing the number of antenna elements.

The proposed PRBs clustering method effectiveness is then tested by considering a DOA estimation algorithm. For this purpose we consider the known Root MuSiC (Multiple Signal

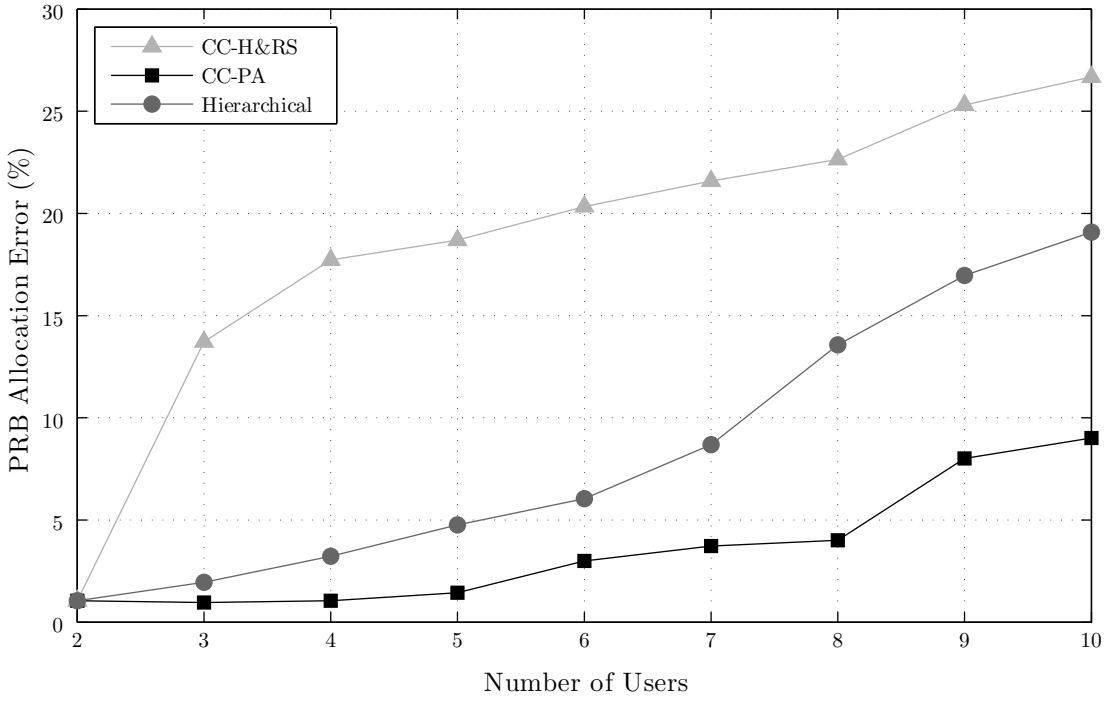

Figure 3-18: Mean percentage error when the number of users varies.

Classification) algorithm that is based on the decomposition of the autocorrelation matrix of the received signal [118]. The effect of snapshot size in DOA estimation algorithms is widely addressed in the literature [110], and it is shown how this heavily affects the performance of the estimate. Usually MuSiC algorithms works optimally for over-sized snapshot which often are not available at the receiver in certain contexts. The snapshot dimension can be increased in the frequency domain by means of PRBs grouping. Fig. 3-21 consider $L = 4$ antennas and shows the DOA estimation capabilities in terms of mean square error of the Root MUSIC estimation when it works on a different number of PRBs. It is possible to note that the performance is poor with a single PRB, while it is possible to get a remarkable improvement even with a few of aggregated PRBs. From this figure it is evident the need to know which PRBs belong to the same user, in order to perform the DOA estimates on an extended snapshot.

Finally we can do some considerations on complexity. K-means algorithm has been selected for its simplicity and execution speed, that are the main reasons for its wide applicability. Its complexity is O(PKI) where I is the number of iterations while the hierarchical agglomerative requires a time complexity that is $O(P^3)$[11] and requires higher storage memory [113]. In all the simulations the number of iterations is limited to $I = 5$. The only additional complexity of our proposed method to determine the initial values is due to the calculation of matrix $\mathbf{Z}$ (matrix $\mathbf{R}$ represents the data set and hence it is needed for every clustering algorithm). It requires $(K')^2$ correlations. The other operations are simply thresholding and row cancellations.

[11]There are some variants that reduce the complexity to $P^2 \log P$.

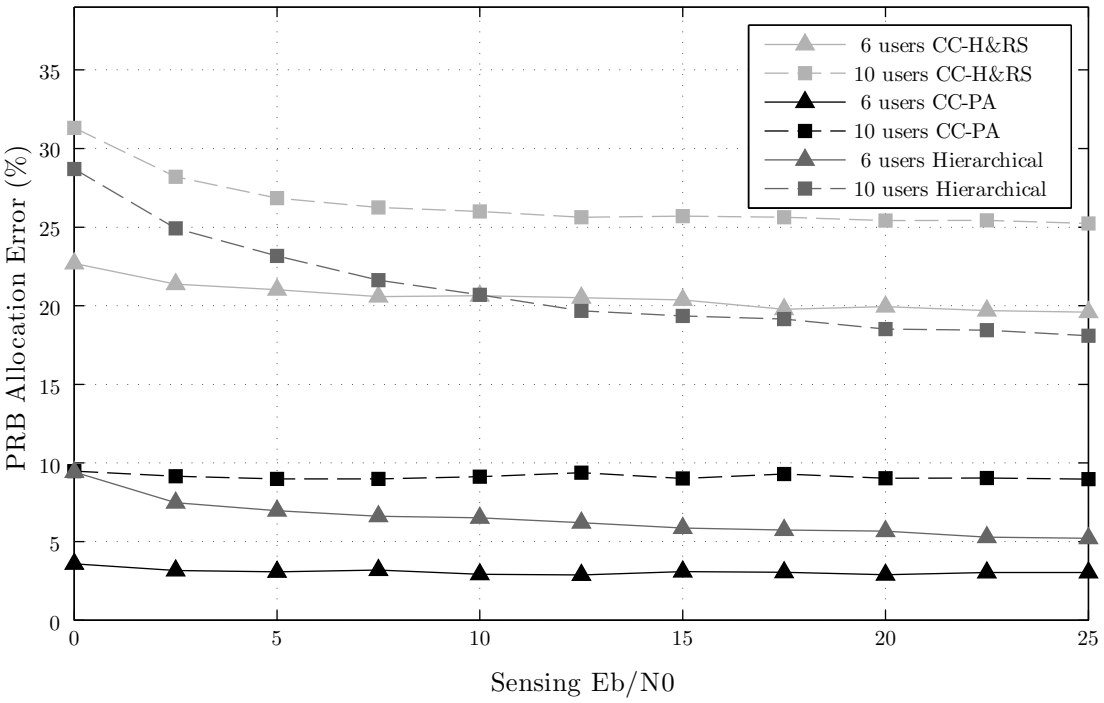

Figure 3-19: Mean percentage error as a function of the SNR value, for different numbers of clusters.

3.6 Conclusion

This chapter provided an analysis of the possible heterogeneous deployment scenarios of LTE-A networks, which represents the most promising approach to maximize the network performance and satisfy the communication service demand. The deployment of small-cells in a traditional network is intended to increase the system coverage and capacity, but the actual benefits are limited by the interference among different cells. The focus was on the discussion of suitable beamforming schemes dedicated to combat the main impairments for different interference scenarios, highlighting how beamforming can support the small-cells deployment and which critical aspects are needed for further investigations to make it more effective. The main research trends have been highlighted by describing the Massive MIMO concept with its main advantages and drawbacks.

Moreover, an interference mitigation scheme for closed access small-cells was presented, where a user-deployed low power cell operated in the coverage area of a traditional macro-cell using the same frequency resources. Through a cognitive approach the small-cell sensed the environment to detect the direction of arrival of the signals transmitted by the Macro-cell User Equipments in its coverage area. This information was then exploited by the small-cell base station to place nulls in its transmission pattern in order to not interferer with the downlink macro-cell communications. The proposed system was investigated by considering actual propagation conditions and taking into account the medium access technique of LTE that allows simultaneous transmission of multiple users on different subcarriers. For this reason, the proposed system operated on a Physical Resource Block basis. The numerical results showed the proposed system is able to efficiently eliminate the interference on macro-cell down link communications. It is particularly efficient for small operational bandwidths that are those more likely used by small-cells. For large frequency bands there is a residual interference due to the high number of propagation paths. However, a significant performance

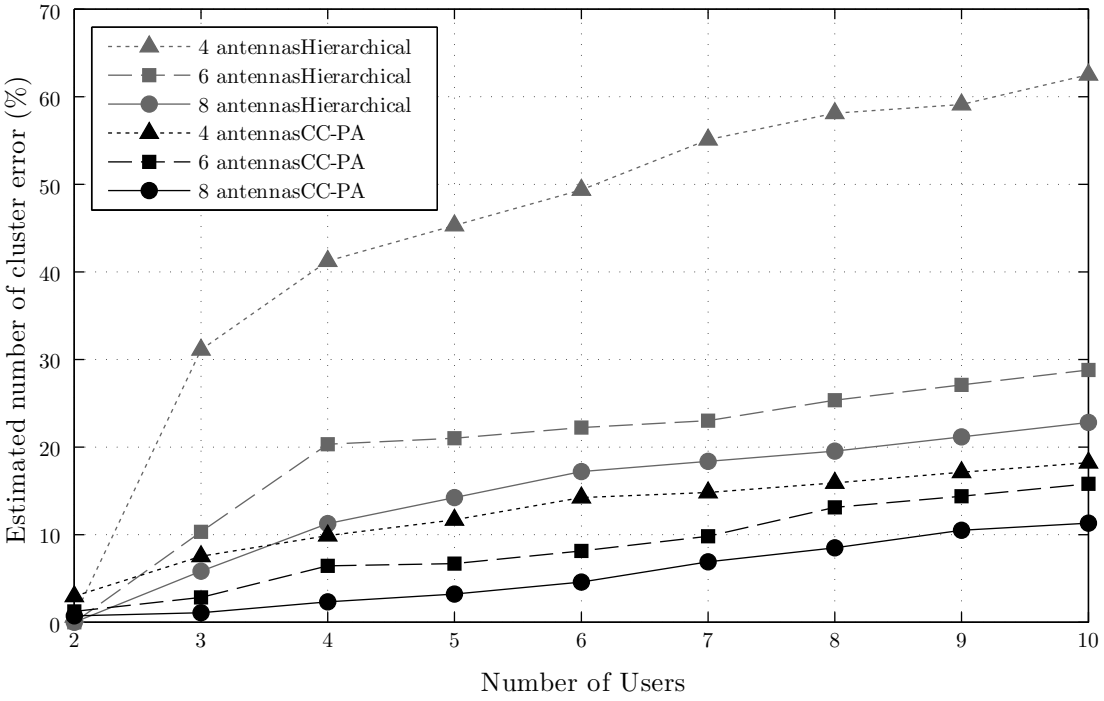

Figure 3-20: Mean percentage error on number of clusters for different number of antennas.

improvement with respect to the case without interference was evident even in this case.

For what concerned the small-cell downlink, two resource allocation schemes were presented. Both methods were based on the joint use of ZF beamforming and suitable time-frequency resource allocation policies. The goal is to reduce or eliminate the interference toward the macro-cell user equipments that are in the small-cell coverage area but, at the same time, maximizing the small-cell capacity. The proposed methods worked using the signal angle of arrival information. The first method was optimal and selected the small-cell user equipments that maximizes the beamforming gain, while the second was sub-optimal but with reduced complexity. It was based on the selection of the user with the higher angle separation from the macro-cell-UE. The AoA were estimated by means of a sensing phase and the performance was compared with that of a conventional maximum gain beamforming and a ZF beamforming. The results showed the good performance of the proposed methods that reached a good trade off between maximization of the small-cell capacity and reduction of the interference level at the MUEs side.

Since the performance showed a possible significant improvement if the physical resource blocks allocation is known at the small-cell base station, i.e., it is possible to perform direction of arrival estimation on groups of physical resource blocks, a PRBs clustering method for an OFDMA system, based on a modified K-means algorithm was proposed. The idea presented here was to use the similarity between the DOA of the incoming signals as attribute for clustering. To achieve this goal, a two stage procedure was introduced. During the first stage, newly proposed here, the input parameters are derived and optimized, then the K-means algorithm is applied, taking into account the specific application context of a heterogeneous network deployment. The PRBs clustering can be very useful in cognitive small-cell systems where the small-cell base station needs to acquire accurate knowledge of the surrounding environments. Indeed, the identification of which PRBs belong to the same group allows the extension of the snapshot used for sensing and for estimation.

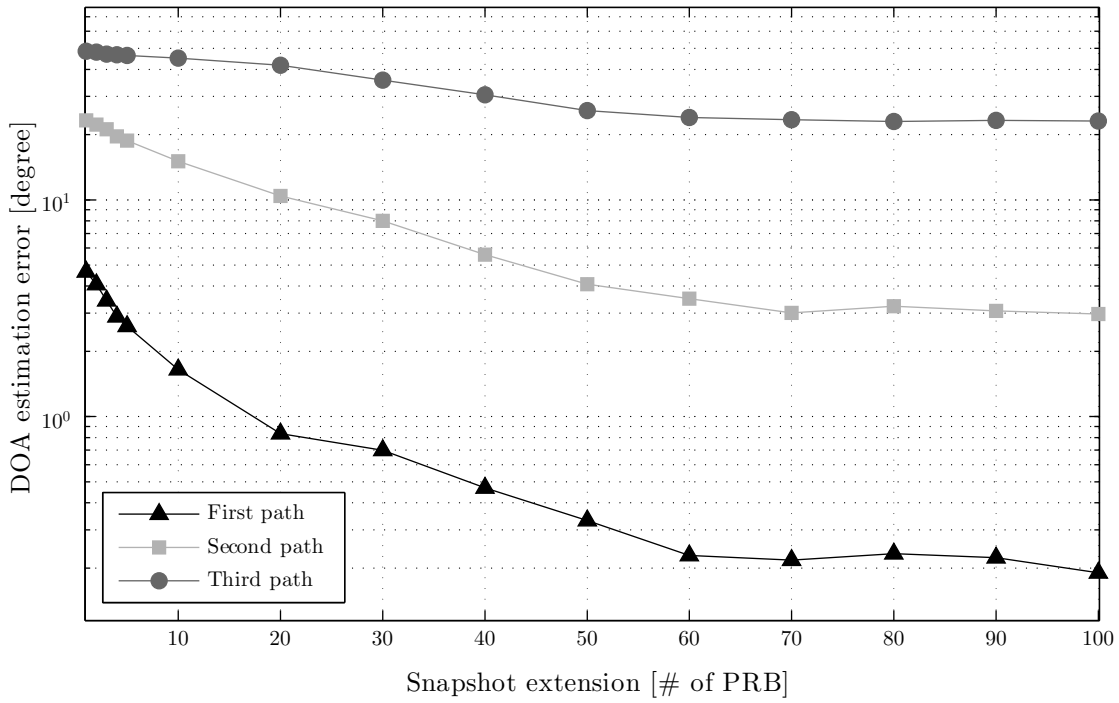

Figure 3-21: Performance for each resolvable path of root MuSiC algorithm when the numbers of sensed PRBs varies.

Procedure 3 Proposed algorithm

• First Iterative thresholding and row deletion
$\mathbf{T} \leftarrow$ random_permutation($[1, \cdots, P]$)
$K' \leftarrow 0$
for $t \leftarrow 1$ to P **do**
  $f = T + t$
  $j = 1$
  while $j < P$ **do**
    if $\tilde{r}_{f,j}^{(t)} > \Gamma \quad \& \quad f \neq j$ **then**
      $K' \leftarrow K' + 1$
      $\mathbf{q}' \leftarrow f$
      $\tilde{\mathbf{r}}_{\mathbf{j}}^{(\mathbf{t})} \leftarrow [0, \cdots, 0]$
      $j = P$
    else
      $j = j + 1$
    end if
  end while
end for
• Matrix Z
for $i \leftarrow 1$ to K' **do**
  for $j \leftarrow 1$ to K' **do**
    $z_{i,j} = \mathbf{r}_{q'_i} \mathbf{r}_{q'_j}$
  end for
end for
• Second Iterative thresholding and row deletion
$K \leftarrow K'$
$\mathbf{q} = \mathbf{q}'$
$\tilde{\mathbf{R}}^{final} = \tilde{\mathbf{R}}^{(P)}$
for $i \leftarrow 1$ to K' **do**
  for $j \leftarrow 1$ to K' **do**
    if $i > j \quad \& \quad z_{i,j} > \Gamma$ **then**
      $K \leftarrow K - 1$
      $\mathbf{q} \leftarrow \mathbf{q} - q_j$
      $\tilde{\mathbf{r}}_{\mathbf{j}}^{\mathbf{final}} \leftarrow [0, \cdots, 0]$
    end if
  end for
end for

Chapter 4

Embracing Interference: Physical Layer Network Coding

Abstract

Physical Layer Network Coding (PLNC) schemes under multipath fading channel propagation conditions are investigated here. PLNC in two way relay networks ideally allows to drastically increase the network throughput. However, under the assumption of actual channel propagation conditions, the performance quickly degrades due to high decoding error probability.

A suitable approach based on a signal pre-equalization technique is proposed for Orthogonal Frequency Division Multiplexing systems. Three subcarriers suppression methods are introduced, differing each other for the performance achieved and the required amount of signalling that nodes have to exchange. The important result obtained here is the enhancement of the system reliability with a slight decrease of the throughput.

Furthermore, a novel multiple access scheme based on the PLNC concept is proposed. This technique can be used in the uplink of any wireless access network to increase the total system throughput. It exploits the multi-user channel diversity to allow different users to send transmissions toward an access point using the same frequency band at the same time. The proposed method allows doubling the system efficiency; its performance is compared with that of a conventional access system where the modulation order is doubled. The effectiveness of the proposed scheme is verified by means of either theoretical analysis or computer simulations.

The performance is investigated for propagation channels characterized by different fading severity. The results show that the comparative performance differences when the channel conditions deteriorate, and it is revealed that the new system has substantial benefits when the channel condition is very bad.

4.1 Introduction

The need for high data rate in mobile communications has led many research efforts to develop new transmission techniques with the goal of enhancing the spectral efficiency. To this goal, recently great attention has been devoted to network coding (NC), which is a possible key technology to maximize the useful throughput in a communication network by combining independent multicast data flows at the intermediate nodes [119]. The NC concept removes the typical requirement that different information flows have to be processed and transmitted independently through the network. Indeed, it is based on the idea that a linear

combination of several communication flows is transmitted at a given time. In particular, when the NC concept is applied to the physical layer (PLNC) the linear combination of the signals is obtained by exploiting the broadcast nature of the propagation channel. In particular, when NC concept is applied to the Physical Layer (PLNC) [120, 121] the linear combination of the signals is obtained by exploiting the broadcast nature of the propagation channel [122].

One of the most promising applications of the PLNC is the two-way relay network (TWRN) [123], where two terminal nodes, $\mathcal{T}_1$ and $\mathcal{T}_2$, exchange informations with the assistance of a central relay node, $\mathcal{R}$. One of the most discussed applications is satellite communication networks, where two satellites exchange aggregated data stream through a base station on the ground [124]. Assuming a conventional time division multiple access scheme, four time slots are needed to achieve the information exchange. Two slots are necessary to convey the signals of the terminals to the relay so that they do not interfere at the receiver. The third and the fourth slots are used by $\mathcal{R}$ to forward the received information to $\mathcal{T}_1$ and $\mathcal{T}_2$. We refer to this classical approach as 4-*slot TWRN*. The PLNC approach reduces the number of necessary slots to two. It allows the terminal nodes to transmit on the same time slot, letting the signals interfere at the relay (multiple access(MA) stage) and the relay to transmit a combination of the received signals (broadcast(BC) stage) in the second slot. In this scheme, the node $\mathcal{R}$ considers the collision of the signals transmitted by the terminal nodes simply as the sum of the two, and performs a suitable preprocessing operation on the received signal before broadcasting. Finally, $\mathcal{T}_1$ and $\mathcal{T}_2$ can recover the data transmitted by each one through the knowledge of the previously transmitted signal and the particular combination performed by $\mathcal{R}$.

The two basic PLNC approaches are *Amplify and Forward* (AF) [120] and *Decode and Forward* (DF) [121]. In the former approach, also known as *Analog Network Coding* (ANC), the relay node simply amplifies and forwards the received collided signal on the next time slot. In the latter approach, often referred to as *DeNoise and Forward*, the relay node performs an ad-hoc detection of the received signal and then uses the decision to forward a new modulated signal to both nodes on the next time slot.

The AF approach is usually less efficient because the noise level is amplified jointly with the useful signal. In particular, in [125] it is highlighted that the AF approach is effective only under high SNR (Signal-to-Noise Ratio) conditions. However, in actual wireless channels, e.g., under multipath fading propagation conditions, each link usually experiences different channel gain and, as a consequence, the DF approach performance degrades due to the power unbalance between the two interfering signals. Several papers in literature deal with different proposals to solve the AF scheme drawbacks [126–130]. Regarding the DF alternative, widely suggested methods are based on ideal pre-equalization of channel [131–133]. The main drawback here is that whenever the signals are affected by deep fading attenuations, pre-equalization at the transmitting sides should require significant amplification that is usually hard to accomplish. The problem of channel pre-equalization (i.e., channel inversion) under power constraints has been investigated in [134] and [135] for the case of two nodes directly connected through the same channel. Moreover, alternatives allowing good performance under multipath fading propagation conditions at the expense of an increased implementation complexity were proposed in [136, 137]. In particular, in [136] a blind signal separation at the relay node is proposed by resorting to complex matrix inversion and diagonalization. Likewise, [137] considers the possibility of integrating PLNC and channel coding schemes and proposes two soft demodulation approaches that can be used adaptively in relation to different channel propagation conditions. In [138] channel fading effects are counteracted with a suitable symbol mapping. Finally, in [139] an approach is outlined based on a suitable

power control technique to be jointly applied at both nodes to lower the influence of multipath fading on system performance. The main drawback of the approach proposed in [139] is the significant increase of the signalling overhead.

In the first section of this chapter, the multi-carrier nature of OFDM is exploited to counteract the inefficiency of channel inversion and, at the same time, to take into account the power constraints. In the second section, the channel imbalance between $\mathcal{T}_1$ and $\mathcal{T}_2$ allows a novel multiple access scheme based on the PLNC concept.

4.2 Enhancing PLNC in Two Way Relay Networks

4.2.1 DF-PLNC approach

We focus on a TDMA based TWRN, where two end nodes ($\mathcal{T}_1$, $\mathcal{T}_2$) and a relay node $\mathcal{R}$ adopt the DF-PLNC approach. Each node exploits the OFDM modulation with K subcarriers, each one modulated through a QPSK scheme[1]. The duration of one TDMA slot has been considered equal to an OFDM symbol. As a consequence, the baseband signal transmitted by node $\mathcal{T}_i$, with $i = 1, 2$, on the k-th subcarrier can be expressed as

$$s_{\mathcal{T}_i}[k] = \frac{\sqrt{2}}{2} \left(a_{\mathcal{T}_i,I}[k] + j a_{\mathcal{T}_i,Q}[k] \right) \tag{4.1}$$

where the in phase $a_{\mathcal{T}_i,I}[k]$ and quadrature $a_{\mathcal{T}_i,Q}[k]$ components of $s_{\mathcal{T}_i}[k]$ may assume the values ± 1 with equal probability, depending on the bits mapped on the symbol. Assuming for the two interfering signals ideal channel conditions, i.e., neither Additive White Gaussian Noise (AWGN) nor multipath fading, ideal symbol and carrier synchronization and the same power level at the $\mathcal{R}$ side, the received signal simply results in their symbol by symbol sum. According to [121], we have that the in phase and quadrature components of the received signal on the k-th subcarrier, $r_{\mathcal{R},I/Q}[k]$ may assume three possible values, i.e., $\pm\sqrt{2}$ if the two nodes transmit the same symbol, 0 otherwise.

The node $\mathcal{R}$ detects if the two terminals have transmitted the same symbol or not, and then sends out the signal $s_{\mathcal{R}}[k] = \frac{\sqrt{2}}{2} \left(a_{\mathcal{R},I}[k] + j a_{\mathcal{R},Q}[k] \right)$, where $a_{\mathcal{R},x}[k]$, with $x = I, Q$, is defined according to the following mapping rule:

$$a_{\mathcal{R},x}[k] = \begin{cases} +1 & \text{if} \quad a_{\mathcal{T}_1,x} \neq a_{\mathcal{T}_2,x} \\ -1 & \text{otherwise.} \end{cases} . \tag{4.2}$$

Each of the two nodes $\mathcal{T}_1$ and $\mathcal{T}_2$ performs the decision on the received QPSK symbols according to the classical coherent approach [66]. Then, by performing a bit-by-bit *xor* operation with the previously transmitted bits, on the I and Q channels, $\mathcal{T}_1$ and $\mathcal{T}_2$ are able to retrieve the information sent by the other node.

DF-PLNC in AWGN channel

By assuming an AWGN communication channel, the signal received at the $\mathcal{R}$ side results as

$$r_{\mathcal{R}}[k] = s_{\mathcal{T}_1}[k] + s_{\mathcal{T}_2}[k] + n_{\mathcal{R}}[k] \tag{4.3}$$

where the terms $n_{\mathcal{R}}[k] \sim \mathcal{CN}(0, \sigma_n^2)$ are complex Gaussian random variables with zero mean and variance σ_n^2.

[1] It is possible to extend this approach to the case of higher order modulation as explained in [121, 140].

In order to correctly detect the received signal, suitable decision regions have to be chosen at the $\mathcal{R}$ side, according to the maximum a posteriori probability (MAP) criterion. From [121], the threshold values that mark off these regions are

$$\Gamma_1 = +\frac{\sqrt{2}}{2}\left[1+\frac{1}{2\gamma}\ln\left(1+\sqrt{1-e^{-4\gamma}}\right)\right] \tag{4.4}$$

$$\Gamma_2 = -\frac{\sqrt{2}}{2}\left[1+\frac{1}{2\gamma}\ln\left(1+\sqrt{1-e^{-4\gamma}}\right)\right] \tag{4.5}$$

where γ represents the mean SNR at the receiver, defined as

$$\gamma = \frac{|s_{\mathcal{T}}[k]|^2}{\sigma_n^2} = \frac{1}{\sigma_n^2}. \tag{4.6}$$

Note that, since the possible received signals are not equiprobable, the decision regions depend on γ [66]. Consequently, $\mathcal{R}$ must know the noise variance σ_n^2 to perform an optimum decoding. The decision rule (4.2) becomes

$$a_{\mathcal{R},x}[k] = \begin{cases} +1 & \text{if} \quad \Gamma_2 < r_{\mathcal{R},x} < \Gamma_1 \\ -1 & \text{otherwise} \end{cases} . \tag{4.7}$$

DF PLNC in multipath fading environment

The communication channel is assumed to be affected by multipath fading with Rayleigh distribution. The channel linking $\mathcal{T}_1$, $\mathcal{T}_2$ to $\mathcal{R}$ is modelled as a FIR filter with L taps. Let $\mathbf{h}_i$ be a vector whose entries $h_i[k]$, with $k = 0, 1, \cdots, L-1$, represent the tap coefficients of the propagation channel between the node $\mathcal{T}_i$ and $\mathcal{R}$, as

$$\mathbf{h}_i = \big[h_i[0], h_i[1], \cdots, h_i[L-1]\big]^T \qquad i = 1, 2 \tag{4.8}$$

where $h_i[l] \sim \mathcal{CN}(0, \sigma_l^2)$, with $l = 0, 1, \cdots, L-1$. Furthermore, we consider that both channels have an identical, independent behaviour, and channel propagation conditions constant over a time interval two time slots long. The channel frequency response at each subcarrier k for the node $\mathcal{T}_i$, $i = 1, 2$ is

$$H_i[k] = \sum_{l=0}^{L-1} h_i[l]\, e^{-2j\pi\frac{k}{K}l}. \tag{4.9}$$

By assuming a pre-compensation of the phases performed at $\mathcal{T}_i$, with $i = 1, 2$, the signal received at the $\mathcal{R}$ side on the k-th subcarrier can be defined as

$$r_{\mathcal{R}}[k] = \big|H_1[k]\big| \cdot s_{\mathcal{T}_1}[k] + \big|H_2[k]\big| \cdot s_{\mathcal{T}_2}[k] + n_{\mathcal{R}}[k]. \tag{4.10}$$

Hence, the possible levels of the received signal depend on the current channels state $\big|H_i[k]\big|$, with $i = 1, 2$ and are different for each subcarrier (i.e, $k = 1, \cdots, K$) [10].

It must be noticed that $\mathcal{R}$ cannot directly equalize the received signal, since the two channels generally have different channel gains at the same subcarrier. Equalization at the $\mathcal{R}$ node requires different and more complex schemes, e.g., the coded-PLNC proposed in [141]. Hence, MAP decision regions, depending on $H_i[k]$ terms, have to be considered in order to correctly detect the received signal. Optimum decision regions have been investigated in [139], where also a sub-optimum threshold value is proposed, (i.e., $\Gamma = \pm \max_{i=1,2}\{|H_i[k]|\}$).

The performance of this method has been provided in Sec. 4.2.3 (named as "PLNC - No Channel Inversion") for comparison. Even considering a sub-optimum implementation, the direct use of this approach is complex to achieve in the case of OFDM based communication systems. Indeed, each node $\mathcal{T}_i$ needs to estimate all the channel gains (i.e., one for each subcarrier) and communicate their values to $\mathcal{R}$, requiring a heavy signalling overhead.

Channel inversion

Under the assumption of subcarriers channel gains known at the end nodes, it is possible to set the amplitude of each subcarrier directly proportional to the reciprocal of the related channel gain (pre-equalization[2]), i.e., $\left|p_i[k]\right| = \left|\frac{F_i}{H_i[k]}\right|$, where $p_i[k]$ denotes the precoding coefficient of the k-th subcarrier for the $\mathcal{T}_i$ node. The normalization factor F_i is derived in order to take into account the bound on the transmitting power, since in actual applications it has to be limited. Assuming the IDFT operation performed at the transmitting side with unit gain, we have

$$\sum_{k=0}^{K-1} |p_i[k]|^2 \;=\; \sum_{k=0}^{K-1} \left|\frac{F_i}{H_i[k]}\right|^2 \;=\; K \tag{4.11}$$

and hence,

$$F_i = f(\mathbf{H}_i) = \sqrt{\frac{K}{\sum_{k=0}^{K-1} \frac{1}{|H_i[k]|^2}}}. \tag{4.12}$$

Each normalization factor F_i in (4.12) depends on the particular channel realization, $\mathbf{H}_i$. When both $\mathcal{T}_1$ and $\mathcal{T}_2$ exploit the channel inversion, the signal received at the $\mathcal{R}$ side can be expressed as

$$r_{\mathcal{R}}[k] = F_1 \cdot s_{\mathcal{T}_1}[k] + F_2 \cdot s_{\mathcal{T}_2}[k] + n_{\mathcal{R}}[k]. \tag{4.13}$$

The channel inversion makes the signal flat on the whole bandwidth and, hence, equal decision regions can be considered at the $\mathcal{R}$ side. As a consequence, $\mathcal{R}$ needs to know only the normalization factors F_1 and F_2. This can be accomplished, for instance, by allocating two subcarriers (one for each terminal) to the exclusive transmission of precoded pilot tones. Hence, the new decision thresholds become

$$\Gamma_1 = +\min_{i=1,2}\{F_i\} \tag{4.14}$$

$$\Gamma_2 = -\min_{i=1,2}\{F_i\}. \tag{4.15}$$

It is important to stress that this method does not need further signalling and, in particular, there is no need of performing power control to balance the two received signal levels at the $\mathcal{R}$ side.

The greater the value of $\min\{F_i\}$, the higher the equivalent SNR at the $\mathcal{R}$ side will be. In particular, the P_e in the MA stage is the same for each subcarrier and can be expressed as

$$\begin{aligned} P_e^{MA}(\mathbf{H_{1,2}}) \;&= Q\big(\sqrt{\overline{\gamma} m^2}\big) - \frac{1}{2} Q\big(\sqrt{\overline{\gamma}(2M+m)^2}\big) + \\ &+ \frac{1}{2} Q\big(\sqrt{\overline{\gamma}(2M-m)^2}\big) \end{aligned} \tag{4.16}$$

[2]This method is also known in literature as ZF precoding.

where $Q(\cdot)$ denotes the Q-function, $m = \min_{i=1,2}\{f(\mathbf{H}_i)\}$, $M = \max_{i=1,2}\{f(\mathbf{H}_i)\}$ and $\overline{\gamma}$ is the mean SNR value at the receiver side. The drawback of this approach is that the normalization factors usually assume small values, leading to high P_e. Thus, with the aim of lowering this effect on the system performance, three subcarriers suppression techniques will be proposed and discussed in what follows.

4.2.2 Subcarriers Suppression methods

As well-known in literature, the channel inversion counteracts the multipath effects but it is a quite inefficient technique, since it leads to poor performance in terms of P_e and hence in terms of useful throughput when F_i is low [139], e.g., under severe attenuation conditions. It is straightforward to note that the behavior of the normalization factors is due to the most attenuated subcarriers which make the mean power level at the $\mathcal{R}$ side very low. Selective subcarriers suppression criteria are used to increase system performance: each subcarrier having a channel gain lower than a specified threshold is suppressed. The saved power is allocated to the remaining subcarriers [142] in order to improve data reliability. This technique exploits channel frequency diversity and knowledge of the channel propagation conditions at the transmitting side. Hence, denoting with λ the selected suppression threshold value[3], the subcarriers are turned off if the following constraint is valid:

$$\left|H_i[k]\right| < \lambda \Longrightarrow s_{\mathcal{T}_i}[k] = 0 \quad \text{for} \quad \begin{matrix} k = 0, \cdots, K-1 \\ i = 1, 2 \end{matrix} . \tag{4.17}$$

This prevents waste of power and allows to fruitfully allocate it on the remaining active subcarriers. As a consequence, the normalization factors F_1, F_2 result to be dependent on λ as follows

$$F_{\lambda,i} = f_\lambda(\mathbf{H}_i) = \sqrt{\frac{K}{\sum_{k=0}^{K-1} \frac{\chi_i^{(\lambda)}[k]}{|H_i[k]|^2}}} \tag{18a}$$

where

$$\chi_i^{(\lambda)}[k] = \begin{cases} 0 & \text{if} \quad \left|H_i[k]\right|^2 < \lambda \\ 1 & \text{otherwise} \end{cases} . \tag{18b}$$

The number of suppressed subcarriers grows as λ increases and, hence, the normalization factor $F_{\lambda,i}$ increases too. Since the P_e depends on $F_{\lambda,i}$, this approach allows an improvement of the system reliability at the expense of a reduced transmitting rate. The receiver needs to know which subcarriers have been suppressed in order to prevent the detection on them, thus requiring additional signalling overhead. A possible solution is proposed in the next section. In the next sub-sections three subcarriers suppression methods will be proposed and compared, taking into account the communication reliability (i.e., P_e), throughput gain and signalling overhead.

Independent Subcarriers Suppression

The first method proposed here is named Independent Subcarriers Suppression (ISS): each source/destination node chooses the threshold value λ in relation to a target P_e, and turns off each subcarrier experiencing a channel gain below the specified threshold. This information is encoded in a vector with dimension equal to the number of subcarriers, whose entries are "1"

[3]We suppose that both terminals choose the same suppression threshold, since the use of different thresholds would lead to intermediate performance.

or "0", with "1" denoting the active subcarriers, conversely, "0" indicates the suppressed ones. A suitable scheduling is adopted to allow both nodes $\mathcal{T}_1$ and $\mathcal{T}_2$ to transmit their streams containing the signalling vectors to $\mathcal{R}$ avoiding collision or interference. The node $\mathcal{R}$ after receiving the two vectors (assumed error-free) forms a new vector through a bit-by-bit *xor* operation and broadcasts it to $\mathcal{T}_1$ and $\mathcal{T}_2$. On the basis of the knowledge of their original vector, nodes $\mathcal{T}_1$ and $\mathcal{T}_2$ can easily retrieve the information concerning the suppressed subcarriers by the other node. Since the marginal distribution of the power of each subcarrier is exponentially distributed with expected value equal to 1, the mean number of active subcarriers[4] $N_\lambda^{(ISS)}$ can be derived as

$$\begin{aligned} N_\lambda^{ISS} &= K \cdot (1 - (1 - Pr\{|H[k]|^2 > \lambda\})^2) \\ &= K \cdot (1 - (1 - e^{-\lambda})^2) \end{aligned} \tag{4.19}$$

During the MA phase, each node transmits only on its active subcarriers so, in order to perform the detection correctly, the $\mathcal{R}$ node has to distinguish for each subcarrier among the following cases:

1. the subcarrier has been used by $\mathcal{T}_1$ and $\mathcal{T}_2$, so DF-PLNC decoding has to be performed.
2. only one of the terminal nodes has used the subcarrier, so classical QPSK detection has to be applied.
3. none of the source nodes has transmitted, so decoding does not have to be applied.

Similarly, during the BC phase, $\mathcal{T}_1$ and $\mathcal{T}_2$ have to distinguish among the cases:

1. the subcarrier carries network coded information, so DF-PLNC decoding has to be applied (i.e., the received bit is *xor*-ed with the previously transmitted one).
2. only the other terminal has transmitted on the subcarrier, so classical QPSK detection has to be applied.
3. the other terminal has suppressed the subcarrier, so the detection is avoided.

During the BC phase, $\mathcal{R}$ allocates the available power only to the active subcarriers, i.e., used by at least one node. Fig. 4-1a briefly outlines the ISS principle.

The overall P_e on the active subcarriers can be calculated taking into account that the active subcarriers can be used for transmission by a single node or both nodes. By averaging the P_e related to the two cases, we have

$$P_{e,ISS}(\lambda) = P_e^{(1)}(\lambda)\mathcal{P}_1(\lambda) + P_e^{(2)}(\lambda)\mathcal{P}_2(\lambda). \tag{4.20}$$

where

- $P_e^{(1)}(\lambda)$ is the P_e of a subcarrier active for both nodes, defined by (B.5) in the Appendix;
- $P_e^{(2)}(\lambda)$ is the P_e of a subcarrier active for a single node defined by (B.10) in the Appendix;
- $\mathcal{P}_1(\lambda)$ is the probability that a subcarrier is active for both nodes defined by (B.1) in Appendix;

[4]In the ISS scheme a subcarrier is defined "active" if is used at least by one node.

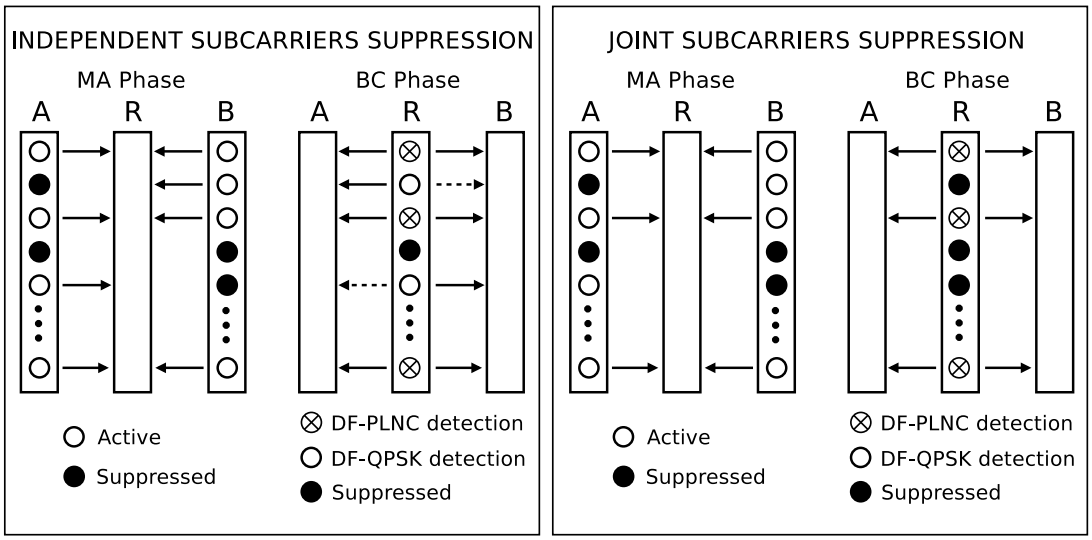

(a) Independent Subcarriers Suppression scheme (b) Joint Subcarriers Suppression scheme

Figure 4-1: Independent and Joint Subcarriers Suppression schemes

- $\mathcal{P}_2(\lambda)$ is the probability that a subcarrier is active for a single node defined by (B.6) in the Appendix.

The main drawback of this method is that the subcarriers suppressed by a single node are turned off during the MA stage but are used in the BC stage by $\mathcal{R}$: during the BC phase the gain of these subcarriers is lower than the suppression threshold. Hence, this method allows performance improvement only at the MA stage, while a significant performance degradation is introduced at the BC stage.

Joint Subcarriers Suppression

The second method proposed here is named Joint Subcarriers Suppression (JSS). Each terminal node chooses a threshold value and communicates to $\mathcal{R}$ which subcarriers are active as for the ISS case. However, according to the JSS scheme, the transmission takes place only on the subcarriers selected by both $\mathcal{T}_1$ and $\mathcal{T}_2$.

The JSS scheme transmission rate is reduced compared with the ISS method. On the other hand, transmission takes place only on the subcarriers which are advantageous for both terminals, so channel conditions are good even during the BC stage, i.e., the gain of every active subcarrier is greater than the suppression threshold either on the MA and the BC stage. The mean number of active subcarriers in the JSS scheme results as

$$\begin{aligned} N_\lambda^{JSS} &= K \cdot Pr\{|H_1[k]|^2 > \lambda\} \cdot Pr\{|H_2[k]|^2 > \lambda\} \\ &= K \cdot e^{-\lambda} \cdot e^{-\lambda} = K \cdot e^{-2\lambda} \end{aligned} \tag{4.21}$$

since the channel conditions for nodes $\mathcal{T}_1$ and $\mathcal{T}_2$ are independent. The expression of the P_e on the active subcarriers corresponds to $P_e^{(1)}(\lambda)$, defined in the Appendix by (B.5)

$$P_{e,JSS}(\lambda) = P_e^{(1)}(\lambda). \tag{4.22}$$

The operation mode of the JSS approach is sketched in Fig. 4-1. This method allows a significant improvement in terms of data reliability and reduces at the same time the

implementation complexity of the data detection process at the nodes sides, at the expense of a reduced transmission rate.

Blind Subcarriers Suppression

The Blind Subcarriers Suppression (BSS) method, originally presented in [10], is the third technique considered in this section. This technique differs from the previous ones since it does not reduce the transmission rate and it does not need any additional signalling information. The subcarriers are suppressed according to a suitable threshold and the saved transmission power is fruitfully allocated to the remaining subcarriers in order to improve the data decision reliability similarly to the other methods. The main difference here is that the informative bits are mapped on all subcarriers, even on the suppressed ones, so that we have to distinguish between effective bit transmissions on active subcarriers and virtual bit transmissions on suppressed subcarriers. It is easy to note that the decision on any virtually transmitted bit at the destination node can be performed with a fair coin toss giving rise to a bit error decision probability of 0.5. However, this detrimental effect is balanced by the benefit of the power allocated to the active subcarriers to enhance the reliability of the bit decisions.

It is important to stress that this method does not require any additional signalling. Differently from the ISS and JSS methods, in this case the end nodes do not need to share information concerning the active subcarriers: the decoding is performed on all subcarriers anyway.

In the BSS scheme the mean number of active subcarriers for each user is $K \cdot e^{-\lambda}$. However, at the $\mathcal{R}$ side, only the subcarriers which are active for both terminals may have P_e different from 0.5, thus we consider only these as "active". Hence, the number of these subcarriers is

$$N_{\lambda}^{BSS} = K \cdot e^{-2\lambda} \tag{4.23}$$

that results equal to N_{λ}^{JSS} given by (4.22).

In order to express the overall P_e, we have to consider that at the $\mathcal{R}$ side the subcarriers suppressed by at least one terminal have 50% of decoding error probability, while the P_e of the subcarriers active for both terminals is equal to $P_e^{MA,1}$, given by (B.2) in the Appendix. So the resulting P_e of the MA stage can be expressed as

$$\begin{aligned} P_{e,BSS}^{MA}(\lambda) &= \frac{1}{2}P_{off} + P_e^{MA,1}(1 - P_{off}) \\ &= \frac{1}{2}(1 - e^{-2\lambda}) + P_e^{MA,1}e^{-2\lambda} \end{aligned} \tag{4.24}$$

where P_{off} is the probability that a subcarrier is suppressed at least by one of the two end nodes.

Likewise, it is straightforward to note that the P_e at the BC stage is equal to the classical bit error probability of a QPSK modulation scheme [66]. Hence, we have

$$P_{e,BSS}^{BC} = \int_0^{\infty} Q\big(\sqrt{\overline{\gamma}H^2}\big) f_r(H) dH \tag{4.25}$$

where $f_r(\,\cdot\,)$ is the Rayleigh probability distribution of $H_i[k]$ with $i = 1, 2$ and $k = 1, \cdots, K$.

Finally, we have that the overall P_e at each end node results as

$$P_{e,BSS}(\lambda) = P_{e,BSS}^{MA}(\lambda)(1 - P_{e,BSS}^{BC}) + P_{e,BSS}^{BC}(1 - P_{e,BSS}^{MA}(\lambda)). \tag{4.26}$$

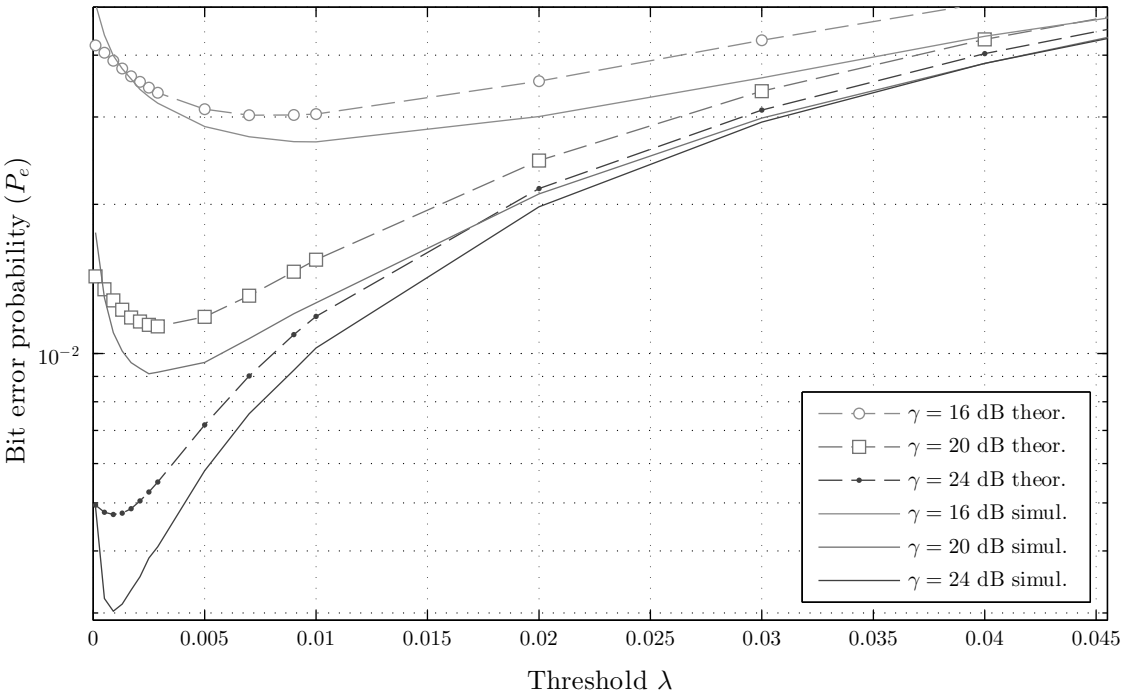

Figure 4-2: P_e as a function threshold λ for different SNR values

.

As shown in [10], each threshold value λ allows an improvement only on a limited range of SNR values. In general, for high $\overline{\gamma}$ values the P_e at $\mathcal{R}$ reaches a floor. Hence, despite the fact the SNR level increases, the performance of the system does not improve. In particular, the P_e has a floor, $P_{e,floor}$, when errors due to the suppressed subcarriers become dominant in comparison with the errors due to the channel noise, i.e., $\frac{1}{2}(1-e^{-2\lambda}) \gg P_{e,ISS}^{MA,1} e^{-2\lambda}$. Hence, we have $P_{e,floor} = \frac{1}{2}(1-e^{-2\lambda})$.

An optimization of the BSS method is possible by selecting the threshold value λ minimizing the overall P_e and, hence, maximizing the useful throughput, i.e., the mean number of error-free received packets per second, at the end nodes.

4.2.3 Numerical results

This section deals with the performance evaluation of the three proposed subcarriers suppression methods carried out on the basis of a suitable analytical approach and computer simulations. The overall available bandwidth of the system under consideration, B, has been assumed equal to 1 MHz and divided in $K = 64$ equally spaced OFDM subcarriers, each one modulated according to a QPSK scheme. Furthermore, we have considered a cyclic prefix CP equal to 16 samples and terminal nodes ($\mathcal{T}_1$ and $\mathcal{T}_2$) using zero-forcing equalization to counteract the multipath effects in the BC stage reception. The ITU-R pedestrian channel model [48], with 4 active paths and maximum delay spread equal to 410 ns has been assumed in deriving the simulation results. Performance of the proposed methods has been evaluated in terms of P_e and useful throughput.

We start our analysis by evaluating the dependence of the BSS performance on the threshold value. In particular, our aim is to derive the optimum threshold value, λ_{opt}, which minimizes the overall P_e as a function of the SNR value at the receiving end, as shown in Fig. 4-2. As expected, the value of λ_{opt} decreases when the SNR gets higher. The number

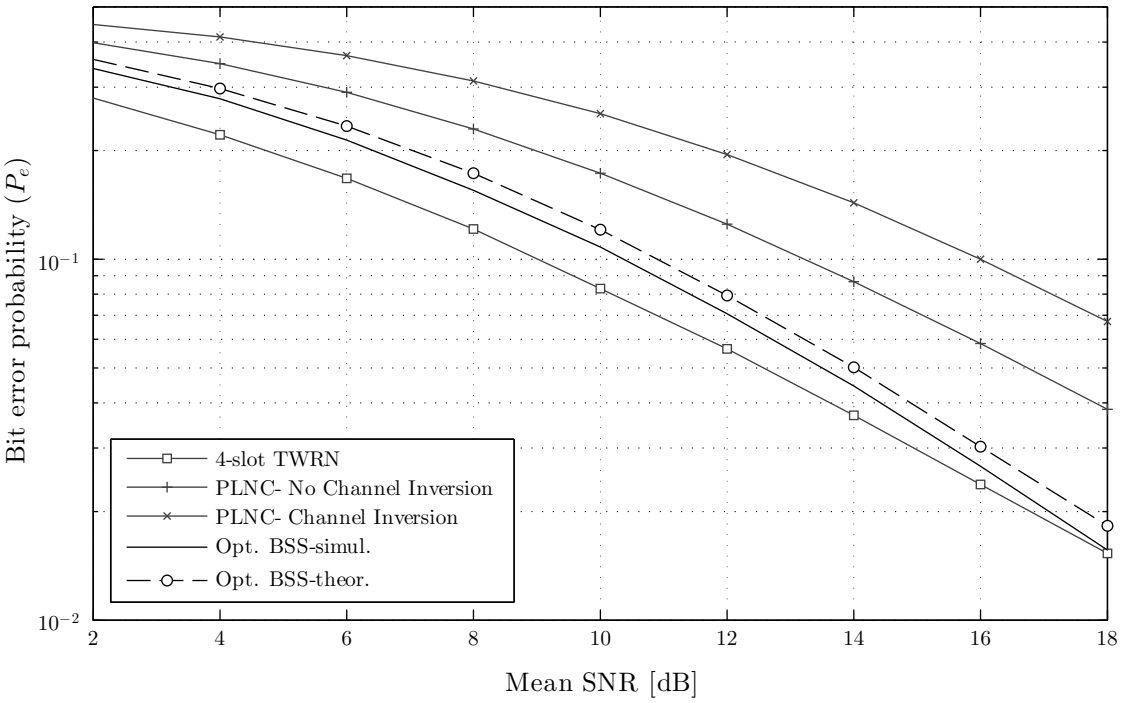

Figure 4-3: P_e of the BSS scheme with optimized threshold values as a function of the mean SNR.

of inactive subcarriers under high SNR conditions must be limited, because the associated bit decision errors become dominant on the overall P_e performance.

Fig. 4-3 shows the P_e achieved by the optimized BSS scheme, i.e., using λ_{opt} values for each SNR. The performance is compared with that of a classical TWRN[5], a PLNC scheme using channel inversion and a PLNC scheme without channel inversion. It is possible to note that the BSS technique achieves a remarkable improvement and approaches the P_e of the system without PLNC (lower bound) under high SNR conditions.

Figs. 4-4 and 4-5 show the P_e performance for the ISS and JSS schemes, respectively, in the case of different threshold values. From Fig. 4-4 it is evident that ISS is affected by errors introduced in the BC stage under high SNR conditions. In particular, it is possible to note in this figure that the P_e reaches a floor when λ increases. Conversely, in the JSS scheme the P_e significantly decreases as λ increases. Furthermore, considering a same λ value, the JSS scheme achieves a lower P_e than the ISS alternative.

The proposed subcarriers suppression schemes have also been evaluated also in terms of outage probability, considering a P_e target value equal to 10^{-2} leading to similar results as shown in Fig. 4-6.

As stated in the previous section, the three carriers suppression approaches turn off a different number of subcarriers, hence, Fig. 4-7 provides a comparison in terms of achieved useful throughput assuming a packet size, D, equal to 64 bits. As a benchmark we consider the maximum value of the useful throughput (i.e., the maximum transmission rate of the system, under the assumption of no transmission errors), defined as

$$R_{max} = \frac{1}{2}\frac{K \cdot b}{K + CP} \cdot \frac{B}{D} = 25 \cdot 10^3 \; pkts/\text{s} \tag{4.27}$$

[5]i.e., when the PLNC approach is not exploited: 4 time slots are used for a bi-directional communications between nodes

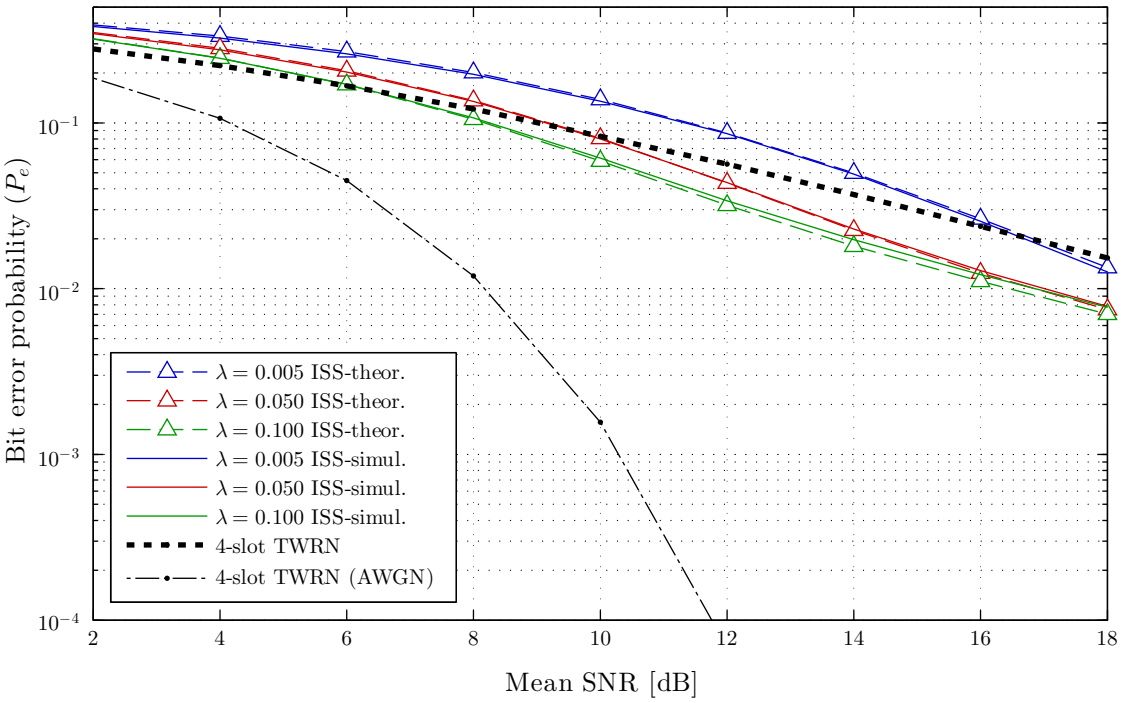

Figure 4-4: P_e of the ISS scheme as a function of the mean SNR for different threshold values.

where b is the number of bits carried by each subcarrier. It is important to point out that in (4.27) the available bandwidth is considered doubled compared to the system not using PLNC since $\mathcal{T}_1$ and $\mathcal{T}_2$ access the channel simultaneously[6]. From Fig. 4-7 it is possible to note that the JSS scheme allows the highest throughput for low SNR conditions and high λ values. Moreover, we can note that ISS and JSS present a lower throughput due to the lack of data reliability, despite the fact they have a higher transmission rate. When the SNR is high, ISS and BSS performance approach that of JSS. Furthermore, it is evident that JSS and ISS performance reaches a floor due to the transmission rate reduction.

Finally, with the aim of a complete performance comparison, it is necessary to consider signalling overhead. With reference to this, we note that BSS method does not require any exchange of information regarding suppressed subcarriers indication. Instead, the JSS and ISS methods need two time slots for the signalling purposes as outlined in Sec. 4.2.2. Moreover, this information has to be updated every time the channel propagation conditions change, so the overhead amount due to the signalling information strongly depends on the coherence time of the channels[7], τ_c, that in turn can be related to the speed of a terminal as

$$\tau_c = \frac{A}{f_d} = \frac{A \cdot c}{v_r f_0} \tag{4.28}$$

where: A is a proportionality constant[8], f_d is the Doppler shift, c is the light speed, f_0 is the carrier frequency, and v_r is the radial speed between nodes.

Denoting by T_{OFDM} the time of an OFDM symbol (equal to one slot), the reduction of

[6]PLNC allows an ideal double the amount of exchanged data at the expense of a reduction of data reliability.

[7]In general the two channels may change with different speeds, τ_c is related to the fastest

[8]A generally depends on the definition of the coherence time.

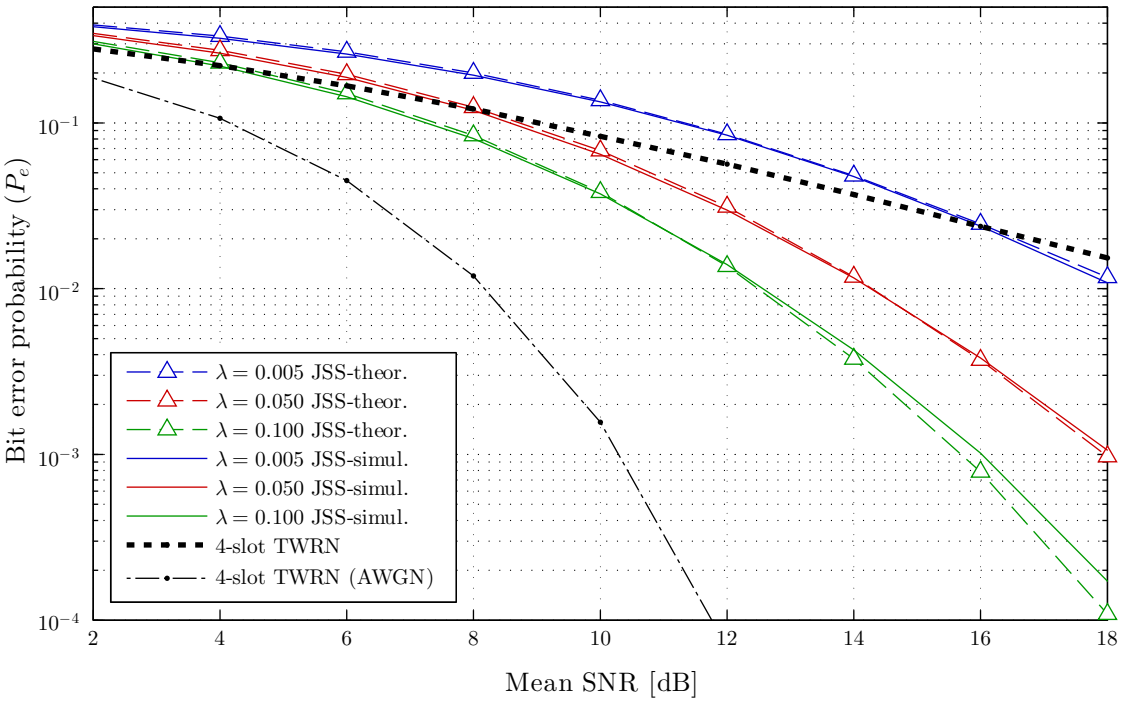

Figure 4-5: P_e of the JSS scheme as a function of the mean SNR for different threshold values.

the throughput due to the signalling overhead can be expressed as

$$\eta = \frac{TP - TP'}{TP} = \frac{3 \cdot T_{OFDM}}{\tau_c} \tag{4.29}$$

where TP indicates the ideal throughput and TP' denotes the throughput by taking into account the signalling overhead.

As an example, assuming $f_0 = 2.4$ GHz, $A = 0.7$ and considering three different node speeds, $v_{r1} = 2$ m/s, $v_{r2} = 10$ m/s and $v_{r3} = 30$ m/s, we have $\tau_{c1} = 12.2$ ms, $\tau_{c2} = 2.4$ ms and $\tau_{c3} = 0.8$ ms. In all these cases the ISS and JSS schemes are affected by of an additional reduction of the useful throughput of 1.97%, 9.87%, 29.62%, respectively.

On the basis of the obtained results, we can state that the BSS has the worst performance in terms of P_e, but it allows a high useful throughput for high SNR conditions, because it does not reduce the transmitting rate. The JSS presents excellent P_e results which reflect in the best throughput performance, despite the large number of inactive subcarriers. The ISS reaches midway performance in terms of P_e even if it is evident from Fig. 4-4 that the resulting P_e has a lower bound regardless of the number of suppressed subcarriers due to the channels propagation conditions. In terms of useful throughput ISS presents performance similar to BSS but requires additional signalling.

4.2.4 Remarkable considerations

The performance evaluations provided for ISS, JSS and BSS methodologies allow us to state that the selection of the best solution depends on the system requirements and specific operational conditions. In general the BSS approach works well under high SNR conditions and low values of λ. It allows high useful throughput without introducing signalling overhead. Hence, it seems to be a suitable solution when high data rates are required and the channel

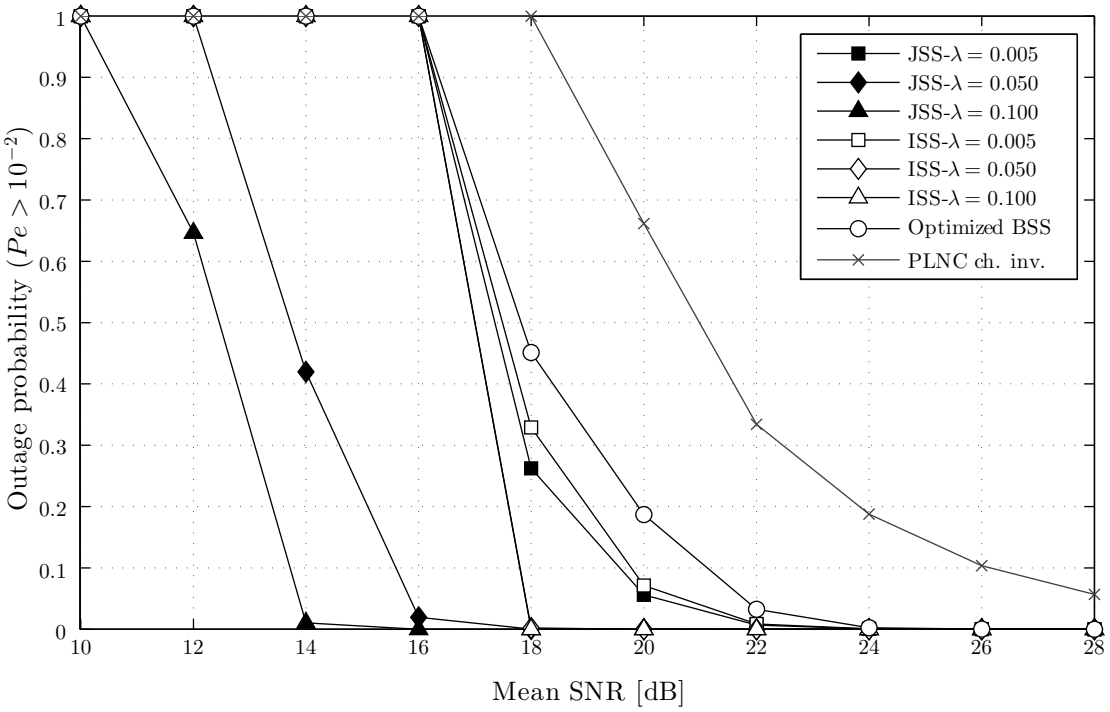

Figure 4-6: Outage probability as a function of the mean SNR for all the methods and different threshold values.

condition is good enough. Conversely, when the data reliability is the main issue, the JSS scheme is the best choice since it allows an efficient use of the subcarriers suppression. Finally, the ISS scheme achieves intermediate results in terms of P_e and throughput.

However, the great improvements achieved here are are strictly related to the network topology. Indeed, the fact that the terminals need to exchange simultaneously informations allows an efficient PLNC. This scenario finds application in satellite communications, where a satellite act as relay between ground stations and/or other satellites, and in mesh networks, where each wireless node routes packets of other nodes. In the next section we propose a more general multiple access scheme, based on the PLNC, suitable for any uplink system.

4.3 Network Coded Multiple Access

This section proposes a new access technique devised on the DF-PLNC concept to be used in any uplink channel affected by severe fading. It can be applied in the uplink of any wireless systems, where several users want to communicate with a central node (i.e., an access point or a base station). The idea is to make two (or more) users communicate simultaneously on the same frequency resources and the central node perform a suitable decoding, newly introduced here, that exploits the multi-user diversity. As stated before, the channel imbalance between the signals is needed to separate the users information.

The fading model assumed here follows the Weibull distribution, which is a flexible statistical model for describing multipath fading channels in both indoor [143], [144] and outdoor [145] radio propagation environments. The Weibull distribution parameters allow studying the behaviour of the system with varying fading severity; the well-known Rayleigh fading can be viewed as the Weibull best case.

The effectiveness of the proposed access method is proved by comparing the performance

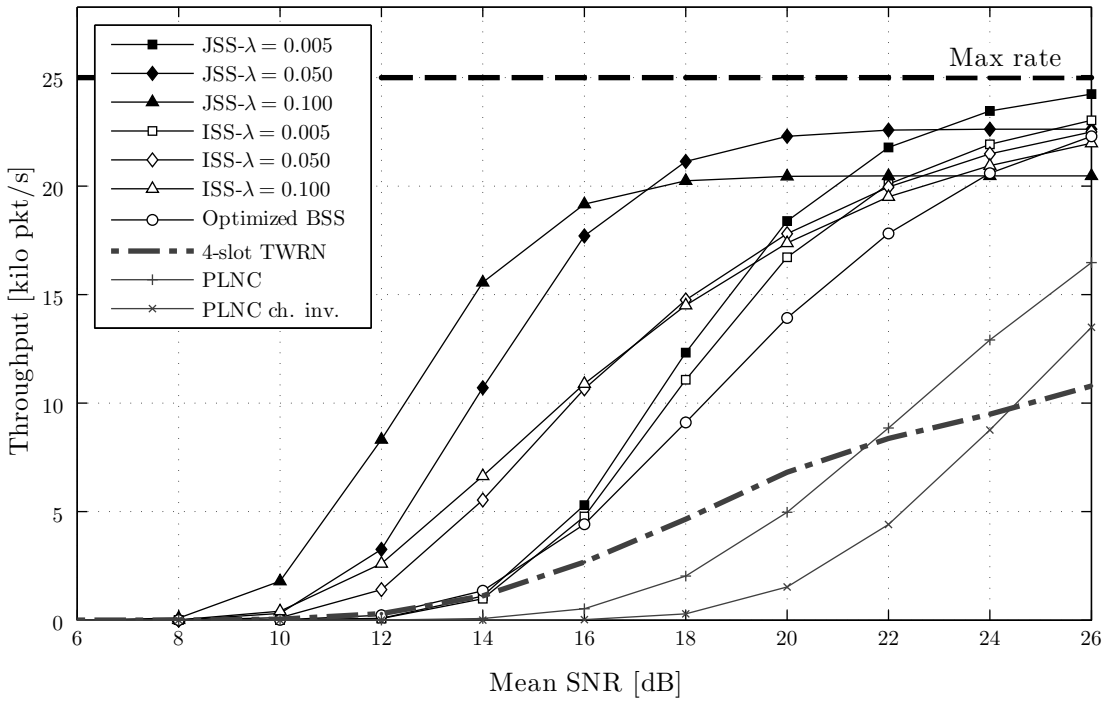

Figure 4-7: BSS, ISS and JSS schemes useful throughput comparison as a function of the mean SNR.

achieved with that of a classical TDMA access scheme (i.e., each user accesses the communication medium in its own time slot) where the modulation order is doubled. The data rate of the two systems are the same, in one case, doubling the number of bits per symbol and in the other case by doubling the number of symbols for time slot.

DF-PLNC in Weibull fading channels

We consider a fading channel whose gain coefficients follow a Weibull distribution. As stated before, the Weibull distribution provides fading characterization that is more flexible than the widely used Rayleigh distribution, that is a special case of Weibull. Indeed, the Rayleigh distribution is used to model fading in environments with a large number of scatterers and is derived theoretically by the central limit theorem, but may be not appropriate in the case of a limited number of incoming radio paths, since the requirements for validity of the theorem may not hold. For example, in [146] it has been shown that the Weibull fading distribution provides a better fit to experimental channel measurements in new wireless applications such as vehicle-to-vehicle communications and wireless sensor networks and aeronautical communications [10].

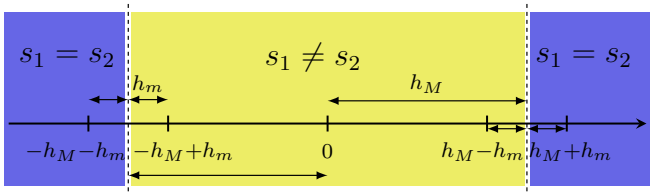

Figure 4-8: Decision regions for the MA stage in a DL-PLNC.

Let us consider communication channels affected by flat fading. We assume ideal phase

Table 4.1: Received signal affected by flat fading

$h_1 s_{\mathcal{T}_1}$	$h_2 s_{\mathcal{T}_2}$	$r_{\mathcal{R}}$	bit
$+h_1$	$+h_2$	$+h_1 + h_2$	0
$-h_1$	$+h_2$	$-h_1 + h_2$	1
$+h_1$	$-h_2$	$+h_1 - h_2$	1
$-h_1$	$-h_2$	$-h_1 - h_2$	0

pre-compensation at the transmitters side. The signal received by the relay can be expressed as

$$r_{\mathcal{R}} = h_1 s_{\mathcal{T}_1} + h_2 s_{\mathcal{T}_2} + n \tag{4.30}$$

where n is a noise sample that we assume follows a Gaussian distribution, $n \sim \mathcal{N}(0, \sigma_n^2)$ and h_i, with $i = 1, 2$, represent the magnitudes of the channel coefficients, considered independent and identically distributed. Each term h_i follows a Weibull distribution, that is

$$f_{h_i}(x; \lambda, \beta) = f_h(x) = \frac{\beta}{\lambda} \left(\frac{x}{\lambda}\right)^{\beta - 1} e^{-\left(\frac{x}{\lambda}\right)^{\beta}} \tag{4.31}$$

where f_{h_i} represents the Weibull probability density function (pdf), and β is a parameter representing the severity of the fading. In particular, when $\beta = 2$ the fading corresponds to the Rayleigh case, while for $\beta = 1$ the Weibull pdf coincides with the exponential distribution, which can be considered a worst case. The scale parameter λ can be expressed as

$$\lambda = \frac{1}{\sqrt{\Gamma\left(1 + \frac{2}{\beta}\right)}} \tag{4.32}$$

since we consider a normalized channel, i.e., $E\left[|h_i|^2\right] = 1$. The possible received signal levels and the associated encoding are depicted in Table 4.1, where the noise at the receiver side $\mathcal{R}$ is omitted for simplicity.

In this case, the decision regions depend on the magnitude of the channel coefficients. In particular, it is useful to denote with h_M and h_m the maximum and the minimum value of h_i, that is

$$h_m = \min_{i=1,2} h_i \tag{4.33}$$

$$h_M = \max_{i=1,2} h_i. \tag{4.34}$$

When the channel is affected by fading it is difficult to find a closed-form expression for the optimum decision thresholds [139]. We consider the suboptimum thresholds $\pm h_M$, leading to the decision regions depicted in Fig. 4-8. If the received signal lies in the central area, the terminal nodes transmitted different symbols, otherwise $\mathcal{T}_1$ and $\mathcal{T}_2$ transmitted the same symbol, that is

$$b_{\mathcal{R}} = \begin{cases} 0 & \text{if} \quad |r_{\mathcal{R}}| < h_M \\ 1 & \text{if} \quad |r_{\mathcal{R}}| > h_M \end{cases} \tag{4.35}$$

where $b_{\mathcal{R}}$ represents the bit that will be encoded and broadcast in the BC stage.

The bit error probability for the MA stage is quite high compared to 4-*slot TWRN*, since the performance strictly depends on h_m, which is usually small. It is straightforward to note that the DF-PLNC can be easily applied to the in-phase and quadrature components of

QPSK modulation. Moreover, in [82], which is the first paper about DF-PLNC in TWRN, the authors show how to extend the PLNC to higher-order modulations.

4.3.1 NCMA

This section presents the proposed multiplexing scheme. It exploits the power imbalance between two users in the MA stage due to the multi-user diversity. Indeed, the underlying idea behind this method arises by noticing that, in presence of uncorrelated fading, it is possible to define decision regions identifying unambiguously all the four possible received signals. This means that the concept of MA stage in PLNC can be used in the uplink to detect and decode two signals arriving in the same time slot and experiencing different channel conditions. Different from the decoding performed by the node $\mathcal{R}$ in a classical DF-PLNC, the proposed method intends to separate the signals of the users and not only determine if the two users transmitted the same information or not; for this reason it is necessary to find the value for the new decision boundaries χ_i, with $i = 1, 2, 3$, for the mapping. Since the possible symbol combinations are equiprobable, it is easy to show that the decision boundaries are

$$\begin{aligned} \chi_1 &= -h_M \\ \chi_2 &= 0 \\ \chi_3 &= +h_M \end{aligned} \tag{4.36}$$

defining the decision regions as follows

$$\begin{aligned} r < \chi_1 \quad &\Rightarrow \quad s_1^{(-)}, s_2^{(-)} \\ \chi_1 < r < \chi_2 \quad &\Rightarrow \quad \begin{cases} s_1^{(-)}, s_2^{(+)} & \text{if} \quad h_1 > h_2 \\ s_1^{(+)}, s_2^{(-)} & \text{if} \quad h_1 < h_2 \end{cases} \\ \chi_2 < r < \chi_3 \quad &\Rightarrow \quad \begin{cases} s_1^{(+)}, s_2^{(-)} & \text{if} \quad h_1 > h_2 \\ s_1^{(-)}, s_2^{(+)} & \text{if} \quad h_1 < h_2 \end{cases} \\ r > \chi_3 \quad &\Rightarrow \quad s_1^{(+)}, s_2^{(+)} \end{aligned}$$

where $s_i^{(\pm)}$ is a contracted notation standing for $s_i = \pm 1$ with $i = 1, 2$. This decision rule is depicted in Fig. 4-9 for the case $h_1 > h_2$.

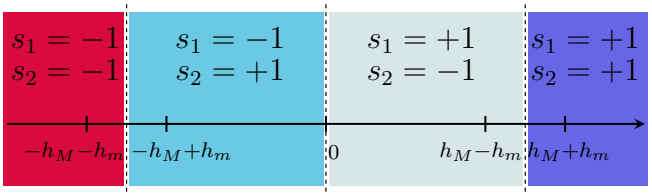

Figure 4-9: Decision regions for the proposed NCMA.

The proposed scheme can be extended to higher order modulations and to a greater number of users: it is easy to show that the number of possible received signal levels L can be expressed as

$$L = m^U \tag{4.37}$$

where m is the PAM modulation order and U is the number of users transmitting simultaneously. The following performance analysis focuses on the case $m = U = 2$ for brevity.

4.3.2 Performance analysis

The performance of NCMA using BPSK modulation with two users is derived here. Then performance of a QPSK modulation scheme can be easily derived by considering a QPSK as two quadrature BPSK modulations. In the following, we refer to s_M and s_m as the signal experiencing the better and the worst channel condition, respectively. By fixing the channel conditions $\mathbf{h} = [h_1, h_2]$, the NCMA bit error probability can be expressed as

$$P_e(\mathbf{h}) = \frac{P_e(s_M|\mathbf{h}) + P_e(s_m|\mathbf{h})}{2} \tag{4.38}$$

where $P_e(s_M|\mathbf{h})$ and $P_e(s_m|\mathbf{h})$ represent the error probability for signal s_M and s_m, respectively. The error probability for s_M will be smaller than that of s_m due to the assumed channel conditions.

By looking at Fig. 4-9, it is clear that s_M determines if the received signal (in the absence of noise) will have positive or negative values. This can be expressed as

$$\begin{aligned} P_e(s_M|\mathbf{h}) &= P(r<0|s_M^{(+)})P(s_M^{(+)}) + P(r>0|s_M^{(-)})P(s_M^{(-)}) \\ &= P(h_M + h_m + n < 0|s_M^{(+)}, s_m^{(+)})P(s_m^{(+)}) + \\ &\quad + P(h_M - h_m + n < 0|s_M^{(+)}, s_m^{(-)})P(s_m^{(-)}) \\ &= \frac{1}{2}\Big[F_n\left(-h_M - h_m\right) + F_n\left(-h_M + h_m\right)\Big] \end{aligned} \tag{4.39}$$

where $F_n(x)$ is the Gaussian cumulative distribution function (cdf), defined as

$$F_n(x) = \frac{1}{\sqrt{2\pi}\sigma_n}\int_{-\infty}^{x} e^{-\frac{t^2}{2\sigma_n^2}}dt. \tag{4.40}$$

As concerns s_m (i.e., the signal affected by the worse channel conditions), the probability of error is

$$\begin{aligned} P_e(s_m|\mathbf{h}) &= \Big[P(0<r<h_M|s_m^{(+)}) \ + \ P(r<-h_M|s_m^{(+)})\Big]\ P(s_m^{(+)}) + \\ &\quad + \Big[P(-h_M<r<0|s_m^{(-)}) \ + \ P(r>+h_M|s_m^{(-)})\Big]\ P(s_m^{(-)}) \\ &= P(0<r<h_M|s_M^{(+)}, s_m^{(+)})P(s_M^{(+)}) \ + \ P(-h_M<r<0|s_M^{(-)}, s_m^{(+)})P(s_M^{(-)}) + \\ &\quad + P(r<-h_M|s_M^{(+)}, s_m^{(+)})P(s_M^{(+)}) \ + \ P(r<-h_M|s_M^{(-)}, s_m^{(+)})P(s_M^{(-)}) \\ &= \frac{1}{2}\Big[P(0<h_M+h_m+n<h_M) \ + \ P(-h_M<-h_M+h_m+n<0) + \\ &\quad + P(h_M+h_m+n<-h_M) \ + \ P(-h_M+h_m+n<-h_M)\Big] \\ &= \frac{1}{2}\Big[F_n(-h_m) \ - \ F_n(-h_M-h_m) + \\ &\quad + F_n(2h_M-h_m) \ - \ F_n(h_M-h_m) + \\ &\quad + F_n(-2h_M-h_m) \ + \ F_n(-h_m)\Big]. \end{aligned} \tag{4.41}$$

Hence, the error probability for fixed channel conditions is

$$\begin{aligned} P_e(\mathbf{h}) = \frac{1}{4}\Big\{&2F_n(-h_m) + F_n(-h_M+h_m) + \\ &+ F_n(2h_M-h_m) + F_n(-2h_M-h_m) - F_n(h_M-h_m)\Big\} \end{aligned} \tag{4.42}$$

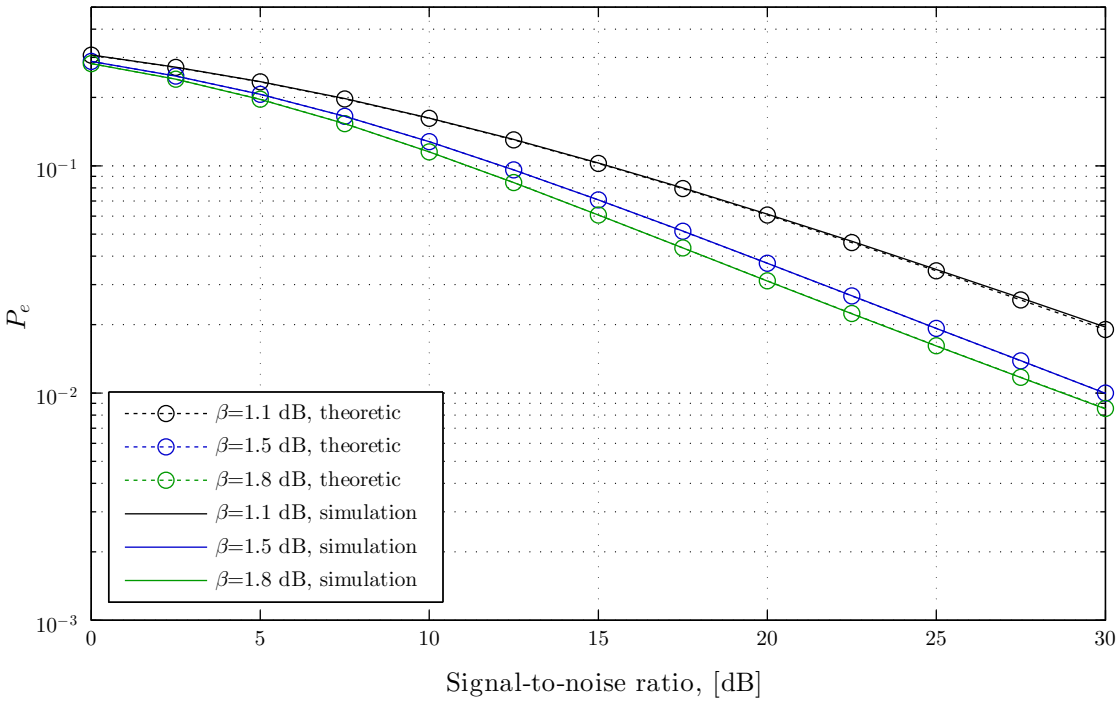

Figure 4-10: The error probability of NCMA obtained through simulations and analytically, for different values of β when the SNR varies.

which can be written in a shorter form as

$$P_e(\mathbf{h}) = \frac{1}{4}\sum_{i=1}^{5} c_i F_n(A_i h_M + b_i h_m) \tag{4.42b}$$

with

$$\mathbf{a}^T = [0, -1, 2, -2, 1] \tag{4.41e}$$
$$\mathbf{b}^T = [-1, 1, -1, -1, -1] \tag{4.41f}$$
$$\mathbf{c}^T = [2, 1, 1, 1, -1] \tag{4.41g}$$

where $(\,\cdot\,)^T$ represents the transpose operator.

In order to obtain the mean bit error probability, it is necessary to average $P_e(\mathbf{h})$ over the pdfs of h_1 and h_2, hence

$$\begin{aligned} P_e = E_{\mathbf{h}}\left[P_e(\mathbf{h})\right] &= \int_{h_1}\int_{h_2} P_e(\mathbf{h}) f_{\mathbf{h}}(\mathbf{h}) dh_1 dh_2 \\ &= \sum_{i=1}^{5} \frac{c_i}{4} \iint_{\mathbf{h}} F_n(a_i h_M + b_i h_m) f_{\mathbf{h}}(\mathbf{h}) d\mathbf{h} \end{aligned} \tag{4.42}$$

where $f_{\mathbf{h}}(\mathbf{h})$ represents the joint pdf of h_1 and h_2, which is given by the product of the marginal pdfs because the two random variables are independent. By focusing on the generic

i-th term of the sum in (4.42), we have

$$\begin{aligned}
&\iint_{\mathbf{h}} F_n(a_i h_M + b_i h_m) f_h(h_1) f_h(h_2) d\mathbf{h} \\
&= \int_{-\infty}^{+\infty} \int_{-\infty}^{h_2} F_n(a_i h_2 + b_i h_1) f_h(h_1) f_h(h_2) dh_1 dh_2 + \\
&\quad + \int_{-\infty}^{+\infty} \int_{h_2}^{+\infty} F_n(a_i h_1 + b_i h_2) f_h(h_1) f_h(h_2) dh_1 dh_2 \\
&= \frac{1}{\sqrt{2\pi}\sigma_n} \int_0^{\infty} \left\{ \int_{-\infty}^{a_i h_2} e^{-\frac{t^2}{2\sigma_n^2}} dt + \right. \\
&\quad + b_i \int_0^{h_2} e^{-\left[\left(\frac{a_i h_2 + b_i h_1}{\sqrt{2}\sigma_n}\right)^2 + \left(\frac{h_1}{\lambda}\right)^{\beta}\right]} dh_1 + \\
Wz \qquad &\quad \left. + a_i \int_{h_2}^{\infty} e^{-\left[\left(\frac{a_i h_1 + b_i h_2}{\sqrt{2}\sigma_n}\right)^2 + \left(\frac{h_1}{\lambda}\right)^{\beta}\right]} dh_1 \right\} f_h(h_2) dh_2.
\end{aligned} \tag{4.43}$$

The correctness of the derived equations is verified through simulations in the next section. Moreover, the aforementioned analysis is valid also for in-phase and quadrature modulation, leading to the same results for the same SNR values.

4.3.3 Numerical results

In this section the performance of the proposed access method is shown. First the theoretical analysis is validated by means of computer simulations. Then, the performance of the NCMA scheme is compared with a possible alternative, showing the benefits achieved.

Fig. 4-10 validates the performance of NCMA obtained analytically in the previous section. This figure shows the mean P_e of a QPSK-NCMA scheme for different values of the Weibull parameter β when the SNR varies. It is possible to see that the simulated performance coincides with that provided by (4.43).

In order to verify the effectiveness of a NCMA scheme we compare its pefromance with that of a classical TDMA scheme providing the same data rate. In particular, we consider a NCMA scheme where two users access simultaneously the channel using a QPSK modulation, hence, the comparison is performed with a TDMA system where the users transmit with a 16QAM modulation. Indeed, the 16QAM allows doubling the transmission rate of a system using a QPSK modulation at the expense of a P_e increase, just like the NCMA. In particular we expect that the performance of the proposed NCMA scheme depends on the fading distribution that determines the power imbalance between the users at the receiver. Hence, we investigate in which conditions the proposed approach represents a better alternative, that is when it allows a smaller P_e at a given information throughput.

First we analyse the special cases $\beta = 1$ and $\beta = 2$, representing the exponential and Rayleigh fading distribution, respectively. Fig. 4-11 shows the behaviour of NCMA and 16QAM when the SNR varies. It is possible to note that for the Rayleigh case the NCMA is the better alternative for low SNR values. On the other hand, for the exponential case the NCMA outperforms the 16QAM for the whole range of SNR values analysed.

Figs. 4-12 and 4-14 extend the analysis to intermediate β values. Fig. 4-12 shows the mean P_e as a function of the SNR level for some values of β, while Fig. 4-14 illustrates the

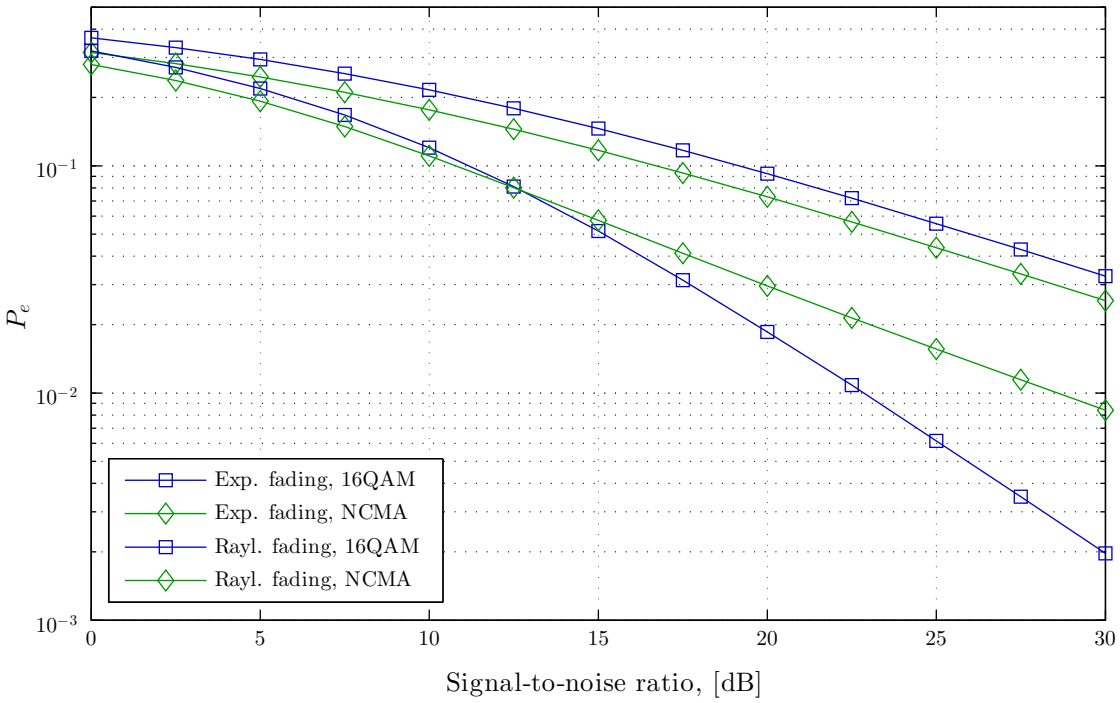

Figure 4-11: The error probability of NCMA and 16QAM modulation for exponential and Rayleigh fading when the SNR varies.

performance of the methods in the whole[9] domain of β. It is possible to see in both figures that the proposed scheme outperforms 16QAM when the channel conditions are bad, i.e., for low SNR and low β. Initially the NCMA performs better, but as the SNR increases the 16QAM gains ground and, finally, after a cross-over point becomes the better alternative. It is interesting to note that the cross-over point occurs at a certain value of SNR, SNR_c, which increases when the shape parameter β decreases. Fig. 4-13 shows SNR_c as a function of β. It is evident that this cross-over point has a vertical asymptote for $\beta = 1$.

4.4 Conclusion

Three methods to implement the Decode-and-Forward Physical Layer Network Coding for TDMA-OFDM system in multipath fading channels have been investigated here. The two major problems concerned the complexity of the detection at the relay side and the resulting decoding P_e. In particular, the former problem has been addressed by exploiting the channel inversion precoding at the end nodes, allowing a simple decoding of the signal received by the relay.

In order to reduce the resulting P_e three subcarriers suppression methods have been proposed at each source node. In the first method, named ISS, the terminal nodes suppress the subcarriers in an independent manner. The second alternative proposed here, named JSS, allows to overcome the performance of the ISS scheme in terms of P_e at the expense of a reduction of the transmission rate. Both these methods need a certain amount of signalling in order to let the relay node know which subcarriers have been turned off. In this sense, the third method (BSS) differs from the other two: it does not need any signalling and avoids

[9]The parameter β of the Weibull distribution can assume any real positive value. However, in order to model the fading, only the values between 1 and 2 are interesting.

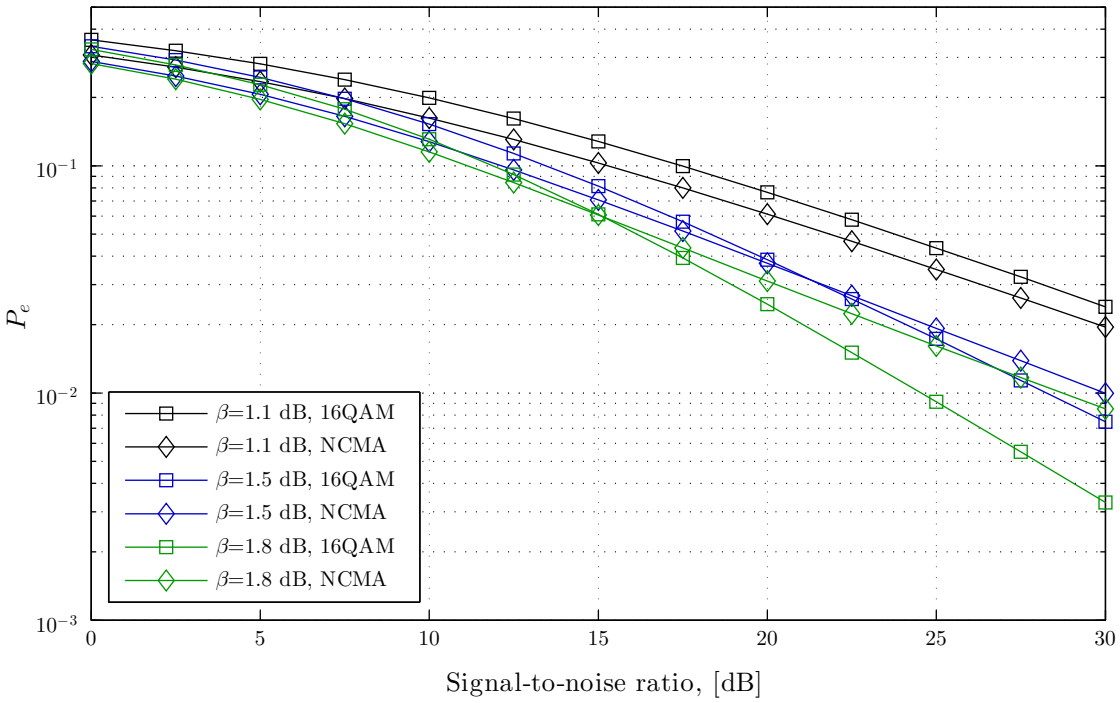

Figure 4-12: The error probability in a channel affected by Weibull fading for different shape factors β when the signal-to-noise ratio varies.

reduction of the transmission rate at the expense of a higher bit error probability.

Furthermore, a novel access technique, named Network Coding Multiple Access (NCMA), suitable for any uplink channel is proposed here. It exploits the basic concept of the Multiple Access Stage of a Physical Layer Network Coding Scheme. Two users can access simultaneously the communication medium, thus doubling the transmission rate, and can be detected at the receiving node exploiting the multi-user diversity provided by the propagation channels. The scheme has been analysed for channels affected by fading with different severity using the Weibull fading model and compared with a classical scheme having the same transmission rate. The results, obtained analytically and through computer simulations, have shown that the scheme under consideration performs well for poor channel conditions. Hence, it can be an important alternative when the propagation condition worsens and improved performance is most needed. Finally, it is important to note that the proposed access scheme can be extended to higher modulation orders and to simultaneous channel access by more than two users.

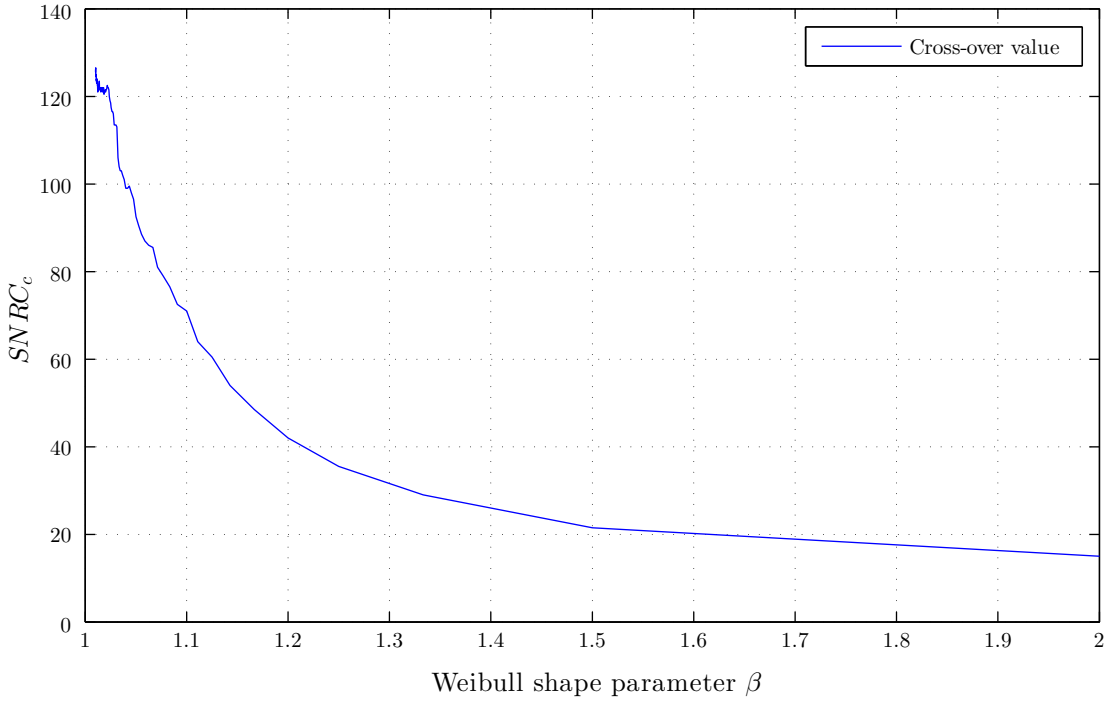

Figure 4-13: The performance cross-over point of NCMA and 16QAM as a function of the shape parameter β.

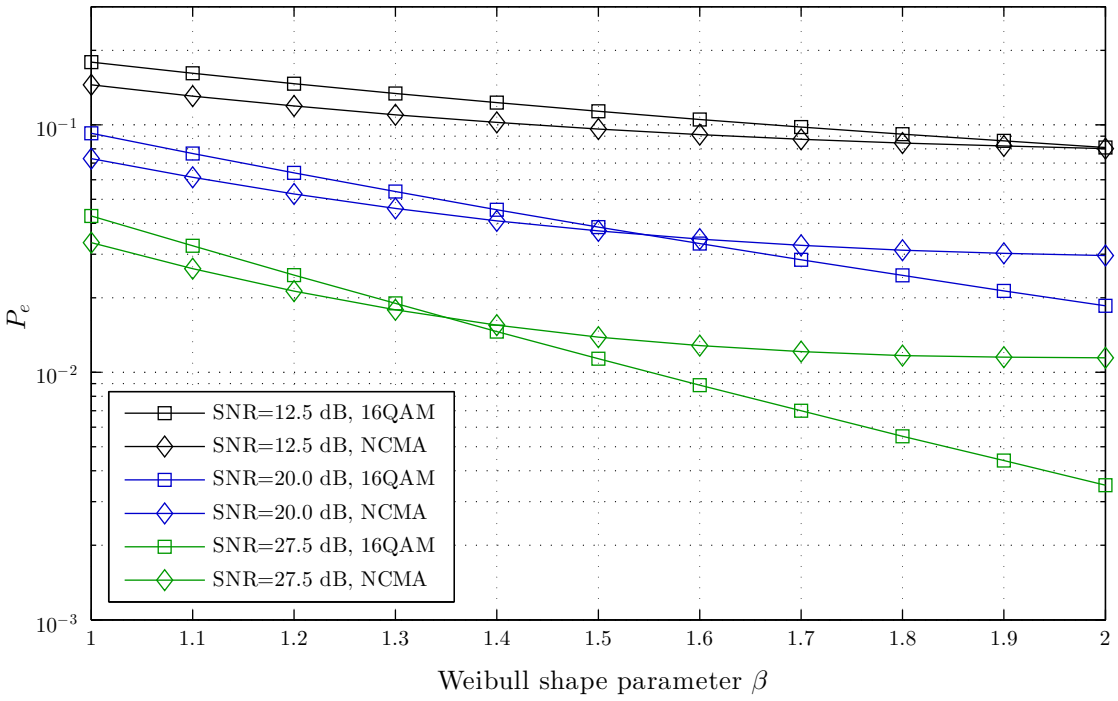

Figure 4-14: The error probability in a channel affected by Weibull fading for different SNR values when the shape factor β varies.

Chapter 5

Conclusion

This thesis dealt with many different topics, joint by a single theme: the interference. It was shown how different types of interference can heavily deteriorate the reliability of a system.

In Chapter 1, impulsive interference with fixed duration was analysed. and its impact on a multi-carrier receiver was evaluated. The results highlighted how the OFDM communication can be negated for some interference configurations. For this reason, a technique based on sensing, blanking, retransmission and soft-combining was presented. This method has shown better performance compared to traditional approaches.

Chapter 2 provided a different model for impulsive interference. Indeed, many works in the literature underline that additive Laplace noise is suitable to model impulsive interference in some cases. Hence, the structure of the optimal continuous-time receiver was derived and its performance evaluated. Moreover, an ARQ-based transmission scheme providing the optimal data-rate was proposed.

Chapter 3 concerned on the interference between cells of different dimensions in LTE heterogeneous networks. First, the main research trends were outlined for this topic. Then, the focus was concentrated on a particular scenario, where a small-cell equipped with a smart antenna system limits the interference and maximize its performance by resorting to a cognitive approach.

Finally, a method to face the interference through a completely different approach was shown. Indeed, Chapter 4 dealt with how the interference can be exploited to increase throughput of a network. In particular, by exploiting the PLNC concept was possible to obtain remarkable improvement in a two way relay network. Furthermore, a new multiple access technique based on the PLNC was proposed. This NCMA was evaluated, showing good performance for channel affected by severe fading conditions.

Appendix A

Interference Configuration PDF for an OFDM Symbol

The interference on a given OFDM symbol depends on the number of samples, d, affecting the symbol. In order to achieve a closed form of the error probability it is needed to remove the dependence on d in (1.27) by averaging its pdf that must be derived.

As stated before we have

- t is the portion of slot at the begin of the OFDM symbol;
- R is the portion of slot at the end of the OFDM symbol;
- N is the number of slots on the OFDM symbol;
- m is the number of slots affected by the interference.

For each possible interference configuration we can detect the number of samples affected by the interference d and the probability of occurrence of this configuration, P. We assume that the presence of the interference in different slots is uncorrelated.

In particular we have

- $m = 0$, represents the event of "absence of interference". This happens with probability $P = (1-p)^N$, and the samples affected by interference are $d = 0$.
- $m = 1$ happens with probability $P = Np(1-p)^{N-1}$. However, the number of corrupted samples depends on where the interference takes place, that is
  - (I) $d = t$, when interference is present in the first slot. This occurs with probability $P = p(1-p)^{N-1}$
  - (II) $d = R$, when interference is present in the last slot. This occurs with probability equal to case (I), $P = p(1-p)^{N-1}$
  - (III) $d = D$, when interference is present in a slot different from the first and the last. This may happen in $N-2$ cases, hence the related probability is $P = (N-2)p(1-p)^{N-1}$
- $m = 2, \cdots, N-2$, represents the general case of an OFDM symbol affected by m interference slots, which has probability $P = \binom{N}{m} p^m (1-p)^{N-m}$. In particular, the $\binom{N}{m}$ configurations can be differentiated in four cases, as follows

(I) interference is present in the first slot and in $m-1$ central slots, hence

$$d = t + (m-1)D. \tag{A.1}$$

This happens with $\binom{N-2}{m-1}$ different interference configurations, so the related probability is

$$P = \binom{N-2}{m-1} p^m (1-p)^{N-m}. \tag{A.2}$$

(II) interference is present in the last slot and in $m-1$ central slots, hence

$$d = (m-1)D + R. \tag{A.3}$$

$$P = P_{m,I} = \binom{N-2}{m-1} p^m (1-p)^{N-m}. \tag{A.4}$$

(III) interference is present in the first, in the last and in $m-2$ central slots. This may occur in $\binom{N-2}{m-2}$ cases, which leads to

$$d = t + (m-2)D + R \tag{A.5}$$

$$P = \binom{N-2}{m-2} p^m (1-p)^{N-m}. \tag{A.6}$$

(IV) interference is present only in central slots, that is

$$d = mD \tag{A.7}$$

$$P = \left(\binom{N}{m} - 2\binom{N-2}{m-1} - \binom{N-2}{m-2} \right) p^m (1-p)^{N-m} \tag{A.8}$$

- $m = N-1$, happens with probability $P = Np^{N-1}(1-p)$ and can be seen as a dual case of $m = 1$. In particular,

(I) interference may be present in the whole symbol with the exception of the first slot, which leads to

$$d = K - t = (N-2)D + R \tag{A.9}$$

$$P = p^{N-1}(1-p) \tag{A.10}$$

(II) interference may be present in the whole symbol with the exception of the last slot, and hence

$$d = K - R = t + (N-2)D \tag{A.11}$$

$$P = p^{N-1}(1-p) \tag{A.12}$$

(III) interference is present in the whole symbol with the exception of a central slot

$$d = K - D \tag{A.13}$$

$$P = (N-2)p^{N-1}(1-p) \tag{A.14}$$

- $m = N$, happens with probability $P = p^N$, the samples affected by interference are $d = K$.

The aforementioned analysis can be generalized. First we introduces an index l that represents the following cases

- l=1, the interference is on the first t samples but not on the last R;
- l=2, the interference is on the last R samples but not on the first t;
- l=3, the interference is neither on the first t samples nor on the last R;
- l=4, the interference is either on the first t samples or on the last R.

We extend the domain of the Binomial function as

$$\left[\begin{array}{c} A \\ B \end{array} \right] = \begin{cases} \binom{A}{B} & \text{if} \quad 0 \leq A \leq B \\ \\ 0 & \text{otherwise} \end{cases} . \tag{A.15}$$

Hence, for a given value of t, we have

$$\begin{aligned} d_{m,t,1} &= t + (m-1)D & \text{(A.16)} \\ d_{m,t,2} &= (m-1)D + R & \text{(A.17)} \\ d_{m,t,3} &= t + (m-2)D + R & \text{(A.18)} \\ d_{m,t,4} &= mD & \text{(A.19)} \end{aligned}$$

and the related probabilities are

$$\begin{aligned} P_{m,t,1} &= \left[\begin{array}{c} N-2 \\ m-1 \end{array} \right] \frac{p^m (1-p)^{N-m}}{D} & \text{(A.20)} \\ P_{m,t,2} &= \left[\begin{array}{c} N-2 \\ m-1 \end{array} \right] \frac{p^m (1-p)^{N-m}}{D} & \text{(A.21)} \\ P_{m,t,3} &= \left[\begin{array}{c} N-2 \\ m-2 \end{array} \right] \frac{p^m (1-p)^{N-m}}{D} & \text{(A.22)} \\ P_{m,t,4} &= \left(\left[\begin{array}{c} N \\ m \end{array} \right] - 2 \left[\begin{array}{c} N-2 \\ m-1 \end{array} \right] - \left[\begin{array}{c} N-2 \\ m-2 \end{array} \right] \right) \frac{p^m (1-p)^{N-m}}{D} & \text{(A.23)} \end{aligned}$$

for $m = 0, 1, \cdots, N$ and $t = 0, 1, \cdots, D-1$.

Now it is possible to express the pdf of the number of samples affected by interference, d, taking in account that certain value of d can be the outcome of different interference configurations. Hence, the pdf of d can be expressed as

$$f_d(x) = Pr(d = x) = \sum_{m,t,l \,:\, n_{m,t,l} = x} P_{m,t,l} \quad , \quad \text{for } x = 0, 1, \cdots, K \tag{A.24}$$

Appendix B

Error Probability of SS Methods

This Appendix deals with the derivation of the theoretical P_e for the proposed methods by means of a suitable analytical approach. In particular, two cases have to be distinguished:

1. the k-th subcarrier is used by both nodes;

2. the k-th subcarrier is used by only one node.

B.1 Case 1: P_e for subcarriers used by both nodes

Case 1 happens when the subcarrier gains are over the threshold for both channels (i.e., $|H_1[k]| > \lambda$ and $|H_2[k]| > \lambda$). By denoting with $P_{\mathbf{on}}$ the probability of an active subcarrier (i.e., $Pr(_{|H_1[k]|^2>\lambda}) = e^{-\lambda}$), as well as $P_{\mathbf{off}}$ the probability of a turned off subcarrier ($P_{\mathbf{off}} = 1 - P_{\mathbf{on}}$), the probability of case 1 happening can be calculated as

$$\mathcal{P}_1(\lambda) = \frac{P_{\mathbf{on}} \cdot P_{\mathbf{on}}}{P_{\mathbf{on}} \cdot P_{\mathbf{on}} + P_{\mathbf{off}} \cdot P_{\mathbf{on}}} = e^{-\lambda}. \tag{B.1}$$

MA stage
The P_e at the $\mathcal{R}$ side is equal for each subcarrier and is given by (4.16) averaged by the Probability Density Function (PDF) of $\mathbf{H_i}$, $f(\mathbf{H_i}; \lambda)$, with $i = 1, 2$. Hence we have

$$P_e^{MA,1}(\lambda) = \int_{\mathbf{H}} P_e^{MA}(\mathbf{H_{1,2}}) f(\mathbf{H_1}; \lambda) f(\mathbf{H_2}; \lambda) d\mathbf{H} \tag{B.2}$$

where $\mathbf{H} = \mathbf{H_1} \times \mathbf{H_2}$, with $\times$ denoting the Cartesian product. The PDF $f(\mathbf{H_i}; 0)$, i.e., without subcarriers suppression, is the joint probability distribution of K complex Gaussian random variable correlated to each other by the FFT operation. When the subcarriers suppression is considered it forces a bound on the magnitude of each random variable, changing the distribution. Observing eq. (4.16) we can note that the expression of $P_e^{MA}(\mathbf{H_{1,2}})$ is function of the normalization factors F_1 and F_2, which are in turn functions of the channels $\mathbf{H_1}$ and $\mathbf{H_2}$. This means that eq. (4.16) can be expressed as

$$P_e^{MA,1}(\lambda) = \iint_{F_1 \times F_2} P_e^{MA}(F_{1,2}) f_F(F_1; \lambda) f_F(F_2; \lambda) dF_1 dF_2 \tag{B.3}$$

where $f_F(F_i; \lambda)$ denotes the PDF of the normalization factor. By means of a fitting procedure it is possible to show that $f_F(F_i; \lambda)$ follows with good approximation a Generalized

Extreme Value distribution [147], whose parameters can be defined by resorting to a numerical approach once the channel model has been identified.

BC stage

In the BC stage the node $\mathcal{T}_i$ performs a classical QPSK demodulation on each active subcarrier having a channel gain, $H_i[k]$, over the threshold. The resulting P_e can be expressed as

$$P_e^{BC,1}(\lambda) = \frac{\int_{\lambda}^{\infty} Q\big(\sqrt{\overline{\gamma} H^2}\big) f_r(H) dH}{\int_{\lambda}^{\infty} f_r(H) dH} \tag{B.4}$$

where $f_r(\,\cdot\,)$ denotes the Rayleigh PDF.

Considering both stages for case 1, the final P_e at node $\mathcal{T}_i$ is given by the probability of having an erroneous decision in only one of the two stages, that is

$$P_e^{(1)} = P_e^{MA,1}(1 - P_e^{BC,1}) + P_e^{BC,1}(1 - P_e^{MA,1}) \tag{B.5}$$

where we omit the dependence by λ for simplicity.

B.2 Case 2: P_e for subcarriers used by only one node

In the second case only one node transmits on a given subcarrier, hence a QPSK demodulation is performed at both $\mathcal{R}$ and $\mathcal{T}_i$. The probability of case 2 happening is

$$\mathcal{P}_2(\lambda) = 1 - \mathcal{P}_1(\lambda) = 1 - e^{-\lambda} \tag{B.6}$$

MA stage

In the MA stage the subcarriers gain is over the threshold and the P_e can be expressed as

$$P_e^{MA,2}(\lambda) = \int_{\mathbf{H_i}} Q\left(\sqrt{\overline{\gamma} F\big(\mathbf{H_i}\big)^2}\right) f(\mathbf{H_i}; \lambda) d\mathbf{H_i} \tag{B.7}$$

$$= \int_{F_i} Q\left(\sqrt{\overline{\gamma} F_i^2}\right) f_F(F_i; \lambda) dF_i. \tag{B.8}$$

BC stage

In the BC stage the subcarriers gain is under the threshold and the P_e can be expressed as

$$P_e^{BC,2}(\lambda) = \frac{\int_{0}^{\lambda} Q\big(\sqrt{\overline{\gamma} H^2}\big) f_r(H) dH}{\int_{0}^{\lambda} f_r(H) dH}. \tag{B.9}$$

The final P_e at node $\mathcal{T}_i$ for the case 2 is given by

$$P_e^{(2)} = P_e^{MA,2}(1 - P_e^{BC,2}) + P_e^{BC,2}(1 - P_e^{MA,2}) \tag{B.10}$$

where we omit the dependence by λ for simplicity.

Bibliography

[1] G. Bartoli, R. Fantacci, D. Marabissi, L. Micciullo, C. Armani, and R. Merlo, "A Novel Mitigation Scheme for JTIDS Impulsive Interference on LDACS System Based on Sensing and Symbol Retransmission," *J. Signal Process. Syst.*, vol. 73, no. 3, pp. 255–266, Jun. 2013.

[2] G. Bartoli, R. Fantacci, D. Marabissi, L. Micciullo, and D. Tarchi, "Detection and Mitigation of Impulsive Interference on OFDM Signals Based on Spectrum Sensing, Blanking and Symbol Retransmission," *Wireless Personal Communications*, pp. 1–17, Feb. 2014. [Online]. Available: http://dx.doi.org/10.1007/s11277-014-1658-6

[3] N. C. Beaulieu, G. Bartoli, D. Marabissi, and R. Fantacci, "The Structure and Performance of an Optimal Continuous-Time Detector for Laplace Noise," *IEEE Commun. Lett.*, vol. 17, no. 6, pp. 1065–1068, Jun. 2013.

[4] G. Bartoli, N. C. Beaulieu, R. Fantacci, and D. Marabissi, "Optimal Data Rate for Reliable Packet Communications in Laplace Noise," *IEEE Commun. Lett.*, vol. 18, no. 1, pp. 2–5, Jan. 2014.

[5] G. Bartoli, R. Fantacci, B. K. Letaief, D. Marabissi, N. Privitera, P. Pucci, and J. Zhang, "Beamforming for Small Cells Deployment in LTE-Advanced and Beyond," *IEEE Wireless Commun. Mag.*, vol. 21, no. 2, Apr. 2014.

[6] G. Bartoli, R. Fantacci, D. Marabissi, and M. Pucci, "Physical Resource Block clustering method for an OFDMA cognitive femtocell system," *Physical Communications*, Oct. 2013. [Online]. Available: http://www.sciencedirect.com/science/article/pii/S1874490713000591

[7] ——, "LTE-A femto-cell interference mitigation with MuSiC DOA estimation and null steering in an actual indoor environment," in *Proc. IEEE Int. Conf. Commun. (ICC)*, Budapest, Hungary, Jun. 2013, pp. 2707–2711.

[8] G. Bartoli, D. Marabissi, R. Fantacci, and S. Simoni, "Subcarriers Suppression Methods for OFDM Systems with Decode-and-Forward Network Coding," *IEEE Trans. Wireless Commun.*, vol. 12, no. 12, pp. 6034–6042, Dec. 2013.

[9] G. Bartoli, R. Fantacci, D. Marabissi, and R. Simoni, "Physical Layer Network Coding in Multipath Channel: Effective Precoding-Based Transmission Scheme," in *Proc. IEEE Global Telecommun. Conf. (GLOBECOM)*, Houston, US-TX, Dec. 2011, pp. 1–5.

[10] G. Bartoli, R. Fantacci, D. Marabissi, L. Micciullo, and M. Fossi, "Carrier Allocation Method for AeroMACS System in Airport Channel," *IEEE Trans. Aerosp. Electron. Syst.*, vol. 49, no. 2, pp. 786–797, Apr. 2013.

[11] G. Bartoli, R. Fantacci, F. Gei, D. Marabissi, and L. Micciullo, "A Novel Emergency Management Platform for Smart Public Safety," *International Journal of Communication Systems*, Dec. 2013. [Online]. Available: http://dx.doi.org/10.1002/dac.2716

[12] G. Bartoli, R. Fantacci, and D. Marabissi, "AeroMACS: A New Perspective for Mobile Airport Communications and Services," *IEEE Wireless Commun. Mag.*, vol. 20, no. 6, pp. 44–50, Dec. 2013.

[13] G. Bartoli, R. Fantacci, D. Marabissi, D. Tarchi, and A. Tassi, "Downlink cross-layer scheduling strategies for long-term evolution and long-term evolution-advanced systems," *Wireless Commun. and Mobile Computing*, Jun. 2013. [Online]. Available: http://dx.doi.org/10.1002/wcm.2406

[14] G. Bartoli, A. Tassi, D. Marabissi, D. Tarchi, and R. Fantacci, "An Optimized Resource Allocation Scheme Based on a Multidimensional Multiple-Choice Approach with Reduced Complexity," in *Proc. IEEE Int. Conf. Commun. (ICC)*, Kyoto, Japan, Jun. 2011, pp. 1–6.

[15] M. Zimmermann and K. Dostert, "Analysis and modeling of impulsive noise in broad-band powerline communications," *IEEE Trans. Electromagn. Compat.*, vol. 44, no. 1, pp. 249–258, 2002.

[16] M. Budsabathon and S. Hara, "Robustness of OFDM signal against temporally localized impulsive noise," in *Proc. IEEE 54th Fall Veh. Technol. Conf. (VTC)*, vol. 3, 2001, pp. 1672–1676.

[17] M. Ghosh, "Analysis of the effect of impulse noise on multicarrier and single carrier QAM systems," *IEEE Trans. Commun.*, vol. 44, no. 2, pp. 145–147, 1996.

[18] S. V. Zhidkov, "Analysis and comparison of several simple impulsive noise mitigation schemes for OFDM receivers," *IEEE Trans. Commun.*, vol. 56, no. 1, pp. 5–9, 2008.

[19] Y. H. Kim, K. H. Kim, H. M. Oh, K. H. Kim, and S. C. Kim, "Mitigation of effect of impulsive noise for OFDM systems over power line channels," in *Proc. IEEE Int. Symp. Power Line Commun. and Applications (ISPLC)*, 2008, pp. 386–390.

[20] D. Marabissi, R. Fantacci, and S. Papini, "Robust Multiuser Interference Cancellation for OFDM Systems With Frequency Offset," *IEEE Trans. Wireless Commun.*, vol. 5, no. 11, pp. 3068–3076, 2006.

[21] C. H. Yih, "Iterative Interference Cancellation for OFDM Signals With Blanking Nonlinearity in Impulsive Noise Channels," *IEEE Signal Process. Lett.*, vol. 19, no. 3, pp. 147–150, 2012.

[22] J. Haring and A. J. H. Vinck, "Iterative decoding of codes over complex numbers for impulsive noise channels," *IEEE Trans. Inf. Theory*, vol. 49, no. 5, pp. 1251–1260, 2003.

[23] S. V. Zhidkov, "Impulsive noise suppression in OFDM-based communication systems," *IEEE Trans. Consum. Electron.*, vol. 49, no. 4, pp. 944–948, 2003.

[24] J. Armstrong and H. A. Suraweera, "Impulse noise mitigation for OFDM using decision directed noise estimation," in *Proc. IEEE Int. Symp. Spread Spectrum Techniques and Applications*, 2004, pp. 174–178.

[25] T. Kitamura, K. Ohno, and M. Itami, "Iterative impulsive noise reduction by generating its replica signal in OFDM reception," in *Proc. IEEE Int Consum. Electron. Conf. (ICCE)*, 2011, pp. 389–390.

[26] R. Fantacci, A. Tani, and D. Tarchi, "Impulse noise mitigation techniques for xDSL systems in a real environment," *IEEE Trans. Consum. Electron.*, vol. 56, no. 4, pp. 2106–2114, 2010.

[27] P. Torio and M. Garcia Sanchez, "Cell interleaving against impulsive noise in OFDM," *IEEE Trans. Consum. Electron.*, vol. 58, no. 2, pp. 269–273, 2012.

[28] T. Yucek and H. Arslan, "A Survey of Spectrum Sensing Algorithms for Cognitive Radio Applications," *IEEE Commun. Surveys Tuts.*, vol. 11, no. 1, pp. 116–130, 2009.

[29] F. F. Digham, M.-S. Alouini, and M. K. Simon, "On the Energy Detection of Unknown Signals Over Fading Channels," *IEEE Trans. Commun.*, vol. 55, no. 1, pp. 21–24, Jan. 2007.

[30] J. F. Cheng, "Coding performance of hybrid ARQ schemes," *IEEE Trans. Commun.*, vol. 54, no. 6, pp. 1017–1029, 2006.

[31] Eurocontrol and FAA, *Communications Operating Concept and Requirements for the Future Radio System*, ICAO Std., Rev. Version 2, May 2007.

[32] SESAR Joint Undertaking. [Online]. Available: http://www.sesarju.eu/

[33] NextGen project. [Online]. Available: http://www.faa.gov/nextgen/

[34] EUROCONTROL web site. [Online]. Available: http://www.eurocontrol.int

[35] U. Epple and M. Schnell, "Overview of interference situation and mitigation techniques for LDACS1," in *Proc. IEEE/AIAA 30th Digital Avionics Systems Conf. (DASC)*, 2011.

[36] S. V. Zhidkov, "Performance analysis and optimization of OFDM receiver with blanking nonlinearity in impulsive noise environment," *IEEE Trans. Veh. Technol.*, vol. 55, no. 1, pp. 234–242, 2006.

[37] A. Al-Dweik, A. Hazmi, B. Sharif, and C. Tsimenidis, "Efficient interleaving technique for OFDM system over impulsive noise channels," in *Proc. IEEE 21st Int. Personal Indoor and Mobile Radio Commun. Symp. (PIMRC)*, 2010, pp. 167–171.

[38] A. Ghasemi and E. Sousa, "Spectrum Sensing in Cognitive Radio Networks: Requirements,Challenges and Design Trade-offs," *IEEE Commun. Mag.*, pp. 32–39, Apr. 2008.

[39] R. Fantacci, "Performance evaluation of efficient continuous ARQ protocols," *IEEE Trans. Commun.*, vol. 38, no. 6, pp. 773–781, 1990.

[40] *Updated LDACS1 System Specification*, SESAR 15.2.4 ET - Task EWA04-1 T2 Std. 00.01.00, Aug. 2011.

[41] *JTIDS System Segment Specification (DCB79S4000C)*, Std.

[42] "A comparison of the minimum coupling loss method, enhanced minimum coupling loss method, and the monte-carlo simulation," European Radiocommunications Committee (ERC) within the European Conference of Postal and Telecommunications Administrations (CEPT), Tech. Rep., 1999.

[43] "Frequency and Distance Separations," International Telecommunication Union, Recommendation SM.337-4, 1997.

[44] "Unwanted emission in spurious domain," ITU-R, Recommendation SM.329-10.

[45] G. Bartoli, D. Marabissi, R. Fantacci, L. Micciullo, C. Armani, and R. Merlo, "Performance Evaluation of a Spectrum-Sensing technique for LDACS and JTIDS Coexistence in L-Band," in *Proc. Wireless Innovation Forum European Conference on Communications Technologies and Software Defined Radio (WInnComm)*, Brussels, Belgium, Jun. 2012.

[46] K. Blackard, T. Rappaport, and C. Bostian, "Measurements and models of radio frequency impulsive noise for indoor wireless communications," *IEEE J. Sel. Areas Commun.*, vol. 11, no. 7, pp. 991–1001, 1993.

[47] I. Mann, S. McLaughlin, W. Henkel, R. Kirkby, and T. Kessler, "Impulse generation with appropriate amplitude, length, inter-arrival, and spectral characteristics," *IEEE J. Sel. Areas Commun.*, vol. 20, no. 5, pp. 901–912, 2002.

[48] "Guidelines for evaluation of radio transmission technologies for IMT-2000," International Telecommunication Union, Recommendation M.1225, Feb. 1997.

[49] R. J. Marks, G. L. Wise, D. G. Haldeman, and J. L. Whited, "Detection in Laplace Noise," *IEEE Trans. Aerosp. Electron. Syst.*, vol. AES-14, no. 6, pp. 866–872, Nov. 1978.

[50] M. Schwartz and L. Shaw, *Signal Processing: Discrete Spectral Analysis, Detection and Estimation.* New York: McGraw-Hill, 1975.

[51] C. W. Helstrom, "Detectability of signals in Laplace noise," *IEEE Trans. Aerosp. Electron. Syst.*, vol. 25, no. 2, pp. 190–196, Mar. 1989.

[52] J. Miller and J. B. Thomas, "Detectors for discrete-time signals in non-gaussian noise," *Information Theory, IEEE Transactions on*, vol. 18, no. 2, pp. 241–250, 1972.

[53] J. Miller and J. Thomas, "Numerical results on the convergence of relative efficiencies," *Aerospace and Electronic Systems, IEEE Transactions on*, vol. AES-11, no. 2, pp. 204–209, 1975.

[54] N. C. Beaulieu and D. J. Young, "Designing Time-Hopping Ultrawide Bandwidth Receivers for Multiuser Interference Environments," *Proc. IEEE*, vol. 97, no. 2, pp. 255–284, Feb. 2009.

[55] M. Chiani and A. Giorgetti, "Coexistence Between UWB and Narrow-Band Wireless Communication Systems," *Proc. IEEE*, vol. 97, no. 2, pp. 231–254, Feb. 2009.

[56] M. W. Thompson and H.-S. Chang, "Coherent detection in Laplace noise," *IEEE Trans. Aerosp. Electron. Syst.*, vol. 30, no. 2, pp. 452–461, Apr. 1994.

[57] S. Jiang and N. C. Beaulieu, "Precise BER Computation for Binary Data Detection in Bandlimited White Laplace Noise," *IEEE Trans. Commun.*, vol. 59, no. 6, pp. 1570–1579, Jun. 2011.

[58] G. L. Turin, "An introduction to digital matched filters," *Proc. IEEE*, vol. 64, no. 7, pp. 1092–1112, Jul. 1976.

[59] N. C. Beaulieu and C. Leung, "On the Performance of Three Suboptimum Detection Schemes for Binary Signaling," *IEEE Trans. Commun.*, vol. 33, no. 3, pp. 241–245, Mar. 1985.

[60] R. Adams and C. Essex, *Calculus: A Complete Course.* Toronto: Pearson Canada, 2010.

[61] A. Papoulis and S. U. Pillai, *Probability, random variables and stochastic processes*, 4th ed. New York: McGraw-Hill, 2002.

[62] H. Cramèr, *Random Variables and Probability Distribution.* Cambridge: Cambridge University press, 1970.

[63] N. C. Beaulieu, "An infinite series for the computation of the complementary probability distribution function of a sum of independent random variables and its application to the sum of Rayleigh random variables," *IEEE Trans. Commun.*, vol. 38, no. 9, pp. 1463–1474, Sep. 1990.

[64] D. P. Bertsekas and R. G. Gallager, *Data networks*, 2nd ed. New Jersey: Prentice Hall, 1992.

[65] R. Fantacci, "Queuing analysis of the selective repeat automatic repeat request protocol wireless packet networks," *IEEE Trans. Veh. Technol.*, vol. 45, no. 2, pp. 258–264, 1996.

[66] J. G. Proakis, *Digital Communications*, 5th ed. New York: Mcgraw-Hill, 2008.

[67] D. Chase, "A Combined Coding and Modulation Approach for Communication over Dispersive Channels," *IEEE Trans. Commun.*, vol. 21, no. 3, pp. 159–174, Mar. 1973.

[68] J. F. Hayes, *Modeling and Analysis of Computer Communications Networks.* Plenum Press, 1984.

[69] A. Larmo, M. Lindstrom, M. Meyer, G. Pelletier, J. Torsner, and H. Wiemann, "The LTE link-layer design," *IEEE Commun. Mag.*, vol. 47, no. 4, pp. 52–59, Apr. 2009.

[70] T. Nakamura, S. Nagata, A. Benjebbour, Y. Kishiyama, T. Hai, S. Xiaodong, Y. Ning, and L. Nan, "Trends in small cell enhancements in LTE advanced," *IEEE Commun. Mag.*, vol. 51, no. 2, pp. 98–105, Feb.

[71] M. Baker, "From LTE-advanced to the future," *IEEE Commun. Mag.*, vol. 50, no. 2, pp. 116–120, Feb. 2012.

[72] A. Attar, V. Krishnamurthy, and O. Gharehshiran, "Interference management using cognitive base-stations for UMTS LTE," *IEEE Commun. Mag.*, vol. 49, no. 8, pp. 152–159, Aug. 2011.

[73] Y. S. Liang, W. H. Chung, G. K. Ni, I. Y. Chen, H. Zhang, and S. Y. Kuo, "Resource Allocation with Interference Avoidance in OFDMA Femtocell Networks," *IEEE Trans. Veh. Technol.*, vol. 61, no. 5, pp. 2243–2255, Jun. 2012.

[74] D. Tarchi, R. Fantacci, and D. Marabissi, "Proposal of a Cognitive Based MAC Protocol for M2M Environments," in *Proc. 24th Annual IEEE International Symposium on Personal, Indoor and Mobile Radio Communications*, London, UK, Sep. 2013, pp. 8–11.

[75] R. Wang, V. Lau, L. Lv, and B. Chen, "Joint cross-layer scheduling and spectrum sensing for OFDMA cognitive radio systems," *IEEE Trans. Wireless Commun.*, vol. 8, no. 5, pp. 2410–2416, 2009.

[76] D. C. Oh, H. C. Lee, and Y. H. Lee, "Cognitive Radio Based Resource Allocation in Femto-Cells," *J. Commun. Networks*, vol. 14, pp. 274–279, Jun. 2012.

[77] F. Khan and Y.-J. Choi, "Joint subcarrier and power allocations in OFDMA-based cognitive femtocell networks," in *18th Asia-Pacific Conference on Communications (APCC)*, Oct. 2012, pp. 812–817.

[78] D. Sun, X. Zhu, Z. Zeng, and S. Wan, "Downlink power control in cognitive femtocell networks," in *Proc. Int. Conf. Wireless Commun. Signal Process. (WCSP)*, Nanjing, China, Nov. 2011, pp. 1–5.

[79] M. Selim, M. El-Khamy, and M. El-Sharkawy, "Enhanced frequency reuse schemes for interference management in LTE femtocell networks," in *International Symposium on Wireless Communication Systems (ISWCS)*, Aug. 2012, pp. 326–330.

[80] C. Bouras, G. Kavourgias, V. Kokkinos, and A. Papazois, "Interference management in LTE femtocell systems using an adaptive frequency reuse scheme," in *Wireless Telecommunications Symposium (WTS)*, Apr. 2012, pp. 1–7.

[81] A. Taherpour, M. Nasiri-Kenari, and S. Gazor, "Multiple antenna spectrum sensing in cognitive radios," *IEEE Trans. Wireless Commun.*, vol. 9, no. 2, pp. 814–823, Feb. 2010.

[82] R. Zhang, T. Lim, Y. C. Liang, and Y. Zeng, "Multi-antenna based spectrum sensing for cognitive radios: a GLRT approach," *IEEE Trans. Commun.*, vol. 58, no. 1, pp. 84–88, Jan. 2010.

[83] S. Kim, J. Lee, H. Wang, and D. Hong, "Sensing performance of energy detector with correlated multiple antennas," *IEEE Signal Process. Lett.*, vol. 16, no. 8, pp. 671–674, Aug. 2009.

[84] W. Lee and D.-H. Cho, "Enhanced Spectrum Sensing Scheme in Cognitive Radio Systems With MIMO Antennae," *IEEE Trans. Veh. Technol.*, vol. 60, no. 3, pp. 1072–1085, Aug. 2011.

[85] R. Zhang and Y.-C. Liang, "Exploiting multi-antennas for opportunistic spectrum sharing in cognitive radio networks," *IEEE J. Sel. Areas Commun.*, vol. 2, no. 1, pp. 88–102, Feb. 2008.

[86] Y. Tawk, S. Jayaweera, C. Christodoulou, and J. Costantine, "A comparison between different cognitive radio antenna systems," in *Proc. Int. Symp. Intelligent Signal Processing and Communications Systems (ISPACS)*, 2011, pp. 1–5.

[87] J. Kim, S. Kim, O.-S. Shin, and Y. Shin, "A Cognitive Beamforming Scheme for Coexistence of Incumbent and Cognitive Radios," in *Proc. 6th IEEE Consumer Communications and Networking Conference (CCNC)*, 2009, pp. 1–4.

[88] S. Yiu, C.-B. Chae, K. Yang, and D. Calin, "Uncoordinated Beamforming for Cognitive Networks," *IEEE Trans. Commun.*, vol. 60, no. 5, pp. 1390–1397, May 2012.

[89] R. Z. F. G. Y.-C. Liang, "Cognitive beamforming made practical: Effective interference channel and learning-throughput tradeoff," in *Proc. IEEE 10th Workshop on Signal Processing Advances in Wireless Communications (SPAWC)*, 2009, pp. 588–592.

[90] H. Lan Zhang; Ying-Chang Liang; Yan Xin; Poor, "Cognitive beamforming made practical: Effective interference channel and learning-throughput tradeoff," *IEEE Trans. Wireless Commun.*, vol. 8, no. 8, pp. 4143–4153, 2009.

[91] D. C. Oh, H. C. Lee, and Y. H. Lee, "Power Control and Beamforming for Femtocells in the Presence of Channel Uncertainty," *IEEE Trans. Veh. Technol.*, vol. 60, no. 6, pp. 2545–2554, 2011.

[92] J. Xie, Z. Fu, and H. Xian, "Spectrum sensing based on estimation of direction of arrival," in *Proc. Int. Conf. Computational Problem-Solving (ICCP)*, Dec. 2010, pp. 39–42.

[93] E. Yaacoub and Z. Dawy, "Enhancing the performance of OFDMA underlay cognitive radio networks via secondary pattern nulling and primary beam steering," in *Proc. IEEE Wireless Commun. Networking Conf. (WCNC)*, Mar. 2011, pp. 1476–1481.

[94] K. Hamdi, W. Zhang, and K. Letaief, "Opportunistic spectrum sharing in cognitive MIMO wireless networks," *IEEE Trans. Wireless Commun.*, vol. 8, no. 8, pp. 4098–4109, 2009.

[95] T. Yoo and A. Goldsmith, "On the optimality of multiantenna broadcast scheduling using zero-forcing beamforming," *IEEE J. Sel. Areas Commun.*, vol. 24, no. 3, pp. 528–541, 2006.

[96] S. Chen, Z. Feng, Q. Zhang, and P. Zhang, "Interference mitigation and capacity optimization in cooperative public femtocell networks with cognitive enabled multi-element antennas," in *Proc. IEEE Global Commun. Conf. (GLOBECOM) Workshops*, 2012, pp. 652–656.

[97] J. Zhang and J. Andrews, "Adaptive spatial intercell interference cancellation in multicell wireless networks," *IEEE J. Sel. Areas Commun.*, vol. 28, no. 9, pp. 1455–1468, 2010.

[98] J. Zhang, R. Chen, J. Andrews, A. Ghosh, and R. Heath, "Networked mimo with clustered linear precoding," *IEEE Trans. Wireless Commun.*, vol. 8, no. 4, pp. 1910–1921, 2009.

[99] Y. Shi, J. Zhang, and K. B. Letaief, "Group sparse beamforming for green cloud radio access networks," in *Proc. IEEE Global Commun. Conf. (GLOBECOM)*, Atlanta, GA, Dec. 2013.

[100] F. Rusek, D. Persson, B. K. Lau, E. Larsson, T. Marzetta, O. Edfors, and F. Tufvesson, "Scaling Up MIMO: Opportunities and Challenges with Very Large Arrays," *IEEE Signal Process. Mag.*, vol. 30, no. 1, pp. 40–60, 2013.

[101] T. Marzetta, "Noncooperative Cellular Wireless with Unlimited Numbers of Base Station Antennas," *IEEE Trans. Wireless Commun.*, vol. 9, no. 11, pp. 3590–3600, 2010.

[102] E. G. Larsson, F. Tufvesson, O. Edfors, and T. L. Marzetta, "Massive MIMO for next generation wireless systems," *submitted to IEEE Commun. Mag.*, 2013. [Online]. Available: http://arxiv.org/abs/1304.6690

[103] H. Q. Ngo, E. Larsson, and T. Marzetta, "Energy and Spectral Efficiency of Very Large Multiuser MIMO Systems," *IEEE Trans. Commun.*, vol. 61, no. 4, pp. 1436–1449, 2013.

[104] C. Shepard, H. Yu, N. Anand, E. Li, T. L. Marzetta, Y. R., and L. Zhong, "Argos: practical many-antenna base stations," in *Proc. ACM Int. Conf. Mobile Computing and Networking (MobiCom)*, 2012, pp. 53–64.

[105] Q. H. Spencer, B. D. Jeffs, M. A. Jensen, and A. L. Swindlehurst, "Modeling the statistical time and angle of arrival characteristics of an indoor multipath channel," *IEEE J. Sel. Areas Commun.*, vol. 18, no. 3, pp. 347–360, Mar. 2000.

[106] 3GPP, "Evolved Universal Terrestrial Radio Access (E-UTRA) - Base Station (BS) radio transmission and reception," Third Generation Partnership Project, Standard TS36.104, Sep. 2012.

[107] F. Boccardi, B. Clerckx, A. Ghosh, E. Hardouin, G. Jongren, K. Kusume, E. Onggosanusi, and Y. Tang, "Multiple-antenna techniques in LTE-advanced," *IEEE Commun. Mag.*, vol. 50, no. 3, pp. 114–121, Mar. 2012.

[108] L. Jiang and S. Y. Tan, "Geometrically Based Statistical Channel Models for Outdoor and Indoor Propagation Environments," *IEEE Trans. Veh. Technol.*, vol. 56, no. 6, pp. 3587–3593, Nov. 2007.

[109] L. Godara, "Application of antenna arrays to mobile communications. II. Beam-forming and direction-of-arrival considerations," *Proc. IEEE*, vol. 85, no. 8, pp. 1195–1245, aug 1997.

[110] G. Ioannopoulos, D. Anagnostou, and M. Chryssomallis, "A survey on the effect of small snapshots number and SNR on the efficiency of the MUSIC algorithm," in *IEEE Antennas and Propagation Society International Symposium (APSURSI)*, Jul. 2012, pp. 1–2.

[111] J. MacQueen, "Some methods for classification and analysis of multivariate observations," in *Proc. Fifth Berkeley Symp. on Math. Statist. and Prob.* Univ. of Claif. Press, 1967, pp. 281–297.

[112] 3GPP, "Evolved Universal Terrestrial Radio Access (E-UTRA) - FDD Home eNode B (HeNB) Radio Frequency (RF) requirements analysis," Third Generation Partnership Project, Standard TS36.921, Sep. 2012.

[113] A. Jain, M. Murty, and P. Flynn, "Data Clustering: A Review," *ACM Computing Surveys*, vol. 31, no. 3, pp. 264–323, Sep. 1999.

[114] A. K. Jain, "Data clustering: 50 years beyond K-means," *Elsevier, Pattern Recognition Letters*, vol. 31, no. 8, pp. 651–666, Jun. 2010.

[115] S. Johnson, "Hierarchical Clustering Schemes," *Psychometrika, Springer*, vol. 32, no. 3, pp. 241–254, Sep. 1967.

[116] A. Jain and R. Dubes, "Algorithms for Clustering Data." Prentice Hall, Englewood Cliffs, NJ, 1988.

[117] B. Chen, P. Tai, R. Harrison, and Y. Pan, "Novel hybrid hierarchical-K-means clustering method (H-K-means) for microarray analysis," in *Proc. IEEE Computational Systems Bioinformatics Conference*, 2005, pp. 105–108.

[118] R. Schmidt, "Multiple emitter location and signal parameter estimation," *IEEE Trans. Antennas Propag.*, vol. 34, no. 3, pp. 276–280, Mar. 1986.

[119] R. Ahlswede, N. Cai, S.-Y. Li, and R. Yeung, "Network information flow," *IEEE Trans. Inf. Theory*, vol. 46, no. 4, pp. 1204–1216, Jul. 2000.

[120] S. Katti, S. Gollakota, and D. Katabi, "Embracing Wireless Interference: Analog Network Coding," in *Proc. Conf. Applicat., Technol, Archit., and Protocols for Comput. Commun. (SIGCOMM)*. Kyoto, Japan: ACM New York, NY, USA 2007, Aug. 2007, pp. 397–408.

[121] S. Zhang, S. C. Liew, and P. P. Lam, "Hot Topic: Physical-Layer Network Coding," in *Proc. 12th Annu. Int. Conf. Mobile Computing and Networking (MobiCom)*. Los Angeles, US-CA: ACM New York, NY, USA 2006, Sep. 2006, pp. 358–365.

[122] J. Laneman, D. Tse, and G. Wornell, "Cooperative diversity in wireless networks: Efficient protocols and outage behavior," *IEEE Trans. Inf. Theory*, vol. 50, no. 12, pp. 3062–3080, Dec. 2004.

[123] T. Cover and A. Gamal, "Capacity theorems for the relay channel," *IEEE Trans. Inf. Theory*, vol. 25, no. 5, pp. 572–584, Sep. 1979.

[124] F. Rossetto, "A comparison of different physical layer network coding techniques for the satellite environment," in *Proc. 5th Adv. Satellite Multimedia Syst. Conf. and 11th Signal Process. for Space Commun. Workshop (ASMA/SPSC)*, Cagliari, Italy, Sep. 2010, pp. 25–30.

[125] I. Maric, A. Goldsmith, and M. Medard, "Analog Network Coding in the High-SNR Regime," in *Proc. IEEE Wireless Network Coding Conf. (WiNC)*, Boston, US-MA, Jun. 2010, pp. 1–6.

[126] F. Gao, R. Zhang, and Y.-C. Liang, "Optimal channel estimation and training design for two-way relay networks," *IEEE Trans. Commun.*, vol. 57, no. 10, pp. 3024–3033, Oct. 2009.

[127] H. Gacanin and F. Adachi, "Broadband analog network coding," *IEEE Trans. Wireless Commun.*, vol. 9, no. 5, pp. 1577–1583, 2010.

[128] G. Wang, F. Gao, Y.-C. Wu, and C. Tellambura, "Joint CFO and Channel Estimation for CP-OFDM Modulated Two-Way Relay Networks," in *Proc. IEEE Int. Conf. Commun. (ICC)*, Cape Town, South Africa, May 2010, pp. 1–5.

[129] Z. Li, X. Xia, and B. Li, "Achieving full diversity and fast ML decoding via simple analog network coding for asynchronous two-way relay networks," *IEEE Trans. Commun.*, vol. 57, no. 12, pp. 3672–3681, 2009.

[130] W. Shiqiang, S. Qingyang, W. Xingwei, and A.Jamalipour, "Power and Rate Adaptation for Analog Network Coding," *IEEE Trans. Veh. Technol.*, vol. 60, no. 5, pp. 2302–2313, 2011.

[131] Z. Ding, K. Leung, D. Goeckel, and D. Towsley, "On the study of network coding with diversity," *IEEE Trans. Wireless Commun.*, vol. 8, no. 3, pp. 1247–1259, Mar. 2009.

[132] T. Koike-Akino, P. Popovski, and V. Tarokh, "Adaptive Modulation and Network Coding with Optimized Precoding in Two-Way Relaying," in *Proc. IEEE Global Telecommun. Conf. (GLOBECOM)*, Honolulu, US-HI, Dec. 2009, pp. 1–6.

[133] T. Cui, F. Gao, T. Ho, and A. Nallanathan, "Distributed Space-Time coding for Two-Way Wireless Relay Networks," in *Proc. IEEE Int. Conf. Commun. (ICC)*, Beijing, China, May 2008, pp. 3888–3892.

[134] E. Al-Susa and R. Onnondroyd, "An improved channel inversion based adaptive OFDM system in the presence of channel errors and rapid time variations," in *Proc. IEEE Veh. Technol. Conf. (VTC)*, vol. 3, Boston, US-MA, Sep. 2000, pp. 1114–1119.

[135] T. Keller and L. Hanzo, "Sub-band adaptive pre-equalised OFDM transmission," in *Proc. IEEE Veh. Technol. Conf. (VTC)*, vol. 1, Amsterdam, Netherlands, Sep. 1999, pp. 334–338.

[136] D. Bing and Z. Jun, "Physical-Layer Network Coding over Wireless Fading Channel," in *Proc. International Conference on Information, Communications and Signal Processing (ICICS)*, 2009.

[137] D. Fang and A. G. Burr, "Soft Bits based fading Correction for Coded Physical Layer Network Coding," in *Proc. 8th Int. Symp. Wireless Commun. Syst. (ISWCS)*, Aachen, Germany, Nov. 2011, pp. 357–361.

[138] M. Noori and M. Ardakani, "On Symbol Mapping for Binary Physical-Layer Network Coding with PSK Modulation," *IEEE Trans. Wireless Commun.*, vol. 11, no. 1, pp. 21–26, Jan. 2012.

[139] E. C. Y. Peh, Y.-C. Liang, and Y. L. Guan, "Power control for physical-layer network coding in fading environments," in *Proc. IEEE 19th Int. Symp. Personal, Indoor Mobile Radio Commun. (PIMRC)*, Cannes, France, Sep. 2008, pp. 1–5.

[140] T. Koike-Akino, P. Popovski, and V. Tarokh, "Optimized constellations for two-way wireless relaying with physical network coding," *IEEE J. Sel. Areas Commun.*, vol. 27, no. 5, pp. 773–787, Jun. 2009.

[141] J. Huang, Z. Wang, S. Zhou, and Z. Wang, "Turbo equalization for OFDM modulated physical layer network coding," in *Proc. 12th IEEE Int. Workshop Signal Process. Adv. Wireless Communications (SPAWC)*, San Francisco, US-CA, Jun. 2011, pp. 291–295.

[142] S. Morosi, D. Marabissi, E. D. Re, R. Fantacci, and N. Del Santo, "A rate adaptive bit-loading algorithm for in-building power-line communications based on DMT-modulated systems," *IEEE Trans. Power Del.*, vol. 21, no. 4, pp. 1892–1897, Oct. 2006.

[143] F. Babich and G. Lombardi, "Statistical analysis and characterization of the indoor propagation channel," *IEEE Trans. Commun.*, vol. 48, no. 3, pp. 455–464, 2000.

[144] H. Hashemi, "The indoor radio propagation channel," *Proc. IEEE*, vol. 81, no. 7, pp. 943–968, 1993.

[145] N. Shepherd, "Radio wave loss deviation and shadow loss at 900 MHz," *IEEE Trans. Veh. Technol.*, vol. 26, no. 4, pp. 309–313, 1977.

[146] D. Matolak and J. Frolik, "Worse than Rayleigh fading: experimental results and theoretical models," *IEEE Commun. Mag.*, vol. 49, no. 4, pp. 140–146, 2011.

[147] S. Coles, *An introduction to statistical modeling of extreme values*, ser. Springer Series in Statistics. London, UK: Springer-Verlag, 2001.